Nuclear Safety
NEA/CSNI/R(2019)15
September 2022
www.oecd-nea.org

Prestressed Concrete Reactor Containment Behaviour in Test Condition Taking into Account Ageing Effects (VeRCoRs)

OECD
BETTER POLICIES FOR BETTER LIVES

NEA
NUCLEAR ENERGY AGENCY

Nuclear Energy Agency

NEA/CSNI/R(2019)15

Unclassified **English text only**

26 September 2022

NUCLEAR ENERGY AGENCY
COMMITTEE ON THE SAFETY OF NUCLEAR INSTALLATIONS

Prestressed Concrete Reactor Containment Behaviour in Test Condition Taking into Account Ageing Effects (VeRCoRs)

This document is available in PDF format only.

JT03503269

ORGANISATION FOR ECONOMIC CO-OPERATION AND DEVELOPMENT

The OECD is a unique forum where the governments of 38 democracies work together to address the economic, social and environmental challenges of globalisation. The OECD is also at the forefront of efforts to understand and to help governments respond to new developments and concerns, such as corporate governance, the information economy and the challenges of an ageing population. The Organisation provides a setting where governments can compare policy experiences, seek answers to common problems, identify good practice and work to co-ordinate domestic and international policies.

The OECD member countries are: Australia, Austria, Belgium, Canada, Chile, Colombia, Costa Rica, the Czech Republic, Denmark, Estonia, Finland, France, Germany, Greece, Hungary, Iceland, Ireland, Israel, Italy, Japan, Korea, Latvia, Lithuania, Luxembourg, Mexico, the Netherlands, New Zealand, Norway, Poland, Portugal, the Slovak Republic, Slovenia, Spain, Sweden, Switzerland, Türkiye, the United Kingdom and the United States. The European Commission takes part in the work of the OECD.

OECD Publishing disseminates widely the results of the Organisation's statistics gathering and research on economic, social and environmental issues, as well as the conventions, guidelines and standards agreed by its members.

NUCLEAR ENERGY AGENCY

The OECD Nuclear Energy Agency (NEA) was established on 1 February 1958. Current NEA membership consists of 34 countries: Argentina, Australia, Austria, Belgium, Bulgaria, Canada, the Czech Republic, Denmark, Finland, France, Germany, Greece, Hungary, Iceland, Ireland, Italy, Japan, Korea, Luxembourg, Mexico, the Netherlands, Norway, Poland, Portugal, Romania, Russia (suspended), the Slovak Republic, Slovenia, Spain, Sweden, Switzerland, Türkiye, the United Kingdom and the United States. The European Commission and the International Atomic Energy Agency also take part in the work of the Agency.

The mission of the NEA is:

– to assist its member countries in maintaining and further developing, through international co-operation, the scientific, technological and legal bases required for a safe, environmentally sound and economical use of nuclear energy for peaceful purposes;

– to provide authoritative assessments and to forge common understandings on key issues as input to government decisions on nuclear energy policy and to broader OECD analyses in areas such as energy and the sustainable development of low-carbon economies.

Specific areas of competence of the NEA include the safety and regulation of nuclear activities, radioactive waste management and decommissioning, radiological protection, nuclear science, economic and technical analyses of the nuclear fuel cycle, nuclear law and liability, and public information. The NEA Data Bank provides nuclear data and computer program services for participating countries.

Committee on the Safety of Nuclear Installations

The Committee on the Safety of Nuclear Installations (CSNI) addresses NEA programmes and activities that support maintaining and advancing the scientific and technical knowledge base of the safety of nuclear installations.

The CSNI constitutes a forum for the exchange of technical information and for collaboration between organisations, which can contribute, from their respective backgrounds in research, development and engineering, to its activities. It has regard to the exchange of information between member countries and safety R&D programmes of various sizes in order to keep all member countries involved in and abreast of developments in technical safety matters.

The CSNI reviews the state of knowledge on important topics of nuclear safety science and techniques and of safety assessments, and ensures that operating experience is appropriately accounted for in its activities. It initiates and conducts programmes identified by these reviews and assessments in order to confirm safety, overcome discrepancies, develop improvements and reach consensus on technical issues of common interest. It promotes the co-ordination of work in different member countries that serve to maintain and enhance competence in nuclear safety matters, including the establishment of joint undertakings (e.g. joint research and data projects), and assists in the feedback of the results to participating organisations. The committee ensures that valuable end-products of the technical reviews and analyses are provided to members in a timely manner, and made publicly available when appropriate, to support broader nuclear safety.

The CSNI focuses primarily on the safety aspects of existing power reactors and other nuclear installations; it also considers the safety implications of scientific and technical developments of future reactor technologies and designs. Further, the scope for the committee includes human and organisational research activities and technical developments that affect nuclear safety.

Foreword

This report was written by members of the Working Group on Integrity and Ageing of Components and Structures (WGIAGE) of the Nuclear Energy Agency (NEA). Members of the concrete subgroup were in charge of developing the responses in this report.

The activity is consistent with NEA strategies for the WGIAGE and was led by Électricité de France (EDF). The main objective was to improve the capability to predict the ageing effects on concrete containment, and consequently to find tools and methods to improve the leak tightness of concrete containment without liner.

The approach to achieve this objective was to use the VeRCoRs, a 1/3 scaled mock-up of a double wall containment used for testing, to share knowledge about the behaviour and leakage assessment of a prestressed concrete containment without liner. The work was largely carried out by the concrete subgroup members of the WGIAGE. As a result, the responses focus on concrete safety-related structures.

The VeRCoRs experiment provides an opportunity to the nuclear civil engineering and research community to study the whole lifetime cycle of a containment building. One of the most challenging scientific objectives is to provide a global understanding of the mechanisms of prestressed reinforced concrete ageing, and their effect on the evolution of leakage rate during integrated leakage rate tests over time. The challenge lies within the numerous complexity levels of the problem. Scientifically, the physical phenomena implied can be complex by themselves (hydration, drying, creep, leakage, damage, etc.) and they are sometimes coupled together. Experimentally, some of the quantities required are also quite difficult to measure and/or to evaluate. Eventually the modelling and prediction work has to deal with all of this complexity.

In 2015 and 2018, EDF organised large benchmarks on the VeRCoRs mock-up, bringing together experts of multiple nationalities from consulting companies or nuclear regulators. The first VeRCoRs benchmark focused on the early age behaviour of the containment in terms of cracking and leakage. The results of the 2015 benchmark are considered as input to the 2018 benchmark.

The present report compares the analysis results of the 2018 benchmark. For privacy purposes, no names of persons or companies are revealed. Team numbers allow comparisons and assessments of differences between the team results.

Objective

The main objective of this report is to give a detailed overview of the benchmark performed in 2018 on the containment mock-up named VeRCoRs. The objective of the benchmark was to improve participants' capability to predict the effects of ageing on concrete containment. The benchmark, which is described in this report, was an open benchmark done with the results of two identical pressurisation tests of the VeRCoRs mock-up.

Scope

The scope of the work is related to the safety of civil engineering structures of nuclear facilities, especially concerning concrete containment ageing effects. As mentioned above, the first VeRCoRs benchmark in 2015 focused on the early age behaviour of the containment, with its implication in terms of cracking and leakage, and the report from that benchmark was made available to the participants of the 2018 benchmark.

The second benchmark, which is covered in this report, focused mainly on the assessment of ageing effects, and on a first assessment of leak rate in test conditions. The behaviour during early age is not included in the report; nevertheless, the synthesis of the 2015 benchmark was considered as an input of this report. This report focuses on ageing effects of the VeRCoRs concrete containment mock-up. Creep and shrinkage have been taken into account to predict the deformations and the leakage. The effect of two successive loadings without ageing has been studied.

The third VeRCoRs benchmark (planned for 2023) will concern severe accident loading.

Acknowledgements, contributors and credits

The NEA wishes to express its sincere gratitude to Mr Manuel Corbin (EDF, France) and Mr Julien Niepceron, who wrote this report, to the members of the VeRCoRs Task Group, and to the authors for their contribution to this report. Additional gratitude is expressed to Dr Miguel Azenha (University of Minho, Portugal), Dr Nico Herrman (Karlsruhe Institute of Technology, Germany) and Dr Jacky Mazars (Grenoble INP, France) for their contribution during the workshop, as well as to Mr Olli Nevander and Dr Diego Escrig Forano of the NEA Secretariat for their support in managing the activity and publishing the report.

Table of contents

List of tables

List of figures

Abbreviations and acronyms

CDP	Concrete damaged plasticity
CPU	Central processing unit
CSNI	Committee on the Safety of Nuclear Installations (NEA)
EDF	Électricité de France
FEM	Finite-Element Method
NEA	Nuclear Energy Agency
MPa	Megapascal
OECD	Organisation for Economic Co-operation and Development
RH	Relative humidity
THM	Thermo-hydro-mechanical
US NRC	United States Nuclear Regulatory Commission
VD	Visite décennale (decennial visit)
VeRCoRs	Vérification réaliste du confinement des réacteurs (Realistic verification of reactor containment)
WGIAGE	Working Group on Integrity and Ageing of Components and Structures (NEA)

Executive summary

Under the Nuclear Energy Agency's (NEA's) co-ordination, the concrete subgroup of the Working Group on Integrity and Ageing of Components and Structures (WGIAGE) of the Committee on the Safety of Nuclear Installations (CSNI) started an activity about concrete containment ageing effects. The activity consisted of a benchmark simulation and analysis of data provided by EDF (Électricité de France) and generated in the experimental facility VeRCoRs.

The VeRCoRs facility mock-up is a reactor containment building at 1/3 scale. The mock-up is instrumented so that its behaviour is monitored from the beginning of construction. More than 700 sensors and 2 km of optic fibre cables have been positioned in the concrete, on the rebars and on the prestressing tendons (grouted tendons). The experimental VeRCoRs campaign consists of daily measurement of all of the sensors and an air pressure test of the mock-up every year. Hundreds of samples of concrete have been prepared and tested to determine their material behaviours and parameters, including hydration, strengths, fracture energy and elastic properties, drying, shrinkage (autogenous and drying), creep (basic and drying), and permeability.

This report summarises the results provided by member organisations of the concrete subgroup of the WGIAGE to the benchmark exercise. The objective of the benchmark was to improve participants' capability to predict the ageing effects on concrete containment. The benchmark, which is described in this report, was an open benchmark done with the results of two identical pressurisation tests of the VeRCoRs mock-up.

In this 2018 benchmark, three main themes were studied:

- Theme 1: Creep modelling – micromechanics and/or multiphysics approaches. The prediction of creep effects is a major challenge with regard to the behaviour over time of concrete structures. The proposition was to analyse the phenomenon at several scales and in several environmental conditions.
- Theme 2: Mechanical behaviour of the containment during pressurisation tests. Predictions were made of the behaviour of the containment wall at different steps: just before the pressurisation test and during the pressurisation up to design pressure (5.2 bar abs.). The strains and stresses were expected in 40 points defined in the raft, the gusset, the cylindrical wall and the dome. Furthermore, the cracking state (inner face cracks, outer face cracks and through cracks) was evaluated.
- Theme 3: Air leakage. The VeRCoRs mock-up underwent five pressurisation tests between November 2015 and March 2018. The global air leakage was measured at the end of the 5.2 bar abs. plateau of each of these pressurisation tests. During the tests, the containment wall was sprayed in order to locate leakage faults and quantify the flow through these defects. Theme 3 of this benchmark consists of predicting air leakage during the pressurisation test, at the end of the 5.2 bar abs. plateau.

After the tests, the following experimental data and measurements were given to the participants to calibrate their models:

- strains before an air test, and during two other different tests;

- gusset cracking history;
- global and local leakage flows.

The results provided by the participants were compared to the detailed experimental results.

In all, over 30 through cracks were identified in the gusset. These cracks were, on average, spaced about 1.1 m apart. At the beginning of the test programme, a crack was identified as a through crack when it appeared in intrados and extrados of the gusset; however, recent local measurements (using optical fibres) show that there are also active cracks that do not fall into this category; active cracks are therefore more numerous than initially listed.

Eighteen participants from different countries and organisations submitted final results. They used a set of different models and tools (codes). Some of the participants provided results for all three themes, others focused on one or two themes, or even on a subset of a theme. The choice was mainly related to the different specialties of each of the participant teams.

For Theme 1, the results provided for creep modelling at concrete scale are numerous. It may be noted that although some results are good and close to the experiment, there are significant differences between the results provided even when the chosen model to represent creep is identical. Beyond the modelling choice, it is the use of the input data and sometimes the presentation of the results which are at the origin of such deviations.

There are also numerous results provided for Theme 2 of the modelling of the containment behaviour and the effects of ageing. Some teams obtained results very similar to the experimental measurements, showing a good understanding of the behaviour of the structure. Nevertheless, there are sometimes significant differences both between the participants and compared with the experimental measurements.

The gusset area, in particular, remains complex to model and its behaviour is poorly mastered, even though there is a clear improvement in dispersion of the results between the 2015 and the 2018 benchmarks per zone of the containment, especially in the gusset area.

Finally, in Theme 3, regarding the prediction of the leakage flow, even if it is a difficult exercise, some improvements have also been made. In 2015, the results showed a factor of 1 to 200 between the lowest and the highest flow. For this second benchmark, the factor has decreased to between 1 and 14. On average, the global leakage predicted values were 30 times higher than the experimental ones in 2015. In 2018, the average value underestimates the experimental value by 55%; one team is only 8% from the experimental value.

The subject of calculating leak through a concrete wall seems better approached by participants. Of course, knowledge from the previous behaviour of the mock-up regarding air leakage also helped to obtain better predictions.

One of the main lessons learnt related to nuclear safety is that determining the cracking state is a major element in forecasting leakage since leakage mainly occurs through cracks. It is therefore necessary to make additional efforts in modelling both crack apparition and airflow through cracks to better predict air leakage for industrial use.

The differences in benchmark results compared to the test results emphasised the need to improve the local measurement capacities of some key parameters, e.g. water content, permeability and cracking during future tests of the mock-up, in order to provide more precise input and comparison data to participants.

1. Introduction

1.1. Background

As part of the Nuclear Energy Agency's (NEA's) continuous efforts to support nuclear safety developments, the concrete subgroup of the Working Group on Integrity and Ageing of Components and Structures (WGIAGE) started an activity about concrete containment ageing effects. The activity consisted of a benchmark simulation and analysis of data provided by Électricité de France (EDF) and generated in the experimental facility VeRCoRs.

As part of EDF's work on safety and the life extensions of its nuclear power plants, an experimental mock-up of a reactor containment building at one-third scale was built at "EDF Lab Les Renardières" near Paris (France). The mock-up construction was completed at the end of 2015. It is finely instrumented so that its behaviour has been monitored since the beginning of construction. More than 700 sensors and 2 km of optic fibre cables have been positioned in the concrete, on the rebars and on the prestressing tendons (grouted tendons).

During construction, measurements were taken just after concreting at one-hour intervals. During the research programme, several measurements are collected on each sensor with a high frequency. Hundreds of samples of concrete have been prepared and tested to determine their material behaviour and parameters, including hydration, strength, fracture energy and elastic properties, drying, shrinkage (autogenous and drying), creep (basic and drying), and permeability.

These data are all stored in a dedicated database making it possible and easier to carry out analyses and comparisons with numerical results.

Figure 1. Picture of the VeRCoRs mock-up – External dome positioning, 11 December 2015

The main objectives of the project are to study:

- behaviour at early age;
- the evolution of the leak tightness under the effect of ageing (drying effects are about nine times faster on the mock-up because of scale effects);
- behaviour under severe accident conditions for which the thermo-mechanical loading is maintained for several days.

Figure 2. Picture of the completed VeRCoRs mock-up, 4 August 2016

The experimental campaign consists of daily measurement through all the sensors and an air pressure test of the mock-up every year. During this test, the containment is pressurised at 5.2 bar absolute (pressurisation at 200 mbar/h and plateaued at 5.2 bar abs. for 12 hours before deflation at 150 mbar/h), all sensors are interrogated each hour and the leakage is measured.

A first benchmark was carried out in 2015, dedicated to early age, mechanical and leak tightness behaviours.

In 2018, a second benchmark was launched. It was proposed to deal with the creep modelling at different scales and in various environmental conditions, and to predict the mechanical and leak tightness behaviour of the mock-up after several years of ageing. In particular, the impact of two successive identical loadings (pressurisation tests) on a concrete structure was studied.

One other benchmark is planned, in 2023, to predict behaviour under severe accident conditions.

1.2. Outline of the report

This report recalls what was expected of the participants and presents the results obtained during the second international benchmark for the three themes proposed. Two comparisons are made for each theme: 1) between the numerical results provided by the participants; and 2) between the numerical results and the experimental data where possible (strains, cracks, global air flow or local air flow). This report provides an overview of the results.

In conclusion, some lessons learnt on each subject are presented.

2. VeRCoRs facilities

2.1. The containment building

The VeRCoRs mock-up is presented in Figure 3, with designations of the specific areas.

Figure 3. Main parts of the mock-up and prestressing principle

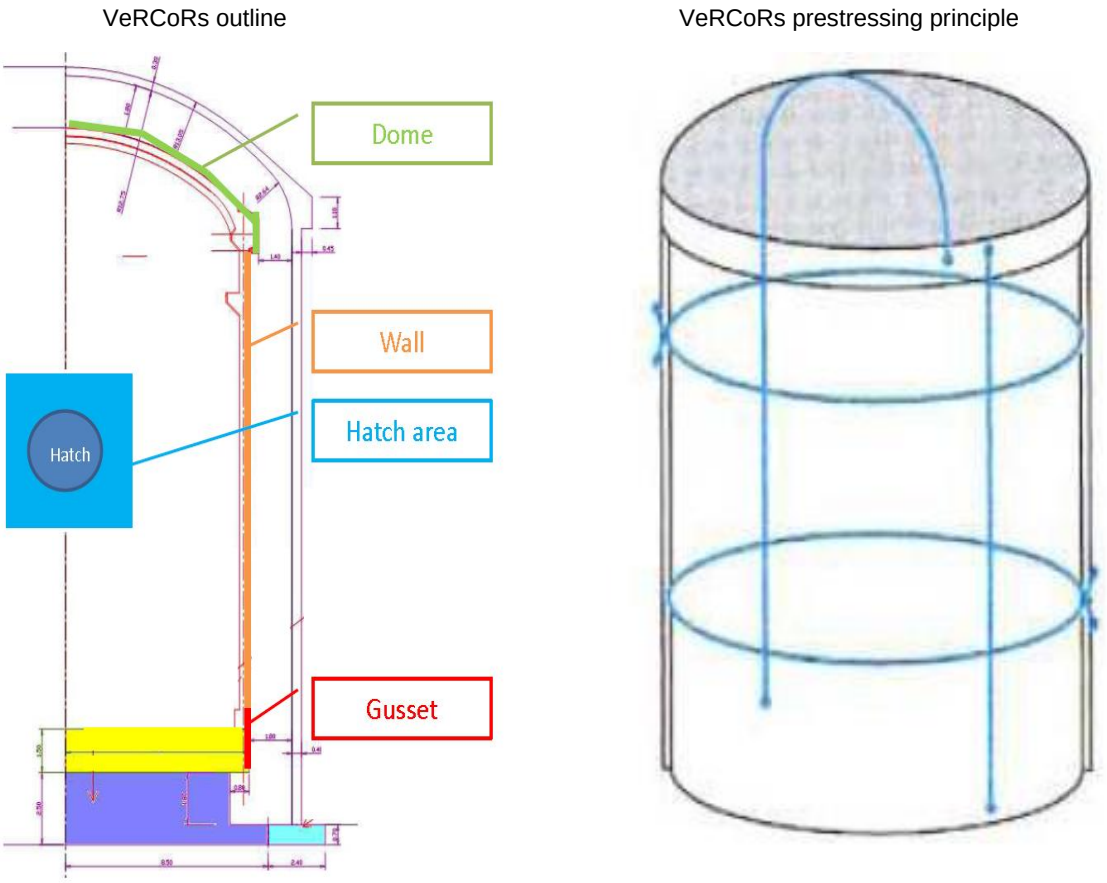

The mock-up consists of a one-third scale prestressed concrete containment model (internal wall), a secondary reinforced concrete wall (external wall) and a flat reinforced concrete base slab anchored in a very thick concrete block foundation.

The external wall's function is to provide thermal and humidity protection, and to recreate an annular space for leakage rate measurements.

The base slab is 2.0 m thick and does not include any prestressing gallery, access for vertical tendons jacking being obtained by the expedient of an overhang of the base slab from the supporting concrete block foundation.

In addition, in order to enable visual inspections and monitoring, a metallic structure supporting various annular floors was erected inside the containment, and another one is anchored in the external wall (Figure 4). Only two structurally significant penetrations have

been modelled through the inner containment wall: 1) the equipment access hatch (and associated wall thickening [Φ2.710 m]) and 2) a personal airlock (Φ1.210 m) at the base have been scaled. Other minor penetrations are not reproduced in the model, but two small ones (Φ500 mm and Φ360 mm) are added to plug necessary pressurisation pipes. The two vertical prestressing buttresses of the inner containment are also scaled.

Figure 4. General view of the VeRCoRs mock-up

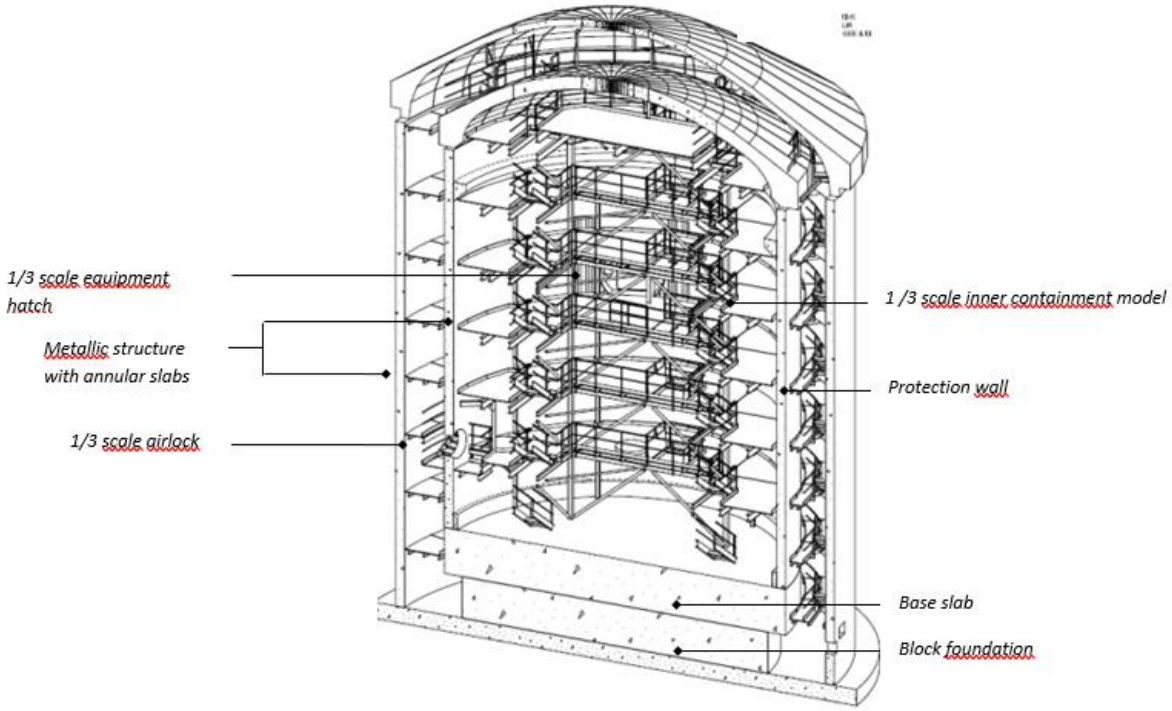

The main dimensions of the inner containment structure are given in Table 1.

Table 1. Geometric characteristics of the inner containment model

	1/3 scale model	Full scale
Height from gusset to the top	20.79 m	62.38 m
Internal radius of cylinder	7.30 m	21.90 m
Thickness of cylinder	0.40 m	1.20 m
Internal radius of the dome (tore)	2.67 m	8.00 m
Internal radius of the dome (centre)	10.67 m	32.00 m
Thickness of the dome	0.30 m	0.90 m
Free volume inside containment	3 160 m^3	85 350 m^3

Materials were selected to be as similar as possible to the ones used in the construction of full-scale containments, including in terms of mechanical and thermal behaviour. Concrete class is 34/37 megapascals (MPa). Nevertheless, the concrete mix microstructure cannot be perfectly scaled due to aggregates size. The prestressing and reinforcement designs are detailed below.

2.1.1. Prestressing design

The prestressing tendons layout is scaled exactly, including any deviations around penetrations: tendons spacing is divided by three, and the ducts diameter is scaled as much as reasonably possible for the contractor (Φ50 mm). Four types of tendons are used (see Figure 3):

- horizontal tendons (spacing 133 mm in typical area);
- vertical tendons (spacing 290 mm in typical area);
- gamma tendons (spacing 205 mm in the dome);
- dome tendons (spacing 205 mm in the dome).

Every tendon has been cement grouted as in full-scale structures, except for instrumented ones (four vertical and two horizontal) in order to follow the prestressing delayed losses or to simulate tendon breaks.

The prestressing tendons are composed of class 1 860 MPa strands T15 (nominal cross section S = 139 mm²). Each tendon has been tensioned at 1 488 MPa at active extremities before anchorage slip, as in full-scale structures.

The number of strands composing each tendon is governed by the following design principle: the initial compressive state of concrete shall be equal to the one in the full-scale containment walls, when the tensioning phase is just over. Consequently, at one-third scale, the tendons section is divided by 9, so that each tendon is made with 4 T15 strands, instead of the 37 T15 in the full-scale structures.

2.1.2. Reinforcement design

Steel class 500 MPa was used for the reinforcement of concrete in the mock-up containment walls. The design principles for the reinforcement are: rebars spacing and diameters are scaled to keep the same ratios ρ (%) as in full-size structures. In typical areas of the cylinder, reinforcement principles are alternatively HB 6/8 @6.7 cm in horizontal direction at both the inner and outer face, and HB 8/10 @0.75 cm in vertical direction. In the dome, reinforcement principles are also alternatively HB 8/10 @9.8 cm at both faces. Stirrups are made with HB 5.

The length of the rebars and the number of overlapping zones are not scaled for practical reasons. Concerning concrete cover, exact scaling is not possible due to the aggregates size.

2.2. **Monitoring**

The monitoring system is composed of:

- a meteorological station;
- for ambient air measurement: 10 thermometers, 10 relative humidity sensors, an atmospheric pressure gauge, and a flow metre;

- 12 pendulums (4 plumb lines each with 3 tables aiming at different heights on 4 vertical lines);
- 4 vertical Invar wires;
- 336 embedded strain metres GEO INSTRUMENTATION – Type SG1 (for each couple of embedded strain metres, the distance between the wall and the sensors is 7.6 cm for the external wall and 7.3 cm for the internal wall);
- 211 thermometers PT100;
- 2 km of optic fibre;
- 31 TDR (time domain reflectometry) sensors;
- 30 "pulse" sensors (permeability measure);
- 6 dynamometers for instrumented tendons;
- 160 strain gauges on rebars.

The positions of the main sensors concerned by the benchmark are given in Figures 5, 6, 7 and 8.

Figure 5. Position of the strain gauges and thermometers in the base slab and the gusset

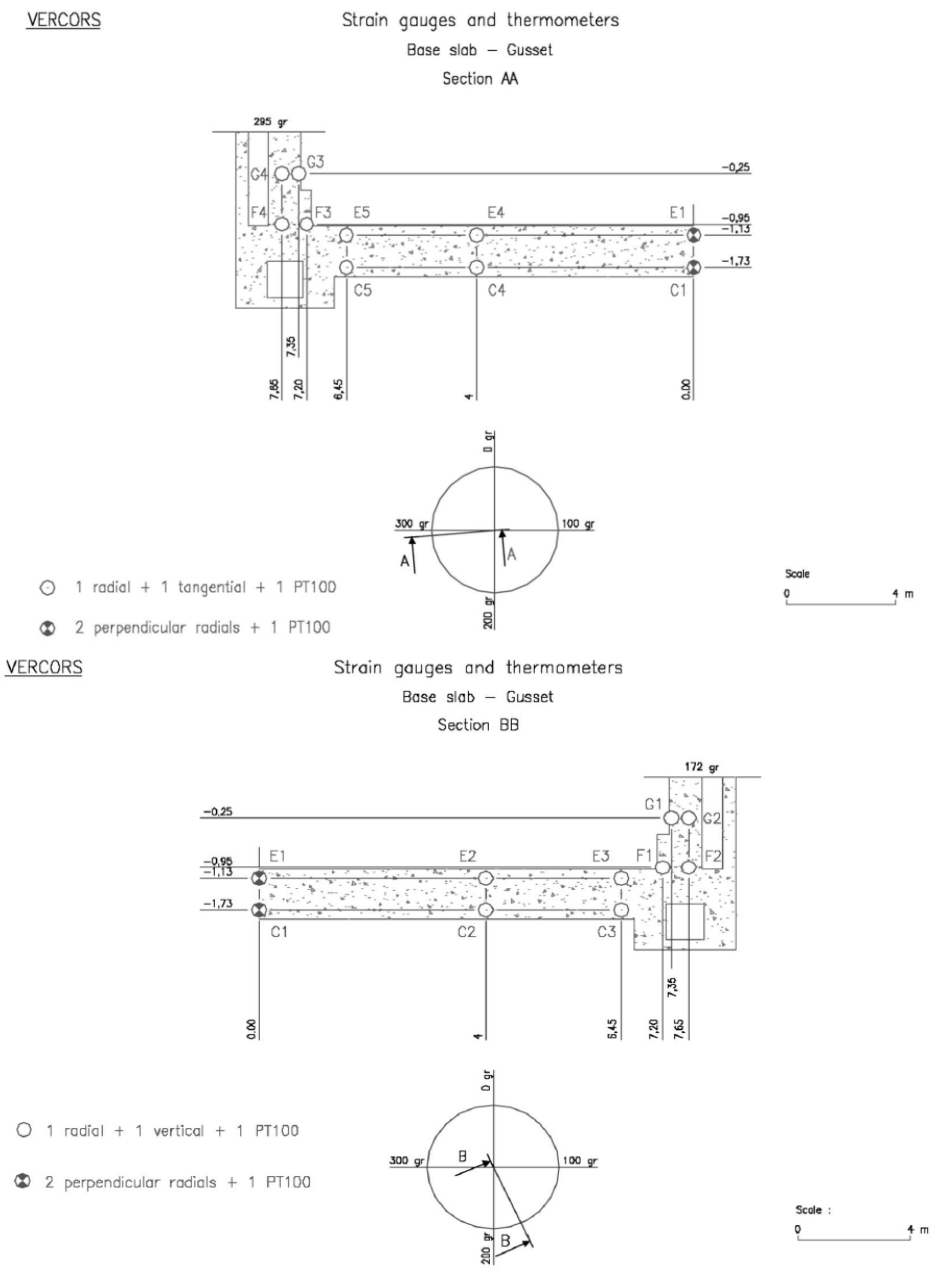

Figure 6. Position of the strain gauges and thermometers in the cylindrical part and the dome: Elevation view

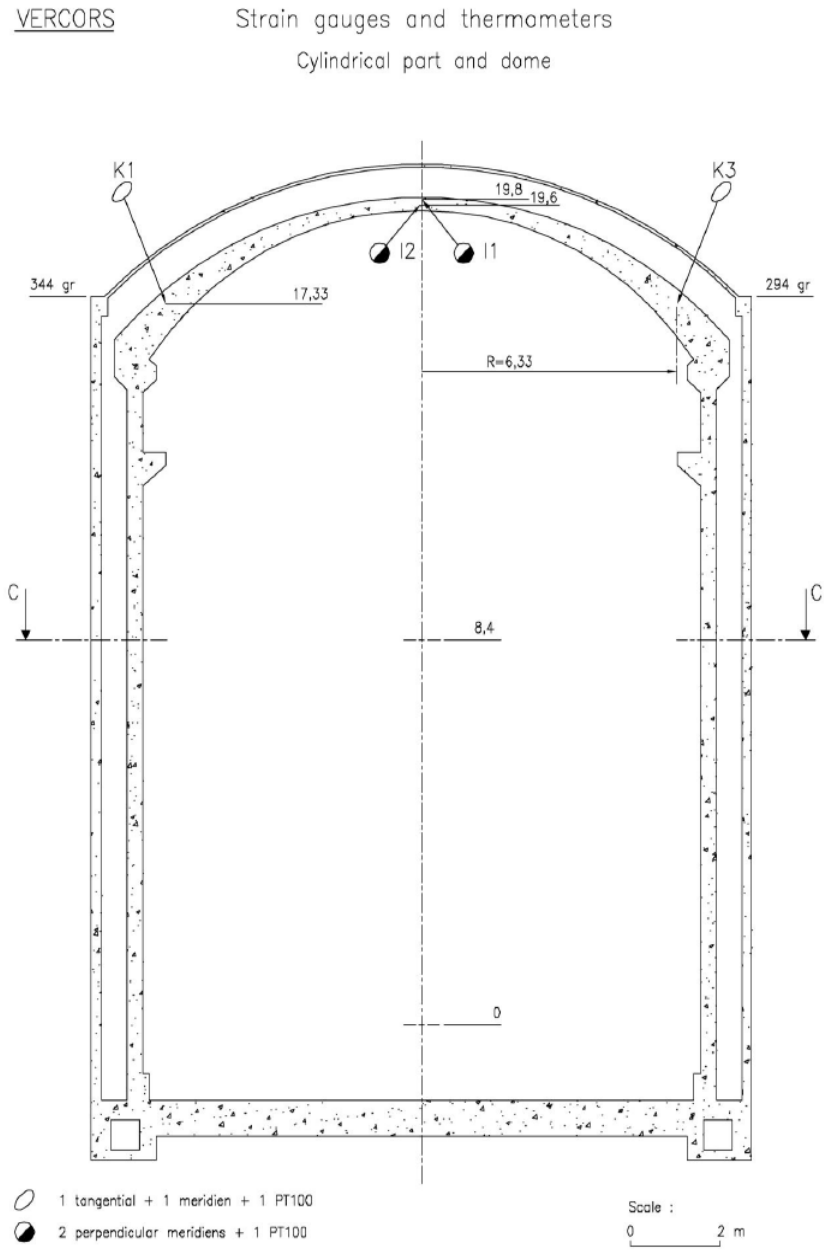

The shape of the base slab is given as an indication. There is no gallery in the base slab of the mock-up.

Figure 7. Position of the strain gauges and thermometers in the cylindrical part: Section view

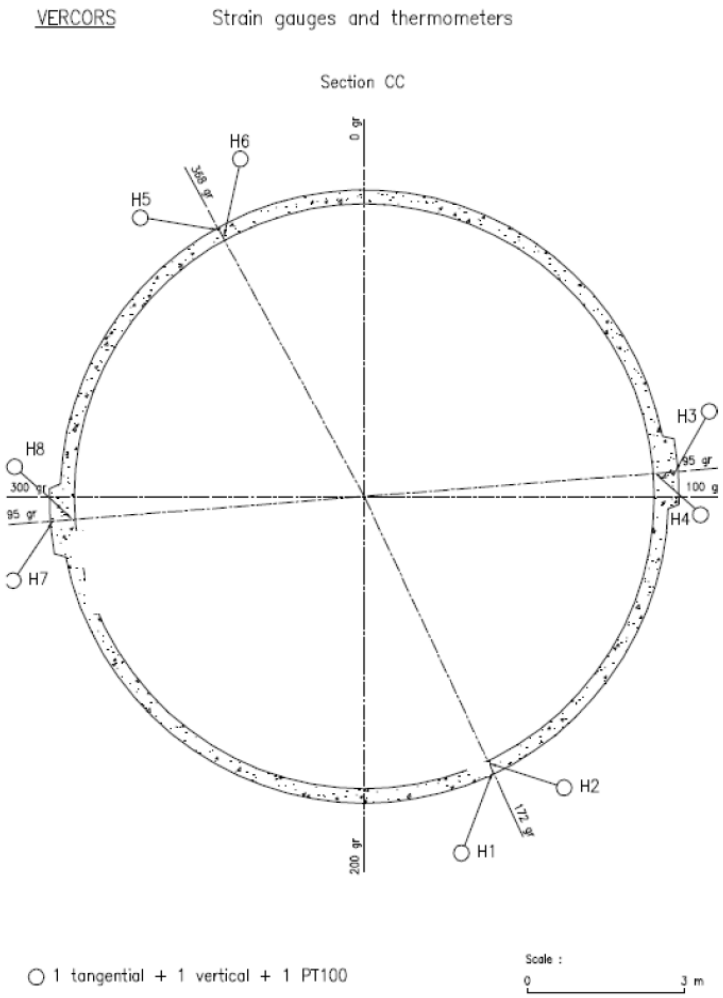

Figure 8. Position of the pendulums and Invar wires

Types	Lines (grades)	Measures's level
Invar wire	95	14,53
Pendulums		14,53
		8,67
		4
Invar wire	170	14,53
Pendulums		14,53
		8,67
		4
Invar wire	295	14,53
Pendulums		14,53
		8,67
		4
Invar wire	370	14,53
Pendulums		14,53
		8,67
		4

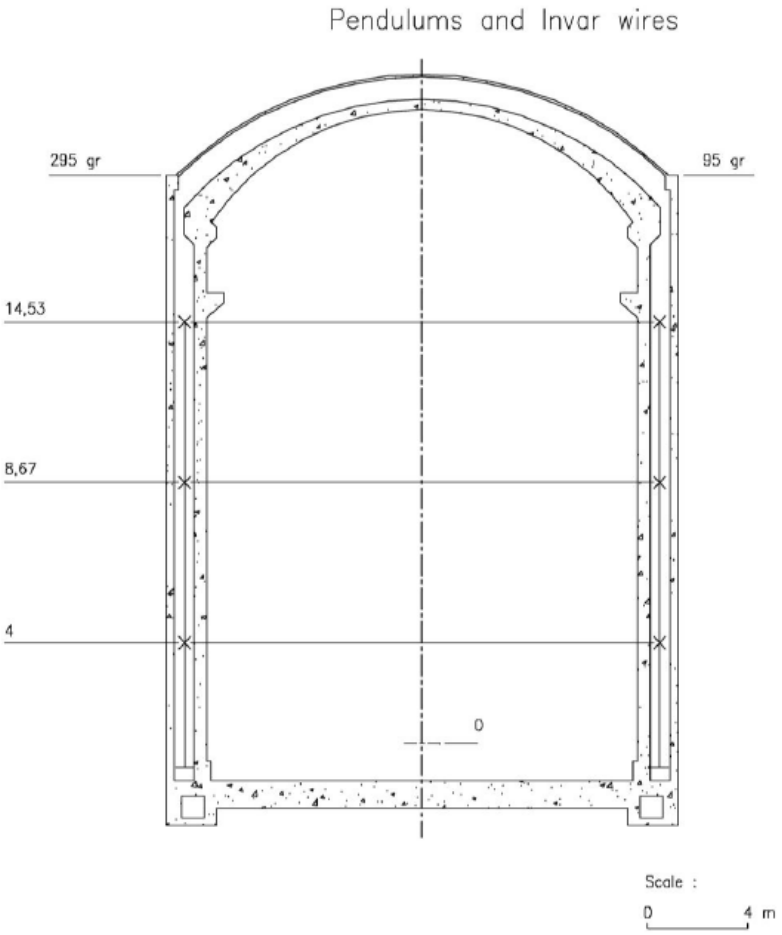

2.3. Strain measures

The experimental results of the strain measures obtained are related to the conditions, involving thermal ones, in which the raw measurements were achieved. The concrete strain gauges give a measure ($\varepsilon_{t,raw}$) that includes the concrete thermal dilatation and the sensor wire dilatation.

The real concrete total strain including thermal effects is given by the following formula:

$$\varepsilon_{t,concrete} = \varepsilon_{t,raw} - \varepsilon_{t0,raw} + \alpha_s (T_t - T_{t0}) \quad (1)$$

where

$\varepsilon_{t,raw}$ is the raw measure at the time t,

$\varepsilon_{t0,raw}$ is the raw measure at the time t0,

α_s is the thermal expansion factor of the sensors ($°C^{-1}$). Typically, α_s ranges between 10 and $12.E^{-6}$ $°C^{-1}$,

T_t is the temperature recorded with the associated thermocouple at the time t (°C),

T_{t0} is the initial temperature recorded with the associated thermocouple (°C).

To obtain the mechanical strains of the concrete (ε_{corr}), a thermal correction must be applied. Various procedures can be proposed for this, depending on the mechanical behaviour of the structure. For example, a determinist approach is the thermo-differential correction method, which can be used in the cylinder part of the containment. The corrected values of strain ε_{corr} are derived from the raw strain ε_{raw} by using the following formula:

$$\varepsilon_{corr} = \varepsilon_{raw} + \alpha_s.(T-T_0) - \alpha_c.(T_m - T_{m0}) \quad (2)$$

where

T is the temperature recorded with the associated thermocouple at the time t (°C),

T_m is the mean temperature of the wall (°C),

T_0 is the initial temperature recorded with the associated thermocouple (°C),

T_{m0} is the mean temperature of the wall at the initial time (°C),

α_s is the thermal expansion factor of the sensors ($°C^{-1}$). Typically, α_s ranges between 10 and $12.E^{-6}$ $°C^{-1}$,

α_c is the concrete thermal expansion factor ($°C^{-1}$). Typically, α_c ranges between 7 and $13.E^{-6}$ $°C^{-1}$.

In this report, the experimental strains represented for Theme 2 are the total strains given by formula (1). For some specific cases, the mechanical strains are given using formula (2) (assuming $\alpha_c = 10.5.10^{-6}$ /°C) or another thermal correction.

3. 2018 VeRCoRs benchmark

3.1. Themes and key dates

Three main themes were proposed for the second benchmark.

3.1.1. Theme 1: Creep modelling – micromechanics and/or multiphysics approaches

The prediction of creep effects is a major challenge with regard to the behaviour over time of concrete structures. The proposition was to analyse the phenomenon at several scales and in several environmental conditions. Two sub-themes were proposed.

1.1. Micromechanics of cementitious materials

Prediction of basic creep taking into account the mix design. The results should present the basic creep at multiple scales and be compared to experimental data:

Cement paste: ageing basic creep, characteristics at early age as measured from the technique described in "Elastic and creep properties of young cement paste, as determined from hourly repeated minute-long quasi-static tests" (Irfan-ul-Hassan et al., 2016).

- Concrete: basic creep at 90 days.

More predictions could be proposed, at cement paste, mortar or concrete scales, for other loading times.

1.2. Multiphysics approach for total creep

Predictions of the creep behaviour of VeRCoRs concrete to show the ability of models to describe creep situations under varying environmental conditions. In particular, the request concerned the prediction of the influence of drying-imbibition cycles on the creep of a specific concrete sample. The prediction had to cover:

- basic creep at 20°C;
- drying creep at 20°C and various relative humidity (RH 50%, RH 30% and RH 70%);
- drying creep with drying-imbibition cycles at 20°C.

3.1.2. Theme 2: Mechanical behaviour of the containment during pressurisation tests

Participants were asked to make predictions of:

- strains, stresses and cracking history of the whole containment wall during "VD1 bis" pressurisation tests;
- the delayed strains between "VD1 bis" and "VD2" pressure tests;
- strains, stresses and cracking history of the whole containment wall during "VD2" pressurisation tests.

3.1.3. Theme 3: Air leakage

This theme consisted of making predictions of air leakage during the pressurisation tests ("VD1", "VD1 bis" and "VD2"), at the end of the 5.2 bars abs. plateau (global, dome area, equipment hatch area, gusset area, cylindrical part).

Teams could choose to contribute to one, two or all three of the themes.

Key dates

The benchmark started 6 February 2017.

Participants' results were expected for 30 March 2018. This deadline was postponed to 30 April 2018.

Additional experimental results were given (to each team that provided results in due time) in June to allow participants to improve, if so desired, the results before the workshop session.

The workshop, which was dedicated to the presentation of the experiments and team results and to discussions in plenary session, was held in Paris Saclay 27-29 August 2018.

3.2. Data

Table 2 presents the data provided to participants for the second benchmark.

Table 2. Data provided for the second benchmark

Concrete

	Unit	From lab composition	From VeRCoRs sample	Comment
Concrete composition	–	–	–	EDF specification
Mortar composition	–	–	–	EDF specification
Cement paste composition	–	–	–	EDF specification
Density	ρb (kg/m^3)	Yes	Each placement	Cylinder 11x22
Air content	%	Yes	Each placement	Specific test
Consistence	mm	Yes	Each placement	SLUMP test
Young modulus	E_b (GPa)	Yes	Several lifts	Cylinder 11x22
Poisson ratio	ν_b (-)	No	No	
Compressive strength (28 days)	f_{c28} (MPa)	Yes	Each placement	Cylinder 11x22
Tensile strength (28 days)	f_{t28} (MPa)	Yes	Each placement	Split test (cylinder 11x22)
Compressive strength (7 days)	f_{cj} (MPa)	Yes	Each placement	
Fracture energy	G_f (J.m^{-2})	Yes	No	
Specific heat	C_v (J.m^{-3}.K^{-1})	Yes	No	

Table 2. Data provided for the second benchmark (Continued)

	Unit	From lab composition	From VeRCoRs sample	Comment
Thermal expansion coefficient	α (m/K)	No	No	
Thermal conductivity	λ ($W.m^{-1}°C^{-1}$)	Yes	No	
Convective exchange coefficient	($W.m^{-2}.°C^{-1}$)	No	No	During erection
Convective exchange coefficient (inner face)	($W.m^{-2}.°C^{-1}$)	No	No	For the closed containment
Convective exchange coefficient (outer face)	($W.m^{-2}.°C^{-1}$)	No	No	For the closed containment
Hydration heat release		Yes	1 sample	Semi-adiabatic test (QAB)
Autogenous shrinkage evolution	ε_{au} (μm/m)	Yes	1 sample	Cylinder 16x100
Drying shrinkage evolution	ε_{ds} (μm/m)	Yes	1 sample	Cylinder 16x100
Basic creep evolution	ε_{bc} (μm/m)	Yes	No	Cylinder 16x100, force applied at 90 days
Drying creep evolution	ε_{dc} (μm/m)	Yes	No	Cylinder 16x100, force applied at 90 days
Porosity	P (%)	Yes	Each placement	
Air permeability	K_g (m^2)	Yes	No	
Water permeability	K_l (m^2)	Yes	No	
Desorption isotherm	$Hr=f(S_w)$	Yes	No	
Loss of mass/hygrometry curve	w=f(Hr)	Yes	No	

Rebars

	Unit	From lab composition	From VeRCoRs sample	Comment
Young modulus	E_a (Gpa)	Yes	No	
Stress/strain relation curve	ε=f(σ)	Yes	No	

Table 2. Data provided for the second benchmark (Continued)

Tendons

	Unit	From lab composition	From VeRCoRs sample	Comment
Relaxation		Yes	No	
Stress/strain relation curve		Yes	No	
Ultimate yield strength warranty	σ_{RG} (MPa)	Yes	No	
Elastic yield strength warranty	σ_{TG} (MPa)	Yes	No	
Relaxation at 1 000 h at 20°C	ρ_{1000} [%]	Yes	No	
Friction coefficient for vertical tendon	f [-] (in curve) φ [-] (in right section)	Yes	No	
Friction coefficient for horizontal tendon	f [-] (in curve) φ [-] (in right section)	Yes	No	

Calculation

VeRCoRs mesh	A mesh was provided but not imposed.

Ambient air conditions

	Unit	Period	Comment
Temperature	°C	From the inner containment closure	Temperature in the inner containment and the annular space
Hygrometry	%	From the inner containment closure	Hygrometry in the inner containment and the annular space

Experimental results

	Unit	Period	Comment
Measured strains	µm/m	From the start of prestressing to the "VD1" test	In some points: raft, gusset, mid-height, dome. Strains are not corrected from thermal effects. Associated temperatures measured are given.
		During pressurisation tests: "Pre-Op" "VC1" "VD1"	In some points: raft, gusset, mid-height, dome. Strains are not corrected from thermal effects. Associated temperatures measured are given.
Global air leakage flow	Nm^3/h	"Pre-Op" "VC1"	
Air leakage repartition		"Pre-Op" " VC1"	Zones: gusset, cylinder, hatch area, dome
Leakage faults location		"Pre-Op" "VC1"	Tables given location, type of the faults, geometric characteristics
Leakage faults measured flows	Nm^3/h	"'Pre-Op" "VC1"	Tables given measured flow for each leakage fault

After the benchmark phase, some experimental data and measurements were given to participants:

- strains before the "VD2" air test and during the "VD14 bis" and "VD2" tests;
- gusset cracking history;
- global and local leakage flows.

3.3. Expected results

3.3.1. Theme 1: Creep modelling – micromechanics and/or multiphysics approaches

Were expected.

1.1 Micromechanics of cementitious materials

- Cement paste: ageing basic creep characteristics at early age:
  - Code used and methodology.
  - List of hypotheses.
  - Results: tables of uniaxial creep functions at repeated loading times according to Irfan-ul-Hassan et al. (2016). Elastic and creep properties of young cement paste, as determined from hourly repeated minute-long quasi-static tests, CCR 82, 36-49.
  - Free comments.
- Concrete: basic creep at 90 days:
  - code used and methodology;
  - list of hypotheses;
  - results: table of uniaxial creep function versus time;
  - free comments.

1.2 Multiphysics approach for total creep

- Concrete: basic creep at 90 days (20°C), drying creep (20°C and various RH), drying creep with drying-imbibition cycles (20°C):
  - code used and methodology;
  - list of hypotheses;
  - results: table of uniaxial creep function versus time;
  - free comments.

3.3.2. Theme 2: Prediction of the strains, stresses and cracking of the whole containment wall

The results were expected at 5.2 bar abs. for the "VD1 bis" and "VD2" air tests.

The following were expected:

- code used (explicit or implicit) or methodology (if not Finite-Element Method [FEM]);
- list of hypotheses:
  - starting point of the calculation;
  - rebar taken into account (yes or no);
  - tendons taken into account (yes or no);
  - type of bonding at the concrete/rebar interface;
  - type of bonding at the concrete/tendon interface.
- boundary conditions:
  - temperatures;
  - displacements and rotations;
  - drying.
- list of data taken into account (for example: modulus, ambient air data, etc.);
- modelling (behaviour law, linear or non-linear):
  - concrete;
  - rebars;
  - tendons.
- mesh
  - type and number of elements for concrete;
  - type and number of elements for rebars;
  - type and number of elements for tendons.
- calculation
  - discretisation in time;
  - time of calculation (CPU) and kind (number) of processor.
- results
  - Table of strains and stresses in ten points defined in the gusset, the containment wall and the dome.
  - Table of cracking state by area (gusset, hatch area, wall and dome), at the inner and outer surface: total length of cracks, maximum opening, spacing between cracks. The through cracks shall be identified.
  - Views of deformations and stresses: complete view centred on the hatch (outer face), for the three pressurisation tests. The scale shall be calibrated from 1 MPa to -10 MPa (compressive stress).
  - Free comments.

3.3.3. Theme 3: Prediction of air leakage during the pressurisation test (global, dome area, equipment hatch area, gusset area, cylindrical part)

The air test consists of inflating the containment with dry air. The inflation speed is 200 mbar/h. At 5.2 bars abs, the inflation is stopped and a pressure plateau starts and lasts over 12 hours. The measurement of the air mass leakage is carried out at the end of this stage. The hypothesis is that inner air and outer air is at 20°C and 60% RH for the calculation.

The results expected concerned the last three pressure tests carried out on the mock-up: VD1, VD1 bis and VD2.

The results expected were:

- code used (explicit or implicit) or methodology (if not FEM);
- global air leakage prediction at the 5.2 bar (absolute pressure) stage;
- air leakage prediction at the 5.2 bar (absolute pressure) stage for the three pressurisation tests:
  - in the gusset area;
  - in the dome area;
  - in the equipment hatch area;
  - of the cylindrical part.

The calculation had to be described and explained:

- Is flow through cracks and through concrete separated?
- Are other results used to calibrate the flow? If yes, which calibration is used? About stress, damage indicator, others?
- How is the leakage through cracks calculated? (analytic formula, model?)
- How is the leakage through concrete calculated?

3.4. **Participants**

In early 2017, those who were interested in participating in the benchmark had to register. Figure 9 shows the origin of the registered participants.

Figure 9. Origin of the registered participants

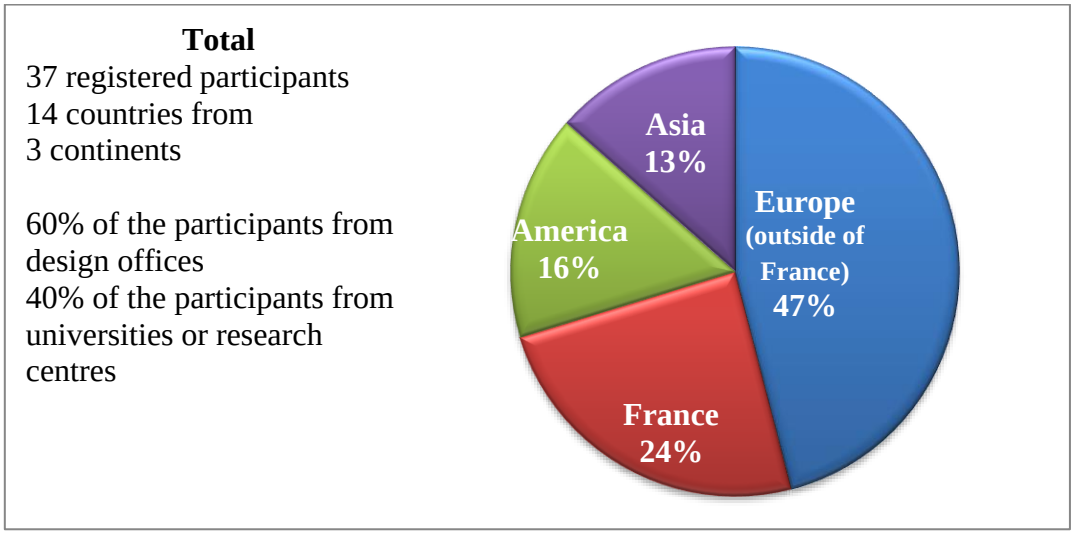

Figure 10 shows the distribution of the effective participants.

Figure 10. Distribution of the effective participants

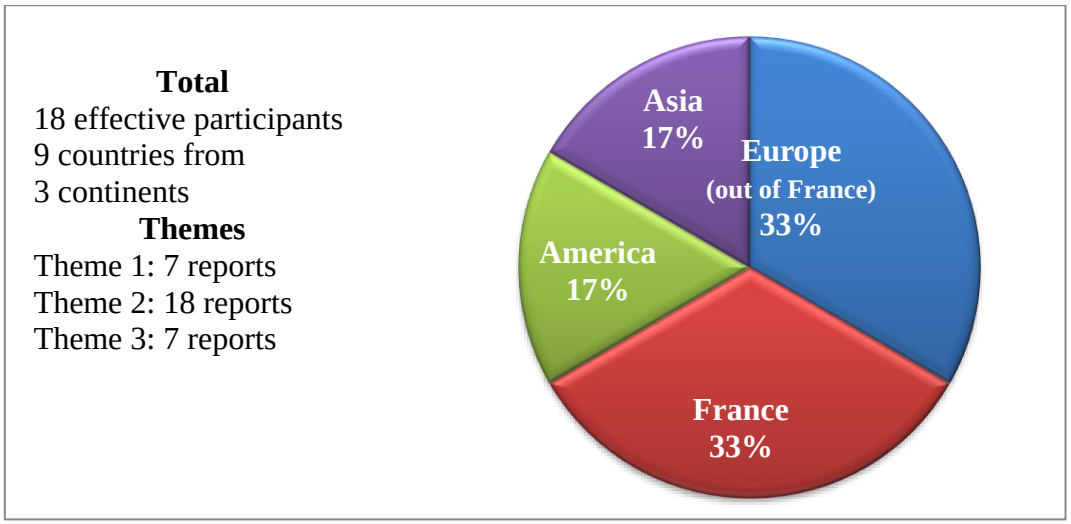

Details on the effective participants by theme are given in Tables 3, 4 and 5.

Table 3. Participants in Theme 1

First name	Last name	Entreprise	Country
Kim	Calonius	VTT Technical Research Centre of Finland Ltd	Finland
Jean-Michel	Torrenti	IFSTTAR/University Paris-Est	France
Mehdi	Asali	OXAND France	France
Bruno	Capra	OXAND France	France
Thibault	Thénint	SIXENCE Necs	France
Keun Kyeong	Kim	Korea Nuclear & Hydro Power Central Research Institute	Korea
Magnus	Ahs	Lund University/KTH Royal Institute of Technology/Vattenfall	Sweden
Joshua	Hogancamp	Sandia National Laboratories/US Nuclear Regulatory Commission (US NRC)	United States

Table 4. Participants in Theme 2

First name	Last name	Entreprise	Country
Homayoun	Abrishami	Candu Energy Inc.	Canada
Xu	Huang	University of Toronto	Canada
Rong	Pan	Nuclear and Radiation Safety Center, Ministry of Environmental Protection	China (People's Republic of)
Jiang-Ying	Wu	South China University of Technology, Guangzhou	China (People's Republic of)
Jan	Stepan	UVJ Rez, a.s. div. Energoprojekt Praha	Czech Republic
Kim	Calonius	VTT Technical Research Centre of Finland Ltd	Finland
Penti	Varpasuo	Fortum Power and Heat Ltd/PVA Engineering Services	Finland
Mehdi	Asali	OXAND France	France
David	Bouhjiti	Chair Pereniti 3SR Grenoble/EDF	France
Sandrine	Kervorkian	Institute for Radiological Protection and Nuclear Safety	France
Georges	Nahas	Institute for Radiological Protection and Nuclear Safety	France
Mahsa	Mozayan	INGEROP/Mines Paris-Tech	France
Jean-Michel	Torrenti	IFSTTAR/University Paris-Est	France
Thibault	Thénint	SIXENCE Necs	France
Keun Kyeong	Kim	Korea Nuclear & Hydro Power Central Research Institute	Korea
Sofia	Aparisio	ITEFI (CSIC) Madrid	Spain
Alex	Barbat	CIMNE/Technical University of Catalonia, Barcelona	Spain
Sergio	Jiménez	CIMNE/Technical University of Catalonia, Barcelona	Spain
Magnus	Ahs	Lund University/KTH Royal Institute of Technology/Vattenfall	Sweden
Joshua	Hogancamp	Sandia National Laboratories/US Nuclear Regulatory Commission (US NRC)	United States

Table 5. Participants in Theme 3

First name	Last name	Entreprise	Country
Xu	Huang	University of Toronto	Canada
Kim	Calonius	VTT Technical Research Centre of Finland Ltd	Finland
Mehdi	Asali	OXAND France	France
David	Bouhjiti	Chair Pereniti 3SR Grenoble/EDF	France
Mahsa	Mozayan	INGEROP/Mines Paris-Tech	France
Thibault	Thénint	SIXENCE Necs	France
Keun Kyeong	Kim	Korea Nuclear & Hydro Power Central Research Institute	Korea

3.5. Models and tools

Eighteen participants submitted final results. Tables 6 and 7 give an overview of the tools (code), mesh and models used.

Table 6. Models used by the participants for creep modelling

Team	Models	Remark
14	Basic creep: Burger model (Code_Aster) modified by Hilaire.	Tension-compression dissymmetry, biaxial effects not identifiable with EDF data sets given.
23	Creep is modelled as a contribution to the strain by using the Eurocode CEN-EN 1992-1-1.	Drying creep calculated as a difference of creep and drying shrinkage.
47	Four strain components (autogenous shrinkage, drying shrinkage, basic creep, drying creep). Modelling based on Eurocode 2 relations.	
76	Viscoelastic Prony series model (Abaqus) fitted to the average of the experimental data sets.	
82	Creep is modelled as a contribution to the strain by using the Eurocode SS-EN 1992-1-1:2005.	
88	Basic creep : Burger model (Code_Aster) – DryiTng : based on Granger model.	No dependence of material parameters with hydration degree.
90	Viscoelastic Prony series model (Abaqus) fitted to the average of the experimental data sets.	Poisson's ratio is assumed constant.

Table 7. Overview of the tools (code) mesh and models used by the participants for structural calculations

Team	Code	Mesh				Rebars and tendons		Models			Remarks
		3D	Shell	Other	Total	Rebar	Tendon	TH model	M model	Crack estimation	
14	Code_Aster 12.3 + MFront	30 384		116 877 Linear Elem	147 261	No	1D Elem	Classical thermics and hydrics computations	Tendons prestressing losses + creep + Mazars damage model	Cracks are obtained by post-treating the mechanical state	Air leakage flow computed with extra cracks from visual inspection
15	ABAQUS 6.13	199 810	61 591	36 530 Linear Elem + 16 MASS	298 834	3D Elem	3D Elem	No thermic calculation performed	The whole model is divided into ten layers with different material behaviour	Cracking pattern not predicted	
23	ABAQUS 6.14-1		189 092	271 758 Linear Elem + 217 758 Connector Elem	624 903	Grid Elem	1D Elem	No thermic calculation performed	Explicit dynamic analysis	Only the results during the overpressure are considered/only through-wall cracks are considered	
24	ABAQUS R2017x	51 460		15 791 Linear Elem	67 251	No	FE mesh provided by EDF		Viscoelastic law used for concrete and tendons	Cracking pattern not predicted	
47	Analytical model						Prestress applied in one day	Evolution of delayed strains performed with next European code (EC2)			
49	Code_Aster 10.6 + extra numerical development	171 071	38 388	43 855 Linear Elem	253 314	Considered using EC2 formulations	Linear elastic model	Multi-physic resolution algorithm		Macro-cracks spacing and the number of the macro-cracks was determined by the formulation suggested by Eurocode 2	Gas leakage classified into different part

Table 7. Overview of the tools (code) mesh and models used by the participants for structural calculations (continued)

50	Code_Aster V14 + MFront	8 736	27 652	29 165 Linear Elem	65 553	Linear Elem	Linear Elem	Strain-based damage model (mu–mazars damage model criterion + Fichant softening law + local damage formulation) – Hillerborg energy-based regularisation for mesh-independency – strain-based crack opening post-processing		The cracking patterns identification is based on a stochastic approach	Modelling of the gusset behaviour at early age/ calculated on a slice of the gusset
56	ANSYS 17	196 512		21 928 LINK Elem	218 440	Grid Elem	1D Elem	No thermic calculation performed		Cracking pattern not predicted	
66	Cast3M 2015	158 238	2 444	572 151 Linear Elem	732 833	1D Elem	1D Elem	No thermic calculation performed	Not detailed	Calculation of the depth of the cracks	
74	VecTor4 v4.10		256	17 Linear Elem	273	Smeared reinforced layers within shell element	Smeared reinforced layers within shell element	No thermic calculation performed		Predicted only near element boundaries	Calculated on a 2D model
76	ABAQUS Smulia 6.14	40 656		5 239 Linear Elem	45 895	Increasing the concrete strength by calculating the rebar ratio in each main concrete section	Truss Elem	Humidity + temperature + tensioning sequence simplified		Damage Plasticity Model + experiment equation to determine the cracking pattern	Reduced integration technique selected
80			59 015	123 134 Linear Elem + 143 Spring	182 292	No	1D Elem	No thermic calculation performed		Cracking pattern not predicted	

Table 7. Overview of the tools (code) mesh and models used by the participants for structural calculations (continued)

82	COMSOL Multiphysics 5.3a	4 664		6 288 Linear Elem	10 592	No	Truss Elem	Not detailed		Cracking pattern not predicted	Calculated 1/8 portion of the structure
84	Plastic Crack Dynamics v16	199 600			199 600	Modification of Young Modulus	Serial-parallel rule of mixtures	No thermic calculation performed	Scalar damage model/post-tensioned concrete is modelled as a composite material/stress relaxation is simulated with a viscoelastic model called Generalized Maxwell	Computation of a damage variable that quantifies the damaged volumetric percentage/crack displacement is computed inside the FE code at each integration point	
86	COMSOL 5.3a	20 334	8 250	1 371 Linear Elem + 60 Vertices Elem + 4 584 mesh verticies	29 955	No	No	Multiphysics model		Cracking pattern not predicted	Calculated on the gusset
88	Code_Aster 12.4 + dev interne	40 656		27 428 Linear Elem + 7 300 Grid	81 126	GRILLE_MEMBRANE Elem	1D BARRE Elem	Using coarse mesh	Damage concrete + cracks prediction	Opening cracks	
90	ABAQUS 6.14	292 866	35 172	44 466 Linear Elem	372 504	Surface Elem	Two-noded bar elements	No thermic calculation performed		Cracking pattern not predicted	
92	ABAQUS 6.14	120 463		54 463 Linear Elem + 154 316 Membrane Elem	329 142	The rebar layer with the element type M3D3/4 is used for the rebars	The element type T3D2 is used for the tendons	No thermic calculation performed	CDP model	Damage factor of the CDP in ABAQUS is used to track the crack	

Note: The information in this table was provided by benchmark participants. Gaps or errors may result from a misinterpretation of this information.

4. Results on Theme 1: Creep modelling – micromechanics and/or multiphysics approaches

The prediction of creep effects is a major challenge with regard to the behaviour of concrete structures. The proposition was to analyse the phenomenon at several scales and in several environmental conditions.

4.1. Theme 1.1 - Micromechanics of cementitious materials

Two different scales were considered: cement paste and concrete. Concerning the cement paste study, early age creep behaviour was considered. For the concrete scale, participants were asked to predict the creep behaviour of 90-day aged concrete.

Participants were free to propose some results at other material scales.

4.1.1. Creep of cement paste at early age

4.1.1.1 Problem to solve

The composition of the VeRCoRs cement paste was given as shown in Table 8.

Table 8. VeRCoRs cement paste composition

Component	Masses for 1 m^3 (kg/m^3)
Cement CEMI 52,5 N CE CP2 NF Gaurain	1 087.6
Sand 0/4 rec GSM LGP1	197.5 (sieving at 0.125 mm)
Admixture: Sikaplast Techno 80	8.84
Added water	564.9

Participants were asked to give the creep properties for different hydration degrees and to give results following the restitution formalism given in Table 9.

Table 9. Restitution formalism for the creep properties for different hydration degrees

	Cement paste creep at early age creep compliance function				
Description of the creep compliance function	Type of law, number of parameters,...				
	Evolution of the parameters of the creep compliance function				
Hydration degree	Parameter 1	Parameter 2	Parameter 3	Parameter 4	Parameter 5
0.2					
0…					
0…					
0…					
0.6					
ξmax					
Time in seconds	Evolution of creep strains over a three-minute creep test at different times (in μm/m)				
	1 day	2 days	3 days	4 days	5 days
0					
5					
10					
15					
20					
25					
30					
60					
…					
140					
145					
150					
155					
160					
165					
170					
175					
180					

The expected results would be compared to experimental results obtained according to the test protocol described in Irfan-ul-Hassan et al. (2016). The main characteristics of this test are given in Table 10.

Table 10. Main characteristics of the creep tests on cement paste

Specimens dimensions	
Cylindrical specimens	
Height	300 mm
Diameter	70 mm
Specimens are moulded using a specific cylindrical tube.	
After filling, the opening of the mould is sealed in order to avoid water evaporation.	
At an age of 20 hours, the specimens are demolded and covered by food preservation foil in order to minimise loss of water via evaporation.	

Figure 11. Views of creep test on cement paste

A. Schematic illustration of symmetric upper half of the test setup

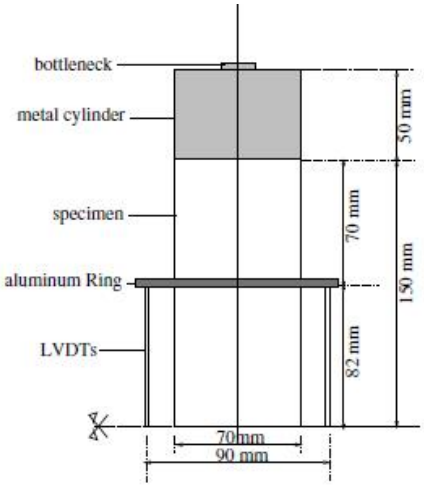

B. Actual test setup inside climate chamber containing two temperature sensors and copper pipes filled with conditioning fluid

Tests were performed between one and ten days after production of the samples.

During testing, the samples were kept at 20°C.

The samples were loaded over 3 minutes, every hour. During the remaining 57 minutes of every hour, a permanent compressive force amounting to 0.2 kN ensured that the whole setup stayed in an upright position.

The three-minute duration load applied to the sample varied with the age of the cement paste.

The specimens were subjected to maximum compressive forces amounting to only 15% of the compressive strength at the time of testing.

Displacements were measured on a length of 164 mm with 5 LVDT sensors (see Figure 11A).

4.1.1.2 Experimental results

Unfortunately, the tests on VeRCoRs cement paste according to the protocol described above could not be achieved in due time. Throughout the remainder of this report, it will not be possible to compare the results submitted by participants to the experimental results.

4.1.1.3 Participants' results

Only one team (Team 76) submitted some results on cement paste creep behaviour.

Team 76 gave the evolution of elastic modulus and compressive strength of the cement paste in function of hydration degree.

Figure 12. Team 76's results: Evolution of elastic modulus

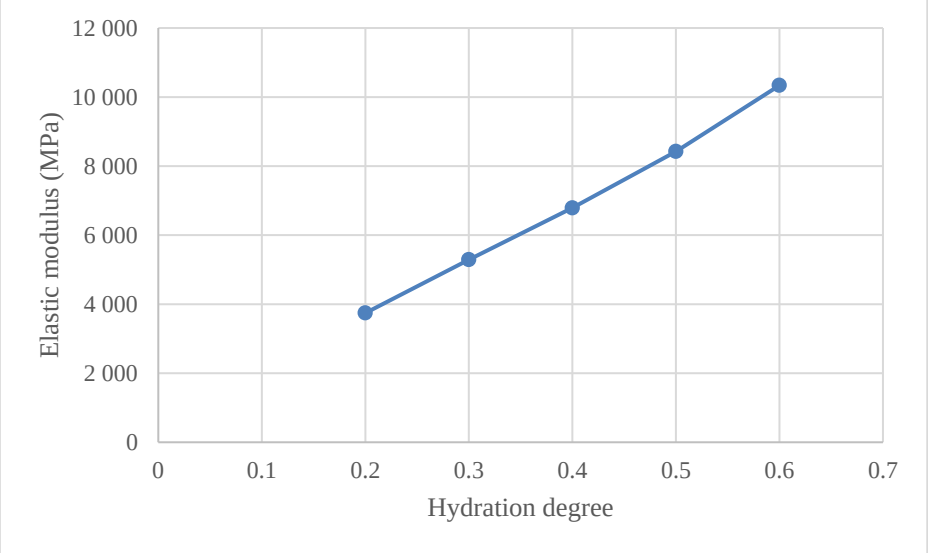

Figure 13. Team 76's results: Evolution of compressive strength

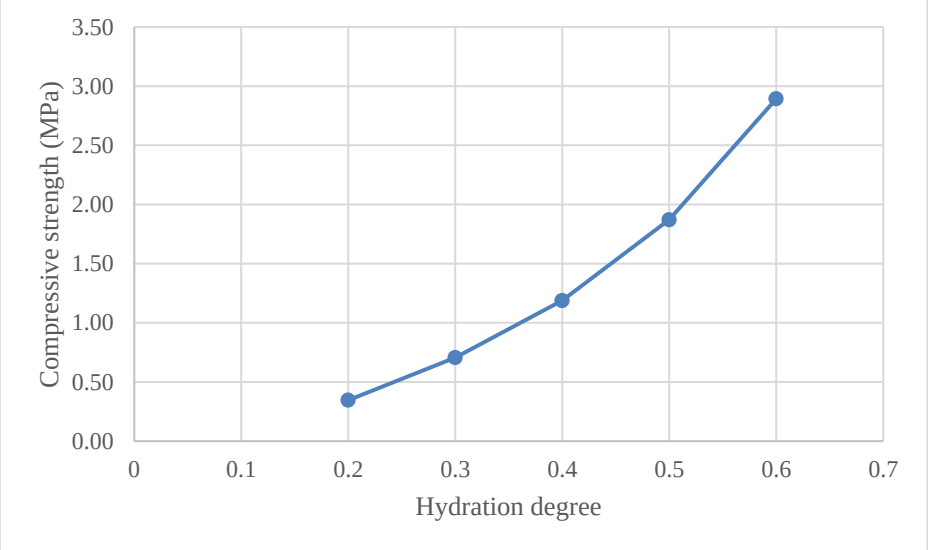

Team 76 also gave the evolution of creep strains over three-minute creep tests for different times: 1 day, 2 days, 3 days, 5 days and 7 days. The curves are shown in Figure 14.

Figure 14. Team 76 results: Creep strains of cement paste

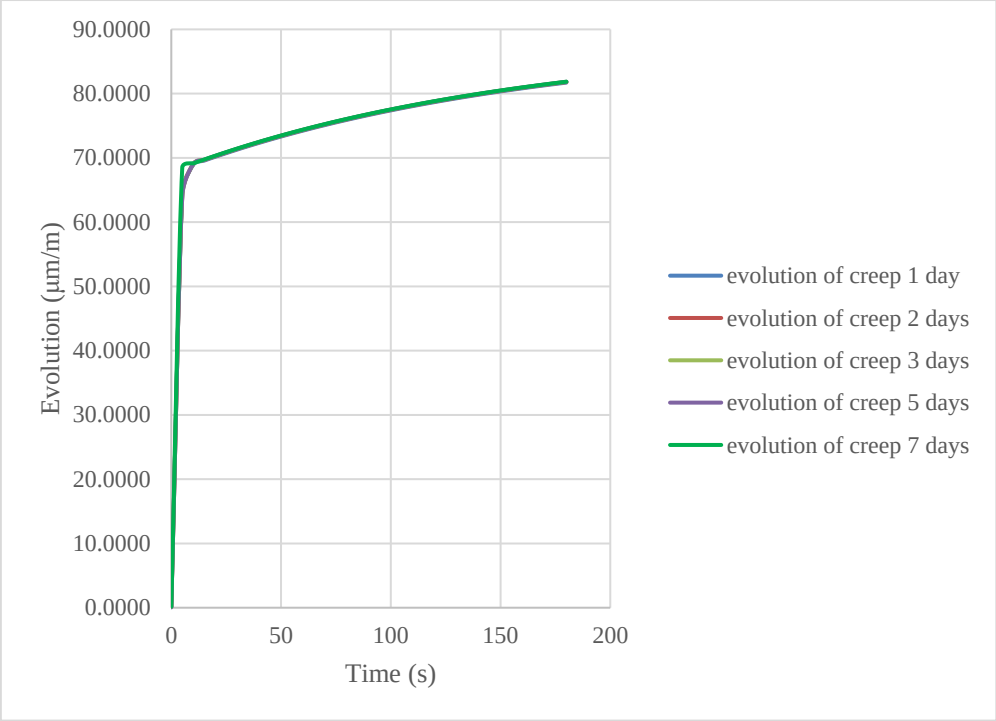

4.1.1.4 Comments

The general procedure used by Team 76 for calculation is the CEB MC90-99 model, using Abaqus for numerical analysis and Excel for regression analysis. For creep, Prony series functions are considered, but results are questionable: there is no change for creep evolution regardless if the time is 1 day or 7 days.

4.1.2. Concrete creep at 90 days

4.1.2.1 Problem to solve

Participants were asked to give the concrete basic creep axial strains without strains due to shrinkage for 90-day aged concrete. Results had to follow the restitution formalism given in Table 11.

Table 11. Restitution formulation for the concrete basic creep axial strains without strains due to shrinkage for 90-day aged concrete

Time (in days)	Concrete basic creep axial strains (in μm/m)
0	
10	
20	
30	
40	
…	
…	
…	
770	

The submitted results can be compared to the experimental results obtained according to the test protocol described in Table 12.

Table 12. Basic creep test protocol

Specimen dimensions	
Cylindrical specimens	
Height	1 m
Diameter	0.16 m
The sample is covered by a leak-tight coating during the entire duration of the test.	
Hygrometry	50%
Temperature	20°C
Load	12 MPa
The load is applied at 91 days.	
Due to creep, the applied force decreases. But when the force reaches the value of 216 kN, the specimen is reloaded to the initial force value (241 kN).	
The axial displacement is given for the central part of the sample (500 mm).	
The measurements start 91 days after pouring.	

Figure 15. View of creep test on VeRCoRs concrete

4.1.2.2 Experimental results

The measured strains are the total strains (basic creep + shrinkage). It is not the pure basic creep strains. In order to compare the basic creep strains obtained by the participants to the experimental results, the measured strains must be corrected using a non-drying shrinkage test on VeRCoRs concrete.

The strain measures obtained on VeRCoRs concrete specimens are given in Figure 16.

From these measures, the pure basic creep strain can be obtained by subtracting the shrinkage strain and the elastic strain due to initial load (read from the first strain measure of creep test). The experimental pure basic creep strain (i.e. the basic creep without elastic strain related to loading) is given by the red curve in Figure 17. This is the curve used to compare with the results submitted by participants.

Figure 16. Axial strains measures during basic creep test on VeRCoRs concrete

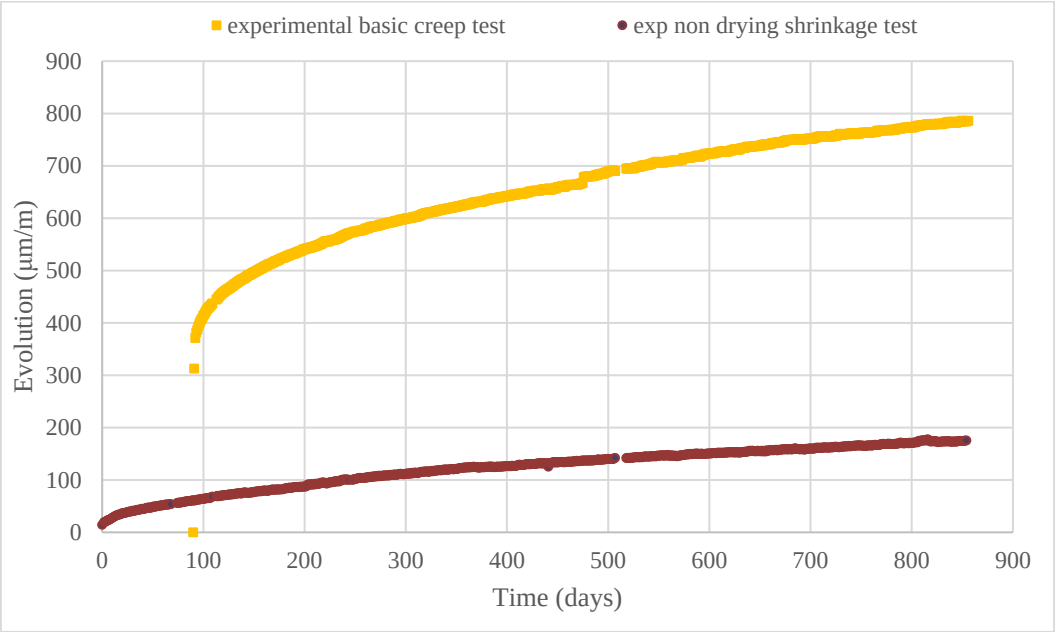

Figure 17. Pure basic creep strains: Experimental curve

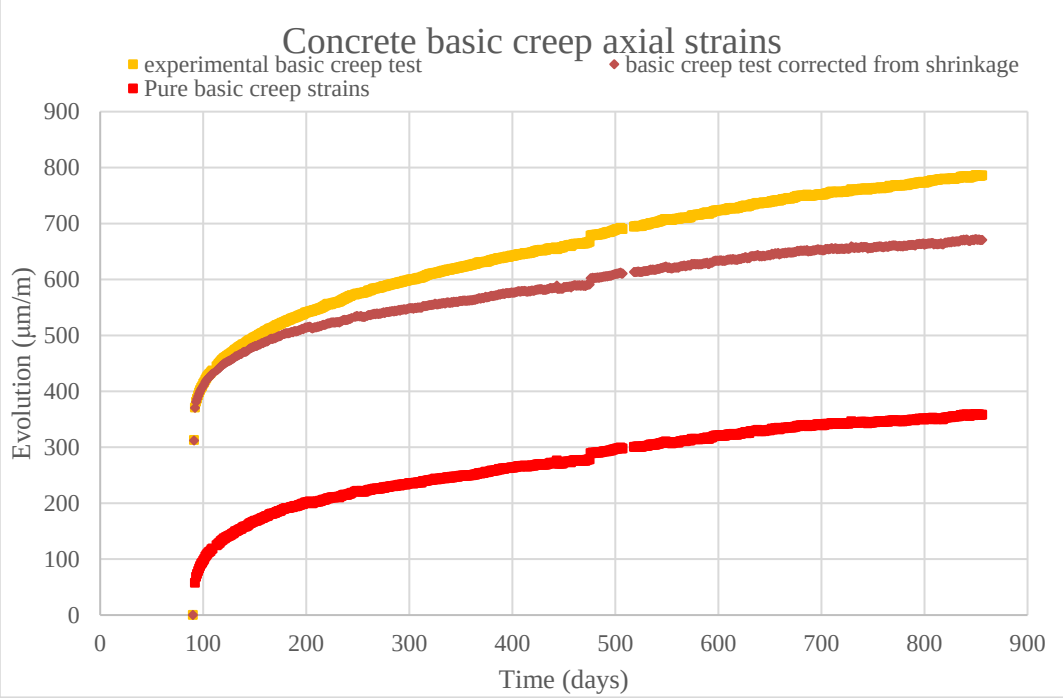

4.1.2.3 Participants' results

For this topic, seven teams submitted results: Teams 14, 23, 47, 76, 82, 88 and 90.

The curves provided by these teams are presented in Figure 18. For ease of comparison, all the curves start from 0 days, but it is the 90-day creep that is considered here.

Figure 18. Basic creep strains: Comparison of participants' results

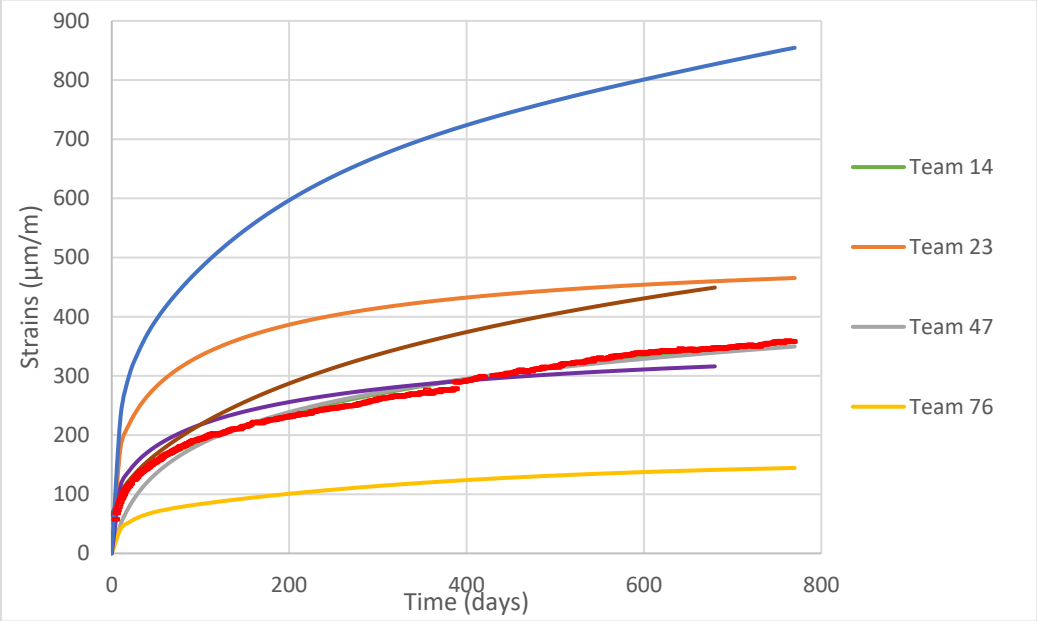

4.1.2.4 Comments

Three teams gave results very close to the experimental measure: Teams 14, 47 and 82.

Team 88's curve shows quite a good level of creep strains but a deformation speed obviously higher than most of the other teams. It seems that this team included some shrinkage strains in its results.

Teams 23 and 90 gave strain curves much higher than the experimental results. For Team 90, it is indicated in the restitution file that the basic creep and drying creep experimental data sets were averaged together, and that the model was fit to the average of the two experimental data sets. This explains why the curve gives such high strain values.

Team 76 provided a curve much lower than the experimental curve.

4.2. Theme 1.2: Multiphysics approach for total creep

In this theme, the idea was to show how different models or laws can describe concrete creep situations under varying environmental conditions. Several conditions were considered on two types of specimens.

The first specimens were concrete-full cylinders of high dimensions submitted to drying creep in various relative humidity. The second specimens were small hollow concrete cylinders on which drying-imbibition cycles were proceeded during a creep test.

4.2.1. Concrete drying creep

4.2.1.1 Problem to solve

Participants were asked to predict the creep axial strains (in µm/m) without strains due to shrinkage of VeRCoRs concrete in environments with different relative humidity: RH 50%, RH 30% and RH 70%.

The comparison of the given results was possible for the RH 50% environment for which one drying creep test was made on VeRCoRs concrete following the protocol described in Table 14.

Results had to follow the restitution formalism given in Table 13.

Table 13. Restitution formalism for creep axial strains without strains due to shrinkage of VeRCoRs concrete in environments with different relative humidity

	Axial strains (μm/m)		
Time (in days)	Drying creep RH 50%	Drying creep RH 30%	Drying creep RH 70%
0			
10			
20			
30			
40			
50			
…			
…			
…			
770			

Table 14. Protocol for the drying creep test

Specimens dimensions	
Cylindrical specimens	
Height	1 m
Diameter	0.16 m
After pouring, the sample is placed in non-drying conditions for 90 days.	
Then the leak-tight coating is removed and the measurements start 91 days after pouring.	
Hygrometry	50%
Temperature	20°C
Load	12 MPa
The load is applied at 91 days.	
Due to creep, the applied force is decreasing. But when the force reaches the value of 216 kN, the specimen is reloaded to the initial force value (241 kN).	
The axial displacement is given for the central part of the sample (500 mm).	
The measurements start 91 days after pouring.	

4.2.1.2 Experimental results

The measured strains are the total strains (creep + shrinkage), not the pure drying creep strains. In order to compare the creep strains obtained by the participants to the experimental results, the measured strains must be corrected using a drying shrinkage test on VeRCoRs concrete.

The strain measures obtained on VeRCoRs concrete specimens are given in Figure 19.

Figure 19. Axial strain measures during drying creep test on VeRCoRs concrete

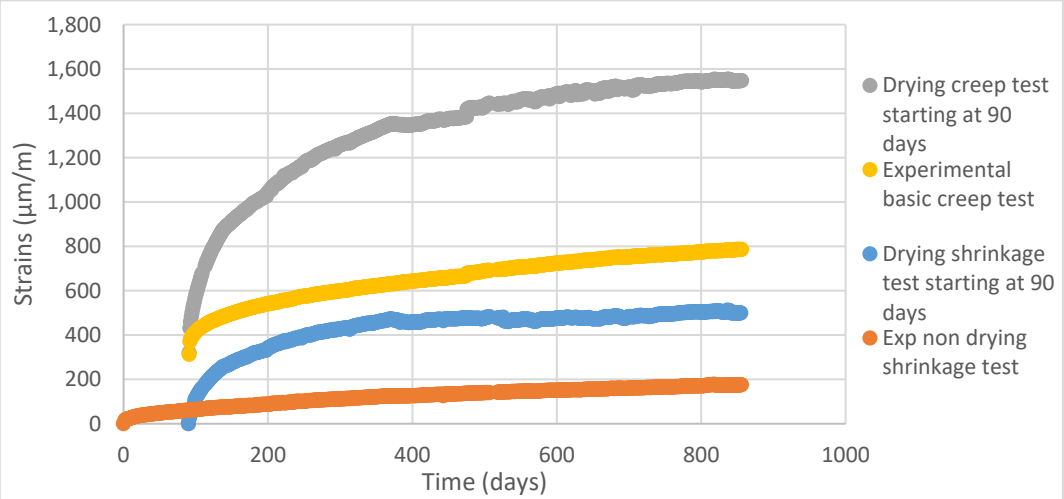

From these measures, the pure drying creep strains (with RH 50%) were obtained by subtracting the drying shrinkage strains, the pure basic creep strains and the elastic strain due to initial load (read from the first strain measure of creep test). The experimental pure drying creep strains (with RH 50%) are given by the red curve in Figure 20. This is the curve used to compare with the results submitted by participants.

Figure 20. Pure drying creep strains (RH 50%): Experimental curve

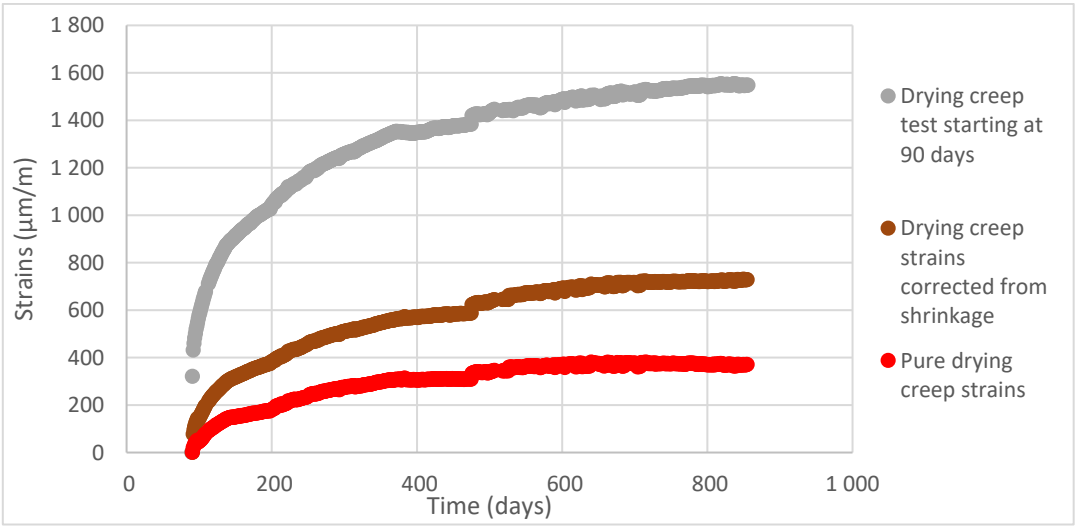

4.2.1.3 Participants' results

The submitted results on this topic are shown in Table 15.

Table 15. Participants' results for the concrete drying creep

	RH 50%	RH 30%	RH 70%
Number of teams	6	5	5
Name of teams	Teams 14, 23, 47, 76, 82, 88	Teams 23, 47, 76, 82, 88	Teams 23, 47, 76, 82, 88

Figure 21 shows the curves for the drying creep with RH 50%.

Figure 21. Drying creep of VeRCoRs concrete at RH 50%: Comparison of the results

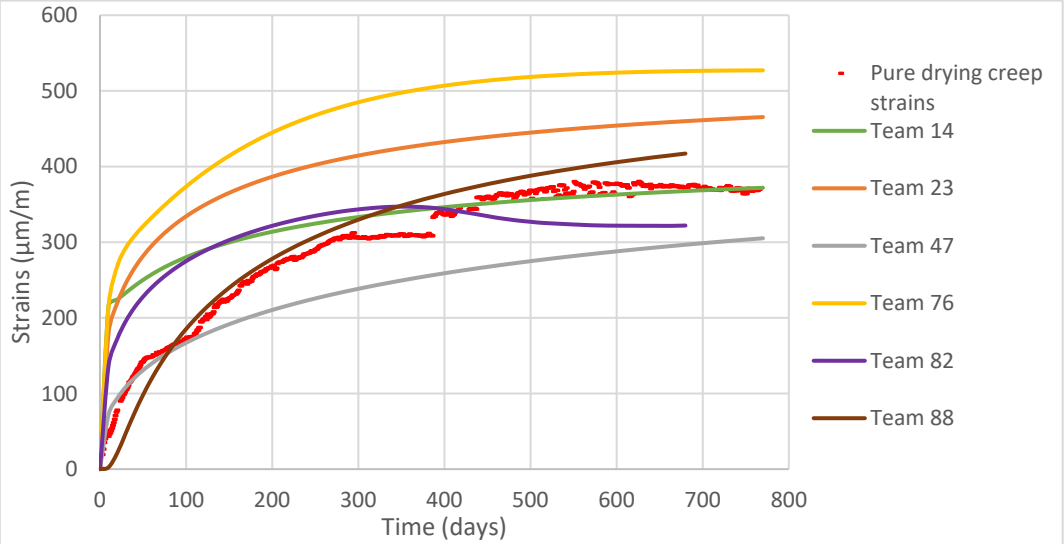

The curves corresponding to the other RH conditions are given in Figures 22 and 23.

Figure 22. Drying creep of VeRCoRs concrete at RH 30%: Comparison of the results

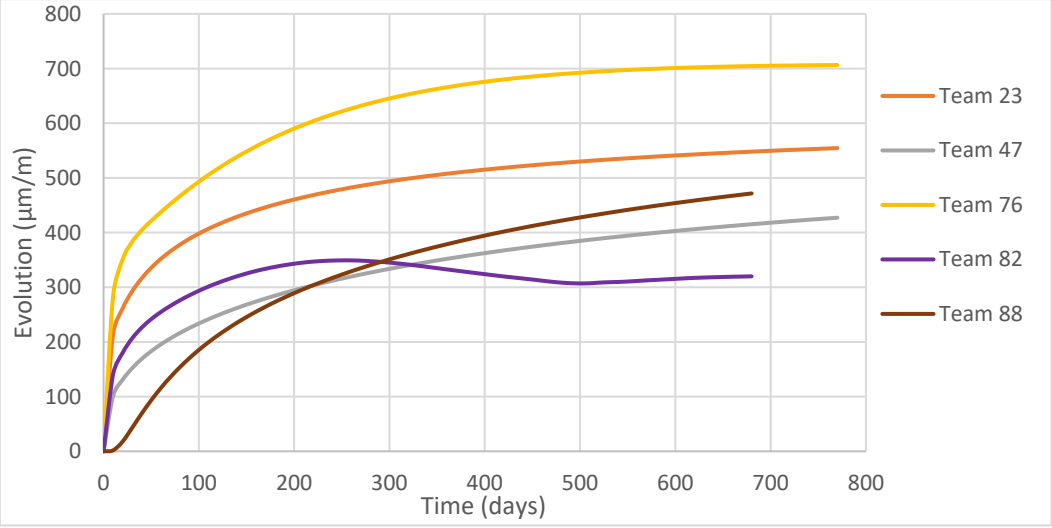

Figure 23. Drying creep of VeRCoRs concrete at RH 70%: Comparison of the results

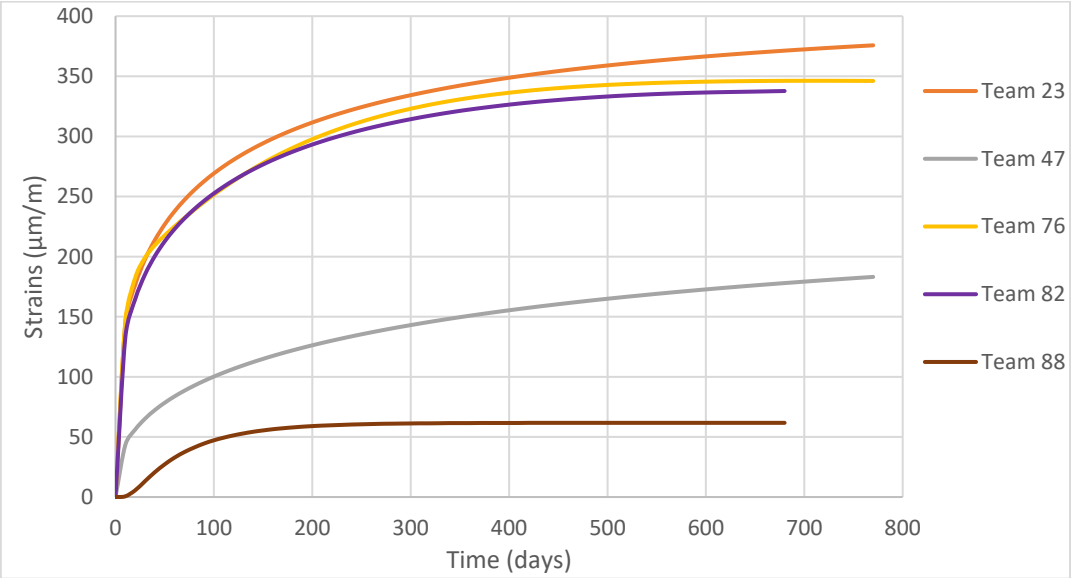

4.2.1.4 Comments

Unlike the curves obtained for the basic creep, the curves here present strong singularities.

For RH 50%, except for Teams 23 and 76, the results are in the same range as the experimental values.

Teams 14, 23, 76 and 82 show a very high deformation speed just after the initial load, compared to Teams 47 and 88. Team 82's curve has an inflexion point approximately 450 days after the initial load, which is an uncommon result. Team 14's curve presents a brutal change in the deformation speed about ten days after the initial load, which has no physical explanation. Concerning Team 88, the beginning of the curve presents an inflexion point which is not a common result.

For RH 30%, the same comments can be made for Teams 82 and 88. Except for Team 82, all teams gave higher strains for RH 30% than for RH 50%, which was expected.

For RH 70%, Team 82's curve no longer has an inflexion point. Three teams have very close curves: Teams 23, 76 and 82. But these three teams propose strains in the same range as the experimental values at RH 50%, which is not an expected result. Team 88 gave very low values of strain.

Among the teams that submitted results for the three drying conditions, Team 47 gave one of the most consistent results.

4.2.2. Drying-imbibition cycles creep behaviour

4.2.2.1 Problem to solve

Participants were asked to model the effect on concrete creep of drying-imbibition cycles. The expected results for this topic were the axial creep strains of a drying specimen and the axial creep strains of a specimen subjected to drying-imbibition cycles. Results were to be given in the following table.

Table 16. Expected results of the drying-imbibition cycles creep behaviour

Axial strains (µm/m)	Time (in days)	Drying creep HR 50% Drying-imbibition cycles creep
0		
10		
20		
30		
…		
…		
…		
450		

The given results could be compared to experimental values obtained from the creep test described below.

Drying- specimens

The hollow cylindrical specimens were loaded on drying conditions (HR 50% and 20°C) for 450 days, without imbibition.

Figure 24. Views of drying-imbibition creep tests on hollow cylindrical specimens

Drying-imbibition cycles specimens

First, the hollow cylindrical specimens are loaded (12 MPa) on drying conditions (RH 50% and 25°C) over 170 days.

At 170 days, the hollow of the cylinder is filled with water, the water is left for 130 days (conditions remain RH 50% and T=25°C).

Three hundred days after the beginning of the test, the water is removed and the specimens start drying again (RH 50% and 25°C).

Four hundred and fifteen days after the beginning of the test, the specimens are filled again with water for a new resaturation (conditions remain RH 50% and T=25°C).

Figure 25. Programme of drying-imbibition cycles during the creep test

4.2.2.2 Experimental results

The strain measures during drying-imbibition cycle creep tests are given in Figure 26. As a comparison, a curve representing a drying creep test (RH 50%) on the same specimen is also given.

Figure 26. Drying-imbibition cycles creep test: Axial strains evolution during test

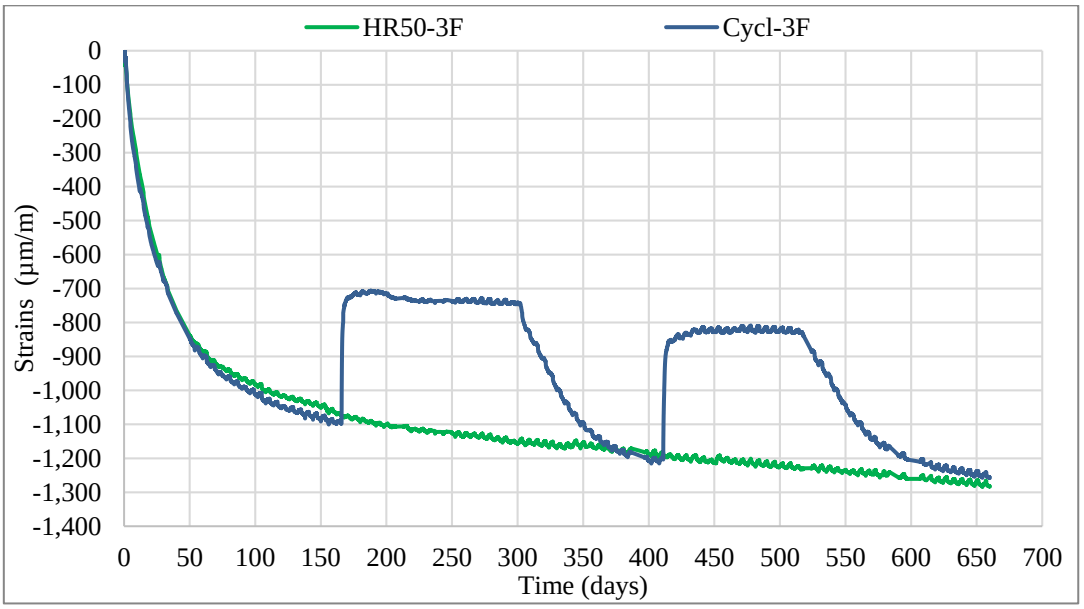

4.2.2.3 Participants' results

No participants submitted results on this topic.

5. Results on Theme 2: Predicting the behaviour of the whole containment wall

5.1. Problem to solve

Predictions were made of the behaviour of the containment wall at different moments: just before the "VD2" pressurisation test, then during the pressurisation tests "VD1", "VD1 bis" and "VD2" (at 5.2 bar abs.).

Strains and stresses at 40 points defined in the raft, the gusset, the cylindrical wall and the dome were expected from the cracking state evaluation (inner face cracks, outer face cracks and through cracks).

5.2. Sensor locations

Figure 27. Sensor locations in the raft and gusset

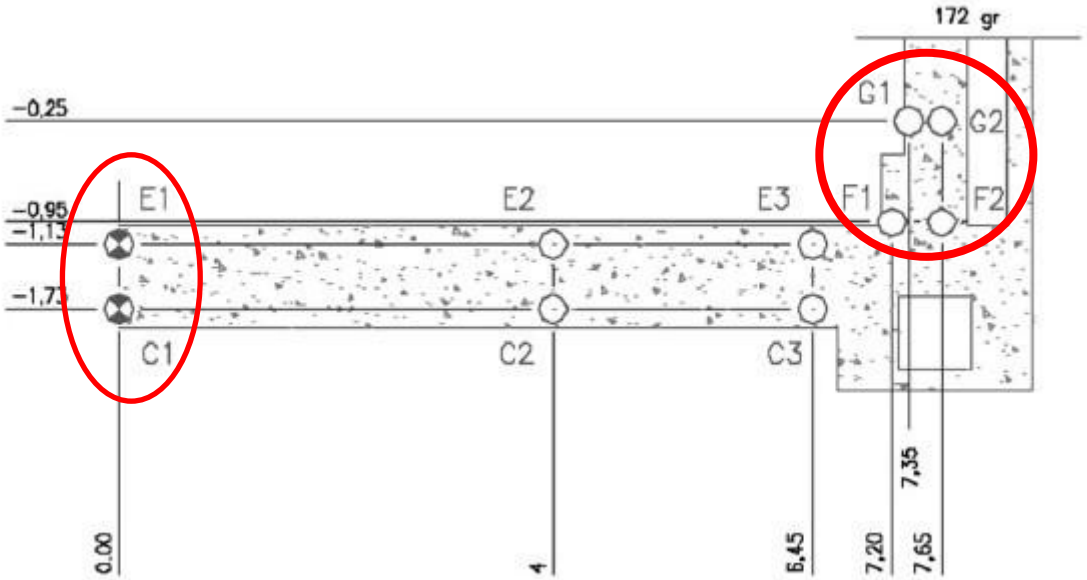

Figure 28. Sensor locations in the cylindrical part

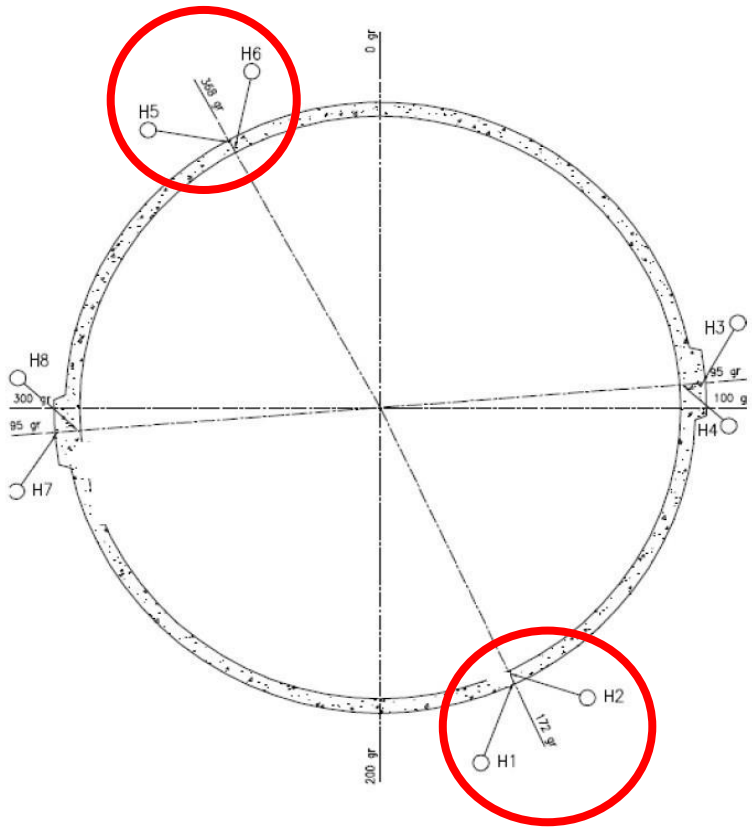

Figure 29. Sensor locations in the dome

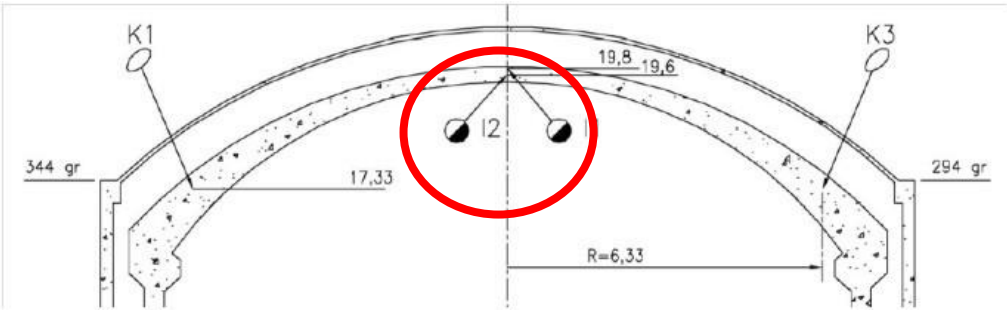

5.3. Strains

5.3.1. Expected results

Two types of strains were examined:

- delayed strains from a reference date to characterise the long-term behaviour (creep and shrinkage);
- instantaneous strains during pressurisation tests to study the effects of repeated pressure loads, with or without ageing between tests.

Concerning the delayed strains from a reference date, participants were asked to predict the delayed strains of the concrete from a reference date to the "VD2" pressure test. The table below was provided to collect participants' results.

Table 17. Results of the predictions of delayed strains of the concrete from a reference date to VD2 pressure test

		Long-term strains (in µm/m)		
		Reference date for strains	Start of VD1 pressure test	Start of VD2 pressure test
Zone	Strain gauge	2 November 2015 12:05	14 March 2017 06:35	2 April 2018 07:00
Raft	C1_CENTRE_95_R	0	-60	
	C1_CENTRE_195_R	0	-67	
	E1_CENTRE_95_R	0	-67	
	E1_CENTRE_195_R	0	-88	
Gusset	F1IV	0	Not available	
	FIIT	0	-73	
	F2EV	0	-181	
	F2ET	0	-119	
	G1IV	0	-344	
	G1IT	0	-117	
	G2EV	0	-206	
	G2ET	0	-114	
Cylindrical part (mid-height)	P1EV	0	-304	
	P1ET	0	-360	
	P2IV	0	-334	
	P2IT	0	-348	
	H1EV	0	-266	
	H1ET	0	-323	
	H2IV	0	-326	
	H2IT	0	Not available	
	H5EV	0	-303	
	H5ET	0	-344	
	H6IV	0	-320	
	H6IT	0	-356	
Equipment hatch	M3EV	0	Not given	
	M3ET	0	Not given	
	M4IV	0	Not given	
	M4IT	0	Not given	

Table 17. Results of the predictions of delayed strains of the concrete from a reference date to VD2 pressure test (Continued)

		Long-term strains (in µm/m)		
		Reference date for strains	Start of VD1 pressure test	Start of VD2 pressure test
Zone	Strain gauge	2 November 2015 12:05	14 March 2017 06:35	2 April 2018 07:00
Equipment hatch	M7EV	0	Not given	
	M7ET	0	Not given	
	M8IV	0	Not given	
	M8IT	0	Not given	
Dome	I1_194_EM	0	-301	
	I1_94_EM	0	-309	
	I2_194_IM	0	-321	
	I2_94_IM	0	-309	
	J1EM	0	Not available	
	J1ET	0	Not available	
	J2IM	0	-258	
	J2IT	0	-231	

Concerning the instantaneous strains, participants were asked to give the strains of the concrete during the "VD1 bis" test and the "VD2" test. Table 18 was provided to collect participants' results.

Table 18. Results of the predictions of the strains of the concrete during the VD1 bis test and the VD2 test

		Strains during pressure test between 0 bar and 4.2 bar rel. (in µm/m)				
Zone	Strain gauge	Pre-op	VC1	VD1	VD1 bis	VD2
Raft	C1_CENTRE_95_R	Not available	-6	-7		
	C1_CENTRE_195_R	Not available	-4	-5		
	E1_CENTRE_95_R	-14	-14	-15		
	E1_CENTRE_195_R	-12	-13	-11		
Gusset	F1IV	Not available	Not available	Not available		
	FIIT	-2	-1	-3		
	F2EV	0	1	0		
	F2ET	-2	-2	1		
	G1IV	142	139	139		
	G1IT	18	17	10		
	G2EV	-5	0	0		

Table 18. Results of the predictions of the strains of the concrete during the VD1 bis test and the VD2 test (Continued)

		Strains during pressure test between 0 bar and 4.2 bar rel. (in µm/m)				
Zone	Strain gauge	Pre-op	VC1	VD1	VD1 bis	VD2
Gusset	G2ET	19	18	16		
Cylindrical part (mid-height)	P1EV	70	71	73		
	P1ET	216	216	216		
	P2IV	86	94	88		
	P2IT	230	231	234		
	H1EV	61	65	60		
	H1ET	217	219	220		
	H2IV	85	90	86		
	H2IT	Not available	Not available	Not available		
	H5EV	63	65	64		
	H5ET	202	201	201		
	H6IV	Not available	98	96		
	H6IT	Not available	236	239		
Equipment hatch	M3EV	Not given	Not given	Not given		
	M3ET	Not given	Not given	Not given		
	M4IV	Not given	Not given	Not given		
	M4IT	Not given	Not given	Not given		
	M7EV	Not given	Not given	Not given		
	M7ET	Not given	Not given	Not given		
	M8IV	Not given	Not given	Not given		
	M8IT	Not given	Not given	Not given		
Dome	I1_194_EM	110	120	120		
	I1_94_EM	150	161	158		
	I2_194_IM	166	171	170		
	I2_94_IM	152	159	158		
	J1EM	Not available	168	Not available		
	J1ET	Not available	29	Not available		
	J2IM	177	178	176		
	J2IT	11	14	10		

5.3.2. Experimental results

The experimental results represented in this part are total concrete strains including temperature effects. They do not correspond to pure mechanical concrete strains.

Figure 30. Raft strains evolution from construction to VD2 pressure test

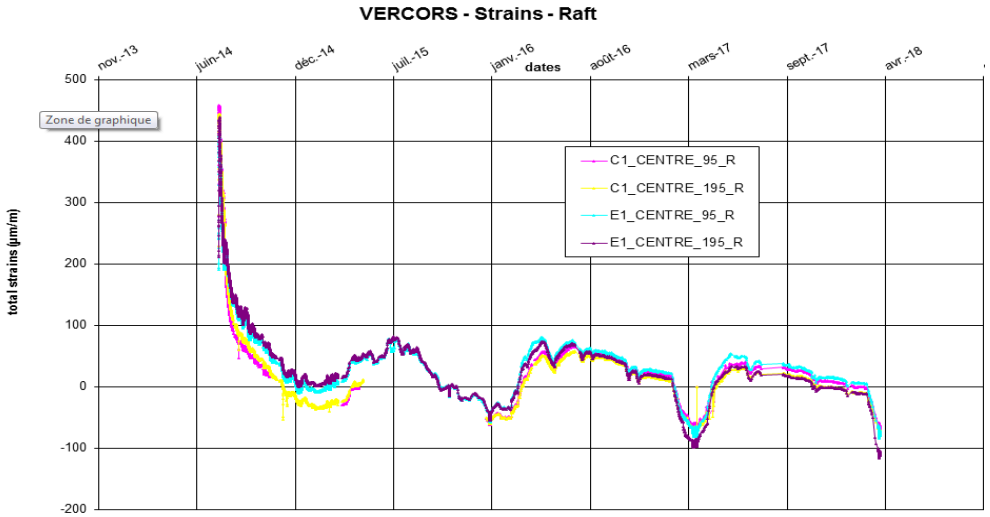

Figure 31. Gusset strains evolution from construction to VD2 pressure test

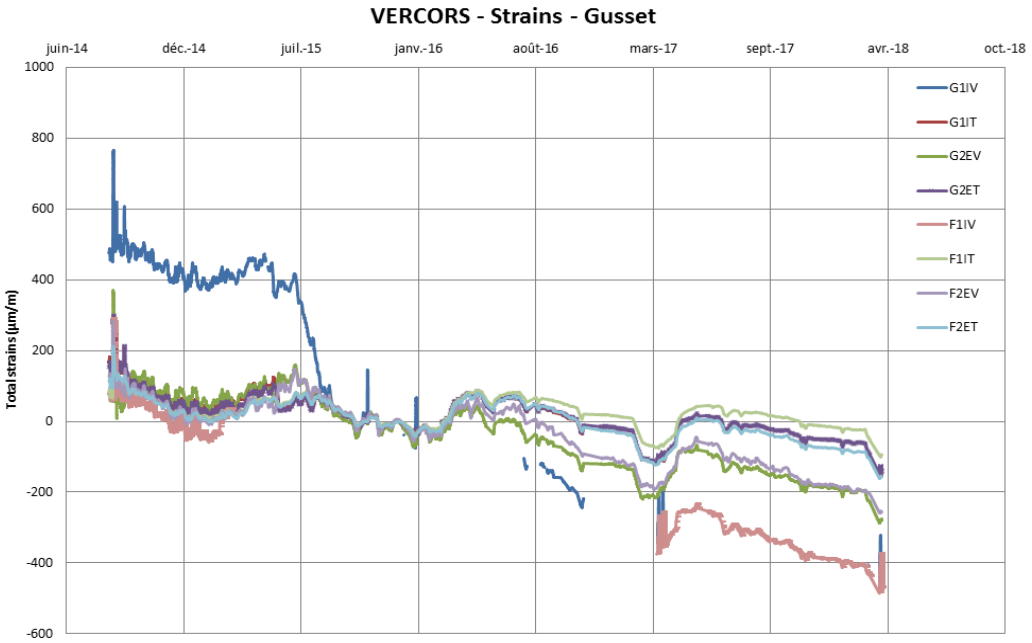

Figure 32. Cylindrical part strains evolution from construction to VD2 pressure test

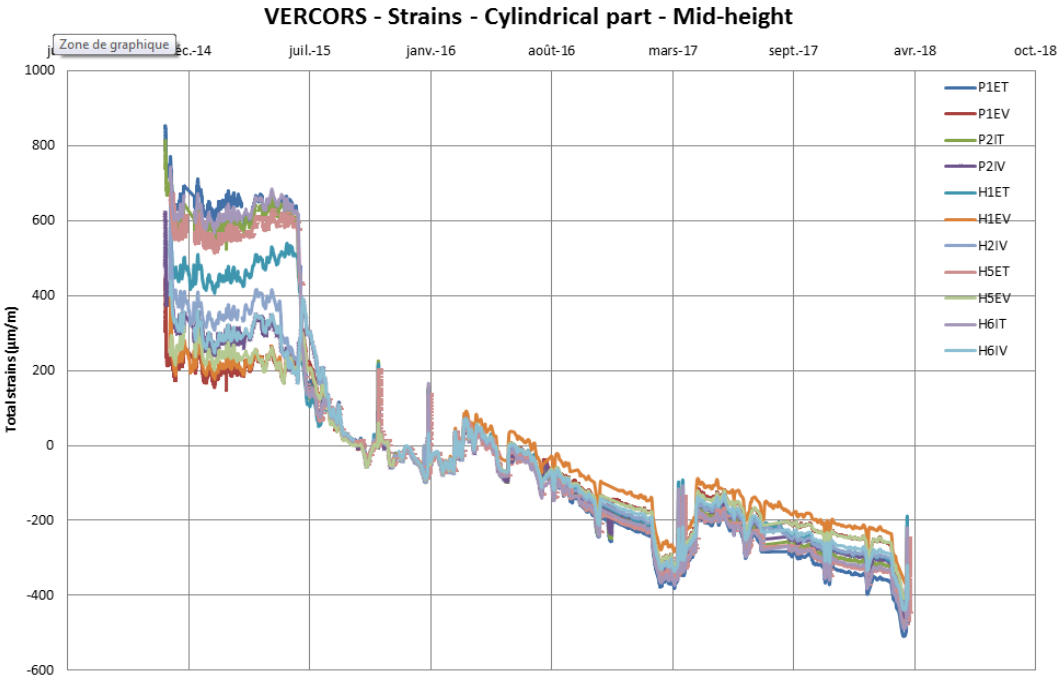

Figure 33. Dome strains evolution from construction to VD2 pressure test

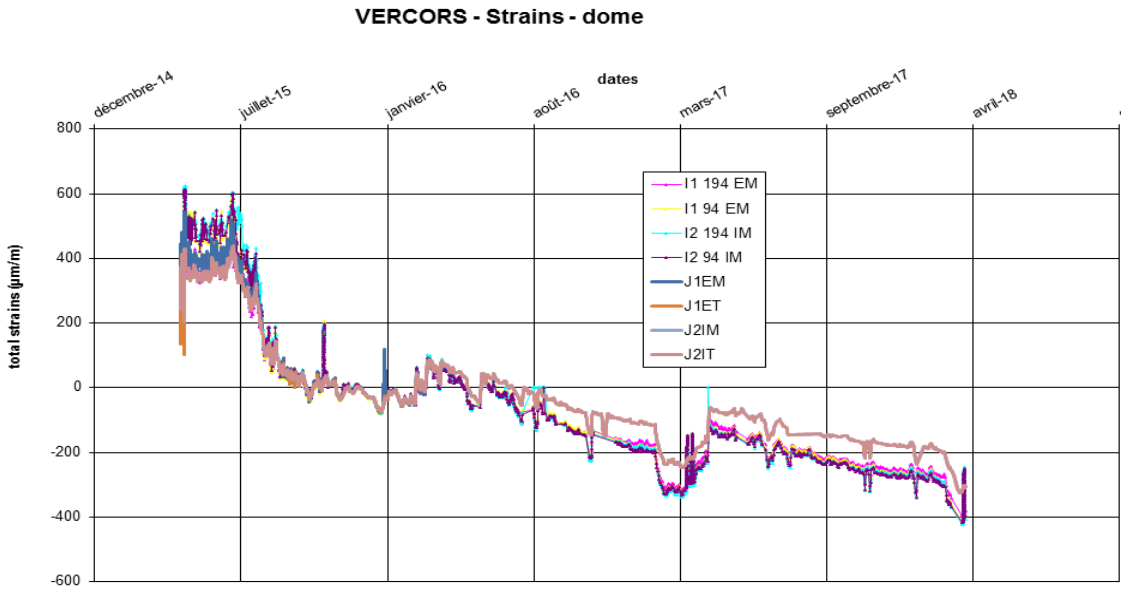

5.3.3. Submitted results

Out of a total of 18 teams participating in this theme, 15 provided results concerning delayed strains, but with a very variable number of results out of a total of 40 analysis sensor positions. Only four teams provided results for all 40 sensor positions. If the raft area is not taken into consideration, seven teams gave full results, and if the focus is only on the gusset, cylindrical part and dome, ten teams submitted full results.

Teams 14 and 47 submitted results for only a few sensors in the cylinder part.

Team 23 gave one unique value of delayed strain for all sensors calculated by applying the Eurocode 2 formula. This value is conserved in the following analysis.

5.3.4. Delayed strains results

The experimental results represented in this part are total strains including thermal effects. The value is represented by an orange horizontal line.

In the following curves, the mean value of the participants' results is represented by a black horizontal line.

5.3.4.1 Raft strain evolution

5.3.4.1.1 Lower level

Figure 34. Delayed strains results comparison: Lower part of the raft (95 Grd)

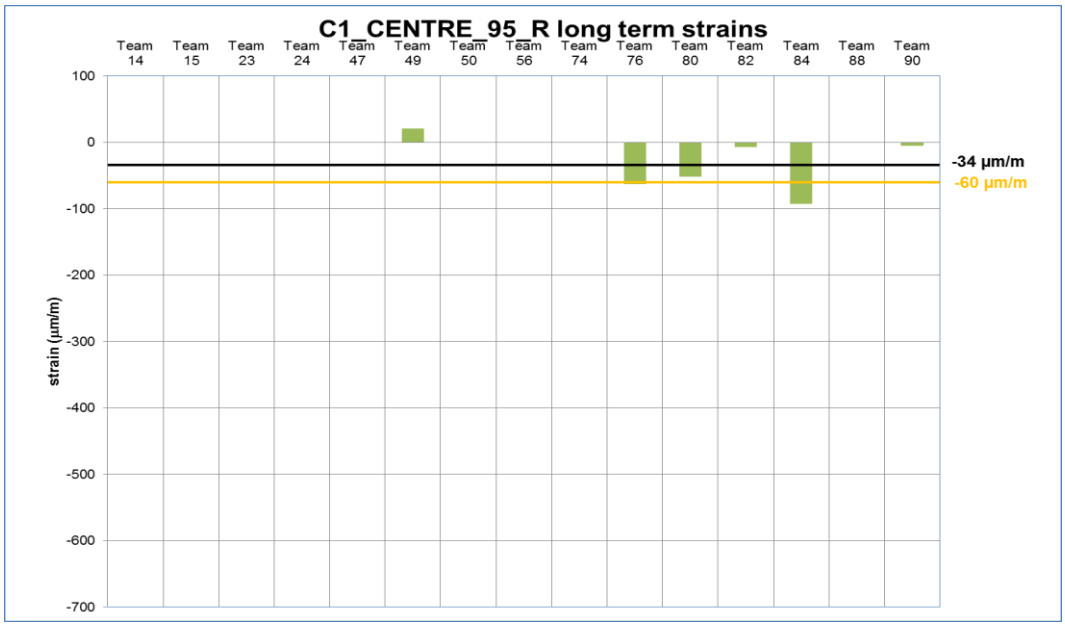

Figure 35. Delayed strains results comparison: Lower part of the raft (195 Grd)

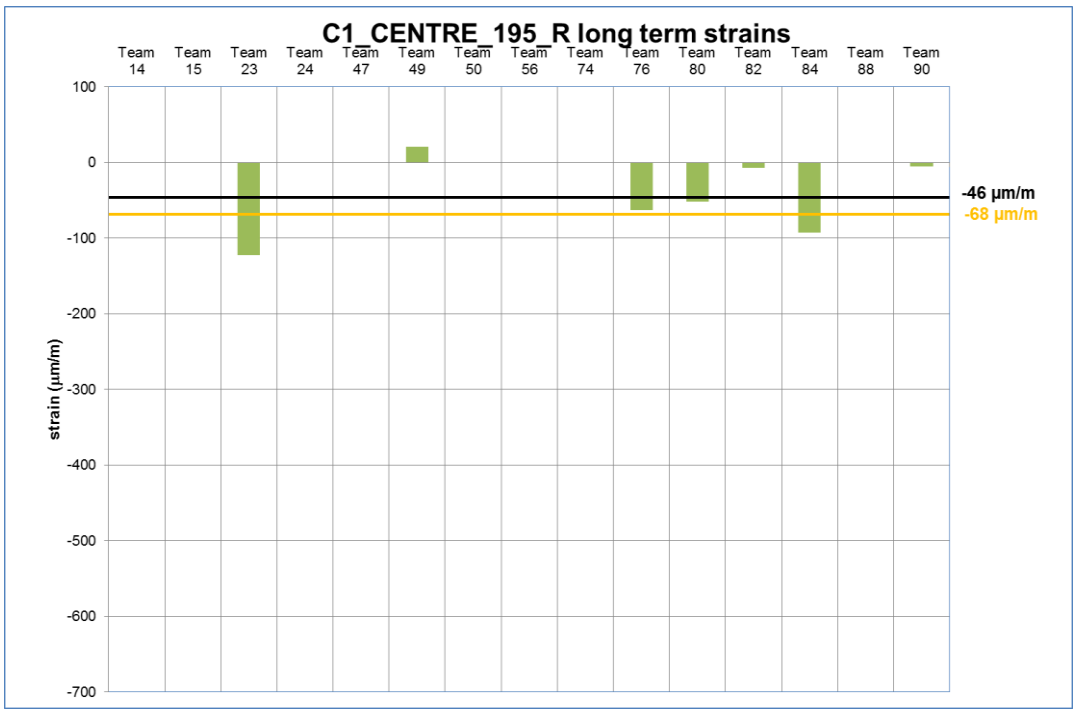

5.3.4.1.2 Upper level

Figure 36. Delayed strains results comparison: Upper part of the raft (95 Grd)

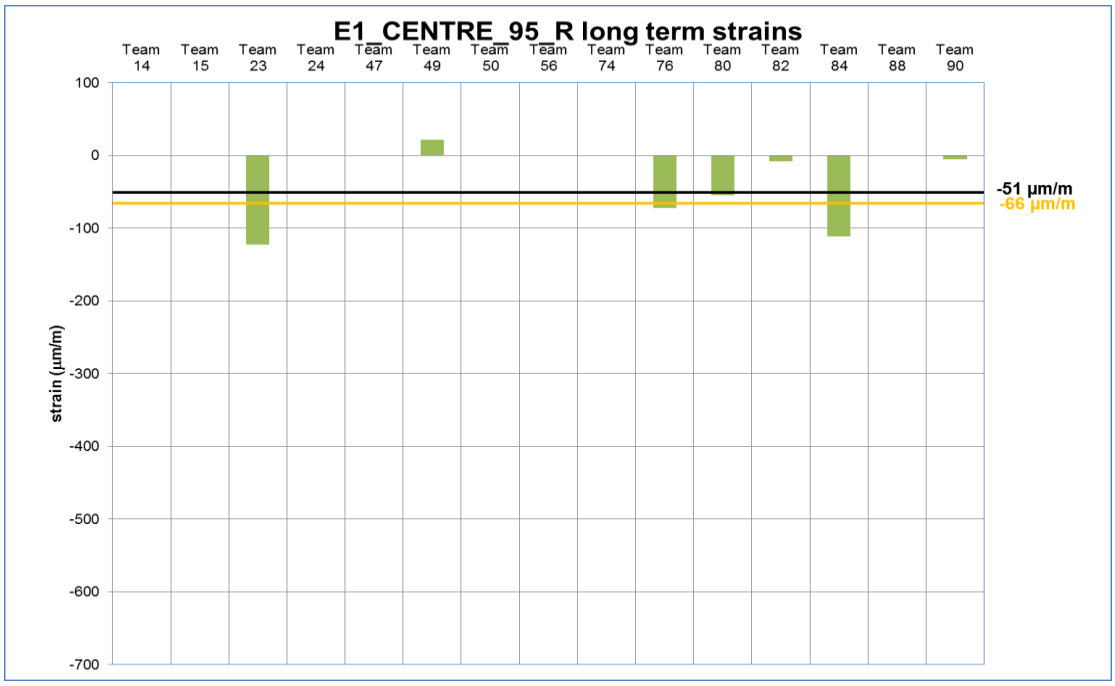

Figure 37. Delayed strains results comparison: Upper part of the raft (195 Grd)

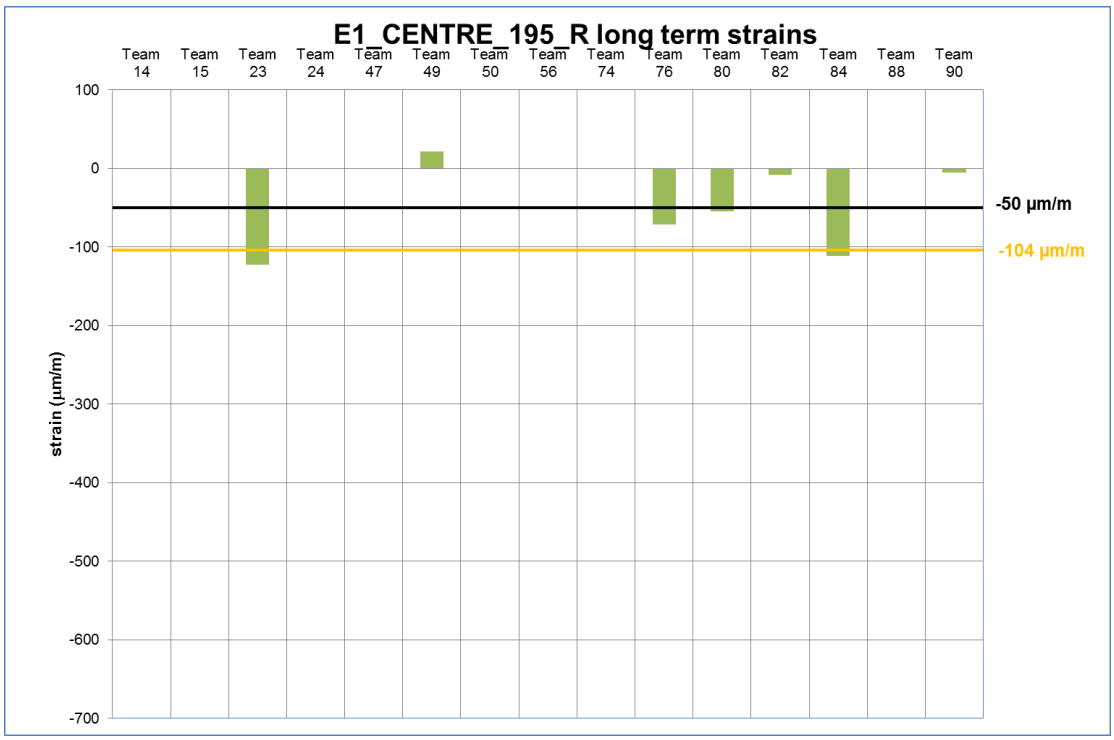

5.3.4.1.3 Comments

Only seven teams gave values for the raft.

Even if the curves seem to show a good mean prediction in comparison to the experimental value, the results are very scattered for both levels.

Team 49 shows a swelling of the raft, which is not observed on the mock-up.

5.3.4.2 Gusset strain evolution

5.3.4.2.1 Vertical direction

Figure 38. Delayed strain results comparison: Gusset – Vertical direction – Bottom – Intrados

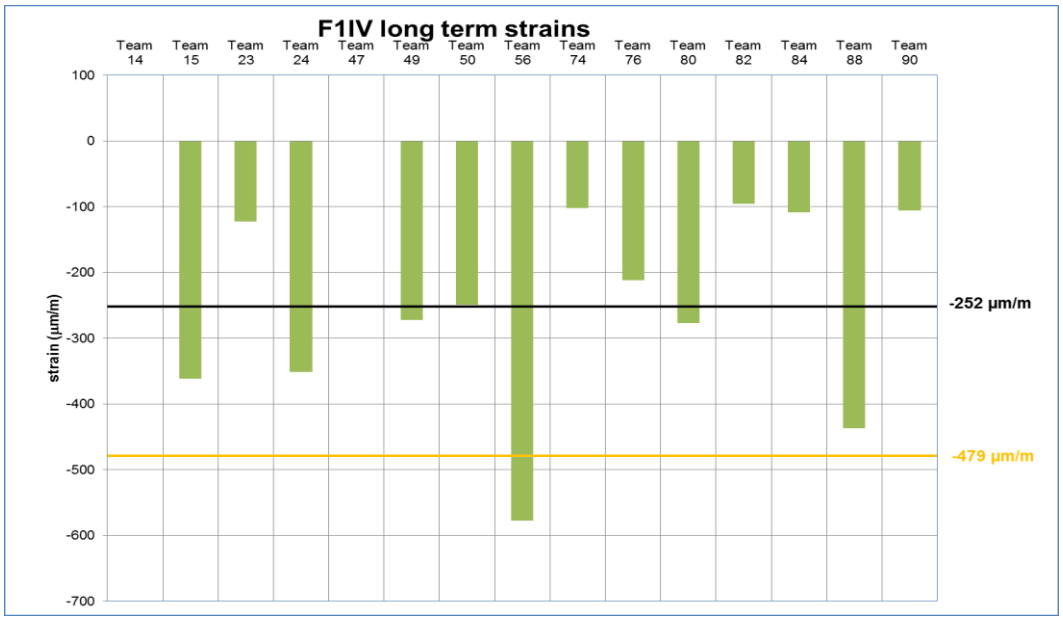

Figure 39. Delayed strain results comparison: Gusset – Vertical direction – Bottom – Extrados

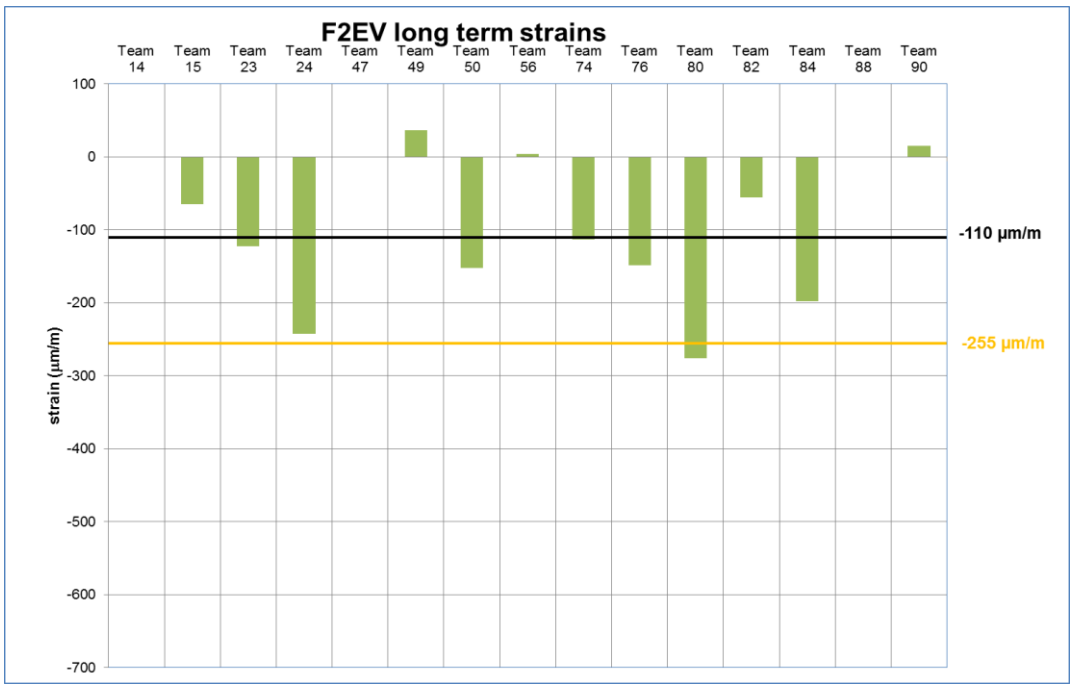

Figure 40. Delayed strain results comparison: Gusset – Vertical direction – Top – Intrados

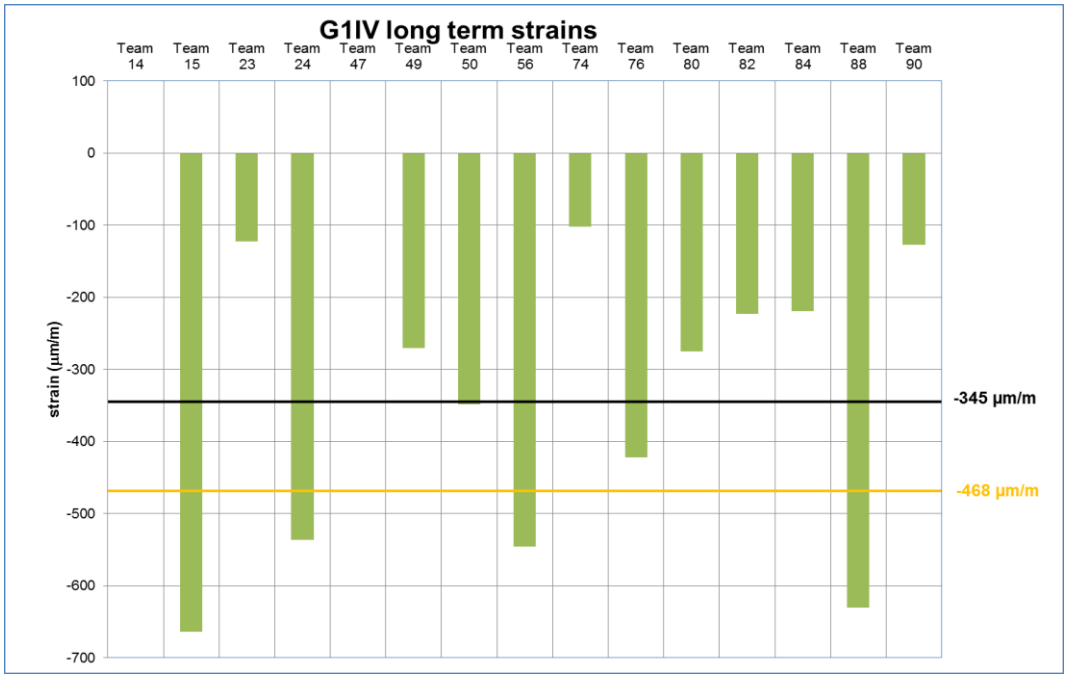

Figure 41. Delayed strain results comparison: Gusset – Vertical direction – Top – Extrados

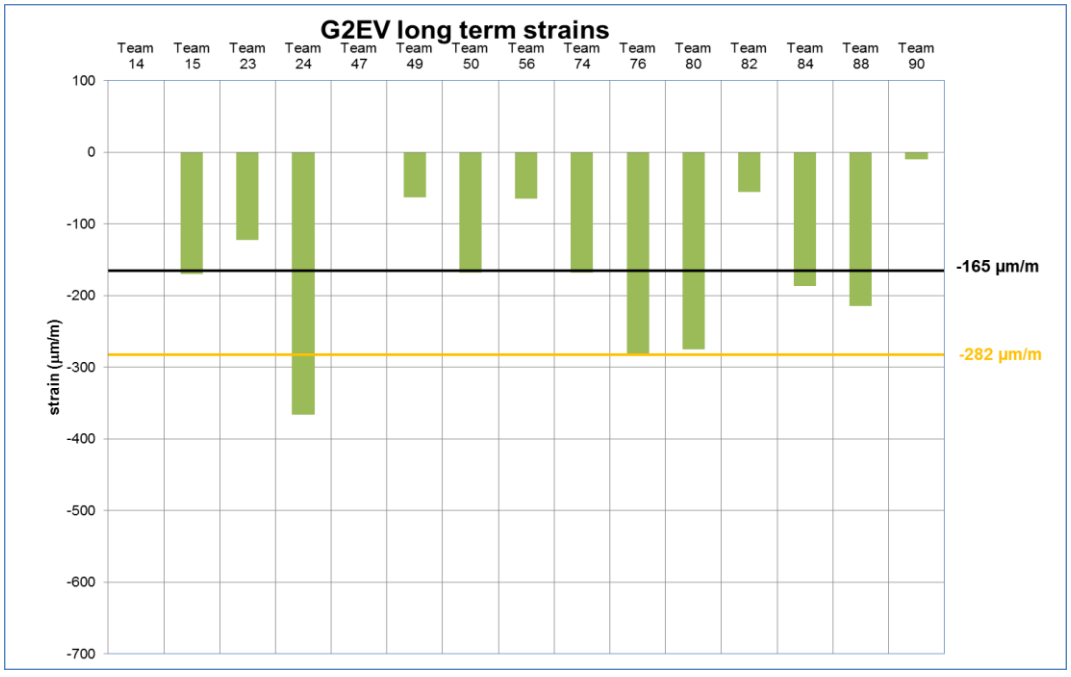

5.3.4.2.2 Tangential direction

Figure 42. Delayed strain results comparison: Gusset – Tangential direction – Bottom – Intrados

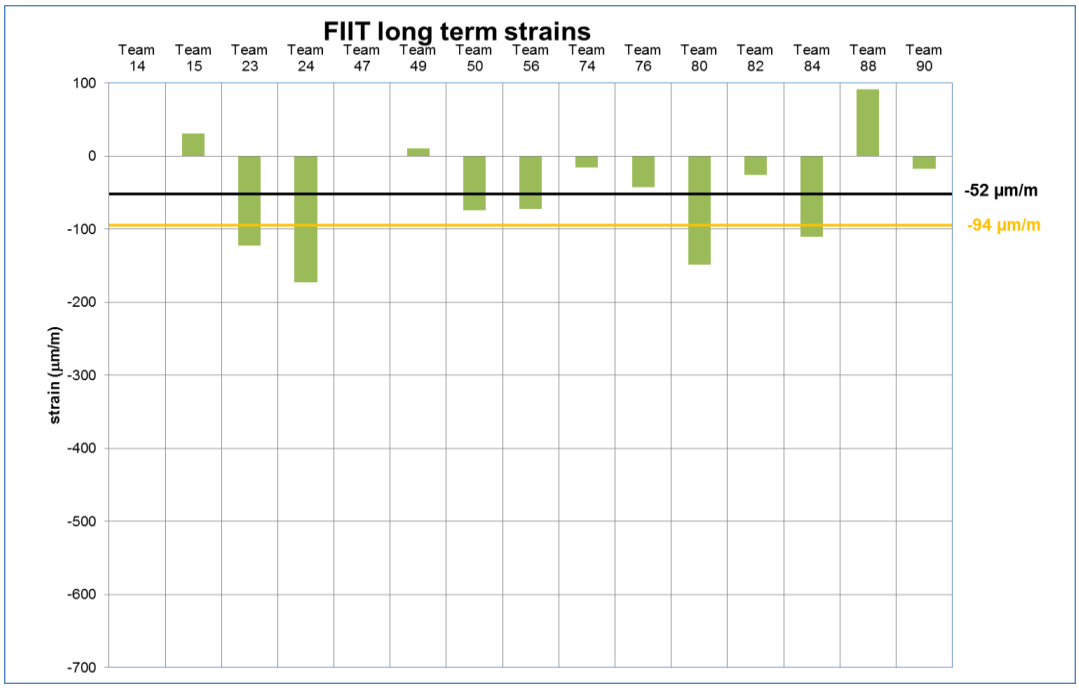

Figure 43. Delayed strain results comparison: Gusset – Tangential direction – Bottom – Extrados

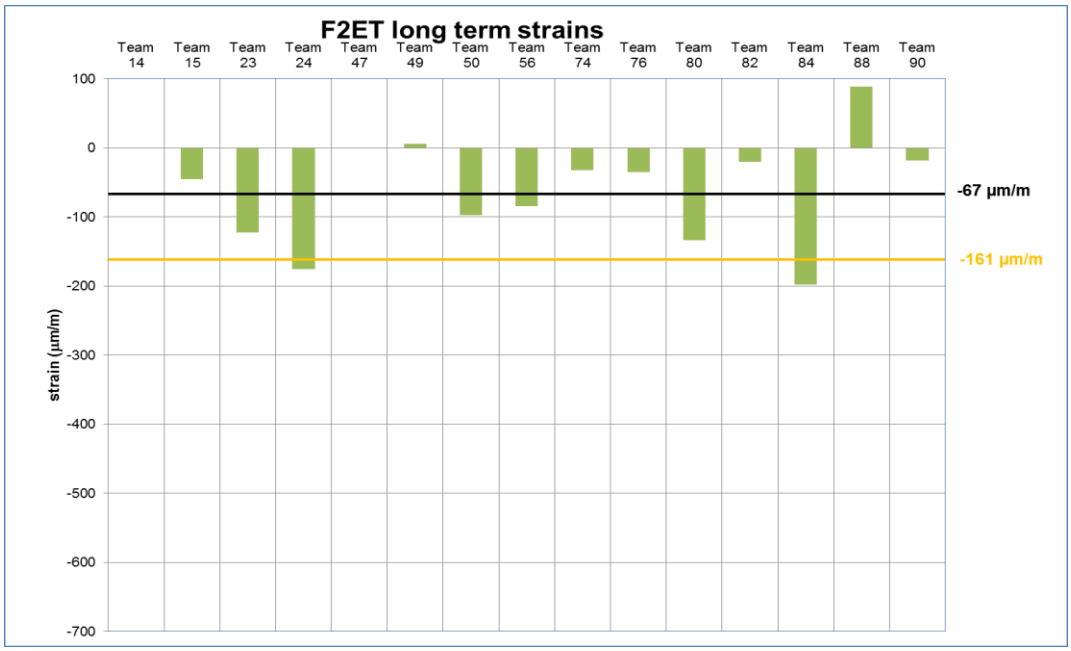

Figure 44. Delayed strain results comparison: Gusset – Tangential direction – Top – Intrados

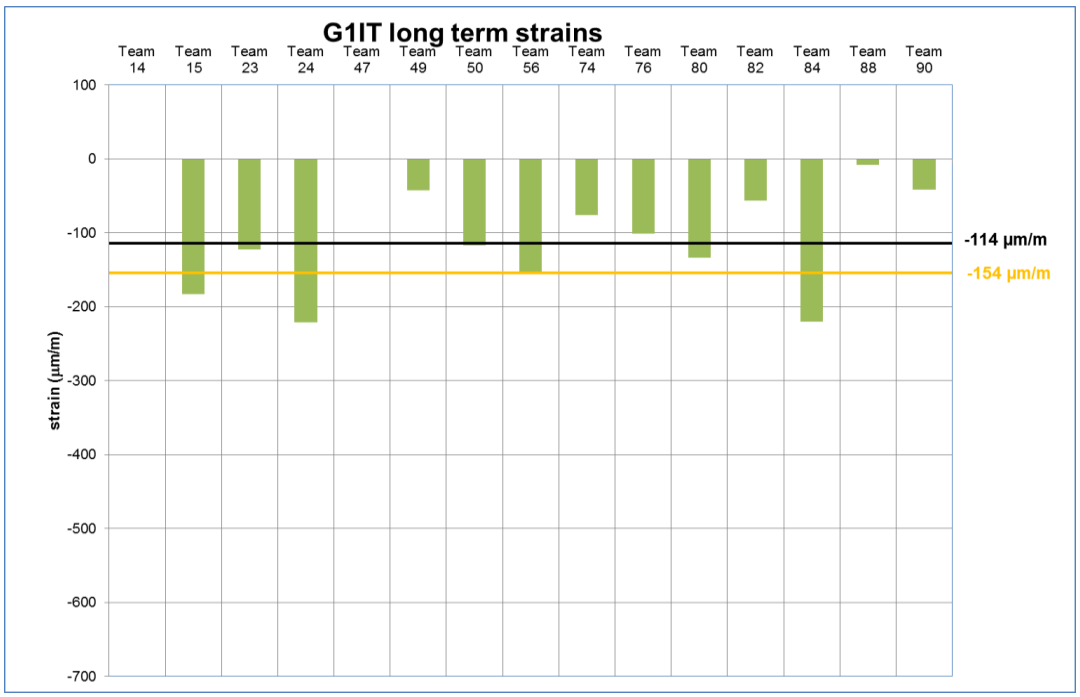

Figure 45. Delayed strain results comparison: Gusset – Tangential direction – Top – Extrados

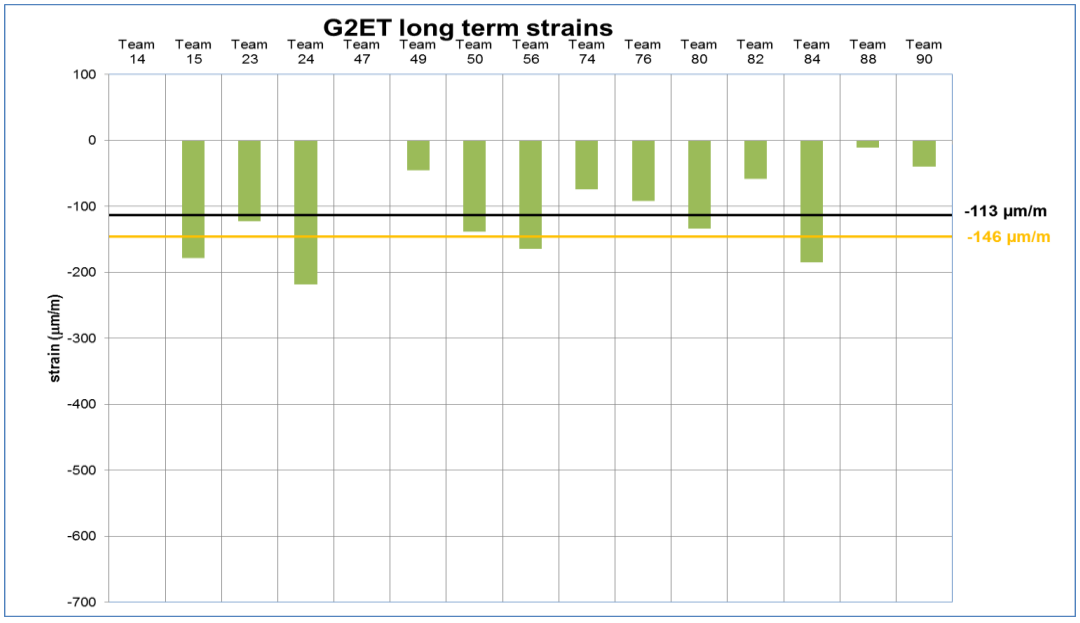

5.3.4.2.3 Comments

Thirteen teams gave results for the gusset area.

In the vertical direction, all teams except three – 74, 80 and 84 – show higher strains on the intrados – as it is observed in the measurements.

In the tangential direction, almost all the teams saw the same level of strain on the intrados and on the extrados for both the bottom and the upper part of the gusset, while the experimental measurements show a difference between intrados and extrados for the bottom part of the gusset.

It can be noted that for both directions, the mean value is closer to the experimental value for the upper part of the gusset. The results are also less scattered in the upper part of the gusset. This could be due to the fact that the behaviour of the upper part is less dependent on the choice of boundary conditions in the numerical models to represent this specific area of the containment.

5.3.4.3 Cylindrical wall strain evolution

5.3.4.3.1 Vertical direction

Figure 46. Delayed strain results comparison: Cylindrical part – Vertical direction – Extrados

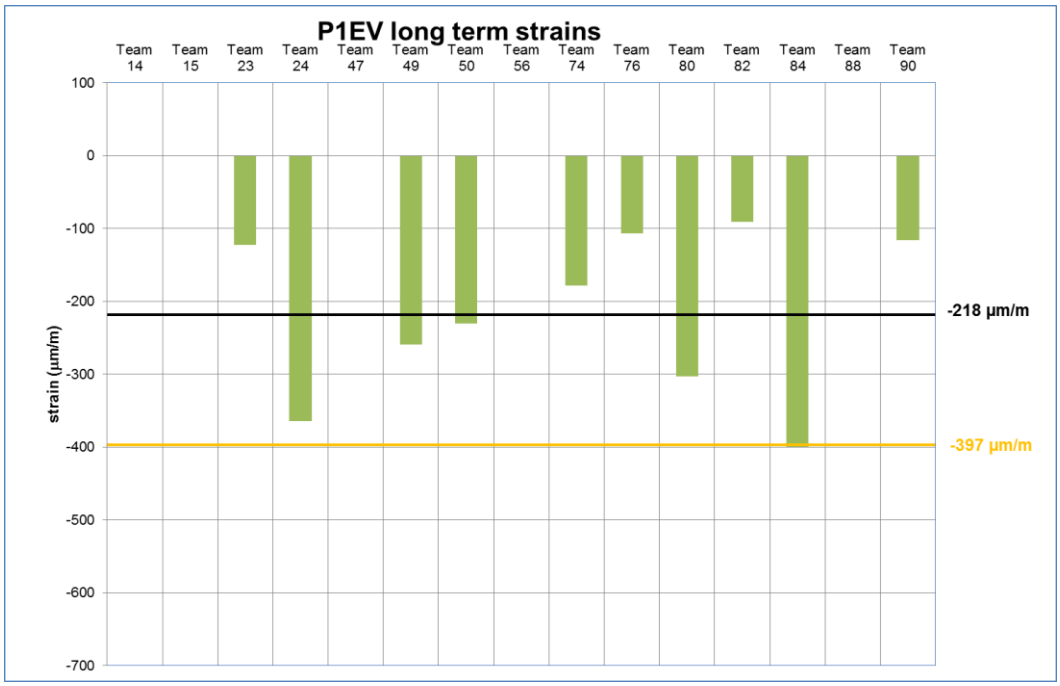

Figure 47. Delayed strain results comparison: Cylindrical part – Vertical direction – Intrados

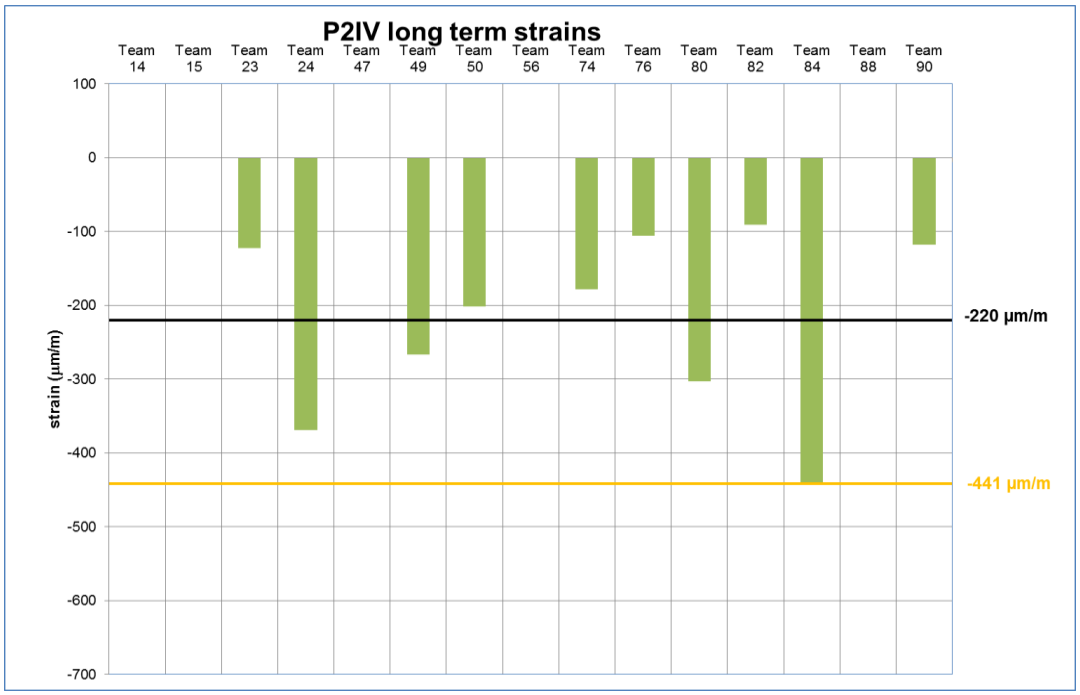

Figure 48. Delayed strain results comparison: Cylindrical part – Vertical direction – Extrados

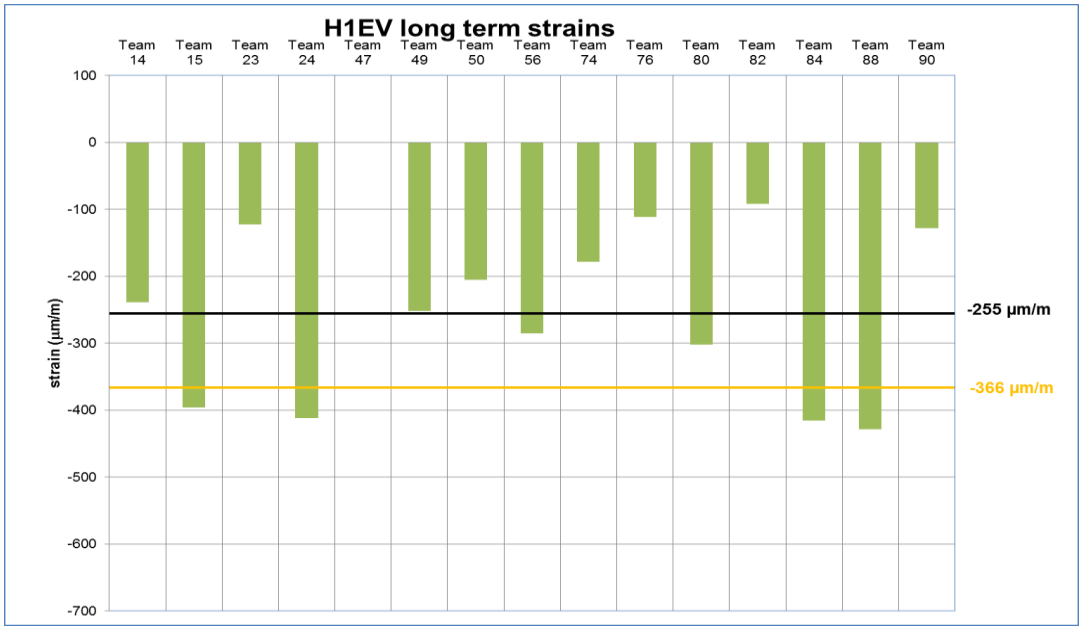

Figure 49. Delayed strain results comparison: Cylindrical part – Vertical direction – Intrados

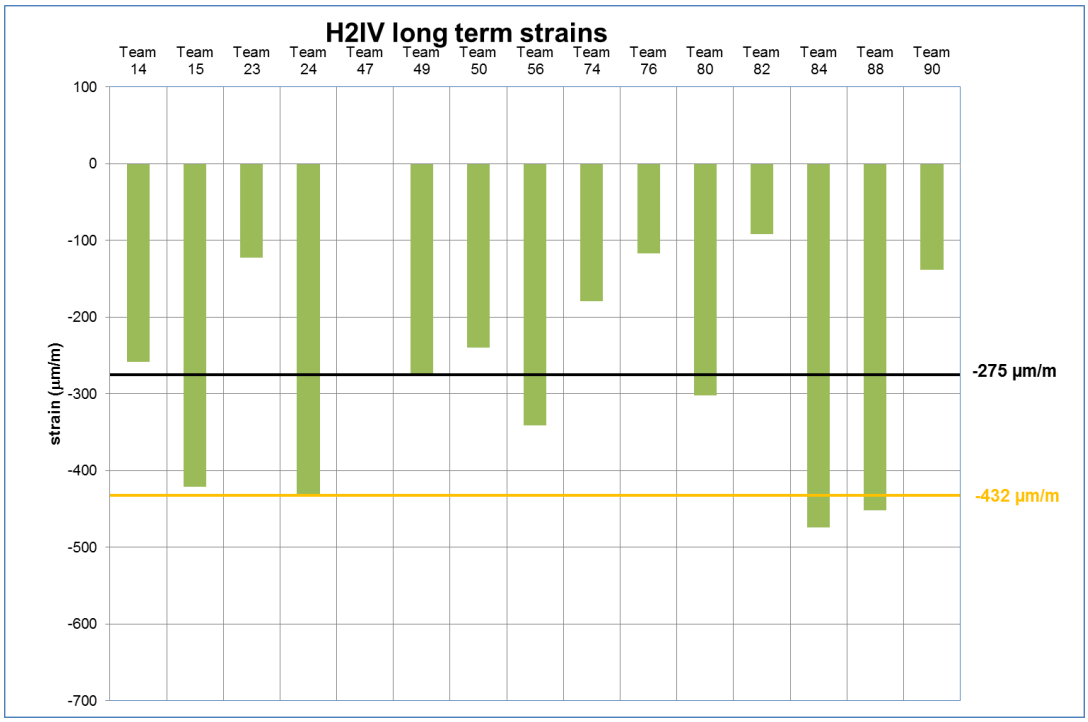

Figure 50. Delayed strain results comparison: Cylindrical part – Vertical direction – Extrados

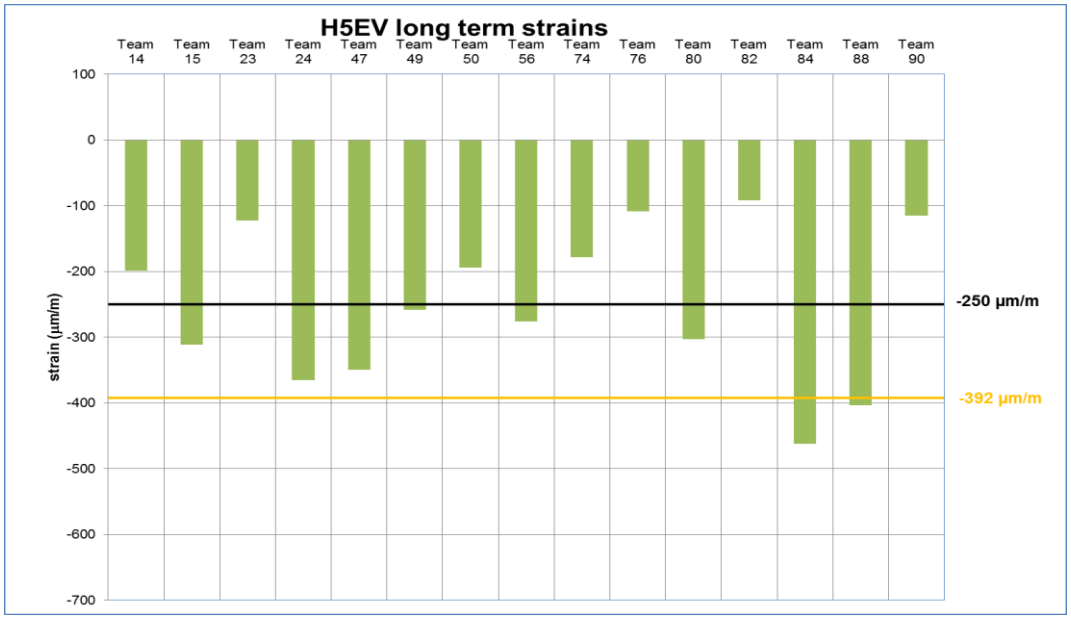

Figure 51. Delayed strain results comparison: Cylindrical part – Vertical direction – Intrados

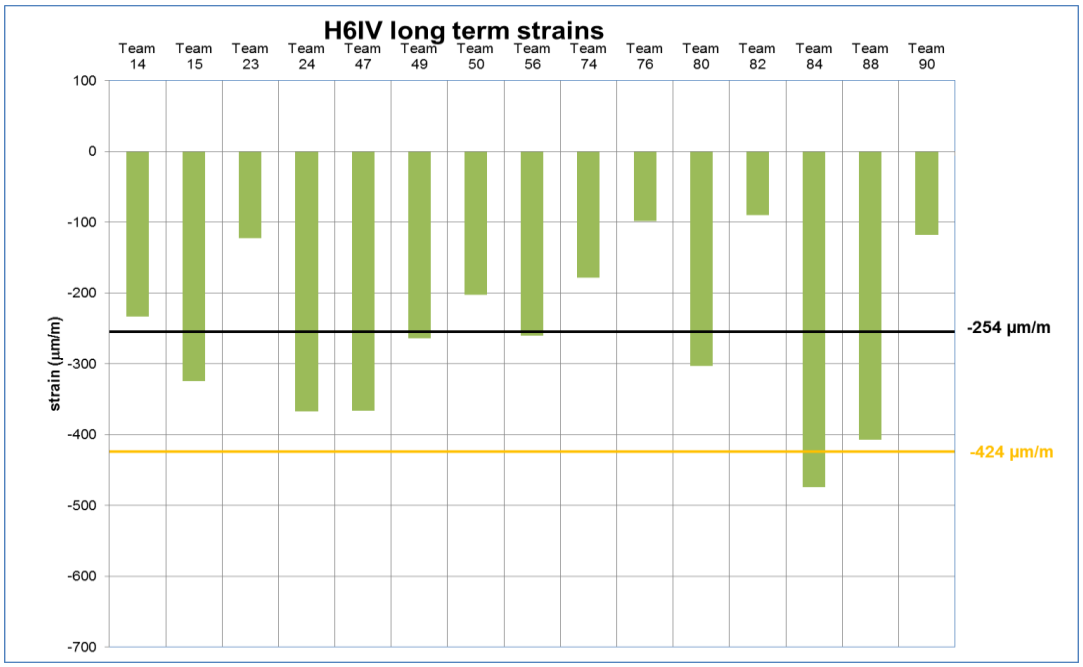

5.3.4.3.2 Tangential direction

Figure 52. Delayed strain results comparison: Cylindrical part – Tangential direction – Extrados

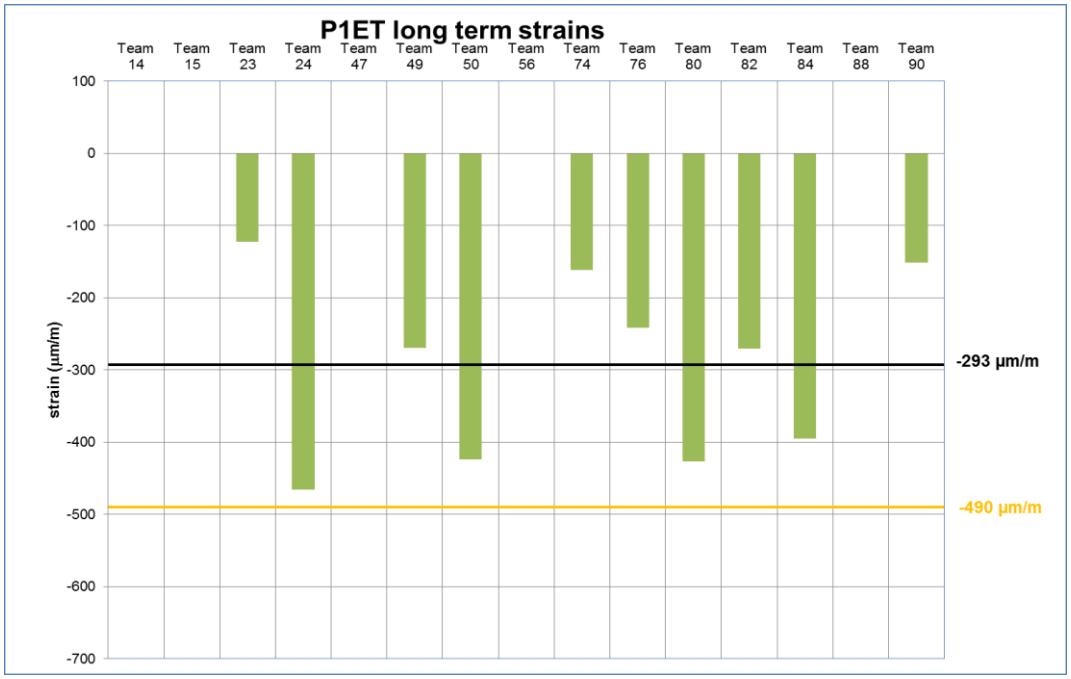

Figure 53. Delayed strain results comparison: Cylindrical part – Tangential direction – Intrados

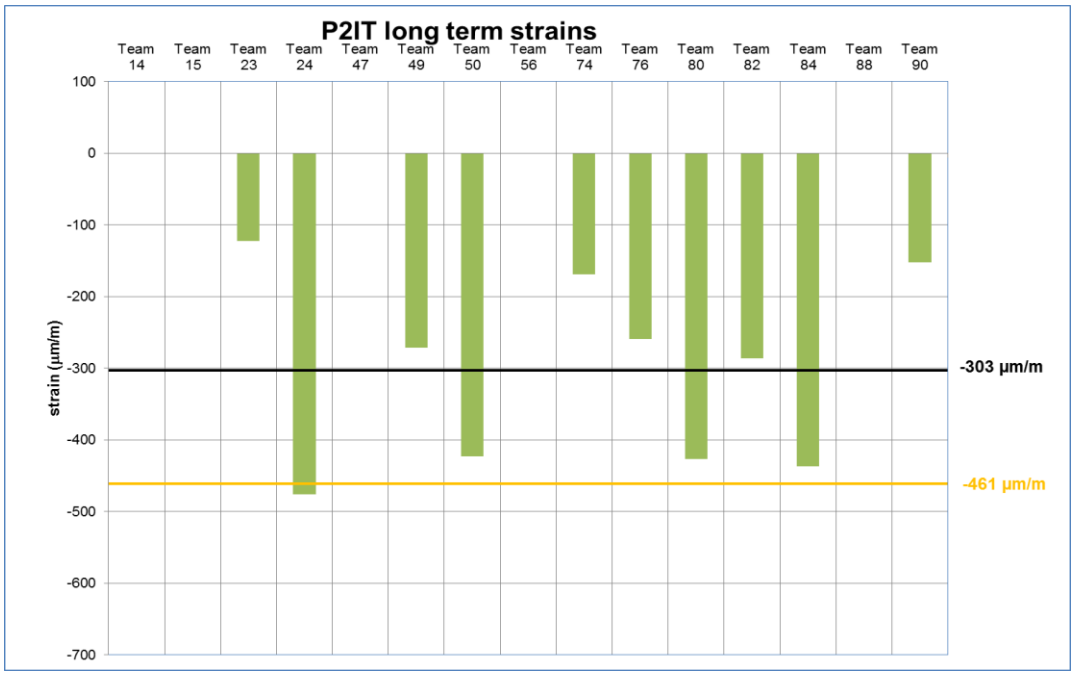

Figure 54. Delayed strain results comparison: Cylindrical part – Tangential direction – Extrados

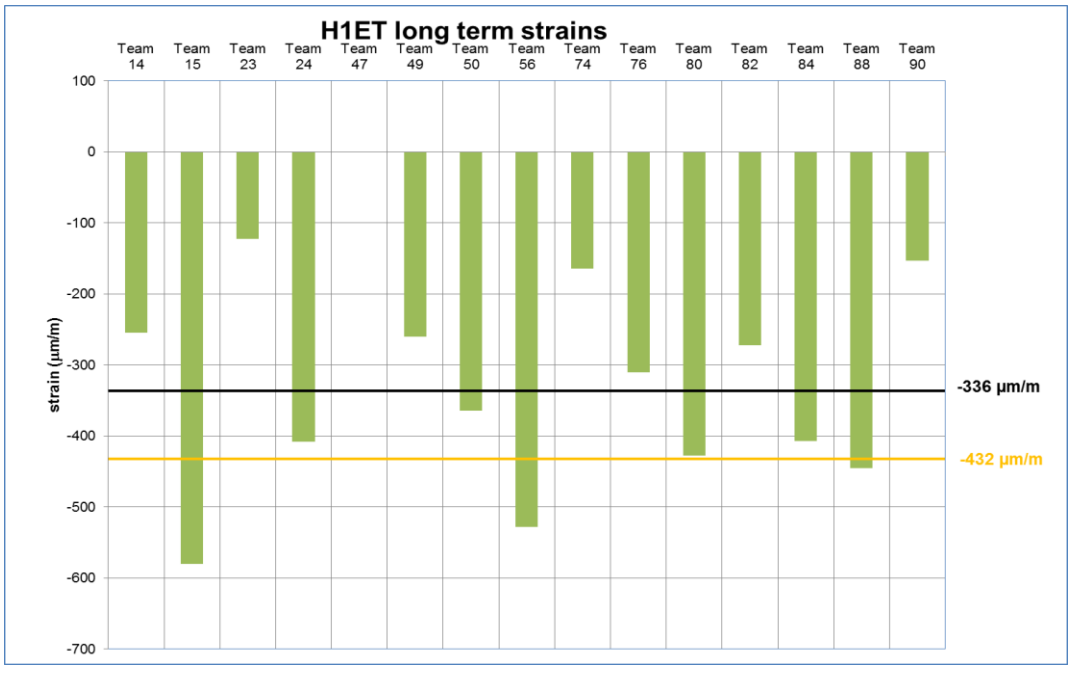

Figure 55. Delayed strain results comparison: Cylindrical part – Tangential direction – Intrados

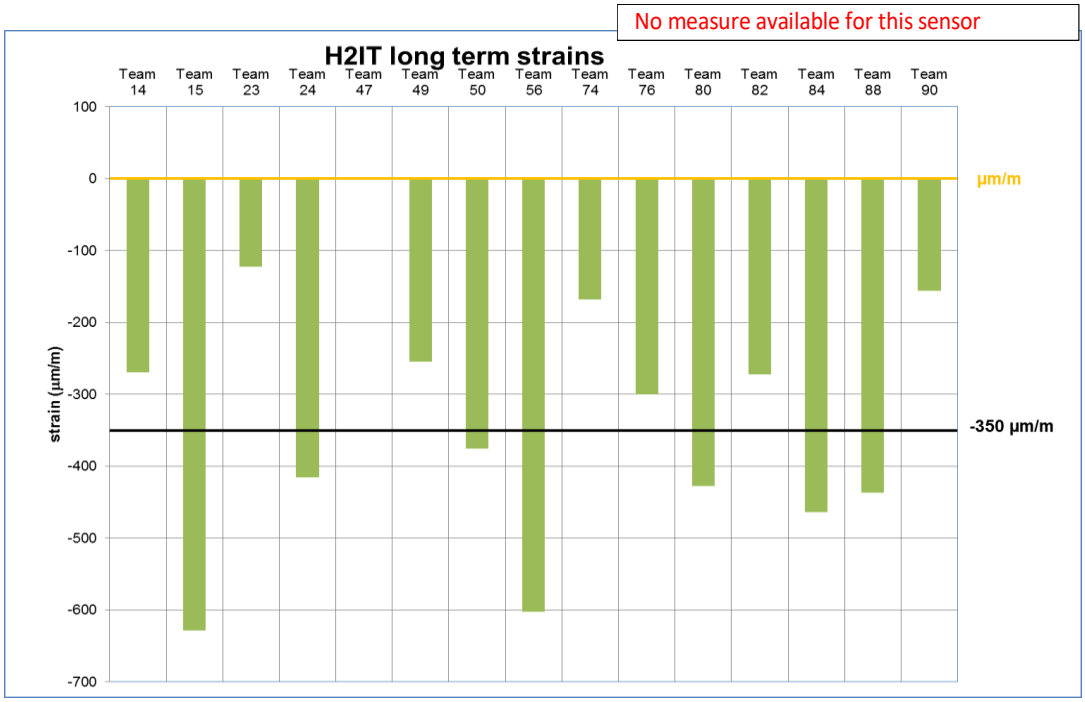

Figure 56. Delayed strain results comparison: Cylindrical part – Tangential direction – Extrados

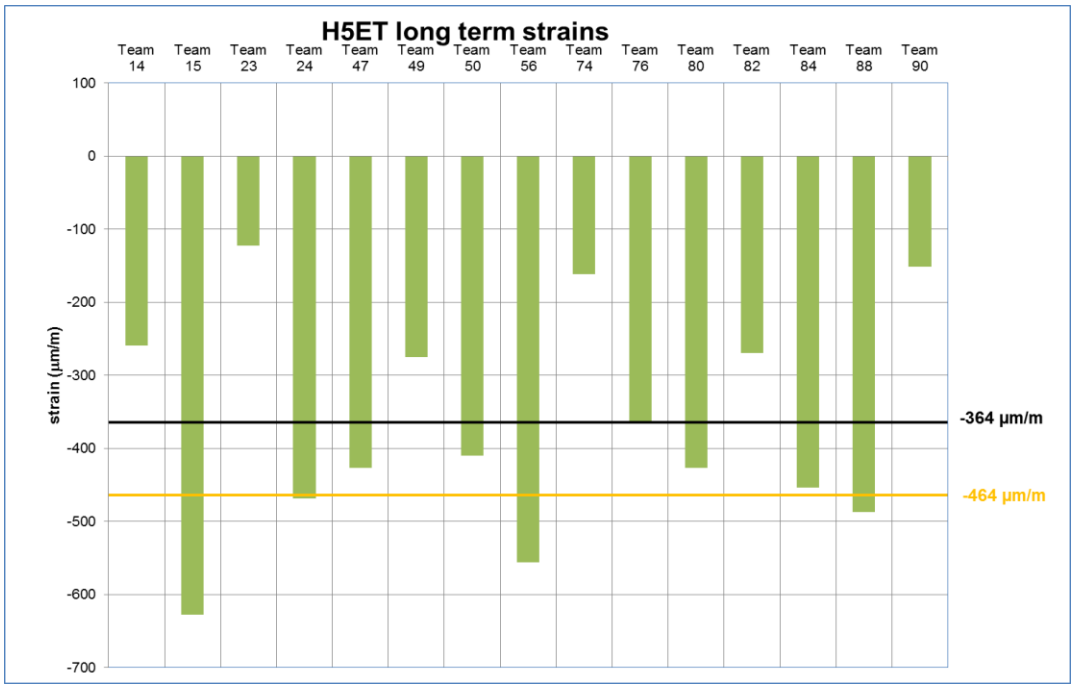

Figure 57. Delayed strain results comparison: Cylindrical part – Tangential direction – Intrados

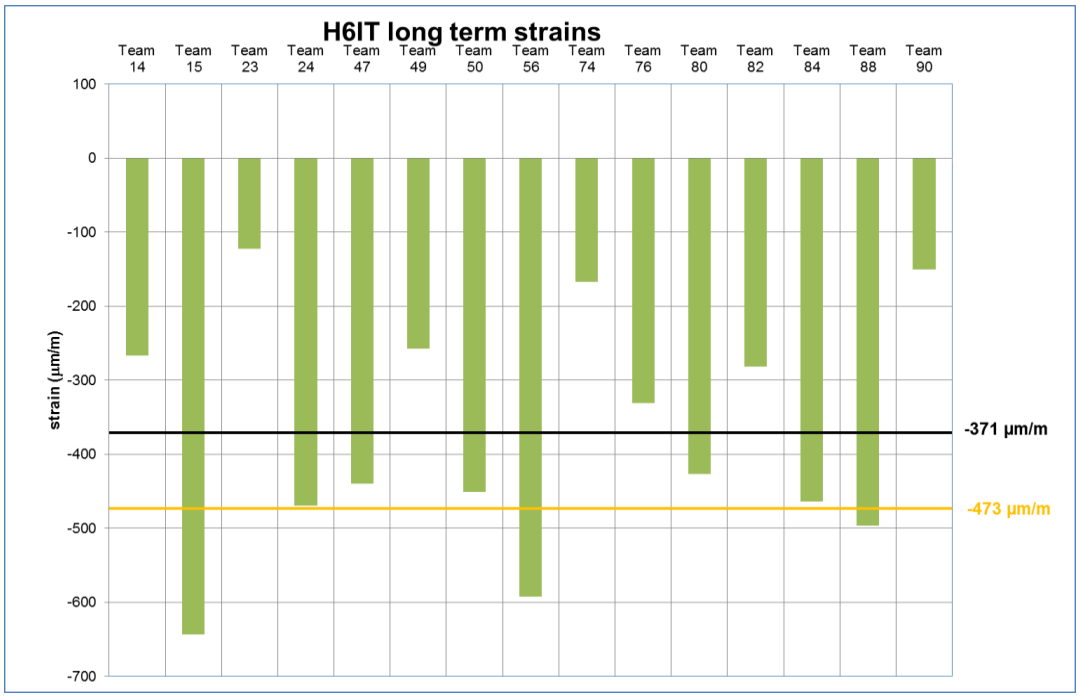

5.3.4.3.3 Comments

For the cylinder part at mid-height, ten participants gave results for sensor positions P1 and P2 and all teams gave results for sensor positions H1, H2, H5 and H6.

In both directions, the results are less scattered than in the previous areas: raft and gusset.

In the vertical direction, the teams' results show equal strain values on the extrados and intrados of the wall for a height of 8.00 m (sensors P1, P2, H5 and H6) as it is observed in the experimental measurements. For sensors H1 and H2 that are not exactly at the same height (8.43 m), experimental strain values are different for the two sides of the wall (about 70 µm/m). All of the teams gave results showing this differential deformation corresponding to the bending moment.

In the horizontal direction, the teams' results show equal strain values on the extrados and intrados of the wall as it is observed on measurements for the sensors P1, P2, H5 and H6.

For this area, some good results can be highlighted and the quality of individual results compared to the experimental values can be appreciated.

Table 19. Quality of the predictions compared to the experimental values

Appreciation of the quality of predictions	Teams
Good predictions in both directions and on numerous sensors	24, 47, 84 and 88
Good predictions in only one direction or only in some sensors	15, 50, 56 and 80
Predictions distant from experimental values in both directions in almost all sensors	14, 49, 76 and 82
Predictions very distant from experimental in all sensors and very much below average values	23, 74 and 90

5.3.4.4 Equipment hatch strain evolution

5.3.4.4.1 Side of the hatch

Figure 58. Delayed strain results comparison: Side of the hatch – Vertical – Extrados

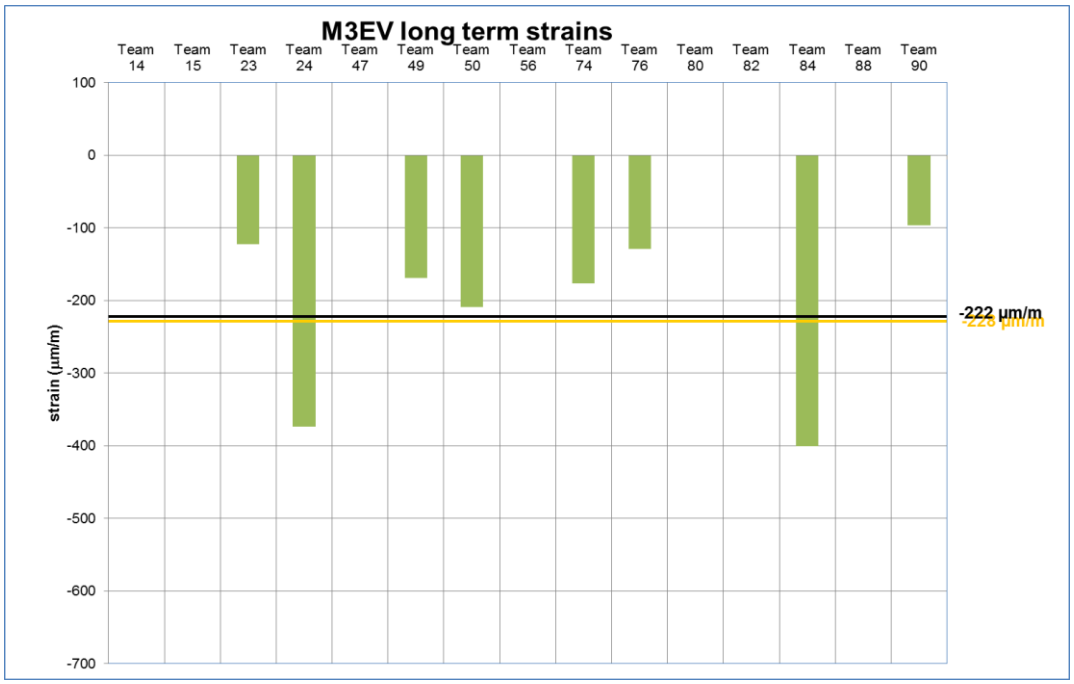

Figure 59. Delayed strain results comparison: Side of the hatch – Tangential – Extrados

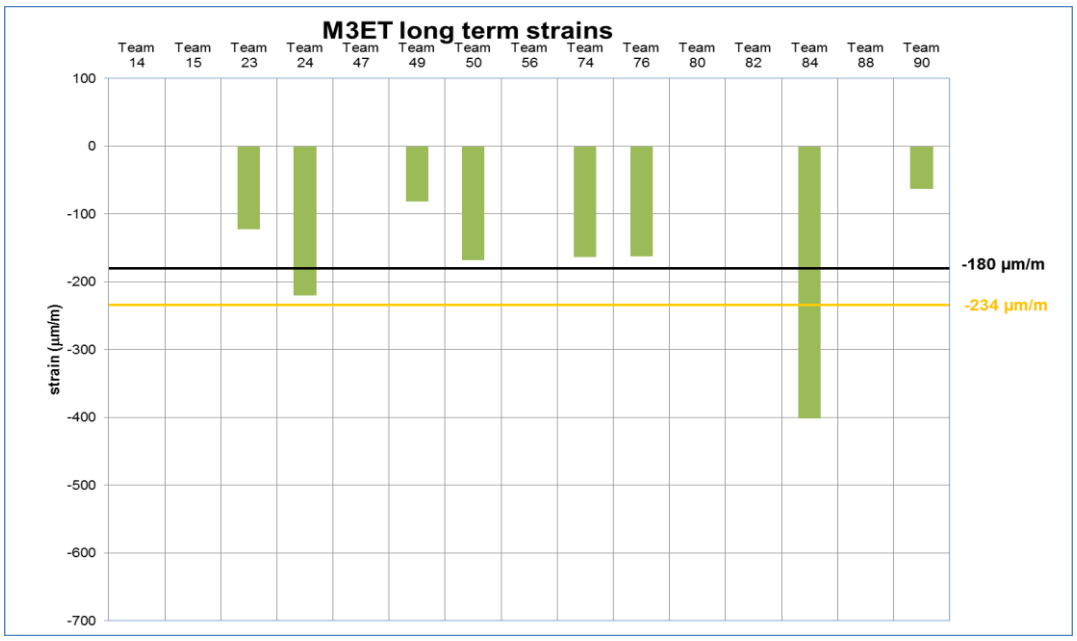

Figure 60. Delayed strain results comparison: Side of the hatch – Vertical – Intrados

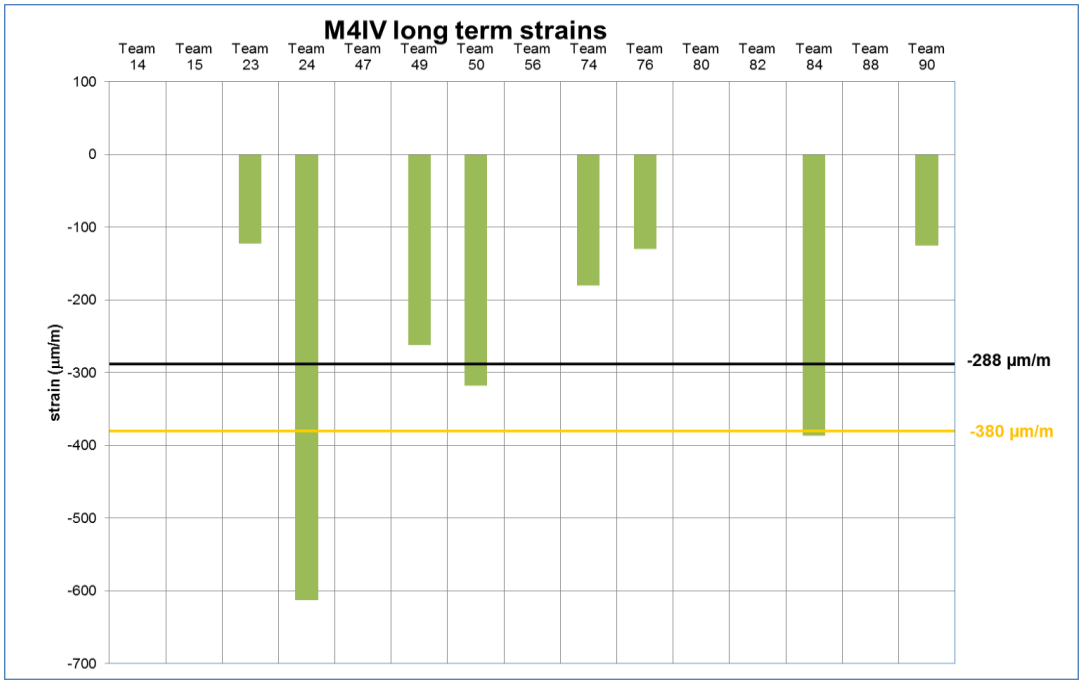

Figure 61. Delayed strain results comparison: Side of the hatch – Tangential – Intrados

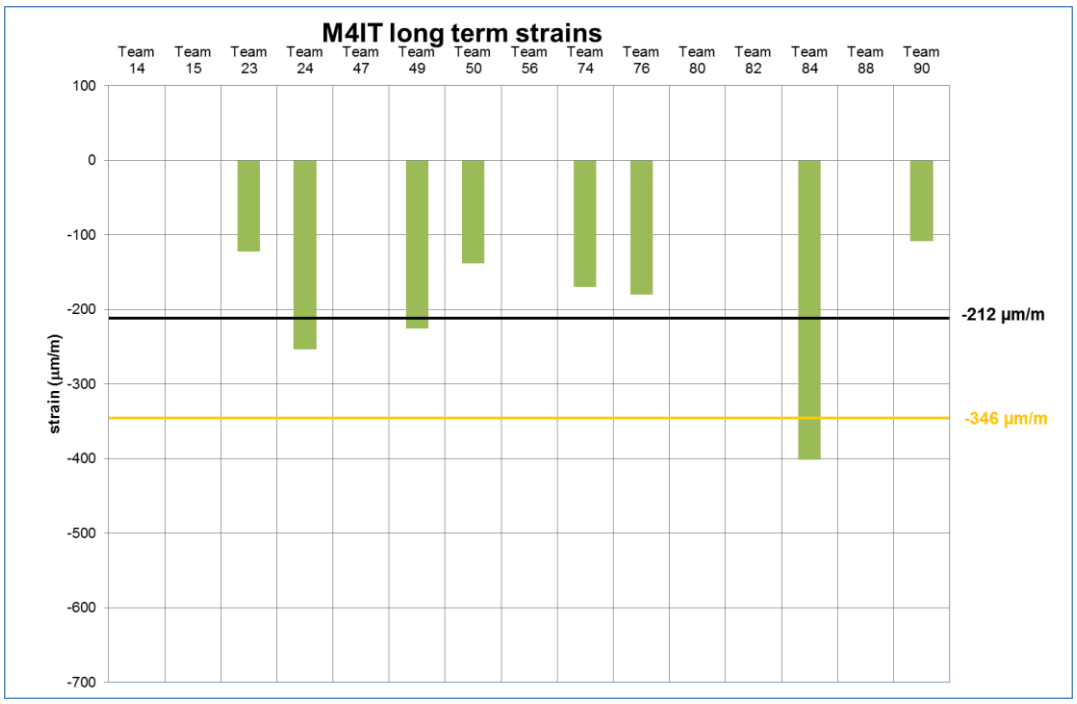

5.3.4.4.2 Above the hatch

Figure 62. Delayed strain results comparison: Above the hatch – Vertical – Extrados

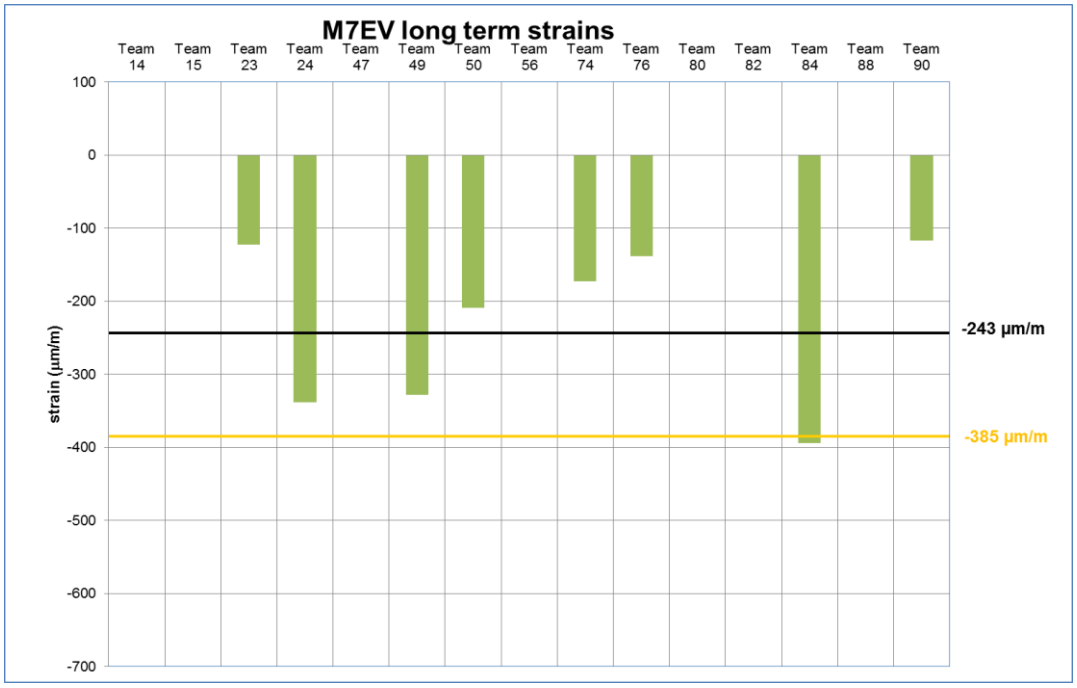

Figure 63. Delayed strain results comparison: Above the hatch – Tangential – Extrados

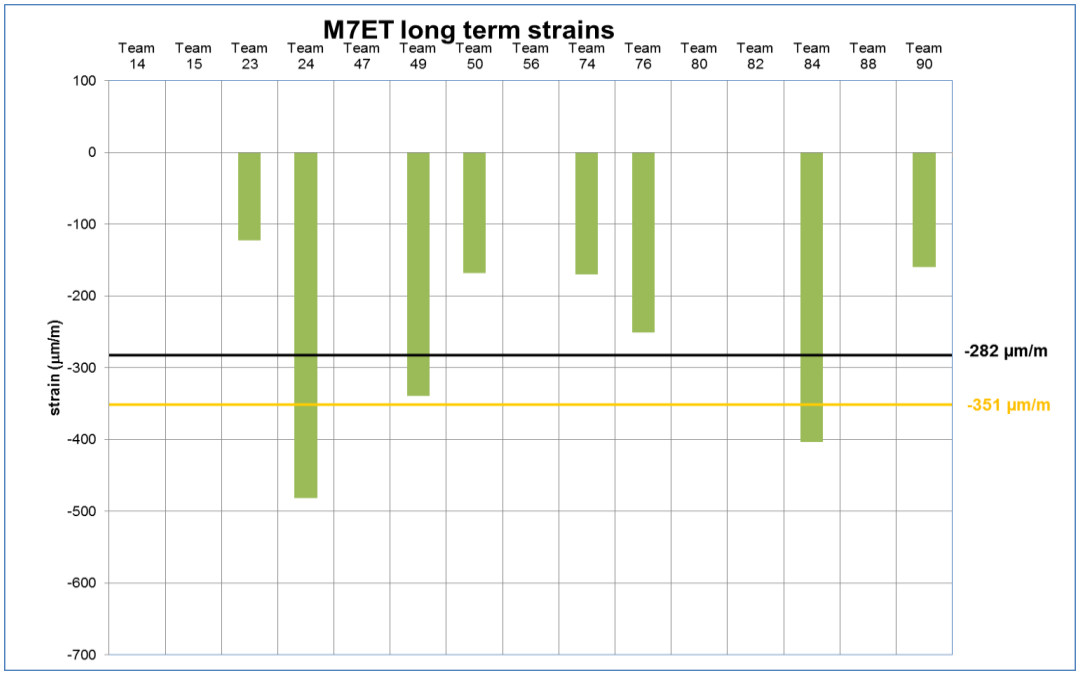

Figure 64. Delayed strain results comparison: Above the hatch – Vertical – Intrados

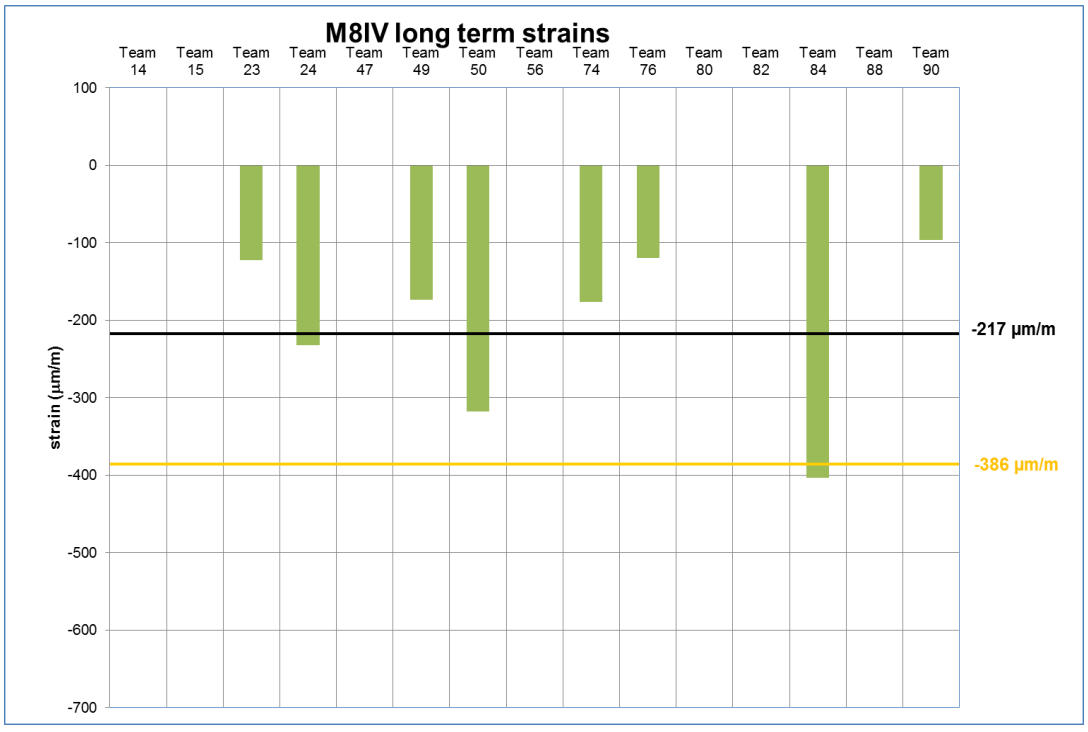

Figure 65. Delayed strain results comparison: Above the hatch – Tangential – Intrados

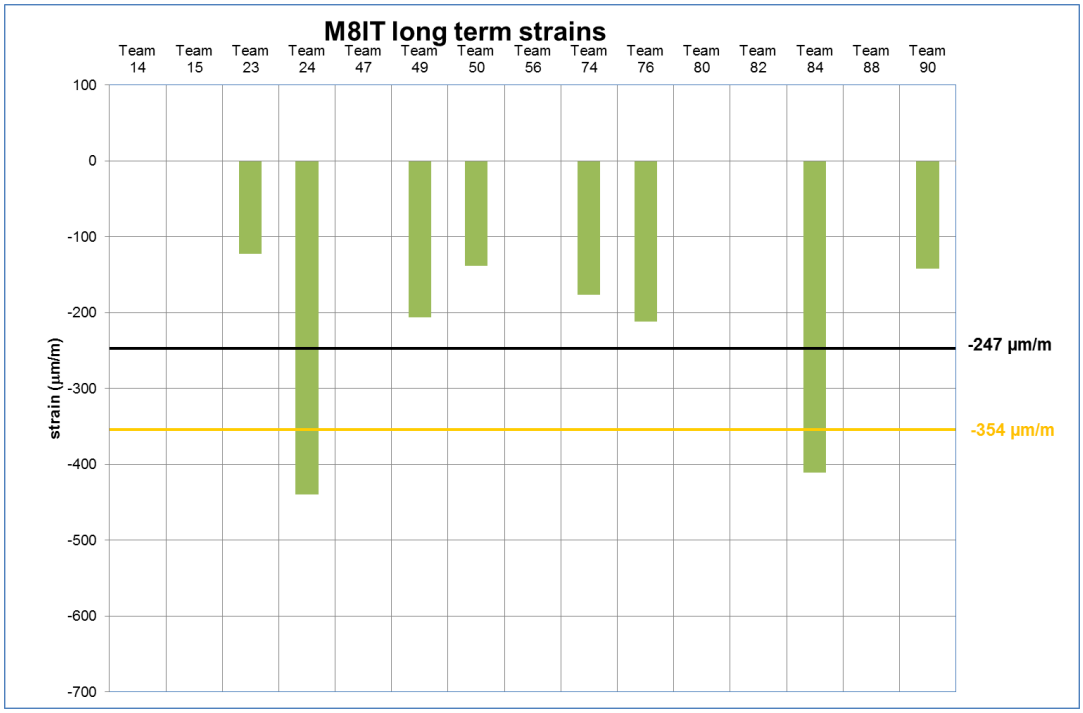

5.3.4.4.3 Comments

Only eight teams provided some results for this part of the containment.

The results are only slightly scattered. Team 84 and on some points Team 24 gave the highest values. Teams 23 and 90 gave the smallest values on each point and each direction around the hatch.

On the side of the hatch, on average, teams predicted vertical strains close to strains given in the current part. In the tangential direction, on average, the predicted strains are almost divided by two compared to the strains given in the current part, representing the effect of a low prestressing in this direction close to the hatch. In both directions, experimental strains are higher on intrados than on extrados. All teams found this result except Teams 50 and 84.

Above the hatch, results are more distant from the experimental values except for Team 84, which gave good predictions. With the exception of Teams 50 and 74, all teams predict higher strains in the tangential direction than in the vertical direction. Experimental values show the opposite.

5.3.4.5 Dome strain evolution

5.3.4.5.1 Results

Figure 66. Delayed strain results comparison: Top of the dome – Extrados (194 Gr)

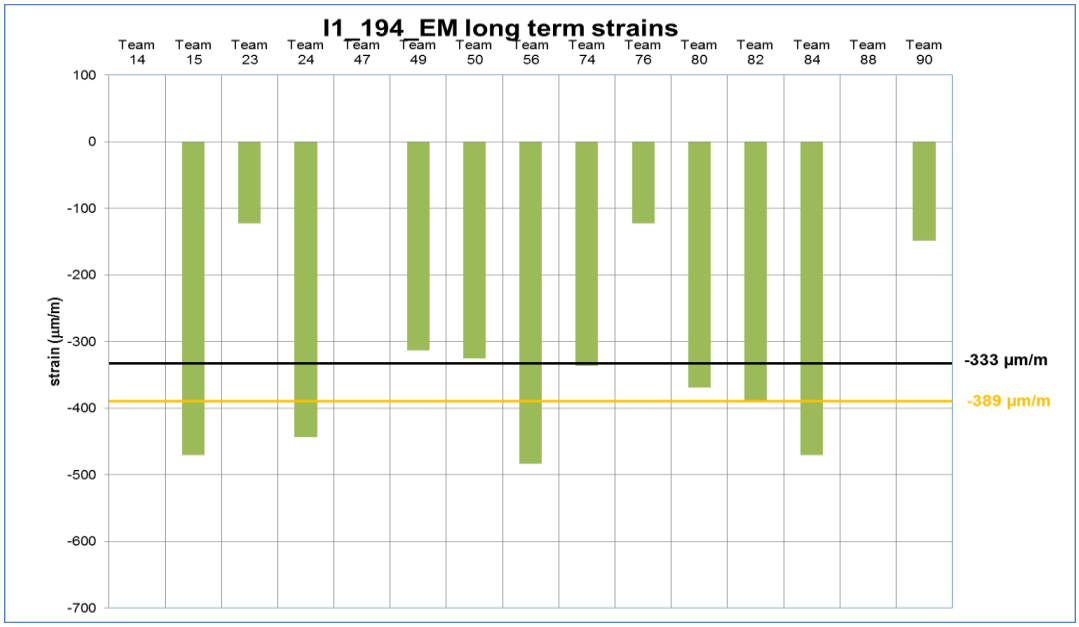

Figure 67. Delayed strain results comparison: Top of the dome – Extrados (94 Gr)

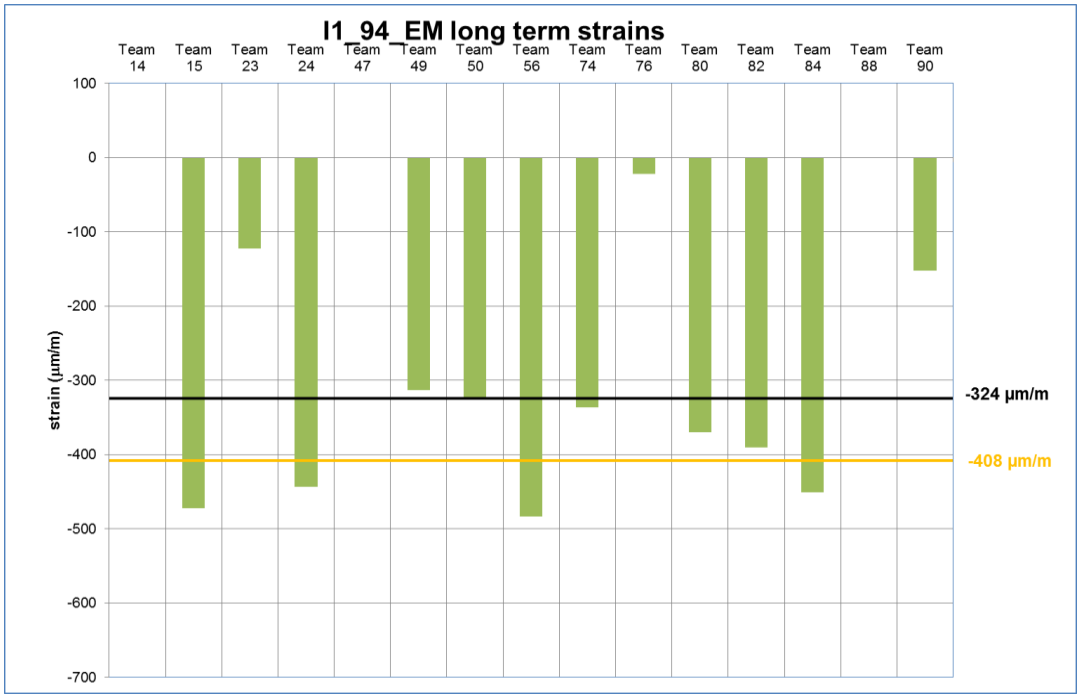

Figure 68. Delayed strain results comparison: Top of the dome – Intrados (194 Gr)

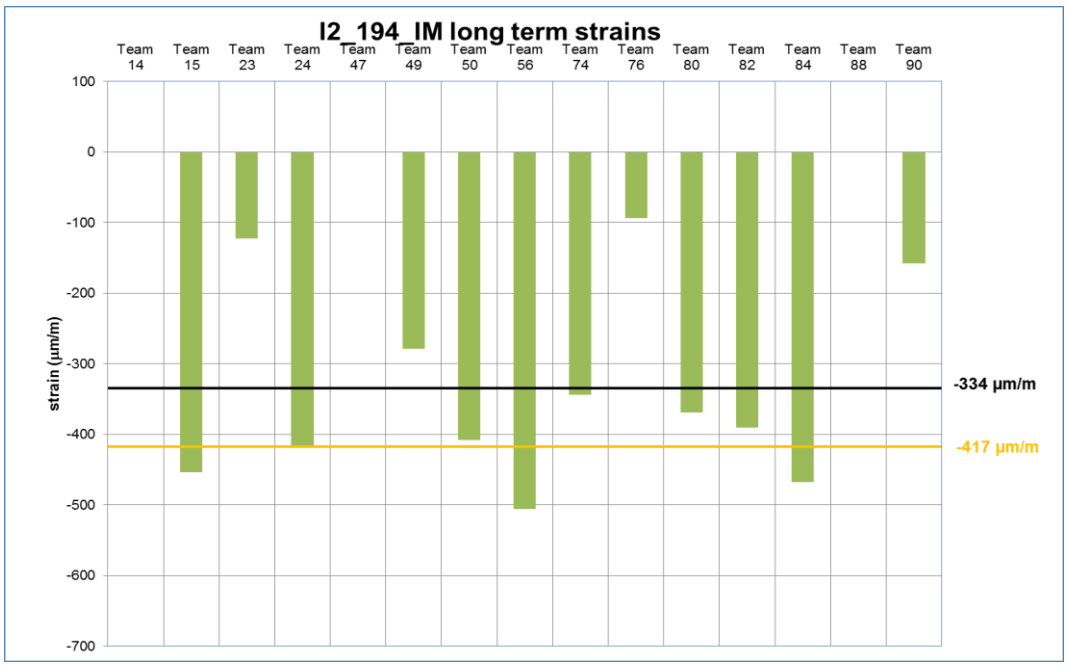

Figure 69. Delayed strain results comparison: Top of the dome – Intrados (94 Gr)

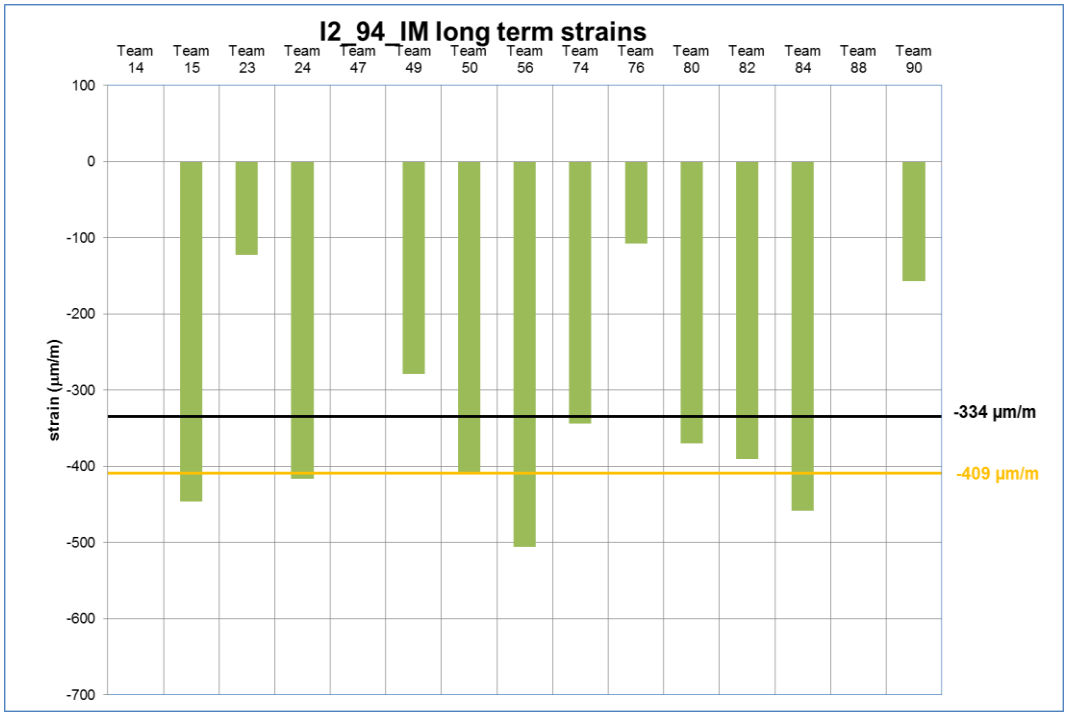

Figure 70. Delayed strain results comparison: Meridian part of the dome – Meridian direction – Extrados

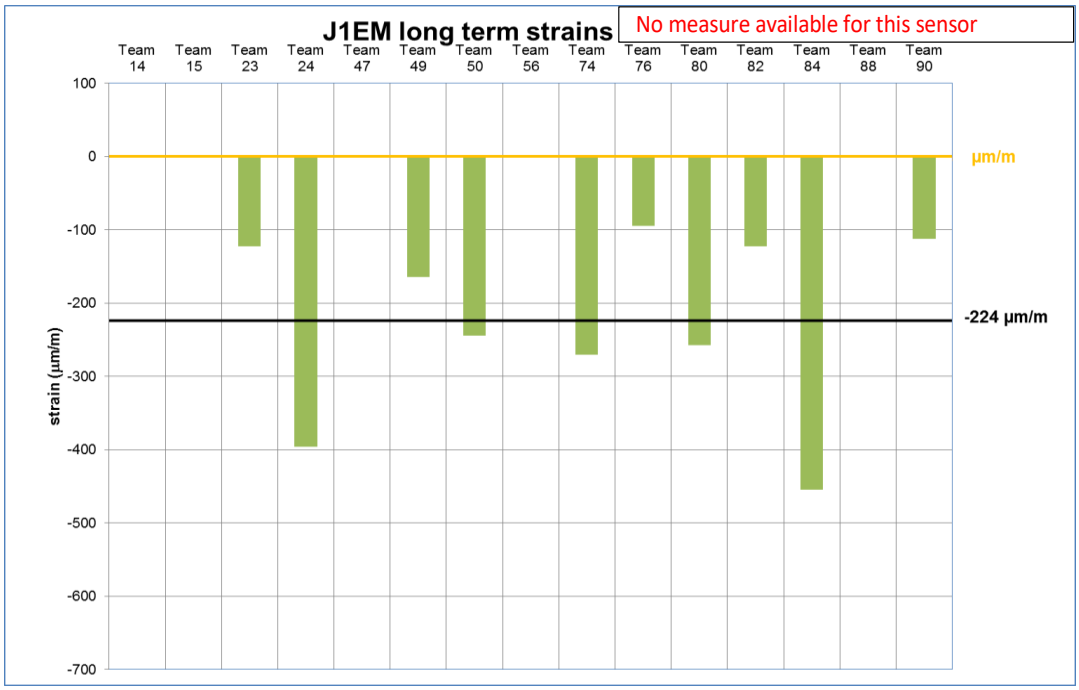

Figure 71. Delayed strain results comparison: Meridian part of the dome – Tangential direction – Extrados

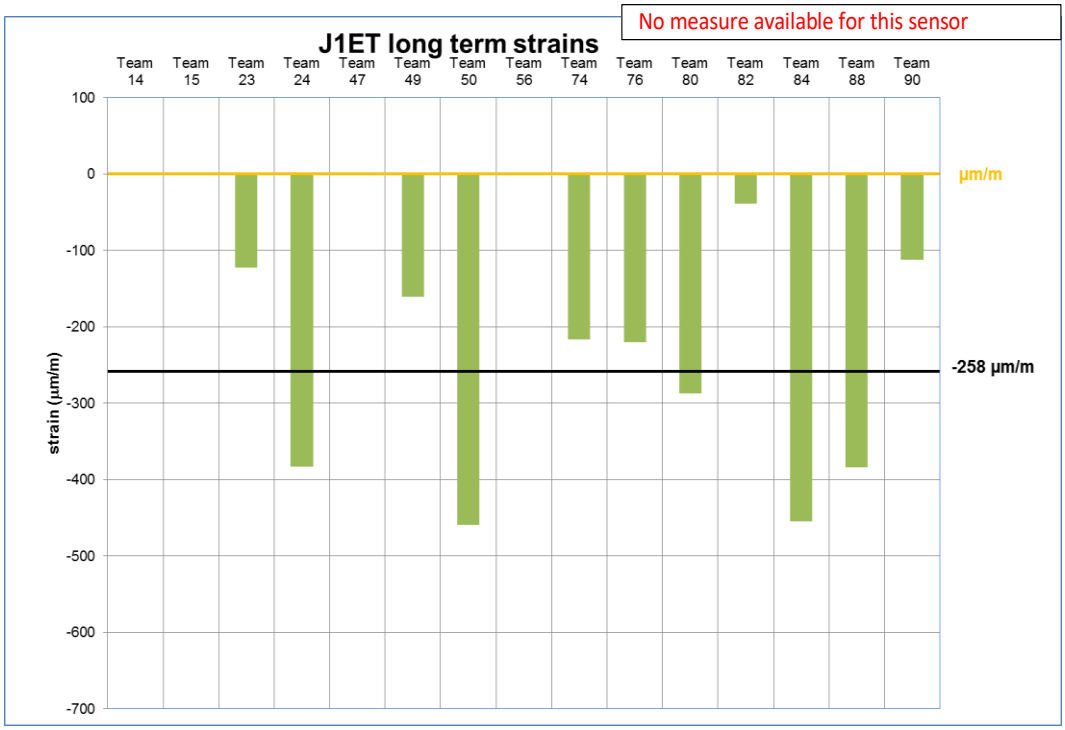

Figure 72. Delayed strain results comparison: Meridian part of the dome – Meridian direction – Intrados

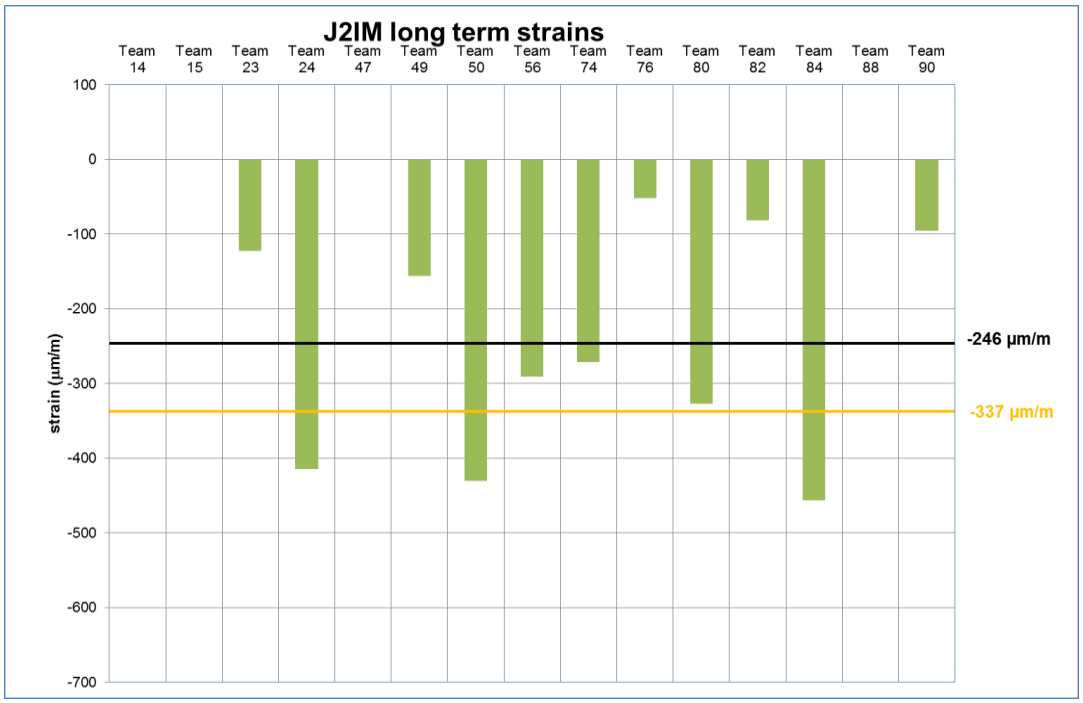

Figure 73. Delayed strain results comparison: Meridian part of the dome – Tangential direction – Intrados

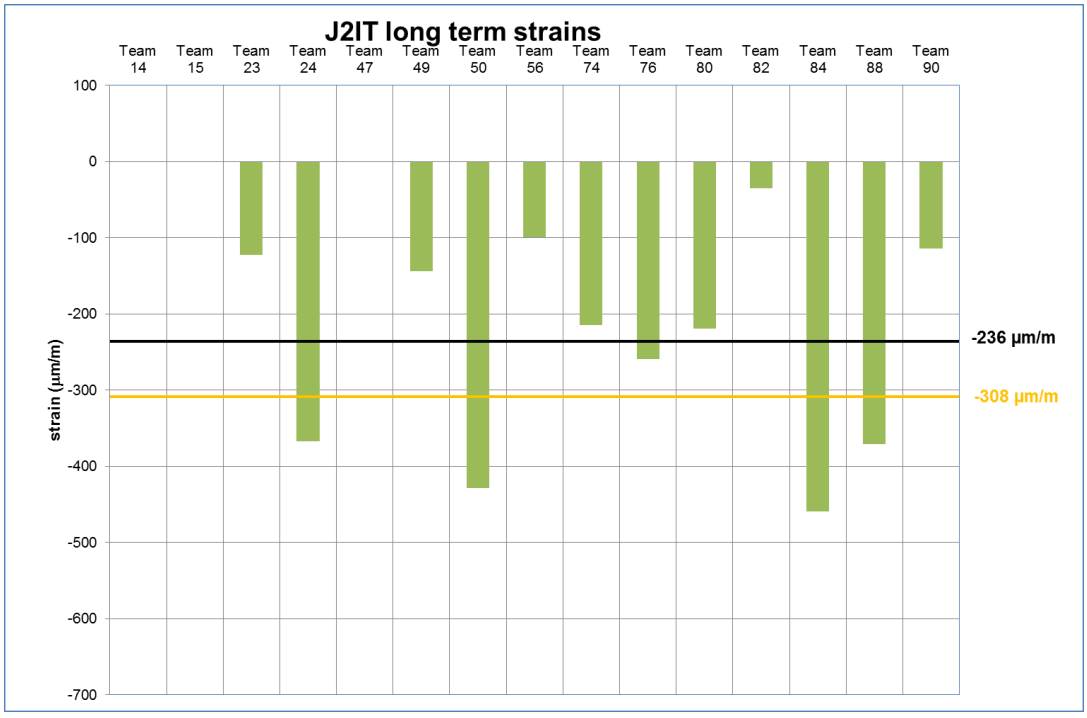

5.3.4.5.2 Comments

For the dome, 12 teams gave results.

For the top of the dome, the results are not very scattered and close to the experimental values, except for Teams 76 and 90, which gave very small values. This part of the dome is well represented by the numerical models.

For the meridian part, the results are more scattered. Team 76 (in the meridian direction), Team 82 and Team 90 gave very small values compared to the experimental ones.

5.3.4.6 Synthesis regarding delayed strains

Concerning delayed strains given by participants, all of the values are underestimated in comparison with the experimental values and on average the distance is about 30%. This value seems high, but it is important to keep in mind that the experimental values are total strains which include thermal effects.

It can be interesting to compare the different areas of the mock-up. Figure 74 gives the average distance between numerical and experimental results for each sensor. It corresponds to the ratio of the distance between numerical value and experimental value to the experimental value. It is given in per cent.

It can be noted that the raft, the gusset and the hatch are the areas where the numerical and experimental values are the most distant.

Figure 74. Delayed strains: Representation of the average distance between numerical and experimental results per zone

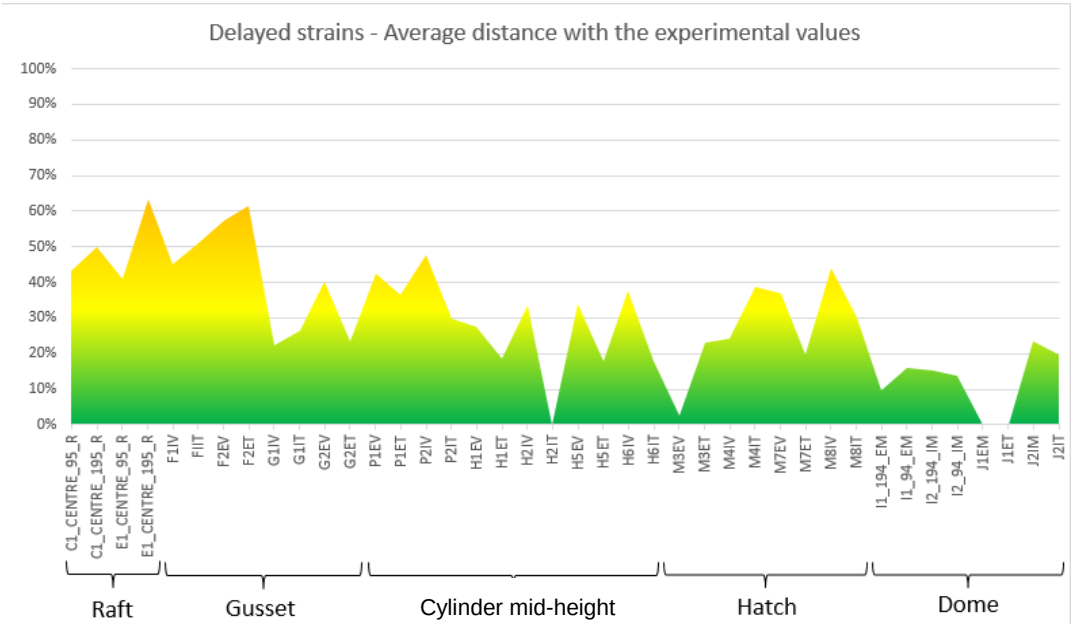

In order to compare results among participants, it is possible to calculate a dispersion by the ratio of standard deviation to mean value. The result is given in per cent (Figure 75).

The dispersion is the lowest in the cylinder part and the top of the dome. For the other areas, dispersion is more important in ascending order in the meridian part of the dome and around the hatch, then in the upper level of the gusset, and finally in the bottom of the gusset and the raft.

Figure 75. Delayed strains: Representation of participants' results dispersion per zone

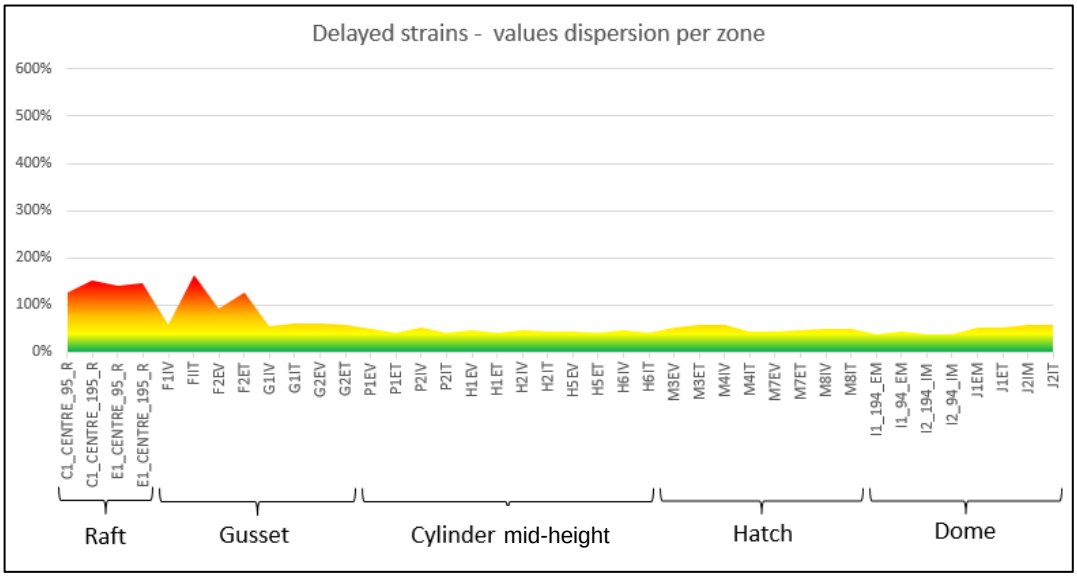

5.3.5. Instantaneous strains during pressurisation tests

The strains represented in this part correspond to strains during the pressurisation tests, representing the effects of inner pressure (between 0 bar relative and 4.2 bar relative) on the mock-up.

The experimental results represented in this part are mechanical strains without thermal effects. The value is represented by a red horizontal line for the VD1 bis test and by a pink horizontal line for the VD2 test.

On the following curves, the mean values of participants' results are represented by green horizontal lines.

Team 82 gave very singular values and far from the expected orders of magnitude. So as not to hinder the comparison of the results of the other teams, their results have been excluded from the analysis in this part.

5.3.5.1 Pressurisation effects in the raft

5.3.5.1.1 Lower level

Figure 76. Instantaneous strain results comparison: Lower part of the raft (95 Grd)

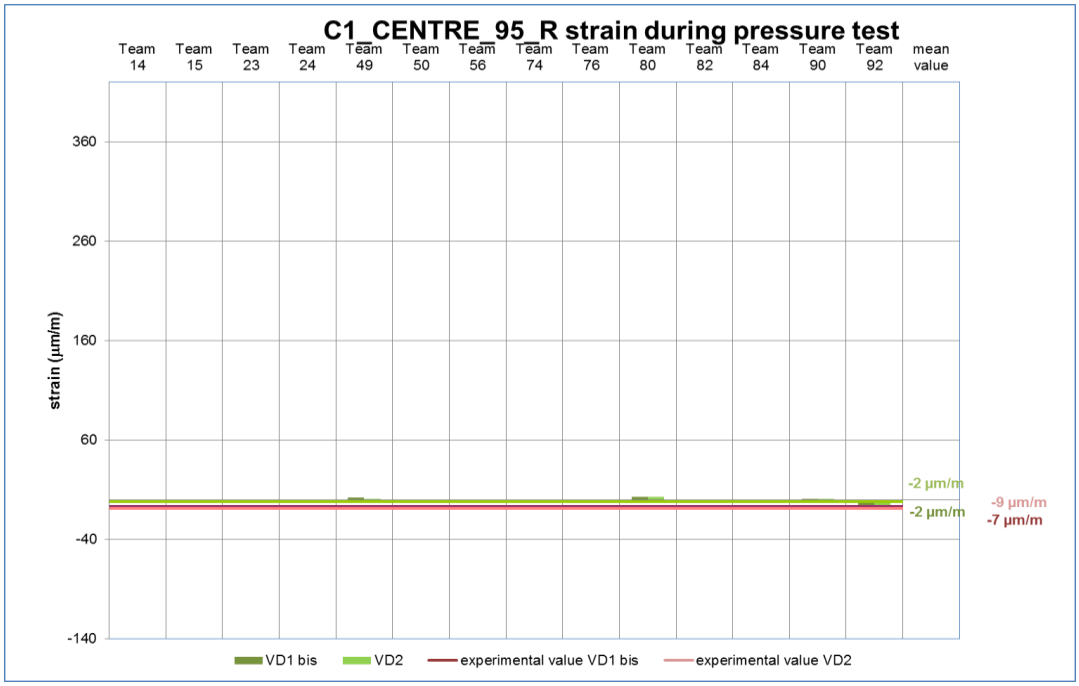

Figure 77. Instantaneous strain results comparison: Lower part of the raft (195 Grd)

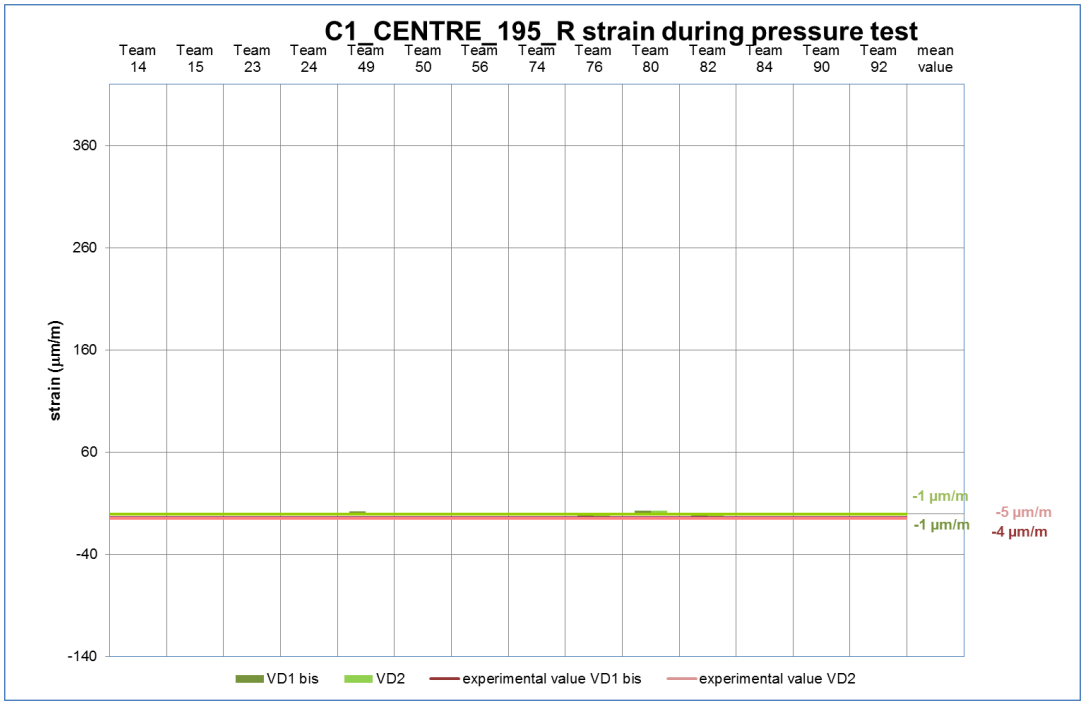

5.3.5.1.2 Upper level

Figure 78. Instantaneous strain results comparison: Upper part of the raft (95 Grd)

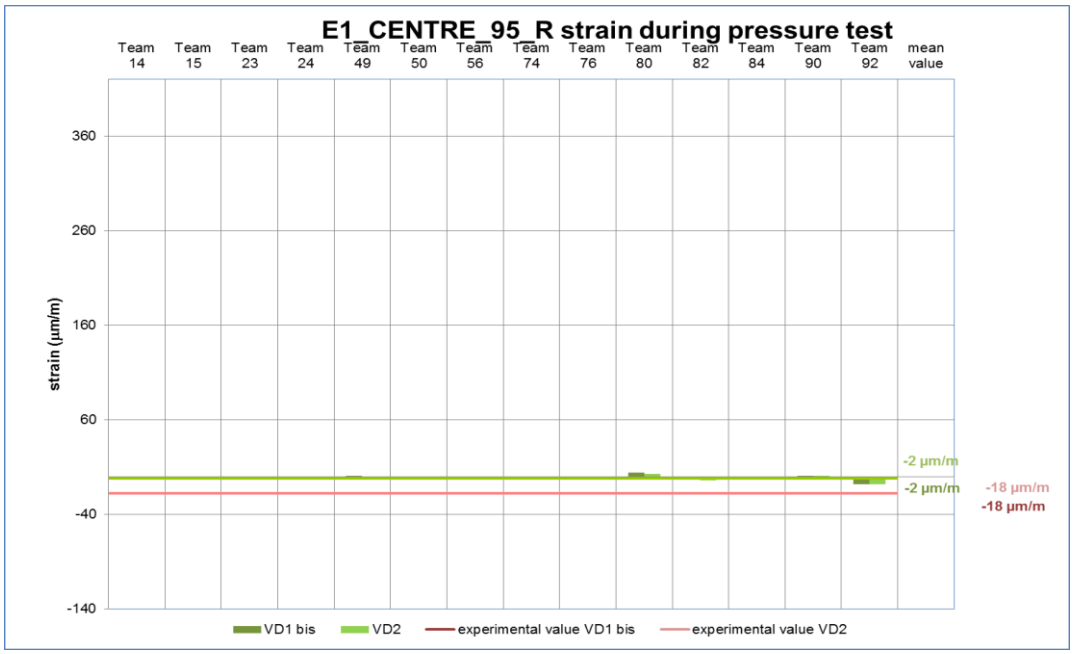

Figure 79. Instantaneous strain results comparison: Upper part of the raft (195 Grd)

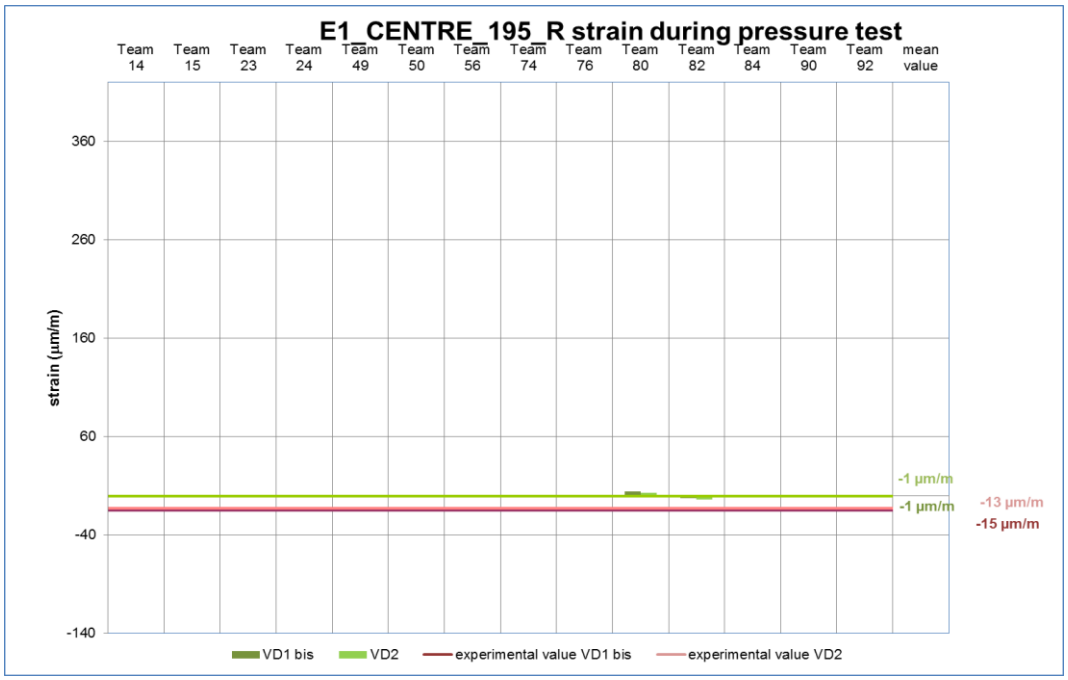

5.3.5.1.3 Comments

Team results gave no strains in the centre of the raft during pressurisation tests, showing that this point is a fixed point in models. It corresponds to the real behaviour of the bottom of the raft as shown by the experimental values. However, measures on the upper level of the raft show a very slight shortening during pressurisation tests, which was not found by the teams.

5.3.5.2 Pressurisation effects in the gusset

5.3.5.2.1 Vertical direction

Figure 80. Instantaneous strain results comparison: Gusset – Vertical direction – Bottom – Intrados

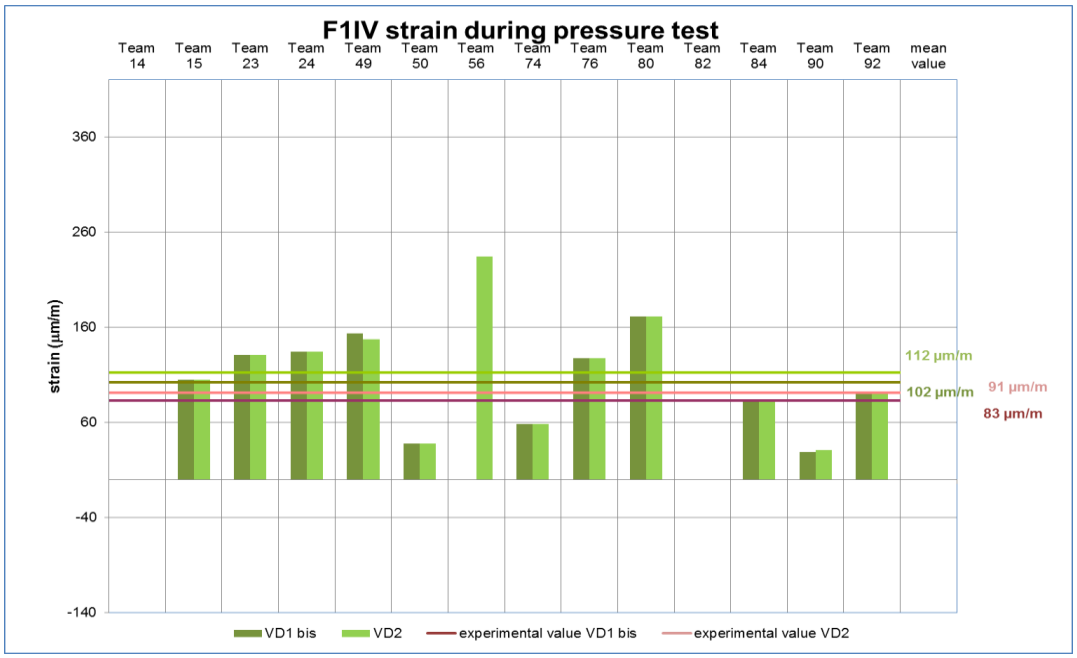

Figure 81. Instantaneous strain results comparison: Gusset – Vertical direction – Bottom – Extrados

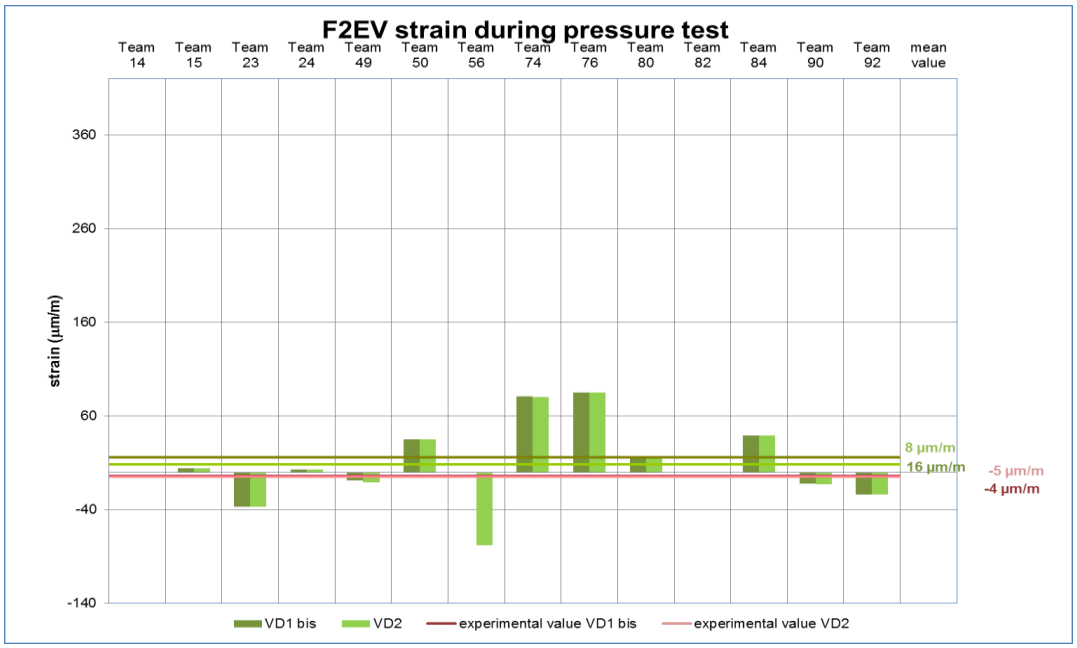

Figure 82. Instantaneous strain results comparison: Gusset – Vertical direction – Top – Intrados

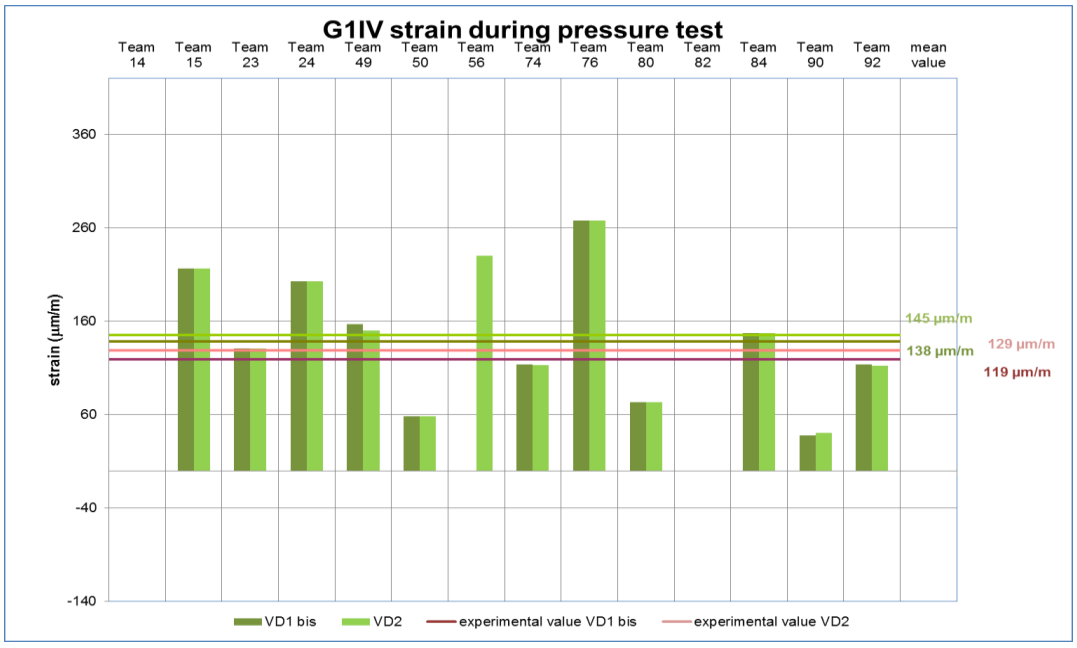

Figure 83. Instantaneous strain results comparison: Gusset – Vertical direction – Top – Extrados

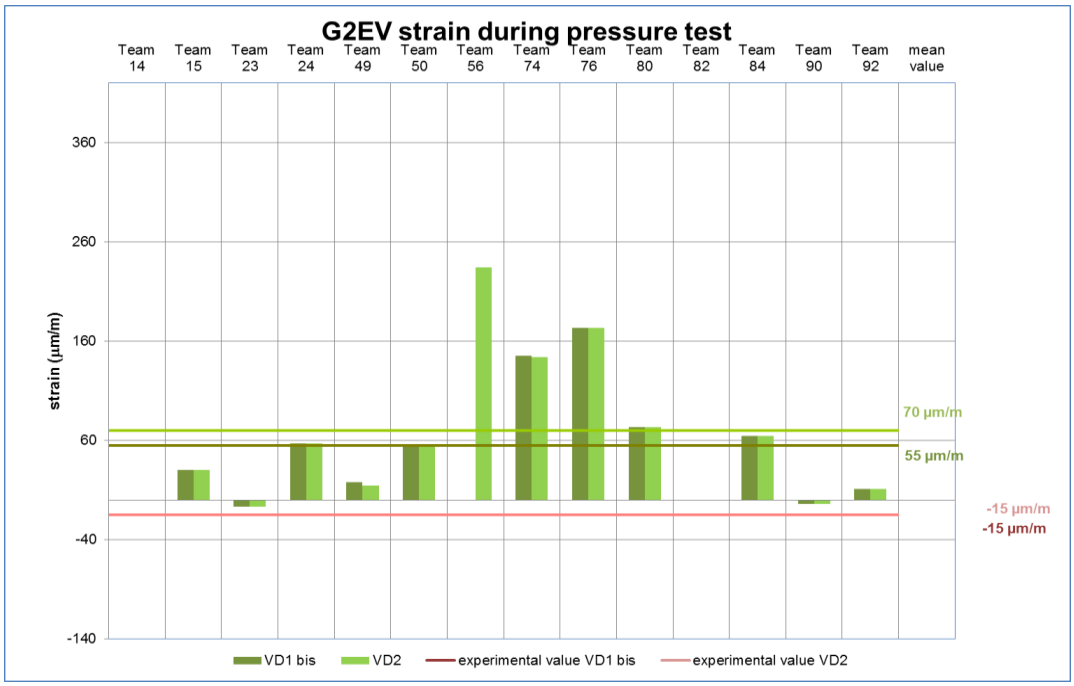

5.3.5.2.2 Tangential direction

Figure 84. Instantaneous strain results comparison: Gusset – Tangential direction – Bottom – Intrados

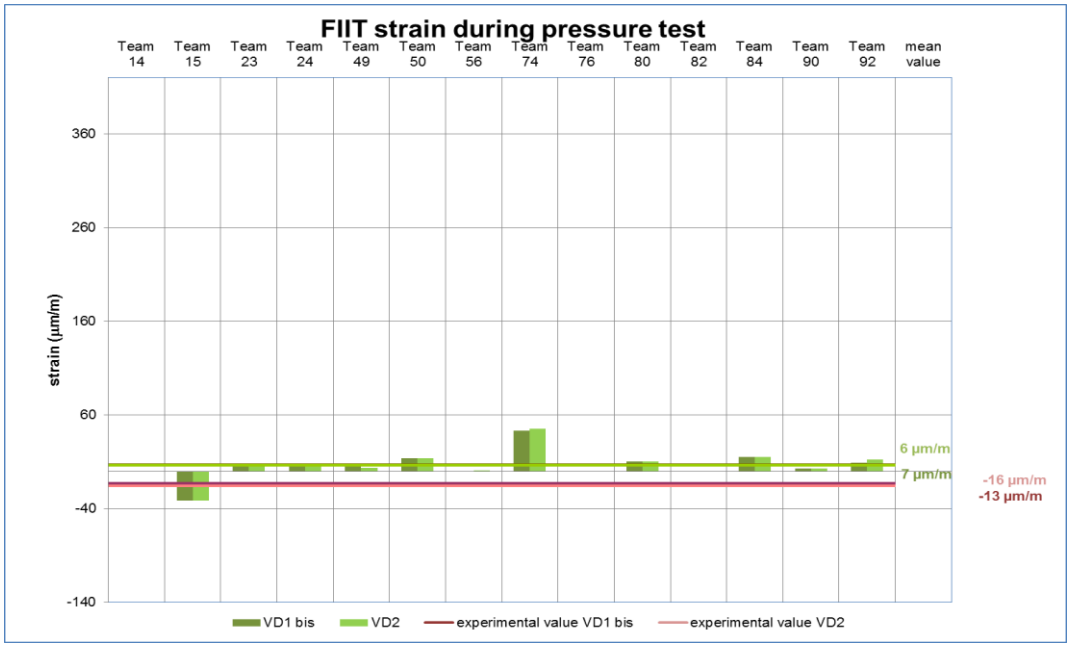

Figure 85. Instantaneous strain results comparison: Gusset – Tangential direction – Bottom – Extrados

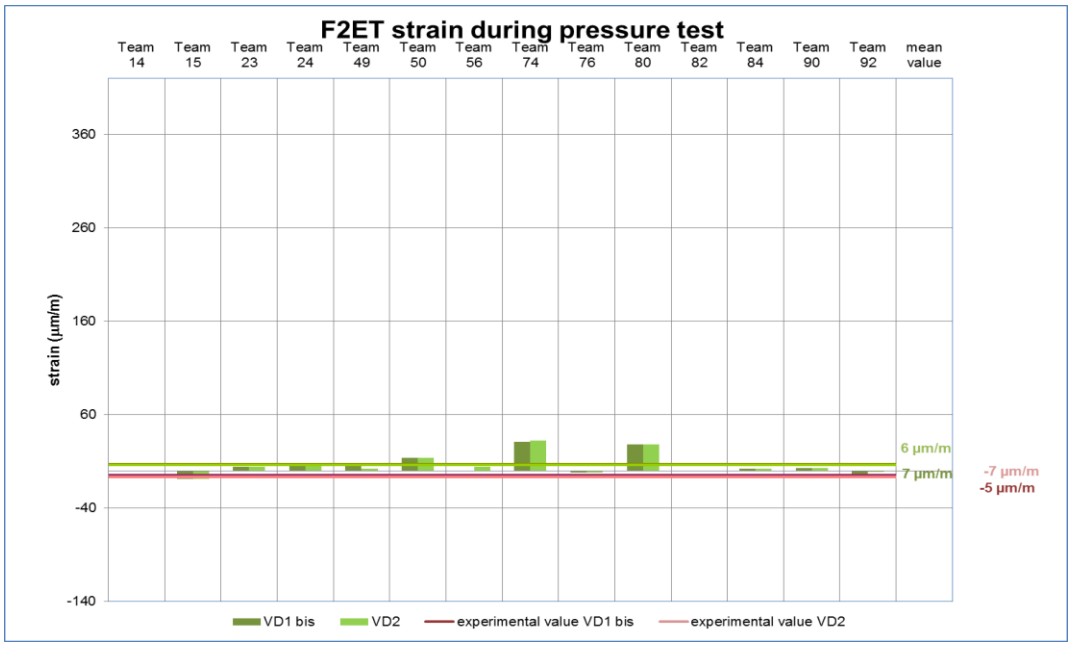

Figure 86. Instantaneous strain results comparison: Gusset – Tangential direction – Top – Intrados

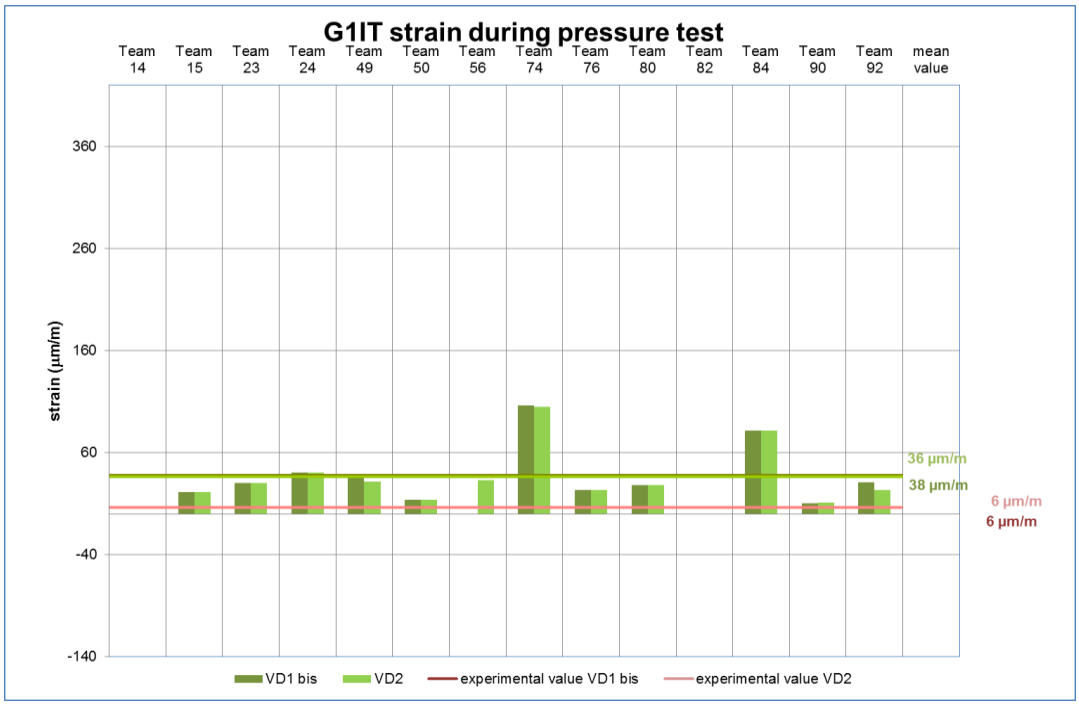

Figure 87. Instantaneous strain results comparison: Gusset – Tangential direction – Top – Extrados

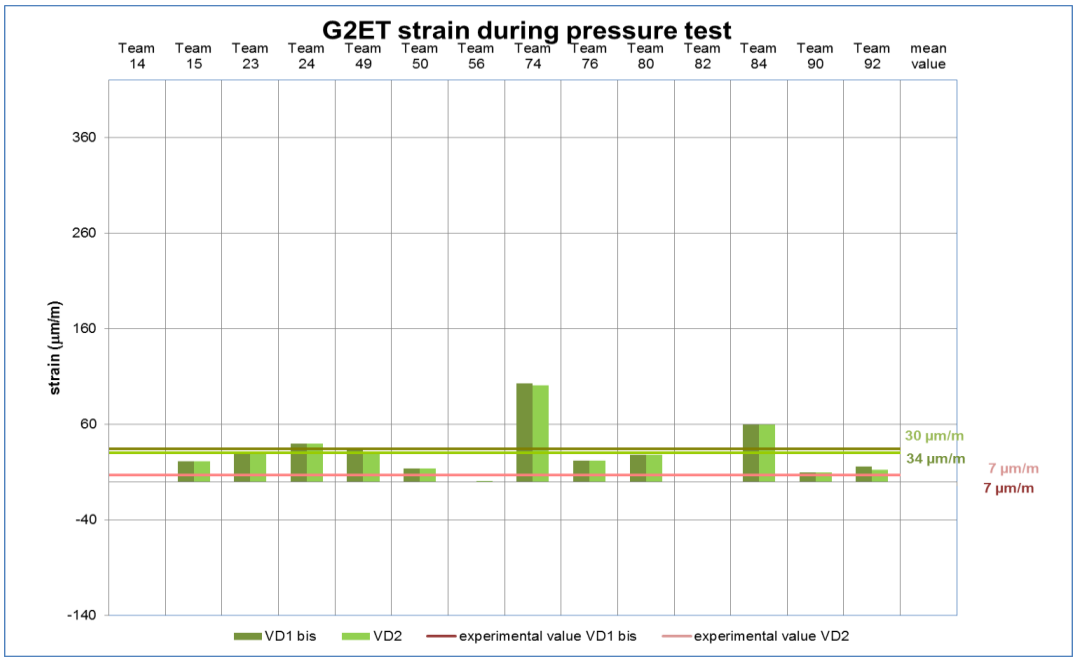

5.3.5.2.3 Comments

The teams' results for this part are very scattered, especially in the lower part of the gusset. The dispersion of the values provided by participants is lower in the upper part of the gusset, in both directions.

In the vertical direction, on average, teams gave good predictions of the strains on the inner face. Teams 84 and 92 gave results that are closest to the experimental measurements. On the outer face, participants saw on average an elongation, while experimental measures show a small shortening. It seems that the rotation of the gusset under pressurisation is not very well represented in the numerical models, except for Teams 23, 49 and 92.

In the tangential direction, the measured strains are close to zero. The raft seems to have an important effect by restraining deformation of the gusset up to the level of sensors G1 and G2. On average, the teams saw very low strains in the lower part of the gusset, but more important strain values at the upper level. It is difficult to explain this finding. It could have been interesting to make a comparison of radial strains in the raft between the models and the experimental measures.

5.3.5.3 Pressurisation effects in the cylindrical wall

5.3.5.3.1 Vertical direction

Figure 88. Instantaneous strain results comparison: Cylindrical part – Vertical direction – Extrados

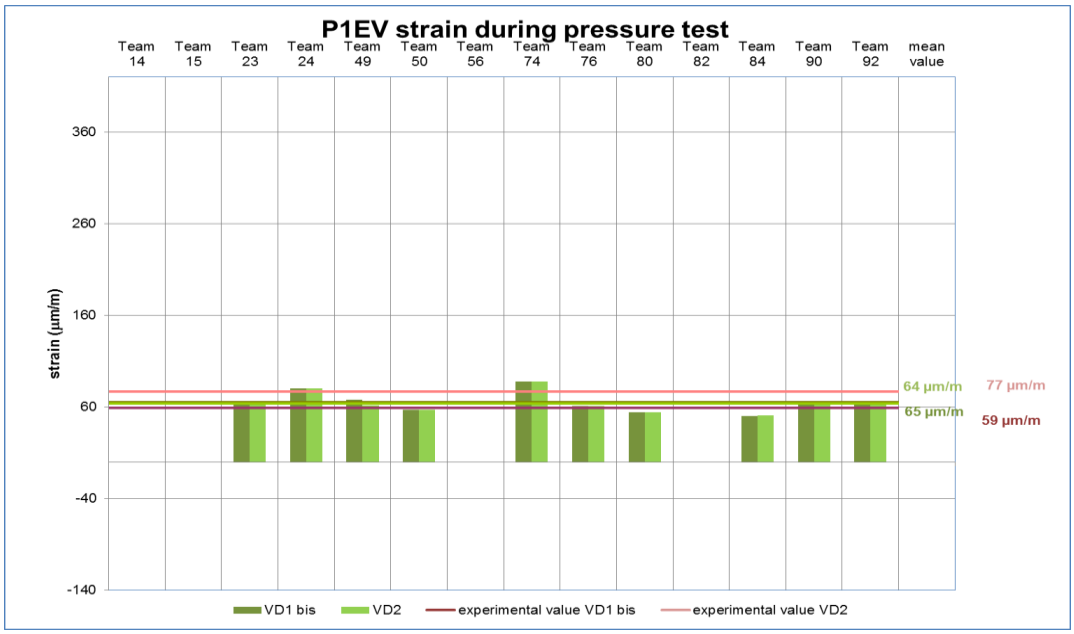

Figure 89. Instantaneous strain results comparison: Cylindrical part – Vertical direction – Intrados

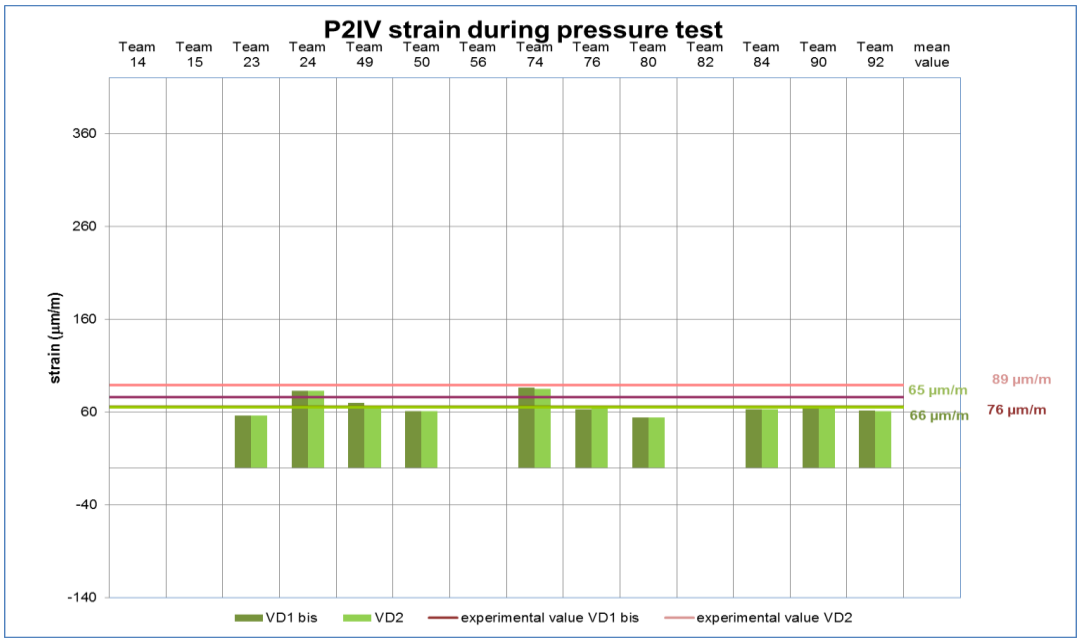

Figure 90. Instantaneous strain results comparison: Cylindrical part – Vertical direction – Extrados

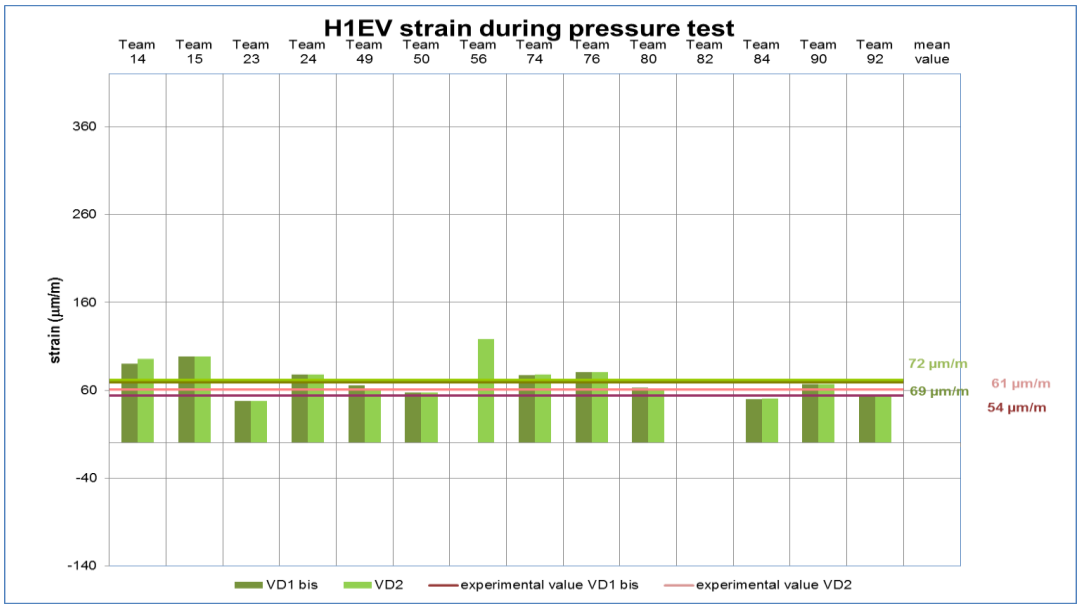

Figure 91. Instantaneous strain results comparison: Cylindrical part – Vertical direction – Intrados

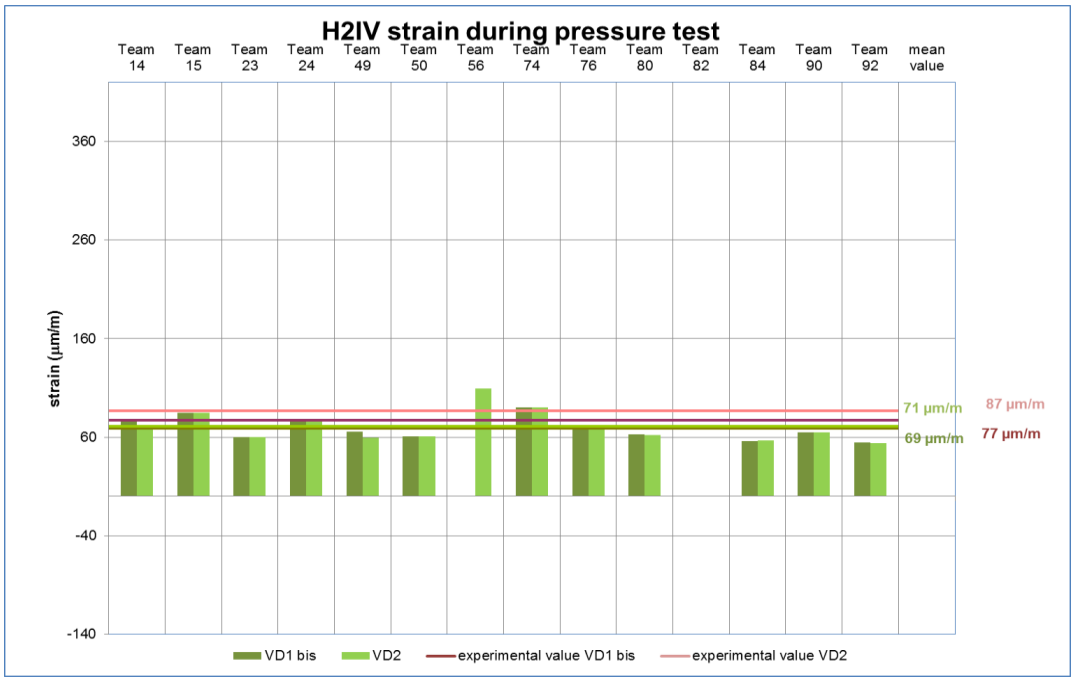

Figure 92. Instantaneous strain results comparison: Cylindrical part – Vertical direction – Extrados

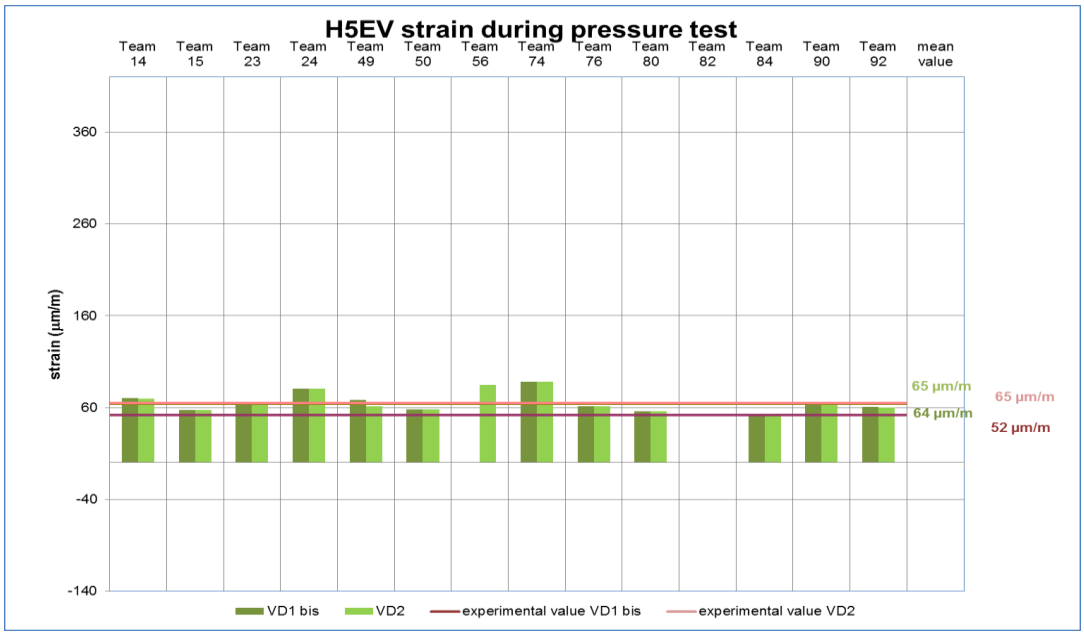

Figure 93. Instantaneous strain results comparison: Cylindrical part – Vertical direction – Intrados

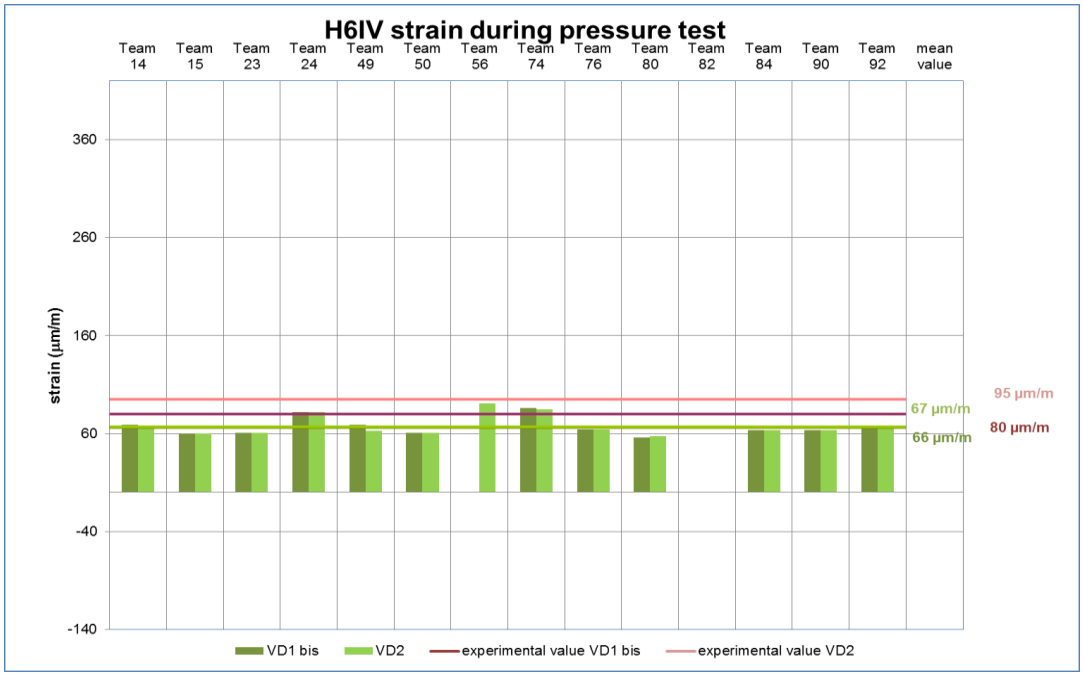

5.3.5.3.2 Tangential direction

Figure 94. Instantaneous strain results comparison: Cylindrical part – Tangential direction – Extrados

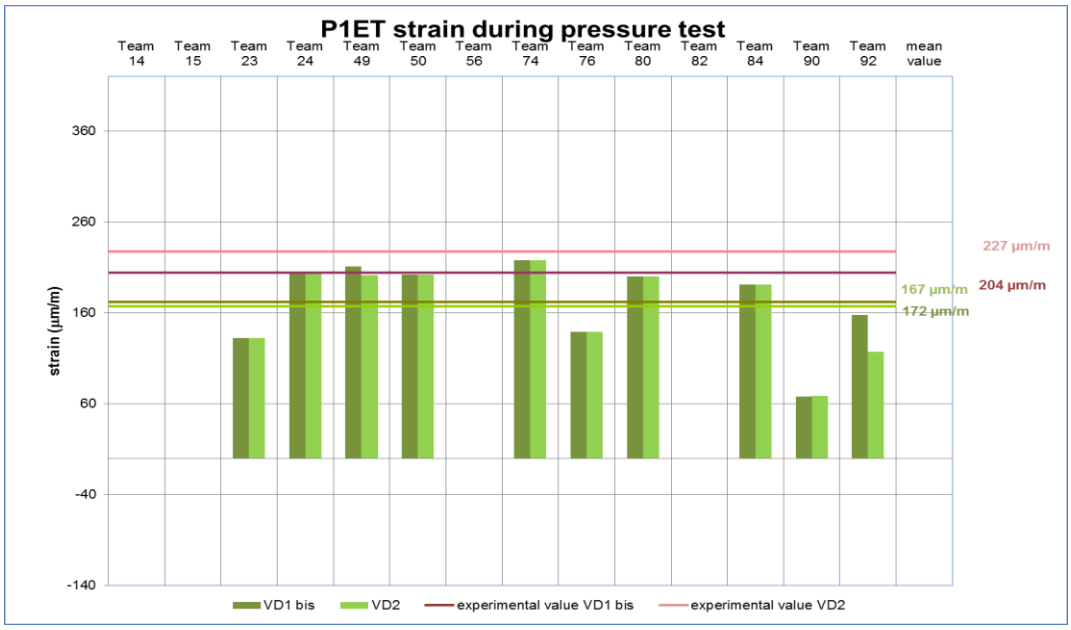

Figure 95. Instantaneous strain results comparison: Cylindrical part – Tangential direction – Intrados

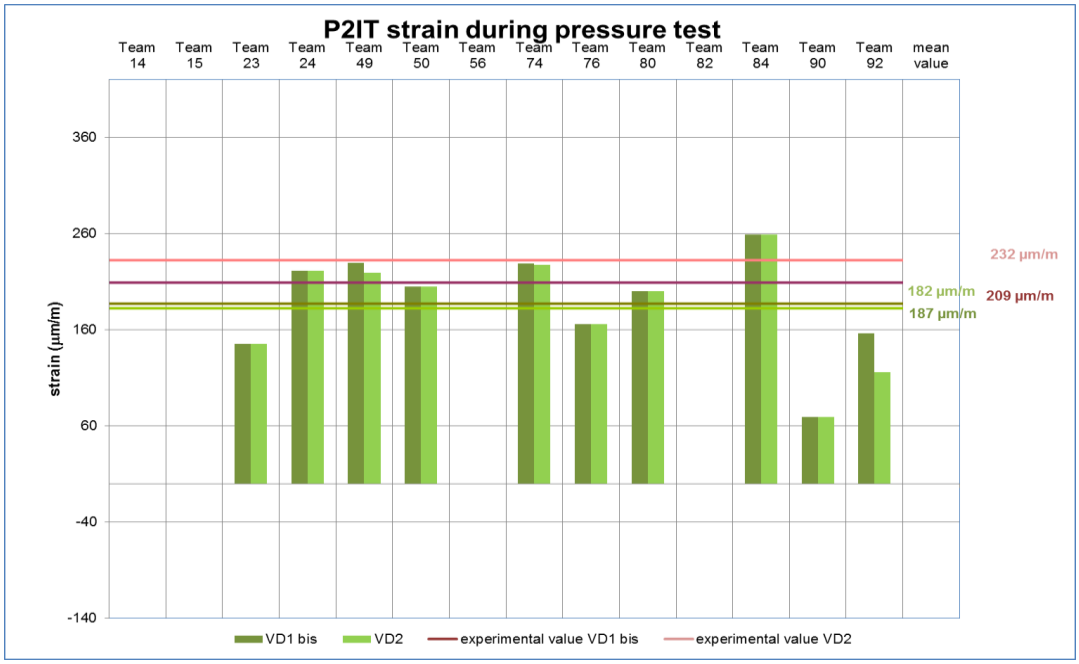

Figure 96. Instantaneous strain results comparison: Cylindrical part – Tangential direction – Extrados

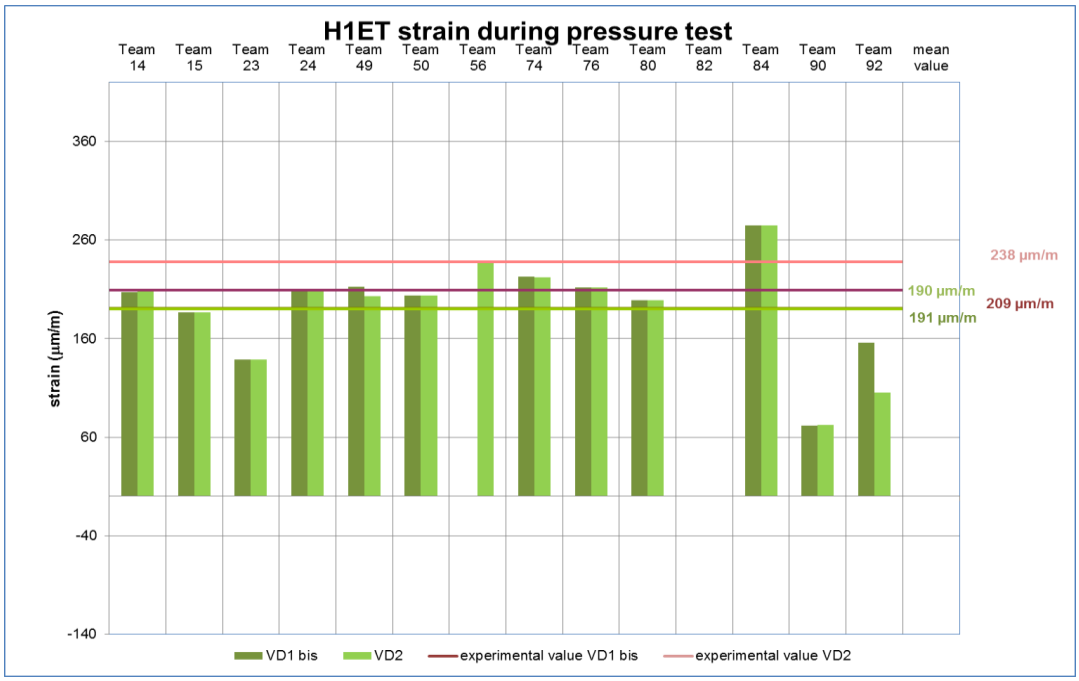

Figure 97. Instantaneous strain results comparison: Cylindrical part – Tangential direction – Intrados

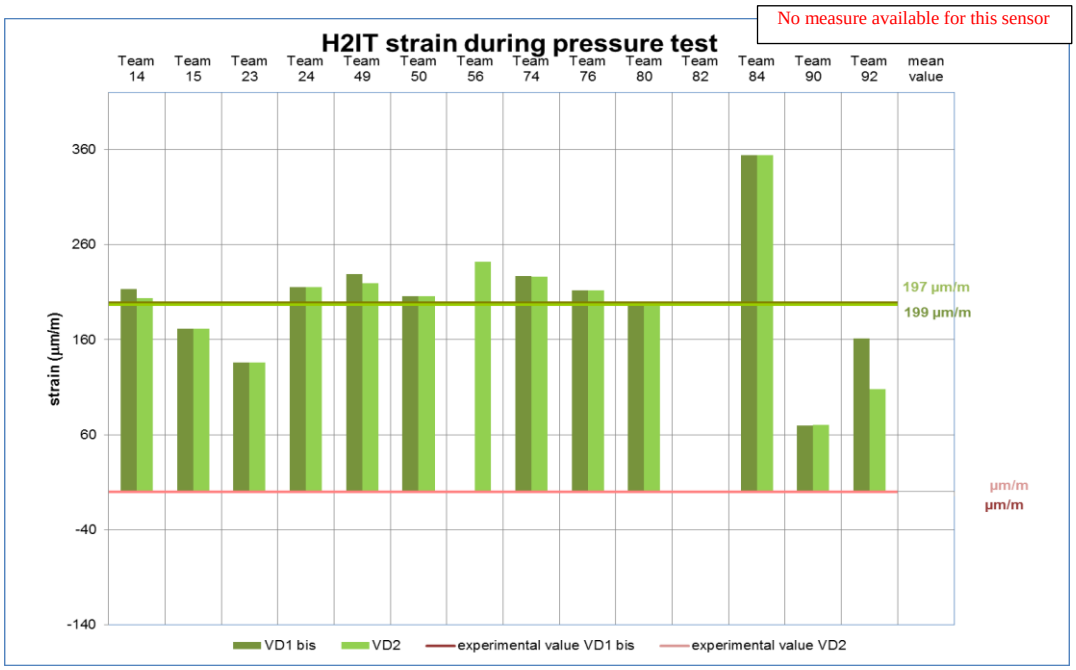

Figure 98. Instantaneous strain results comparison: Cylindrical part – Tangential direction – Extrados

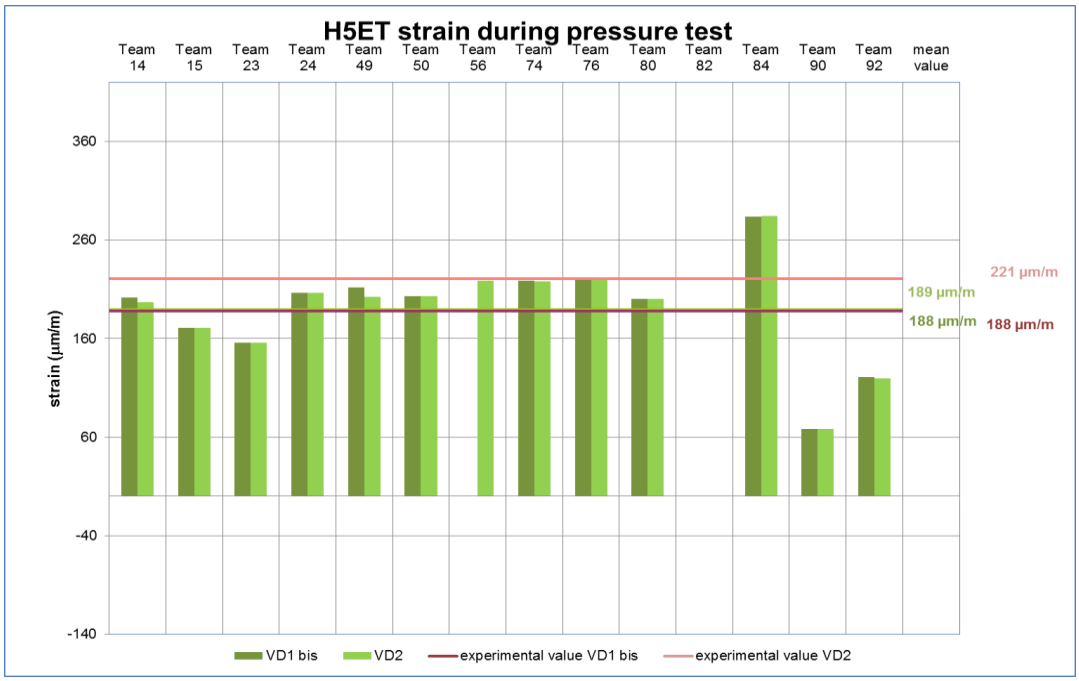

Figure 99. Instantaneous strain results comparison: Cylindrical part – Tangential direction – Intrados

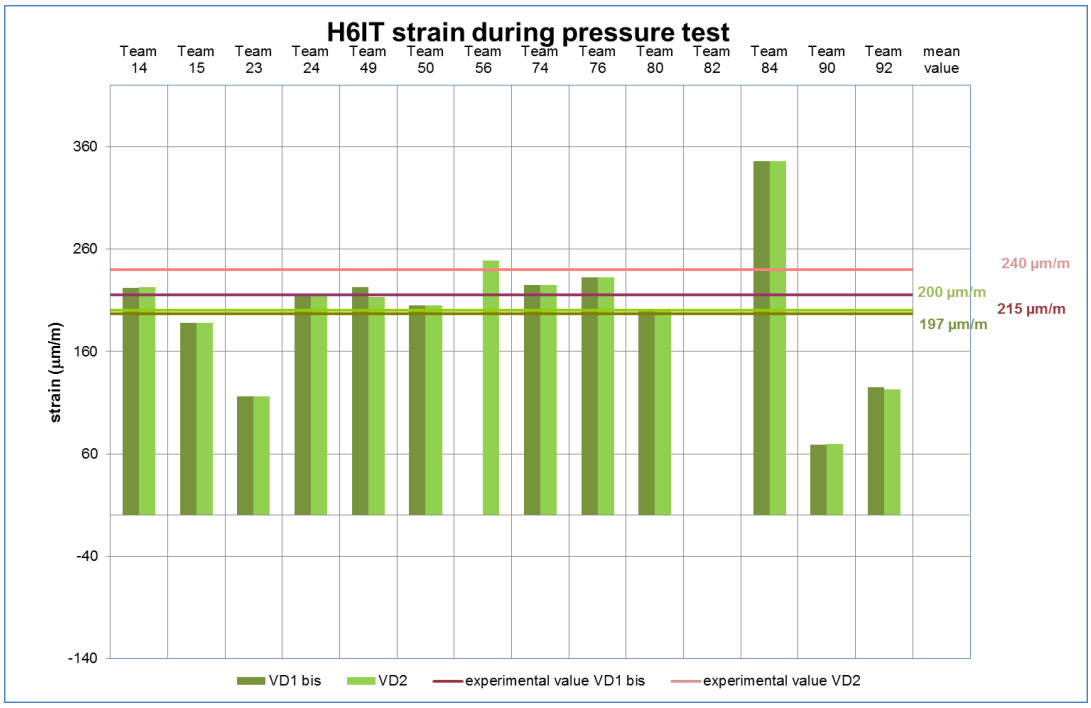

5.3.5.3.3 Comments

On this part of the containment, the dispersion of participants' values is very low. It was already the case in the 2015 benchmark. It can be noted that in the tangential direction, Team 90 had very low strain values compared to the other teams.

There is very good compliance of the numerical results with the experimental measures. In the tangential direction, Teams 14, 49, 50, 56, 74 and 80 gave results closest to the experimental measurements.

No team predicted higher strains in VD2 than in VD1 bis as it was observed in the mock-up.

5.3.5.4 Pressurisation effects around the equipment hatch

5.3.5.4.1 Side of the hatch

Figure 100. Instantaneous strain results comparison: Side of the hatch – Vertical – Extrados

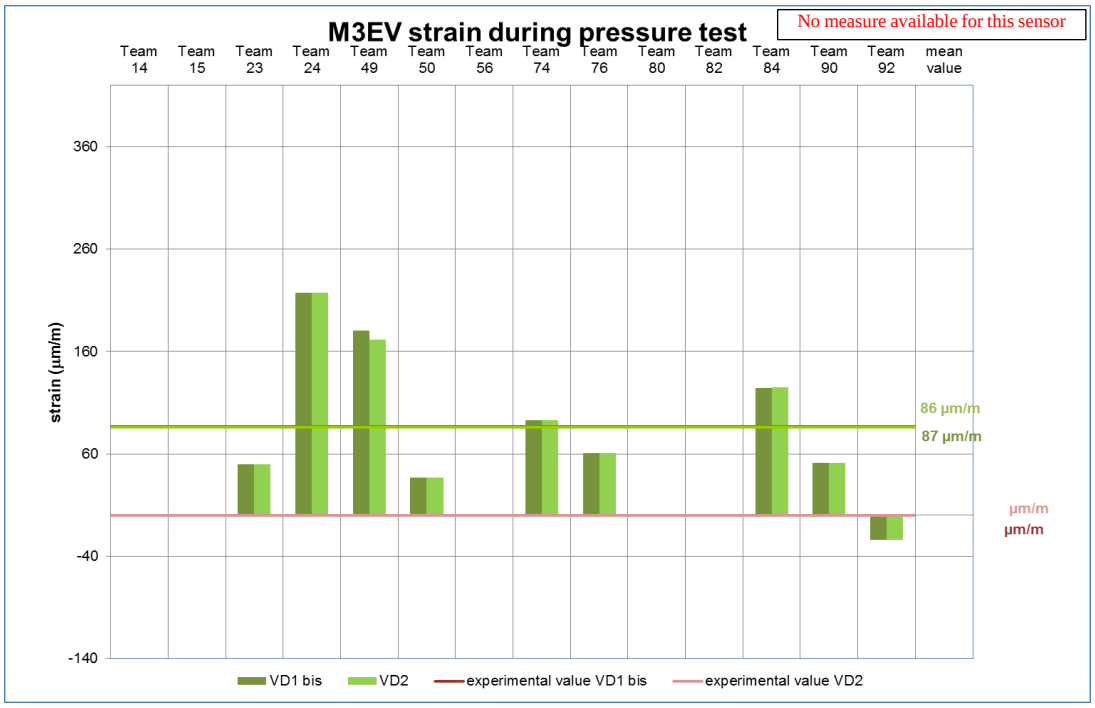

Figure 101. Instantaneous strain results comparison: Side of the hatch – Tangential – Extrados

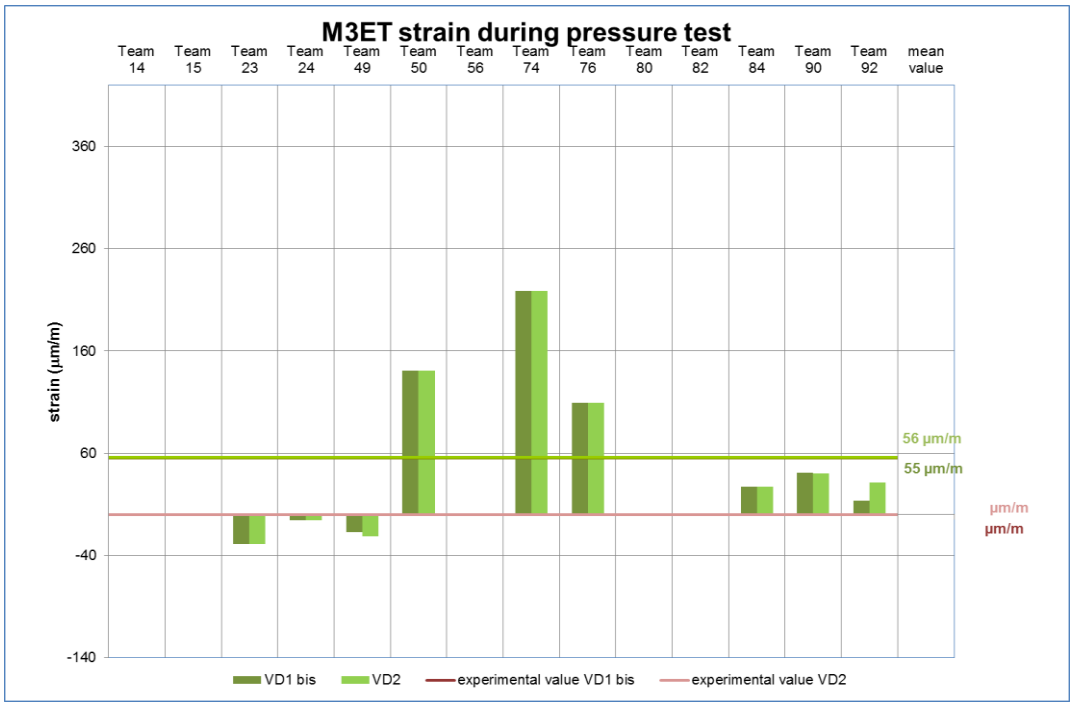

Figure 102. Instantaneous strain results comparison: Side of the hatch – Vertical – Intrados

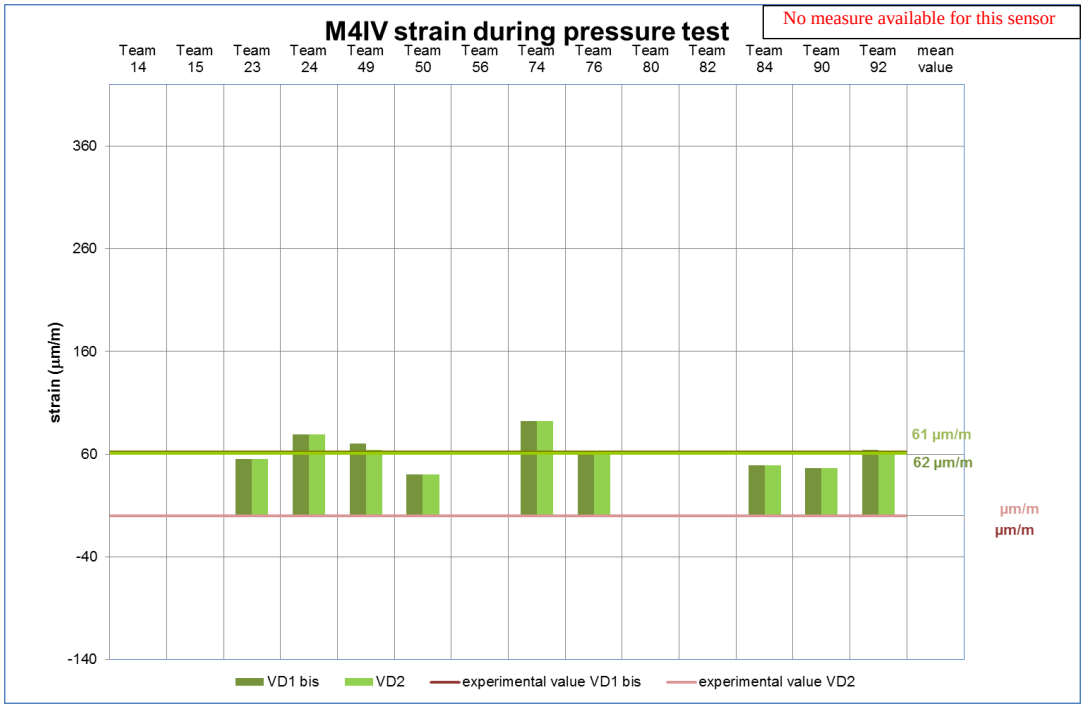

Figure 103. Instantaneous strain results comparison: Side of the hatch – Tangential – Intrados

No measure available for this sensor

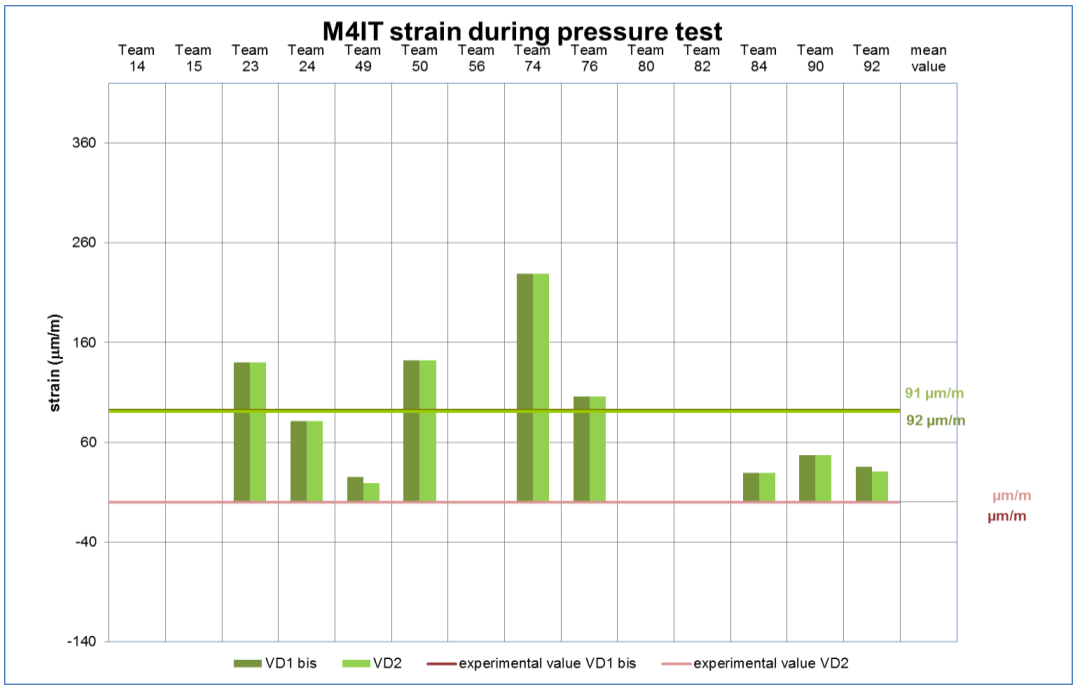

5.3.5.4.2 Above the hatch

Figure 104. Delayed strain results comparison: Above the hatch – Vertical – Extrados

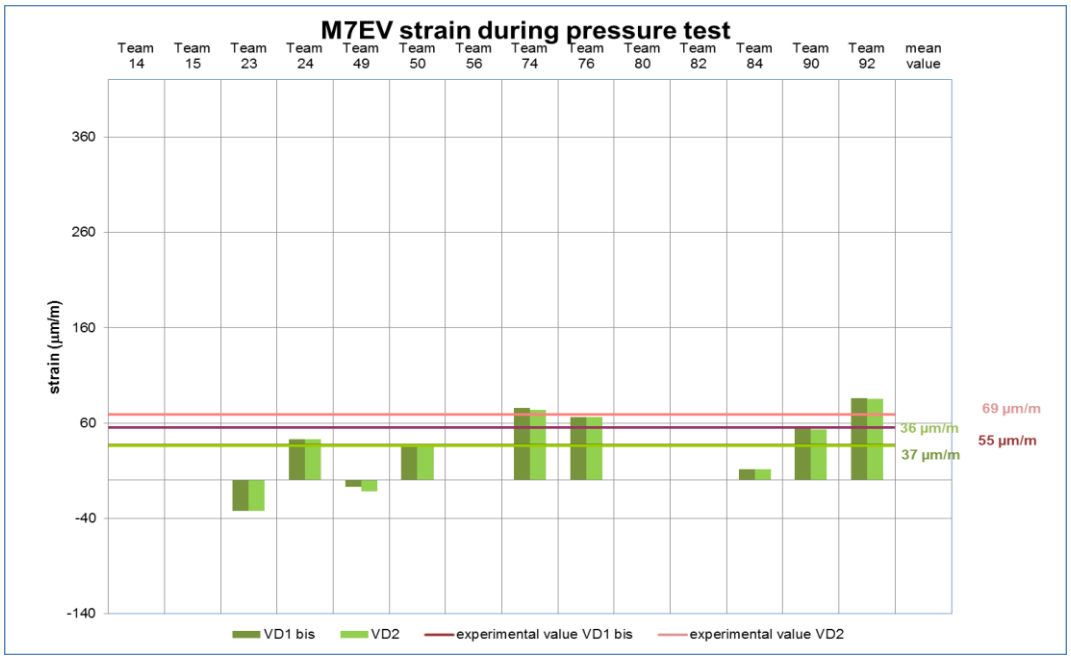

Figure 105. Delayed strain results comparison: Above the hatch – Tangential – Extrados

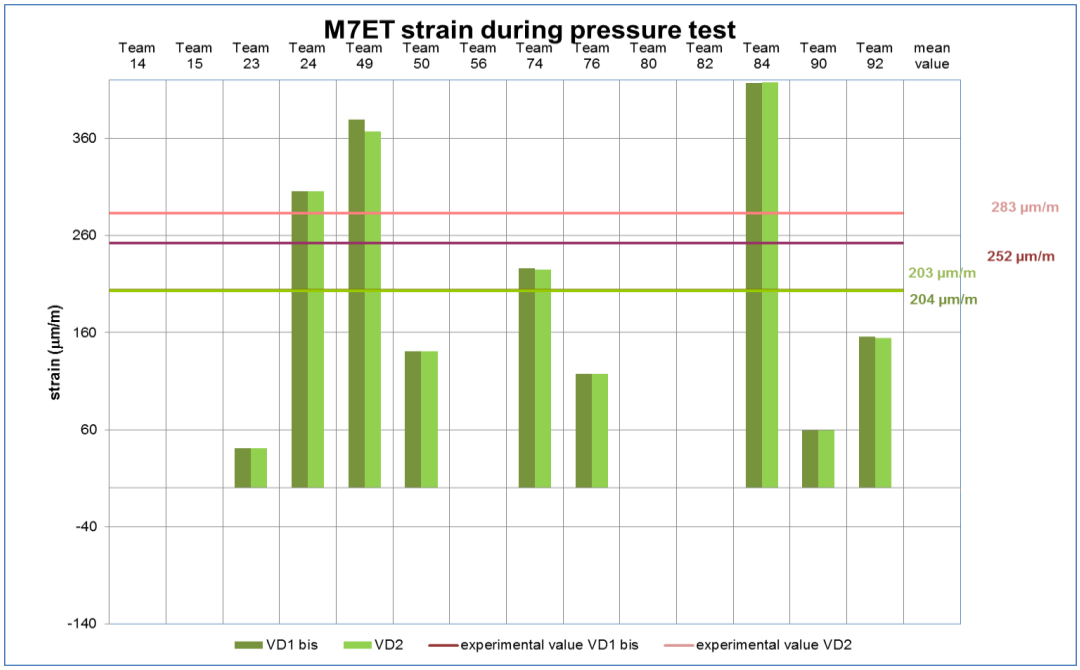

Figure 106. Delayed strain results comparison: Above the hatch – Vertical – Intrados

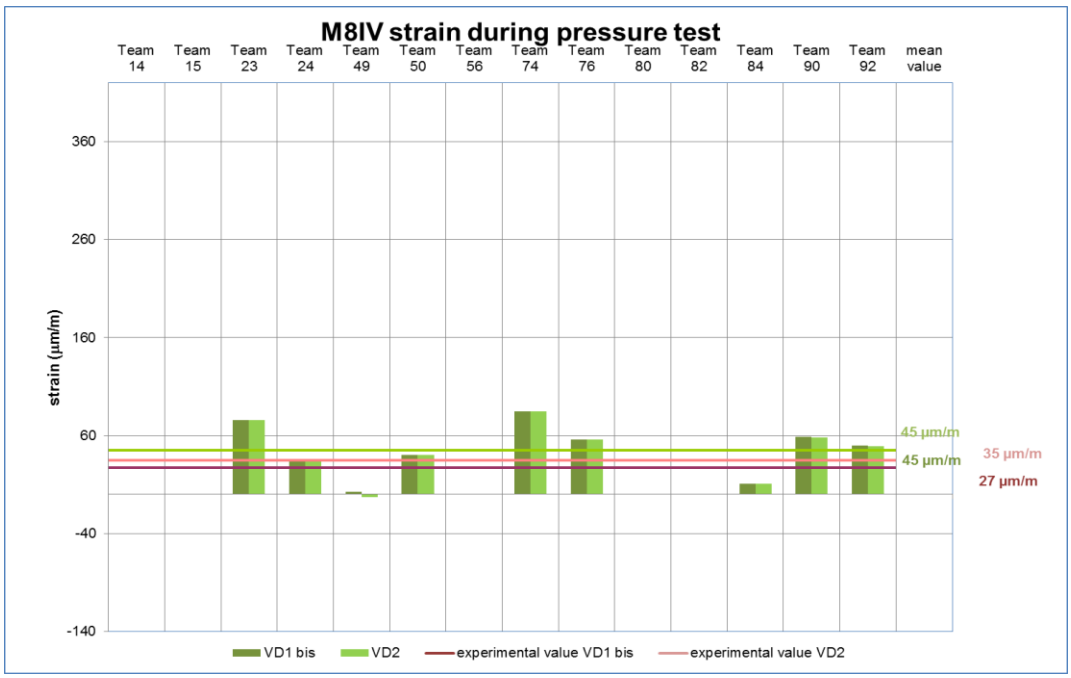

Figure 107. Delayed strain results comparison: Above the hatch – Tangential – Intrados

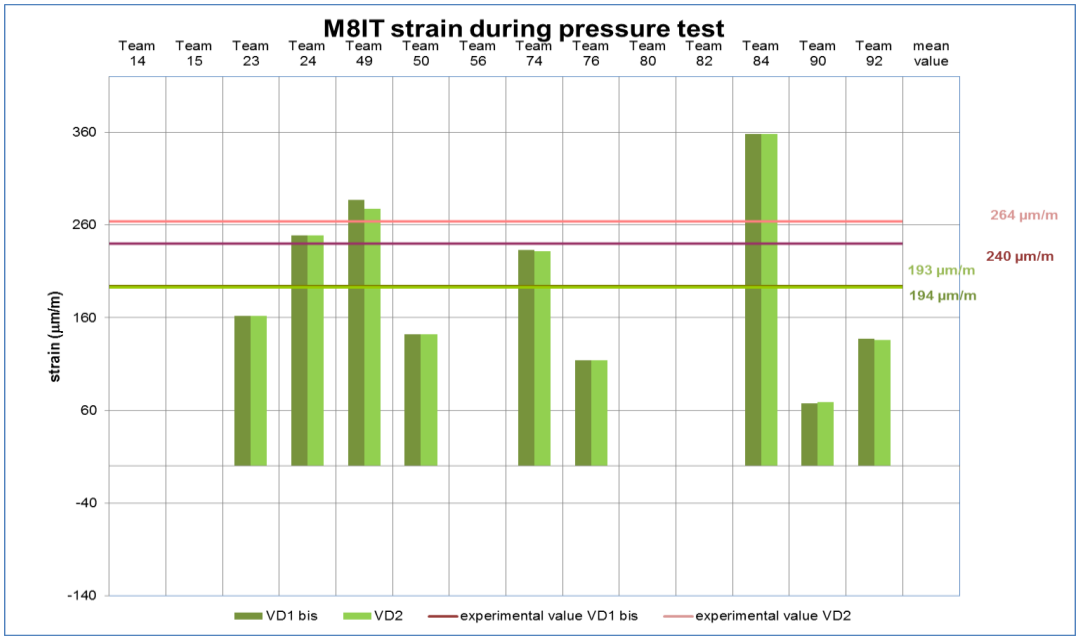

5.3.5.4.3 Comments

For this area, only nine teams submitted results. The results are more scattered for this specific part of the containment.

On the side of the hatch, on average, teams predicted vertical strains close to strains given in the current part. In tangential direction, the predicted strains are on average divided by two in comparison to strains given in the current part, representing the hatch rigidity. But in this direction, results are very scattered. Some teams gave a small shortening, others predicted an elongation of more than 200 µm/m.

Above the hatch, results are still scattered. On average, in the vertical direction, the predicted strains are around 40 µm/m (compared to about 65 µm/m in the current part). In the tangential direction, teams predicted on average the same strains as in the current part (but values range from 41 µm/m to 417 µm/m), while experimental measurements give an elongation between 240 µm/m and 283 µm/m.

No team predicted an increase of strains between VD1 bis and VD2 as it was measured on the mock-up (more than a 10% increase).

5.3.5.5 Pressurisation effects in the dome

5.3.5.5.1 Results

Figure 108. Instantaneous strain results comparison: Top of the dome – Extrados (194 Gr)

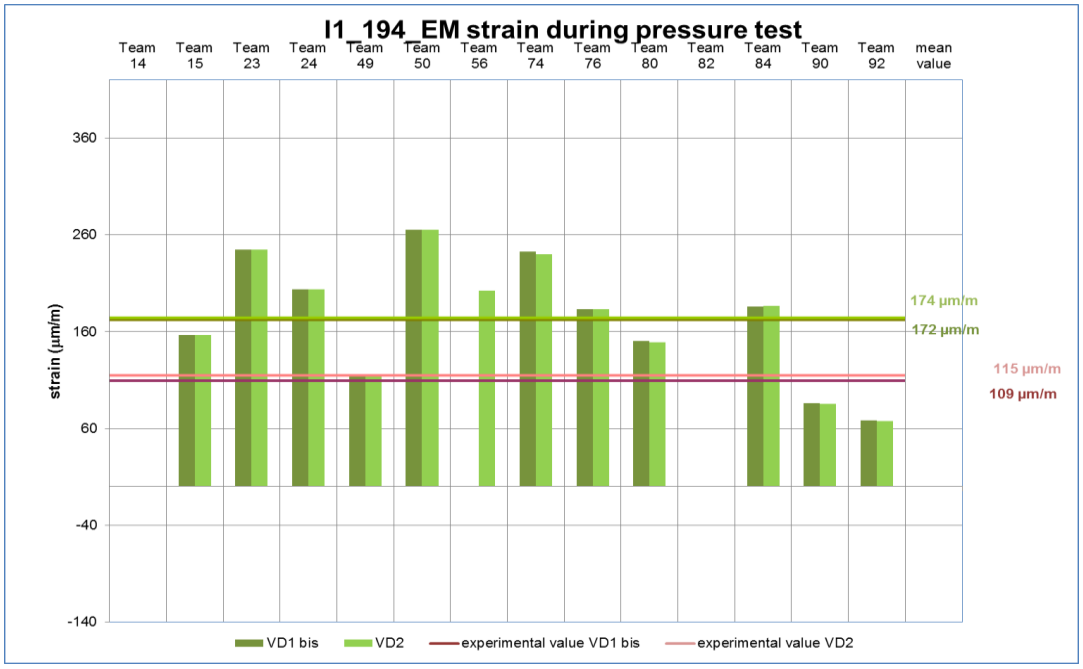

Figure 109. Instantaneous strain results comparison: Top of the dome – Extrados (94 Gr)

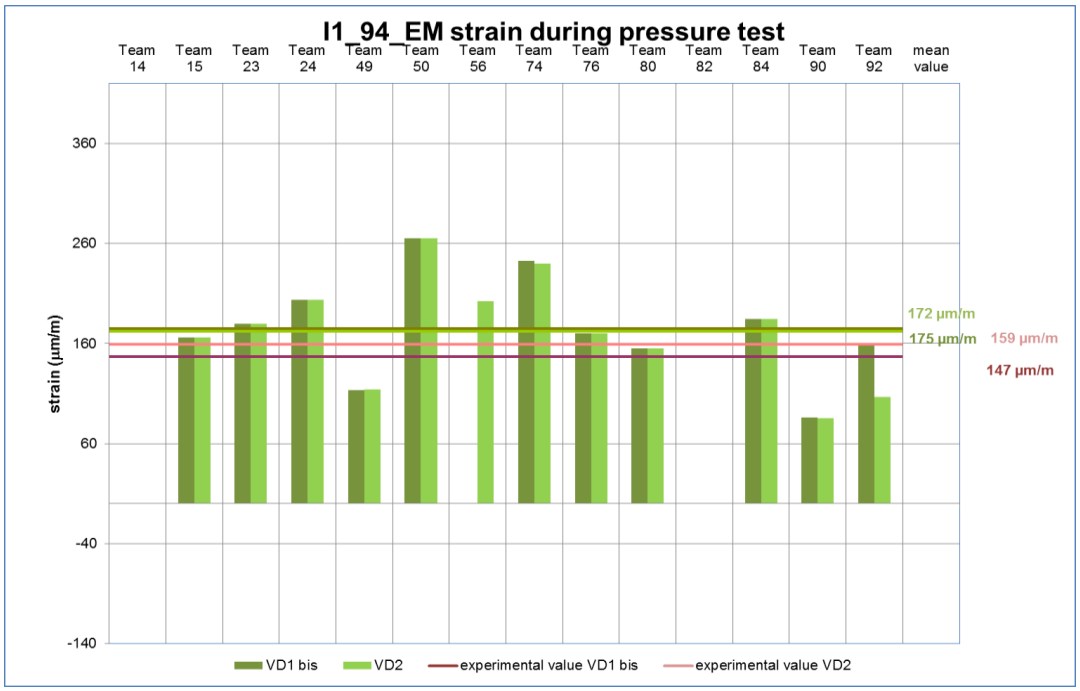

Figure 110. Instantaneous strain results comparison: Top of the dome – Intrados (194 Gr)

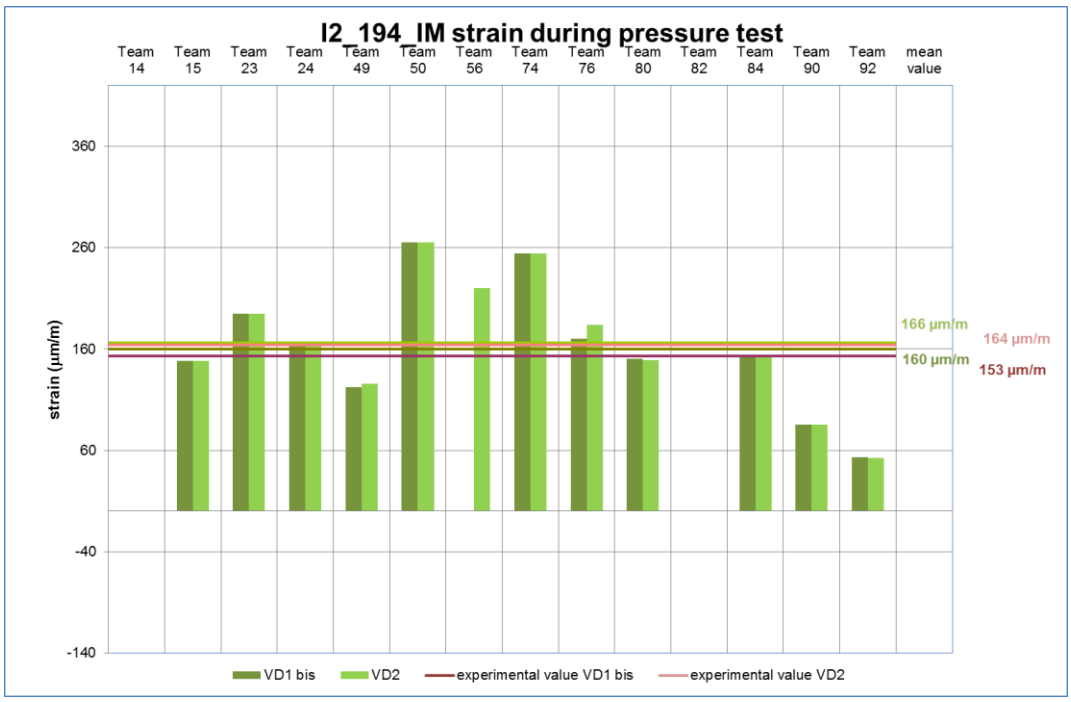

Figure 111. Instantaneous strain results comparison: Top of the dome – Intrados (94 Gr)

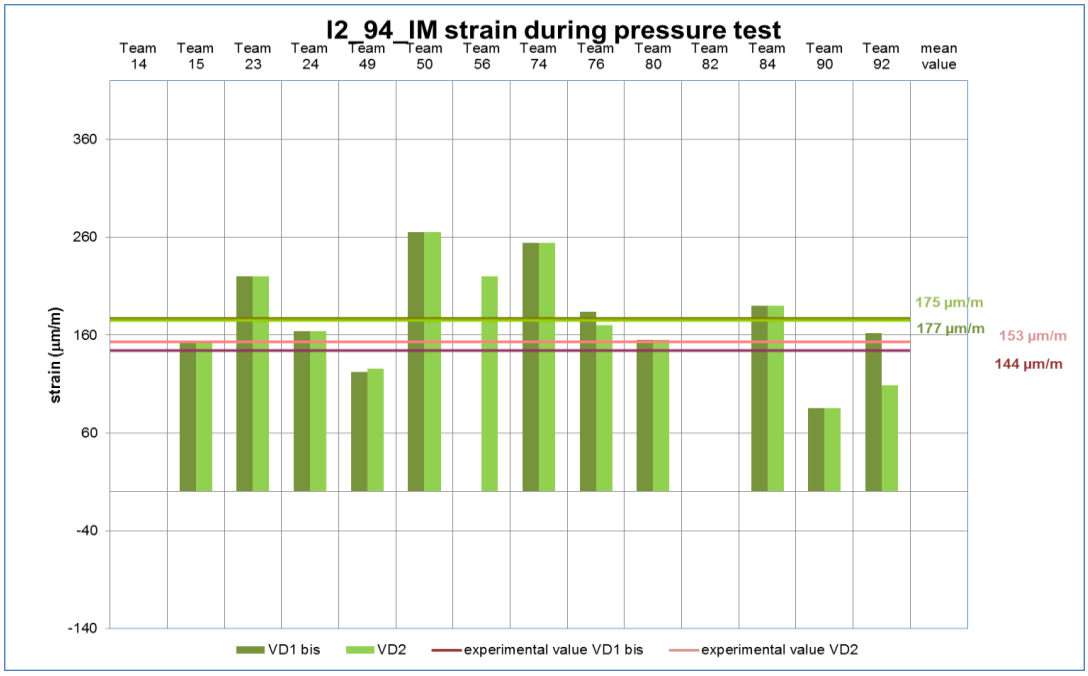

Figure 112. Instantaneous strain results comparison: Meridian part of the dome – Meridian direction – Extrados

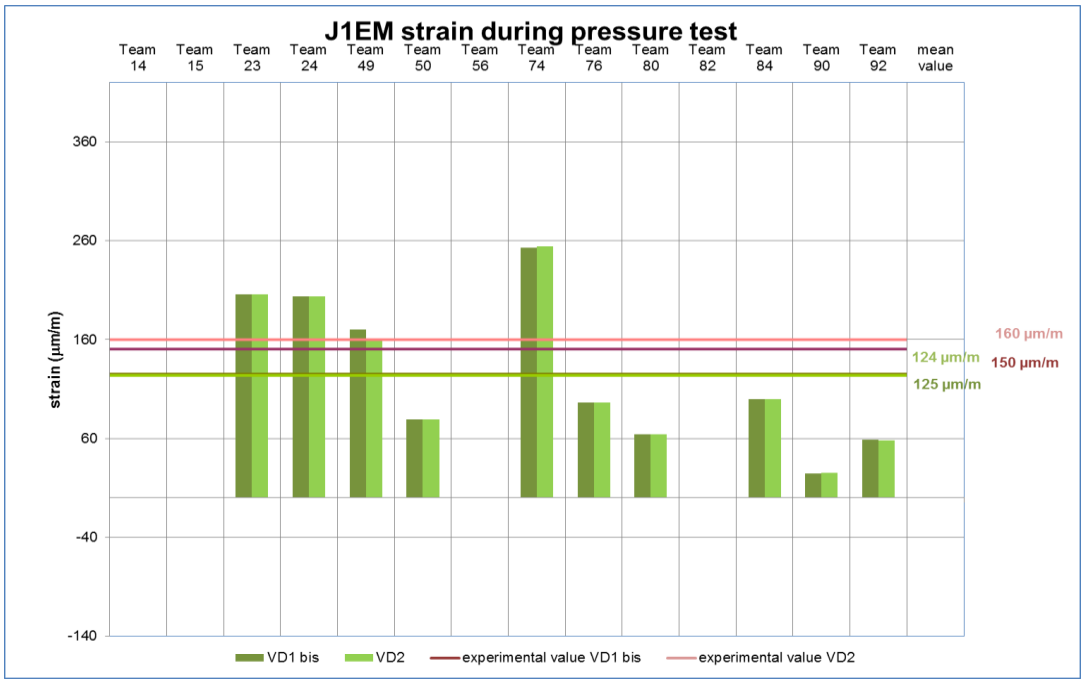

Figure 113. Instantaneous strain results comparison: Meridian part of the dome – Tangential direction – Extrados

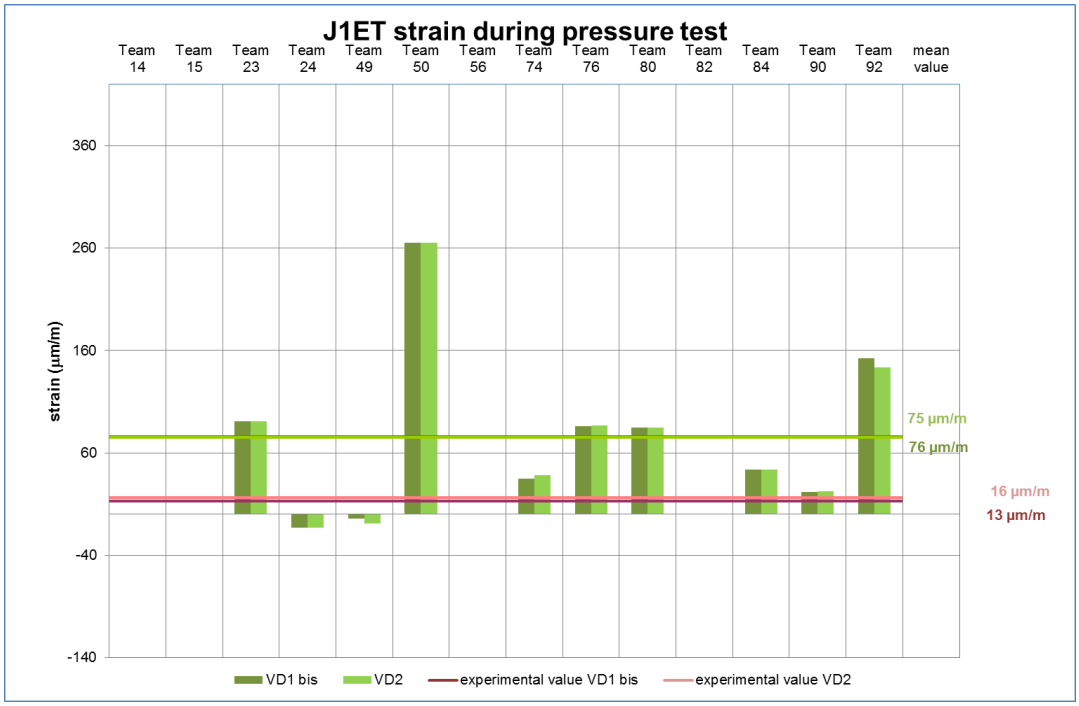

Figure 114. Instantaneous strain results comparison: Meridian part of the dome – Meridian direction – Intrados

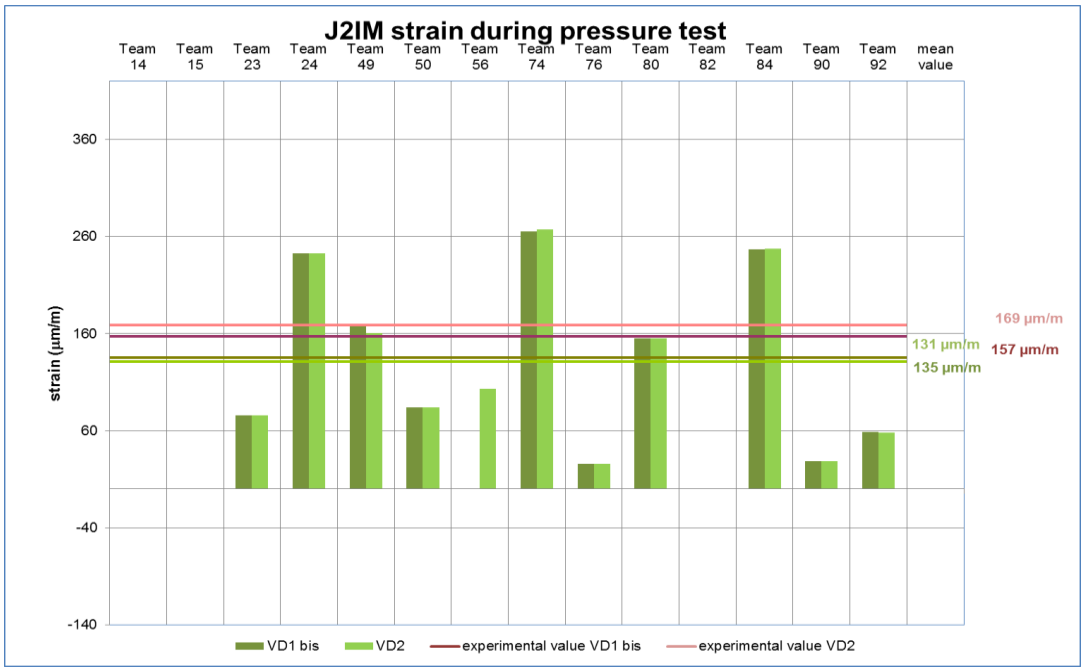

Figure 115. Instantaneous strain results comparison – Meridian part of the dome – Tangential direction – Intrados

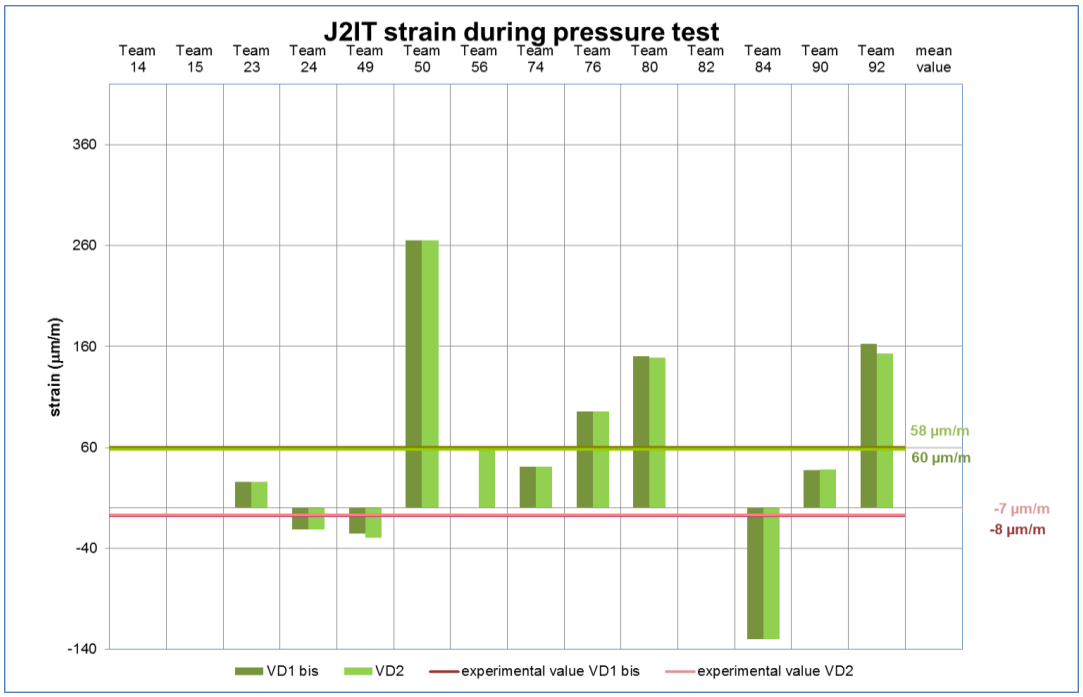

5.3.5.5.2 Comments

At the top of the dome, the results are fairly homogeneous. On average, results are close to experimental values, except for I1_194_EM. Teams 15, 24, 76 and 80's results were the closest to the experimental measurements. Only one team (Team 49) predicted an increase of strains between VD1 bis and VD2, but underestimated the values.

In the meridian part of the dome, the results are more scattered. On average, in the meridian direction, results are not so far from the experimental measurements, but submitted values range from 25 µm/m to 265 µm/m. Team 74 predicted a small increase of strains between VD1 bis and VD2, but with strain values much higher than the experimental measurements. In tangential direction, participants' results are very scattered and on average distant from the experimental values.

5.3.5.6 Synthesis regarding instantaneous strains results

Overall, the effects of the pressure test were well represented by the participants; in most areas the distance from the experimental values is small, except for the gusset and some points in the dome (Figure 116). This can be explained by the fact that the applied load is relatively simple. The representation of structural connection between raft and cylinder remains an area of improvement for modellers.

Figure 116. Instantaneous strains: Representation of the average distance between numerical and experimental results per zone

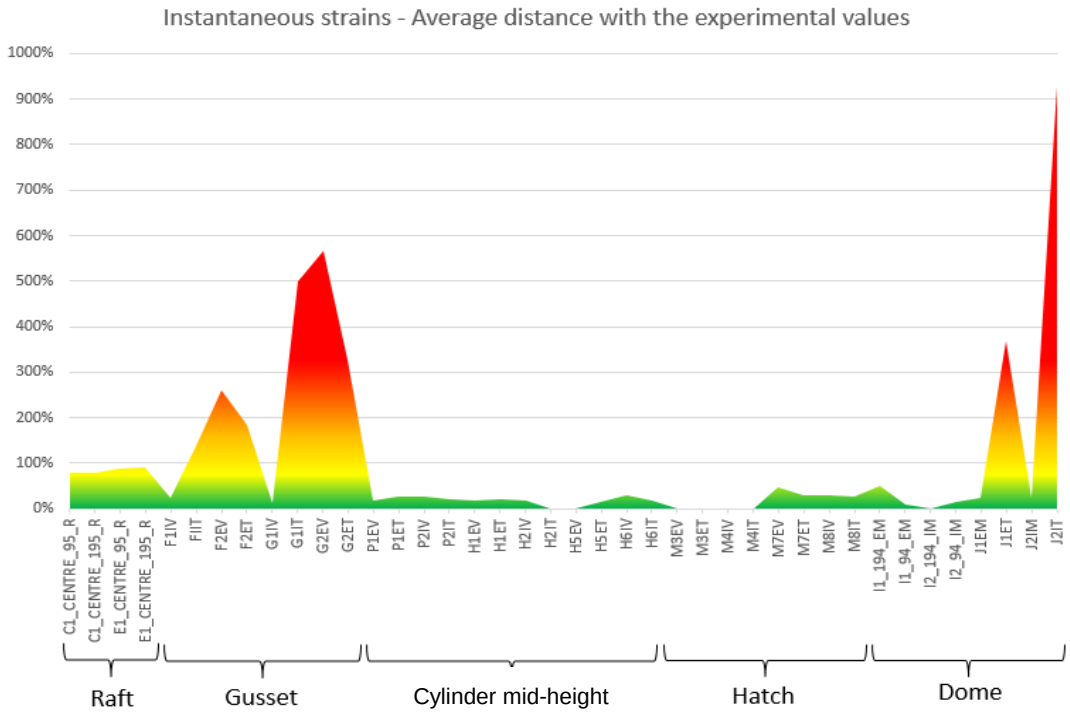

Regarding the numerical results dispersion, the lower part of the gusset is the part of the structure where the results are most scattered (Figure 117). Some other areas generate significant differences in the results provided, for example around the hatch and in the meridian part of the dome. The mid-height of the cylinder is the area that produces very little scattered values.

Figure 117. Instantaneous strains: Representation of participants' results dispersion per zone

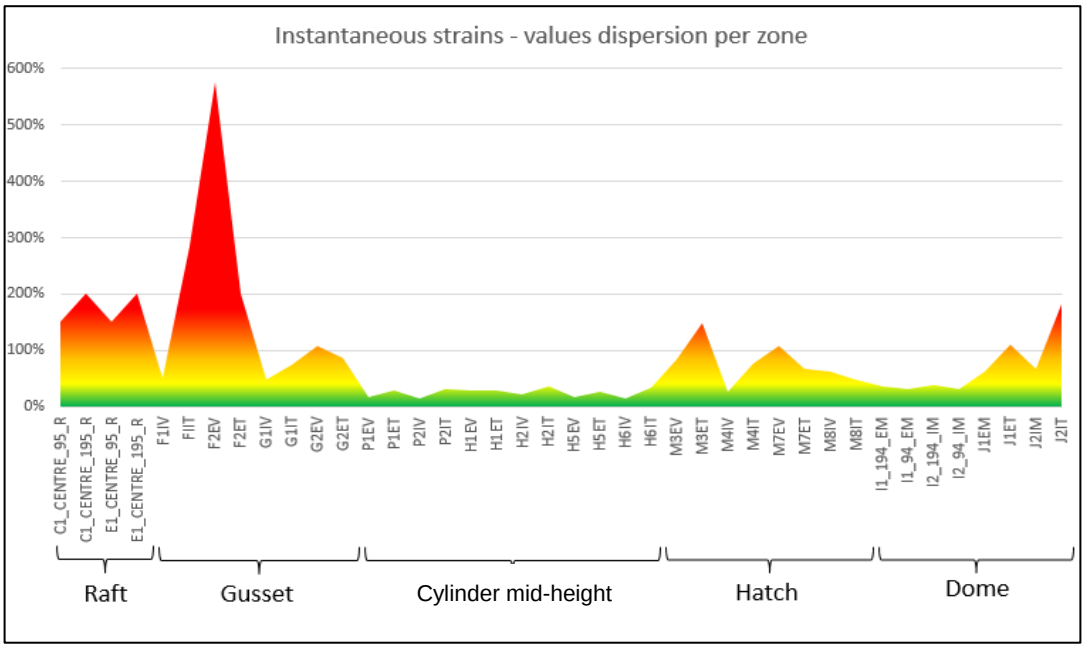

5.4. Stresses

5.4.1. Expected results

Participants were asked to give the stresses evolution in the whole containment over time. Values were expected at three times: VD1, VD1 bis and VD2.

The stresses evolution is analysed for two states of the containment: without inner pressure (i.e. at 0 bar relative) and with inner pressure (i.e. at 4.2 bar relative).

Table 20 was provided to collect participants' results.

Table 20. Participants' predictions of stresses evolution in the whole containment over time

		Stresses in the concrete (in MPa)					
		VD1		VD1 bis		VD2	
		0 bar	4.2 bar rel.	0 bar	4.2 bar rel.	0 bar	4.2 bar rel.
Zone	Strain gauge	14 March 2017 06:35	15 March 2017 09:05	21 March 2017 07:06	22 March 2017 09:06	2 April 2018 07:00	3 April 2018 09:00
Raft	C1_CENTRE_95_R						
	C1_CENTRE_195_R						
	E1_CENTRE_95_R						
	E1_CENTRE_195_R						

Table 20. Participants' predictions of stresses evolution in the whole containment over time (Continued)

		Stresses in the concrete (in MPa)					
		VD1		VD1 bis		VD2	
		0 bar	4.2 bar rel.	0 bar	4.2 bar rel.	0 bar	4.2 bar rel.
Zone	Strain gauge	14 March 2017 06:35	15 March 2017 09:05	21 March 2017 07:06	22 March 2017 09:06	2 April 2018 07:00	3 April 2018 09:00
Gusset	F1IV						
	FIIT						
	F2EV						
	F2ET						
	G1IV						
	G1IT						
	G2EV						
	G2ET						
Cylindrical part (mid-height)	P1EV						
	P1ET						
	P2IV						
	P2IT						
	H1EV						
	H1ET						
	H2IV						
	H2IT						
	H5EV						
	H5ET						
	H6IV						
	H6IT						
Equipment hatch	M3EV						
	M3ET						
	M4IV						
	M4IT						
	M7EV						
	M7ET						
	M8IV						
	M8IT						
Dome	I1_194_EM						
	I1_94_EM						
	I2_194_IM						
	I2_94_IM						
	J1EM						
	J1ET						
	J2IM						
	J2IT						

5.4.2. Submitted results

Out of the 18 teams participating in Theme 2, 14 submitted stress values, but with a varying number of sensor locations answered. Without considering the raft, which is not an area of interest regarding stresses evolution, eight teams gave stress values for all of the sensors and for each time. Three teams (Teams 15, 80 and 82) provided results for the whole containment except the hatch area. Two teams (Teams 14 and 47) gave partial results for only some of the sensors locations in the cylinder part. Team 86 only gave some values in the gusset and only for VD1.

5.4.3. Stresses evolution at 0 bar

Experimental results are not available for this part. Results are compared between teams. In the following figures, the mean value of participants' results is represented by a horizontal line.

This part analyses the stresses evolution over time without inner pressure in the containment; that is to say, the effects of delayed strains and tendons relaxation on the concrete stresses.

5.4.3.1 Raft stresses evolution

5.4.3.1.1 Lower level

Figure 118. Stresses evolution at 0 bar: Raft - Lower level (95 Gr)

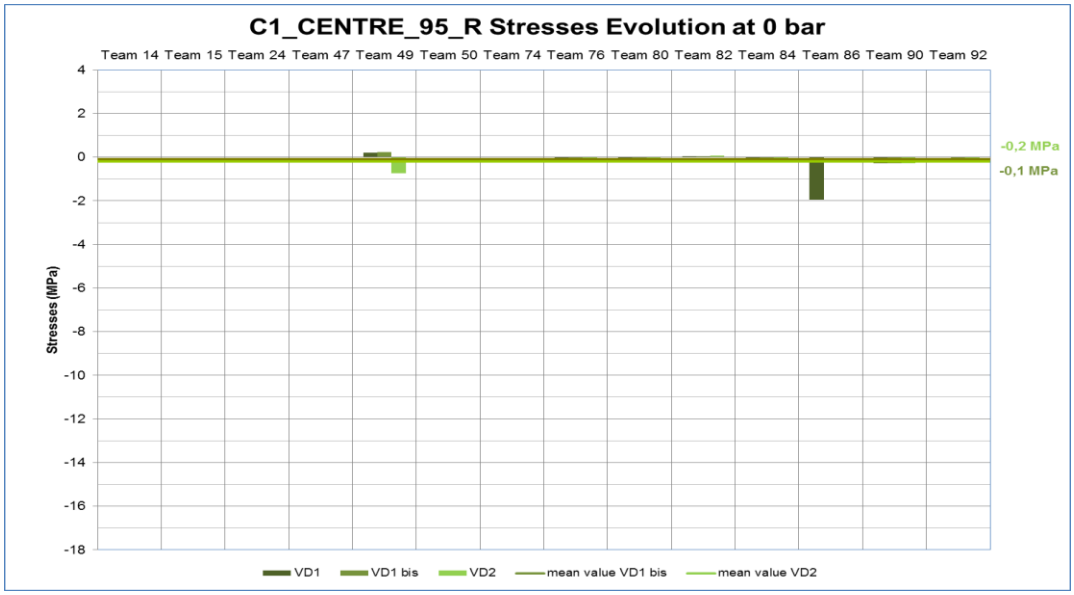

Figure 119. Stresses evolution at 0 bar: Raft – Lower level (195 Gr)

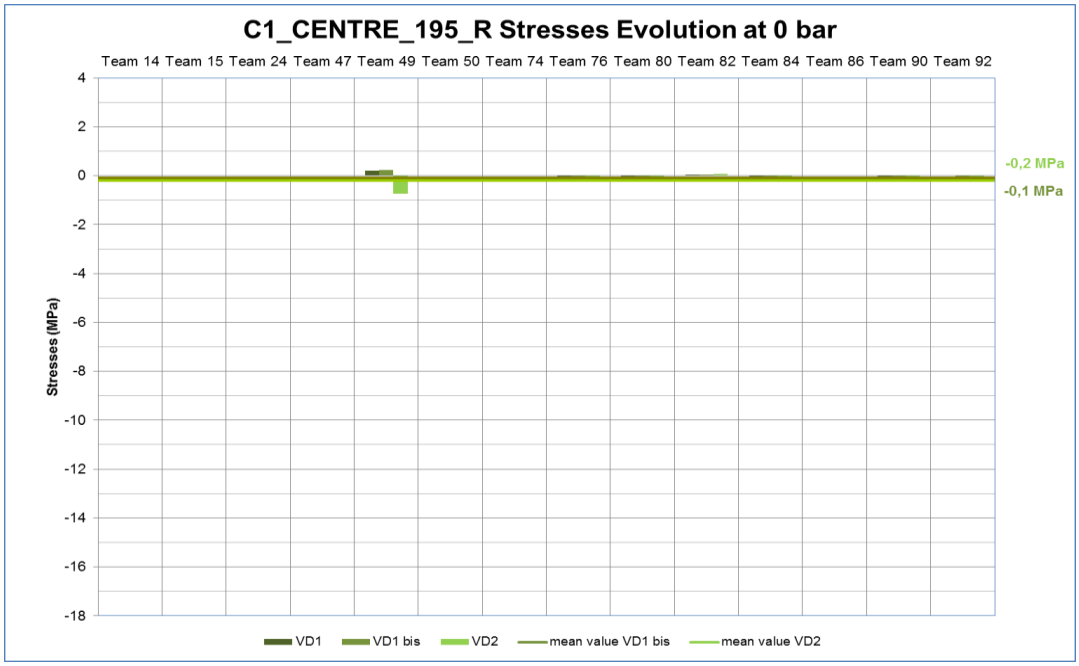

5.4.3.1.2 Upper level

Figure 120. Stresses evolution at 0 bar: Raft – Upper level (95 Gr)

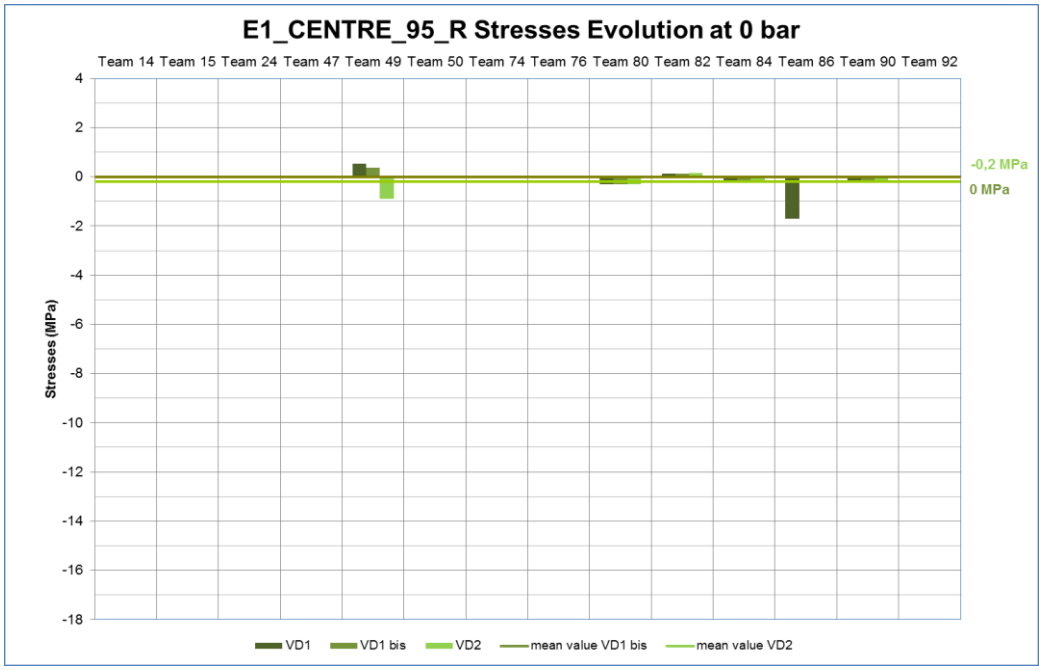

Figure 121. Stresses evolution at 0 bar: Raft – Upper level (195 Gr)

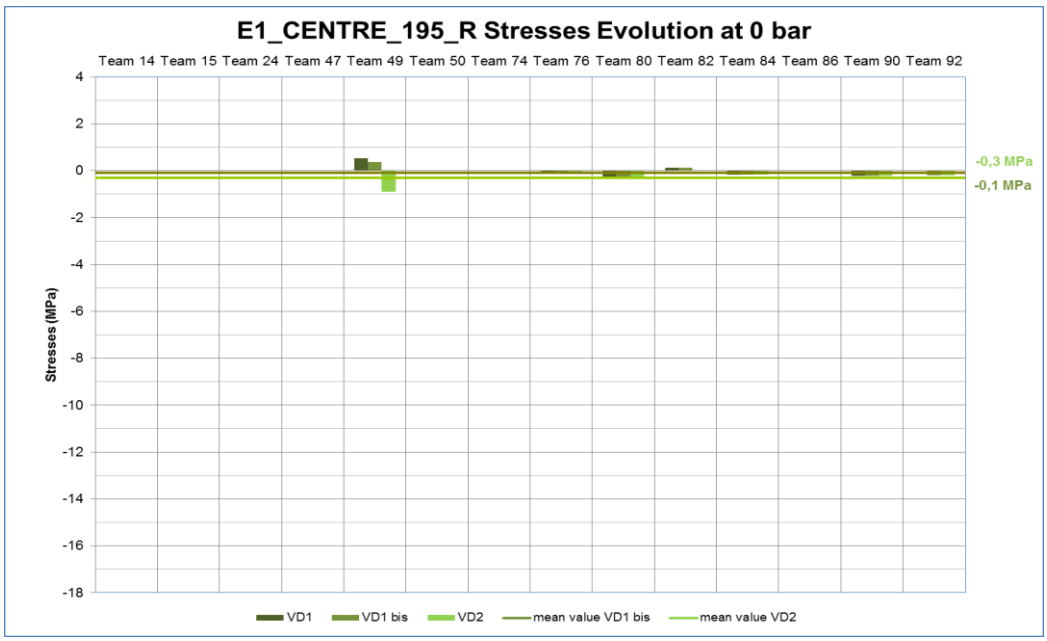

5.4.3.1.3 Comments

Participants gave on average no stresses in the centre of the raft, except for Team 49, which predicted an evolution from slight tensile stress to slight compressive stress over time, and Team 86, which gave a compressive stress of almost 2 MPa for VD1 considered to be a strange value.

5.4.3.2 Gusset stresses evolution

5.4.3.2.1 Vertical direction

Figure 122. Stresses evolution at 0 bar: Gusset – Vertical direction – Bottom – Intrados

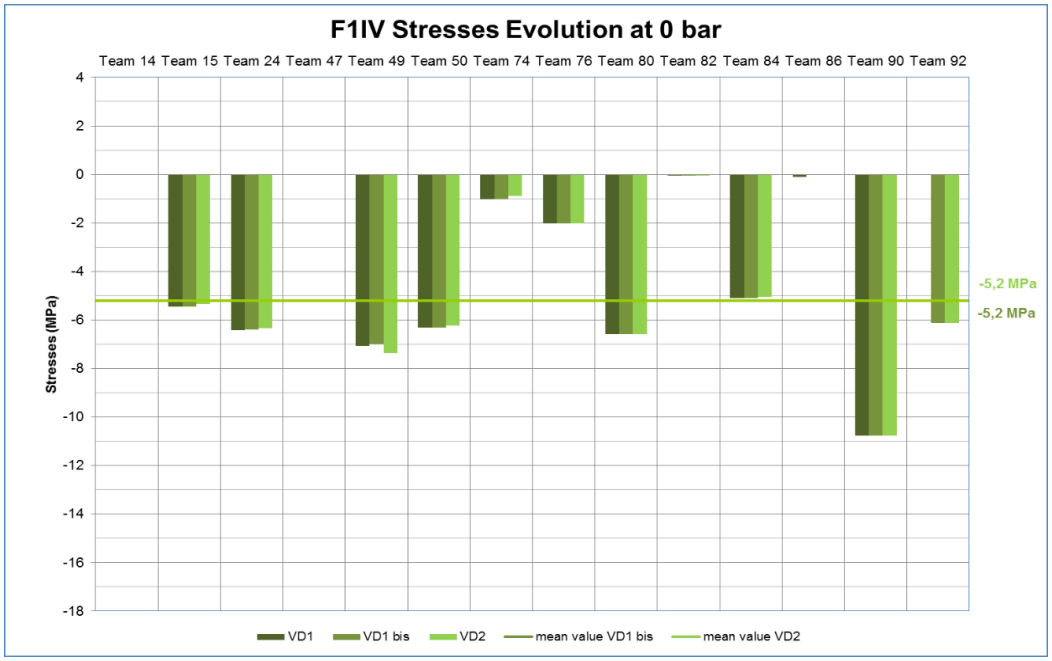

Figure 123. Stresses evolution at 0 bar: Gusset – Vertical direction – Bottom – Extrados

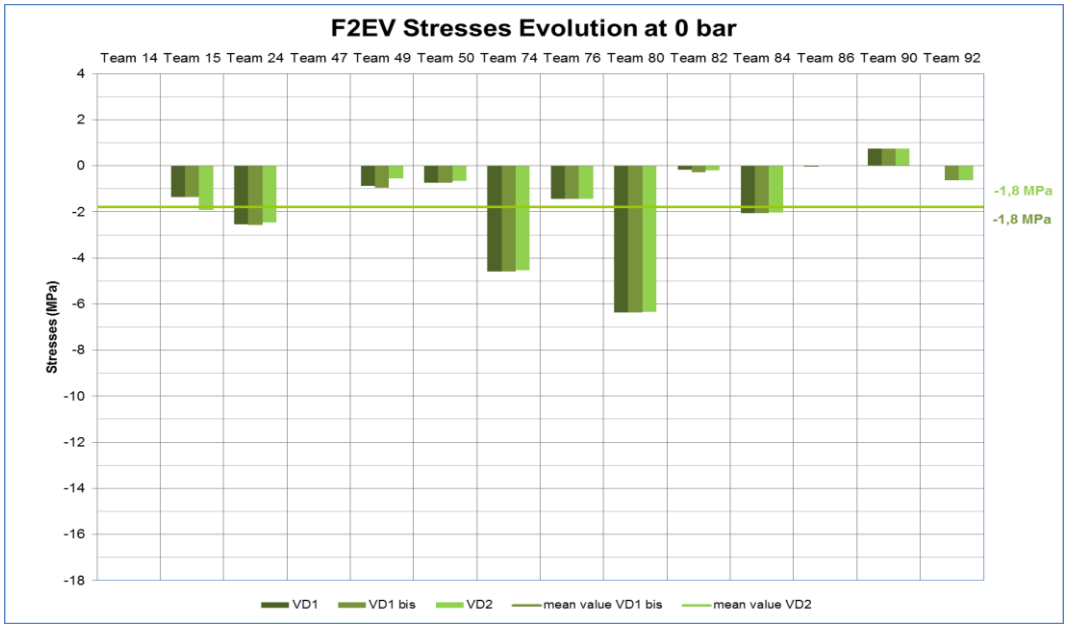

Figure 124. Stresses evolution at 0 bar: Gusset – Vertical direction – Top – Intrados

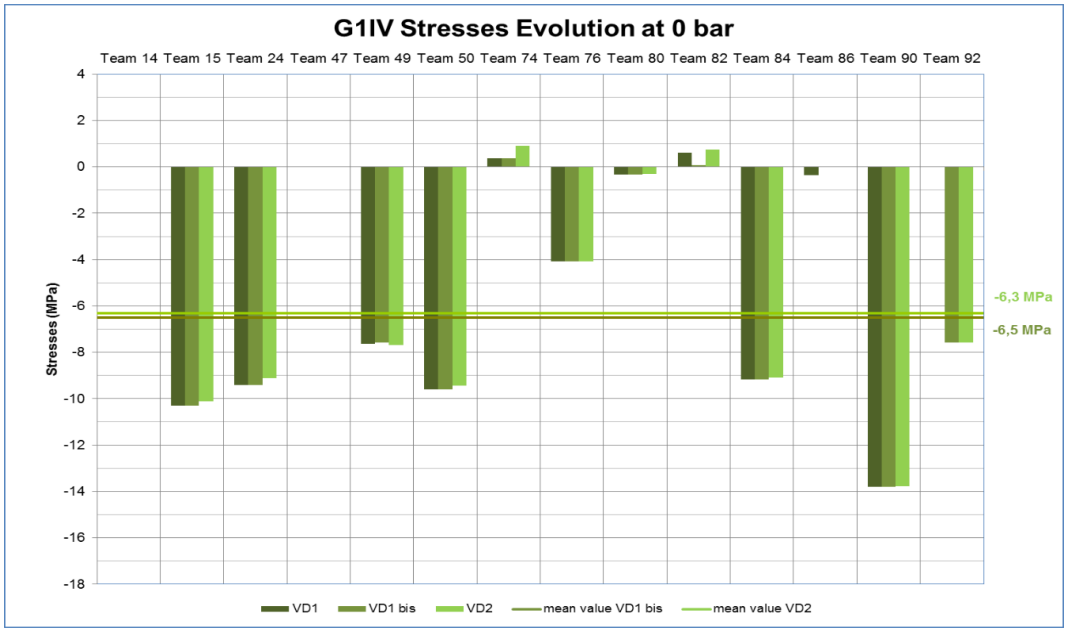

Figure 125. Stresses evolution at 0 bar: Gusset – Vertical direction – Top – Extrados

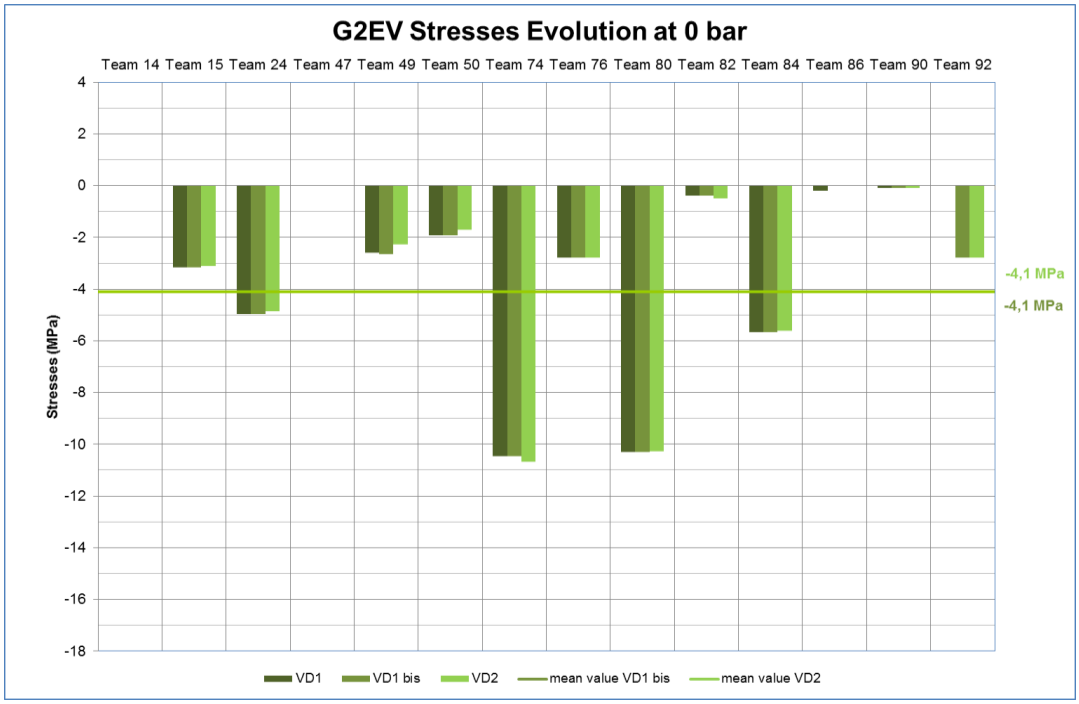

5.4.3.2.2 Tangential direction

Figure 126. Stresses evolution at 0 bar: Gusset – Tangential direction – Bottom – Intrados

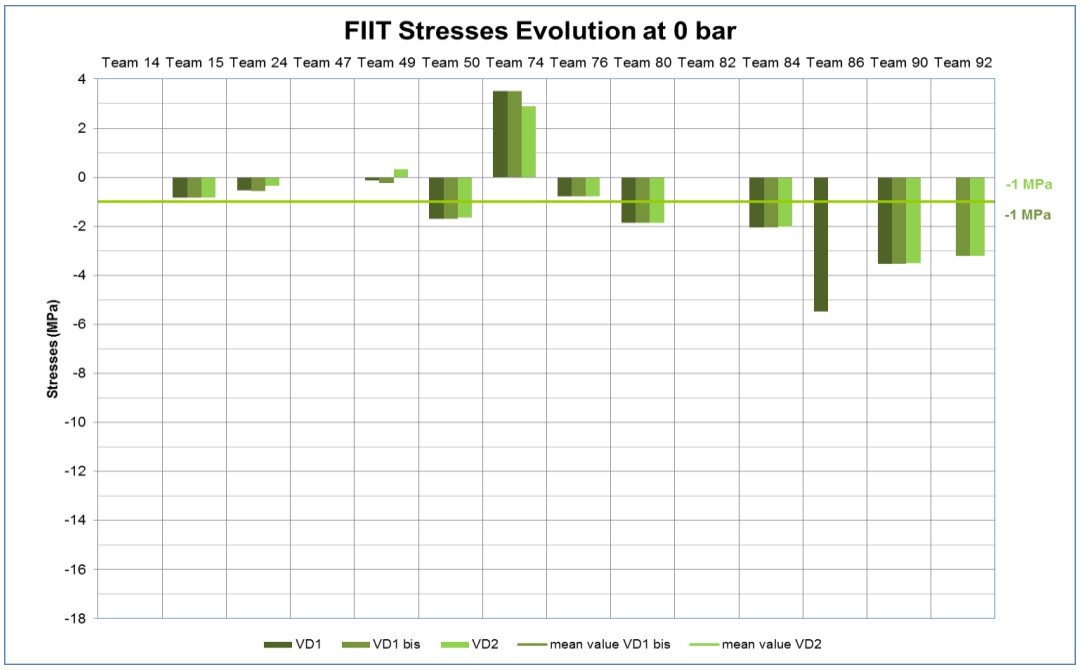

Figure 127. Stresses evolution at 0 bar: Gusset – Tangential direction – Bottom – Extrados

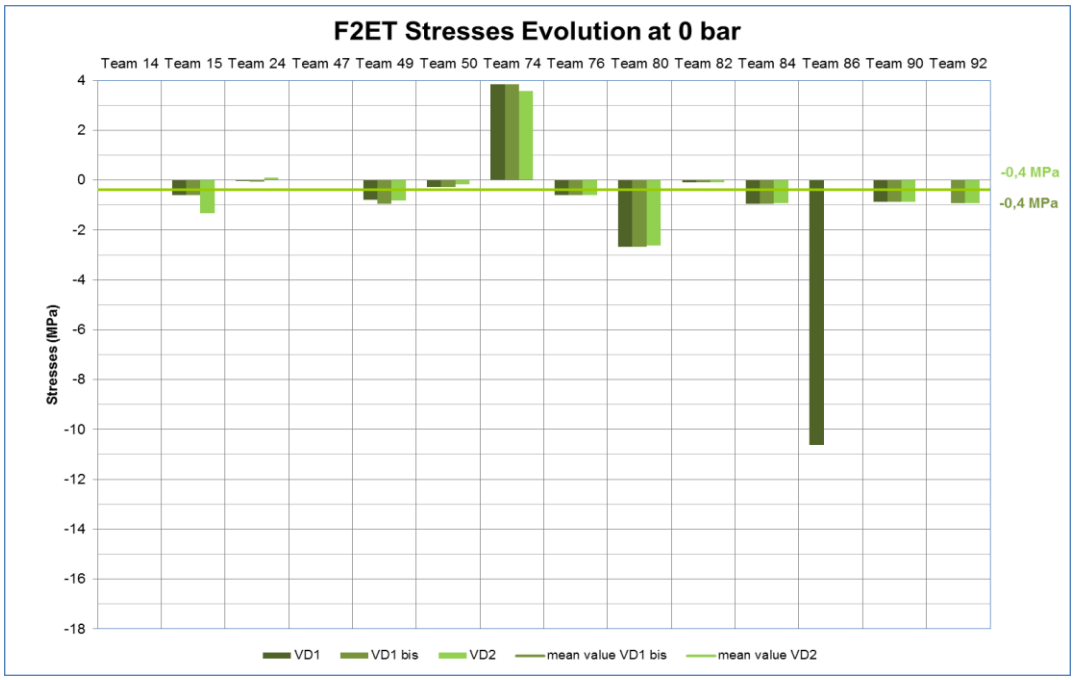

Figure 128. Stresses evolution at 0 bar: Gusset – Tangential direction – Top – Intrados

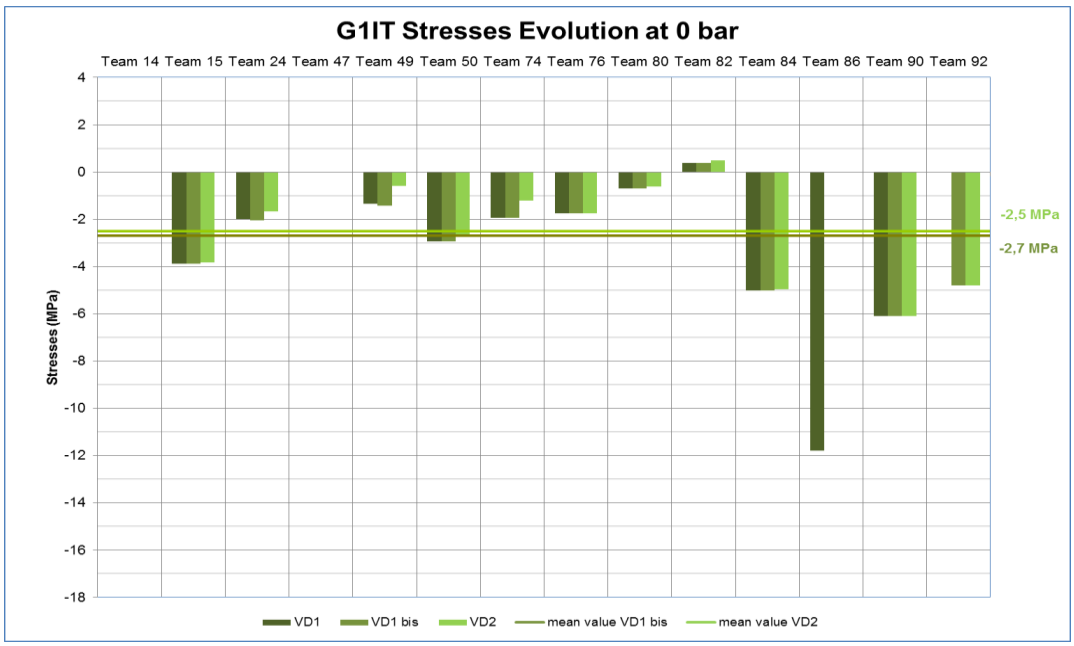

Figure 129. Stresses evolution at 0 bar: Gusset – Tangential direction – Top – Extrados

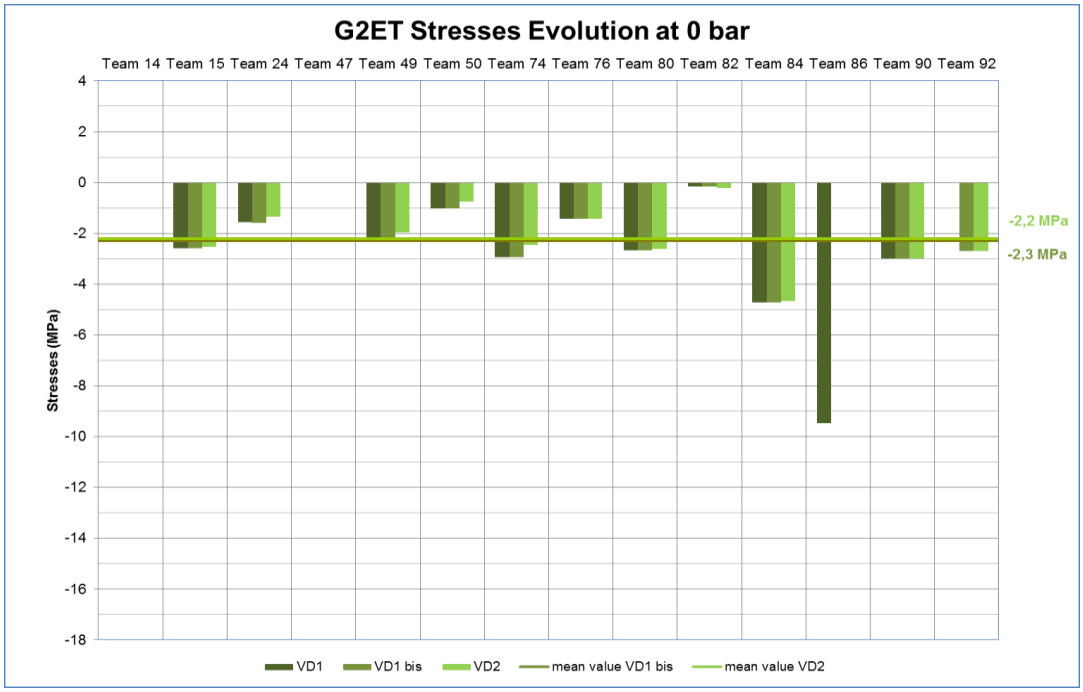

5.4.3.2.3 Comments on gusset stresses evolution

The results are very scattered, especially for the lower part of the gusset.

In the vertical direction, on average, participants found that intrados is more compressed than the extrados, except for Teams 74 and 80. Team 82 gave very low values of stress, even some tensile stress in G1IV. Team 86, which only submitted results in the gusset, gave almost no compressive stress in this direction.

In the horizontal direction, participants gave, on average, a low compressive stress in the bottom part of the gusset, except for Teams 74 and 88, which gave a tensile stress of almost 3 MPa. In the upper part of the gusset, participants showed on average a compressive stress of about 2.5 MPa. As in vertical direction, Team 82 gave a very low value of compressive stress, even a tensile stress on intrados. Team 86 gave very high values of compressive stress in this direction (between 5 MPa and 12 MPa).

Table 21 shows the distribution of participants' results concerning the stress evolution between VD1 bis and VD2.

Table 21. Participants' results of the gusset stresses evolution between VD1 bis and VD2

	Stress decreases in all points of the gusset	Stress decreases in some points of the gusset	Stress does not decrease in the gusset
Vertical direction	Teams 15, 24, 50, 80, 84	Teams 49, 74	Teams 76, 82, 90, 92
Tangential direction	Teams 24, 49, 50, 80, 84	Teams 15, 74	Teams 76, 82, 90, 92

5.4.3.3 Cylindrical wall stresses evolution

5.4.3.3.1 Vertical direction

Figure 130. Stresses evolution at 0 bar: Cylindrical part – Vertical direction – Extrados

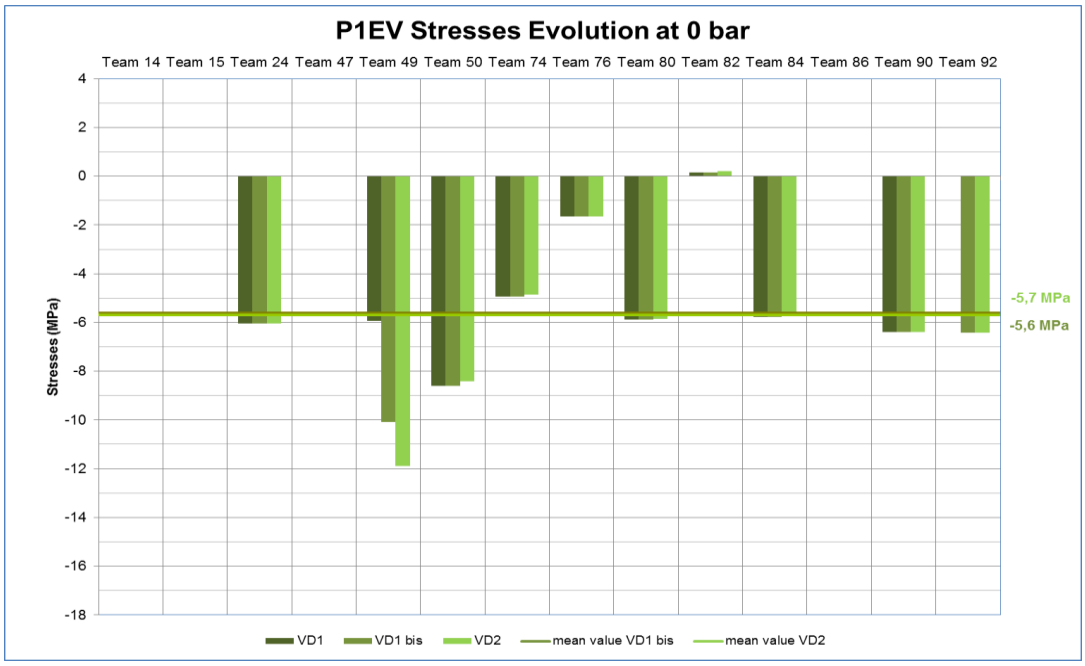

Figure 131. Stresses evolution at 0 bar: Cylindrical part – Vertical direction – Intrados

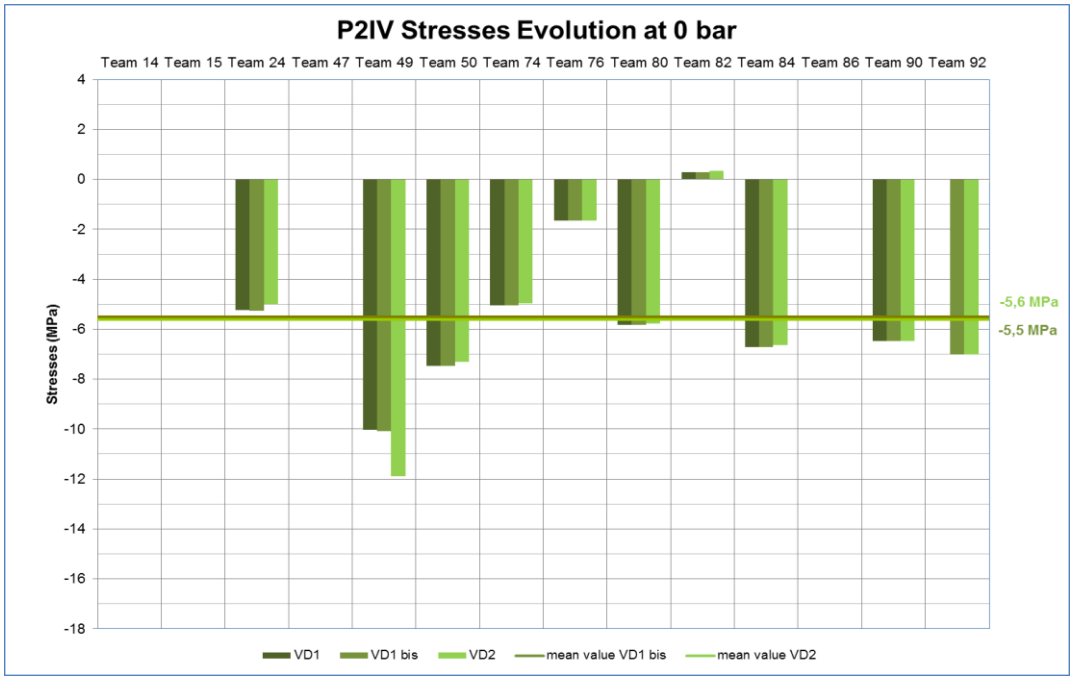

Figure 132. Stresses evolution at 0 bar: Cylindrical part – Vertical direction – Extrados

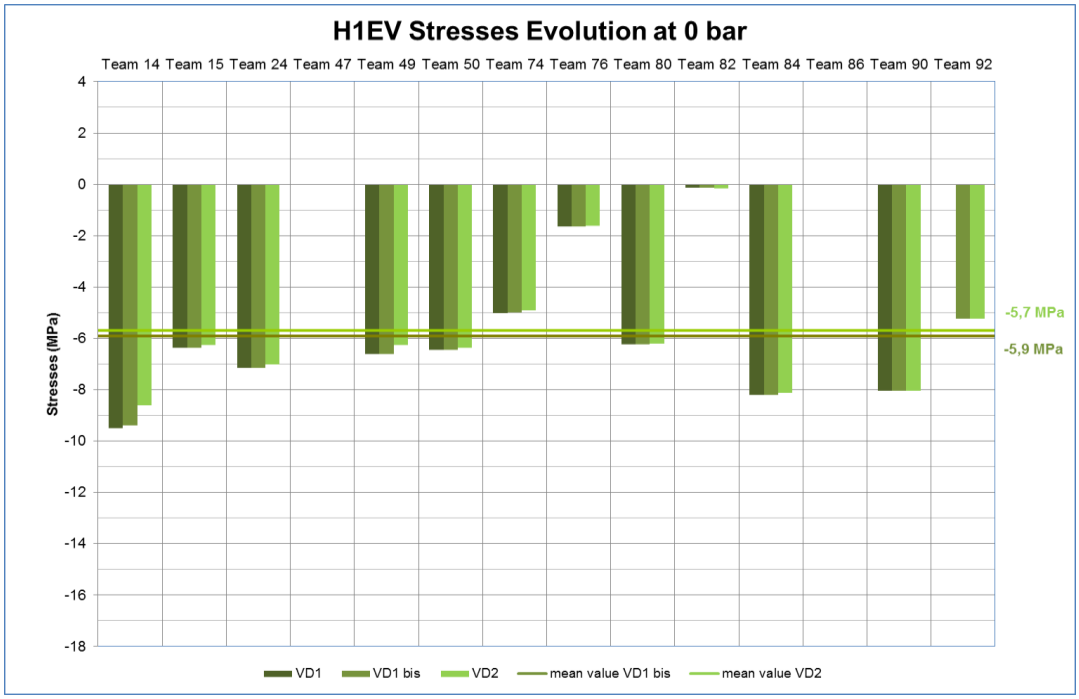

Figure 133. Stresses evolution at 0 bar: Cylindrical part – Vertical direction – Intrados

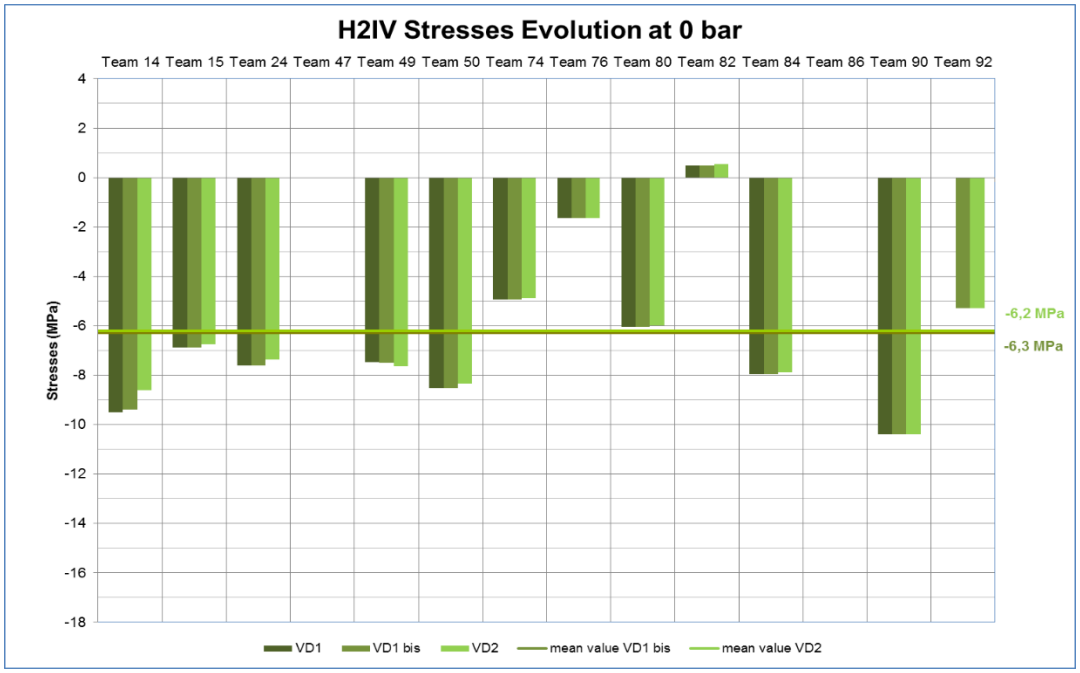

Figure 134. Stresses evolution at 0 bar: Cylindrical part – Vertical direction – Extrados

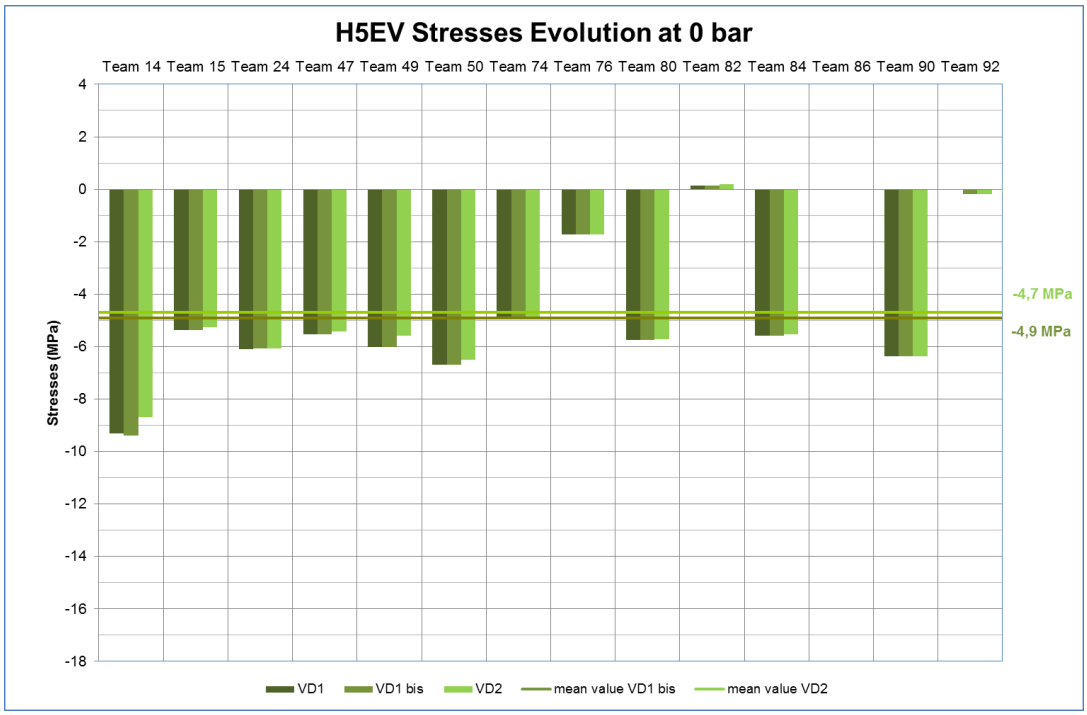

Figure 135. Stresses evolution at 0 bar: Cylindrical part – Vertical direction – Intrados

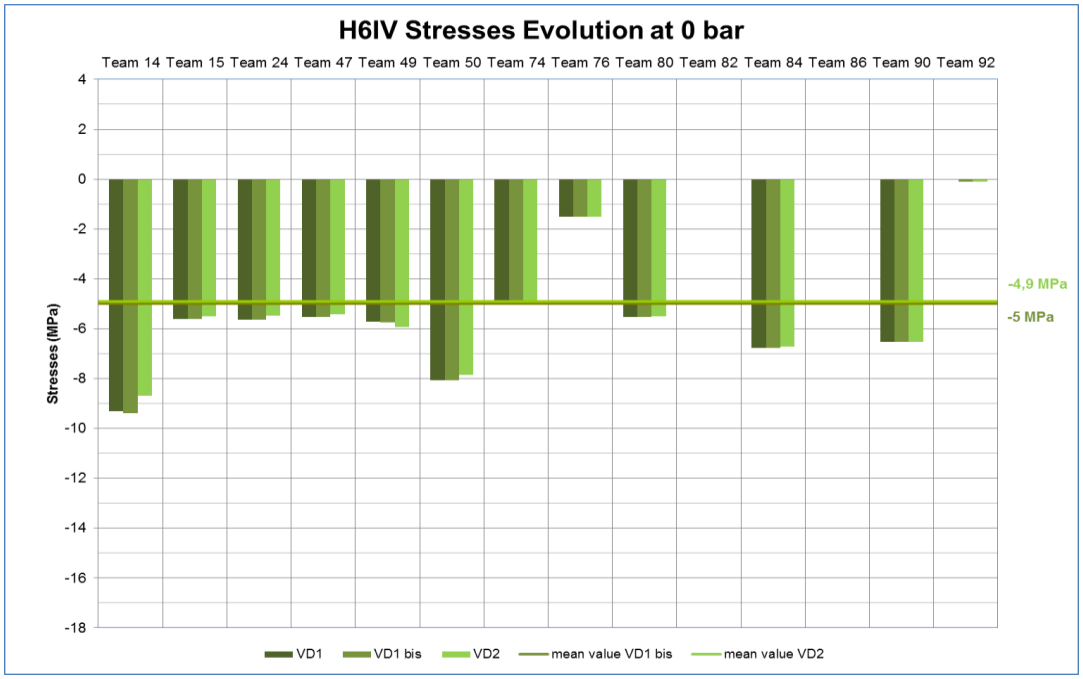

5.4.3.3.2 Tangential direction

Figure 136. Stresses evolution at 0 bar: Cylindrical part – Tangential direction – Extrados

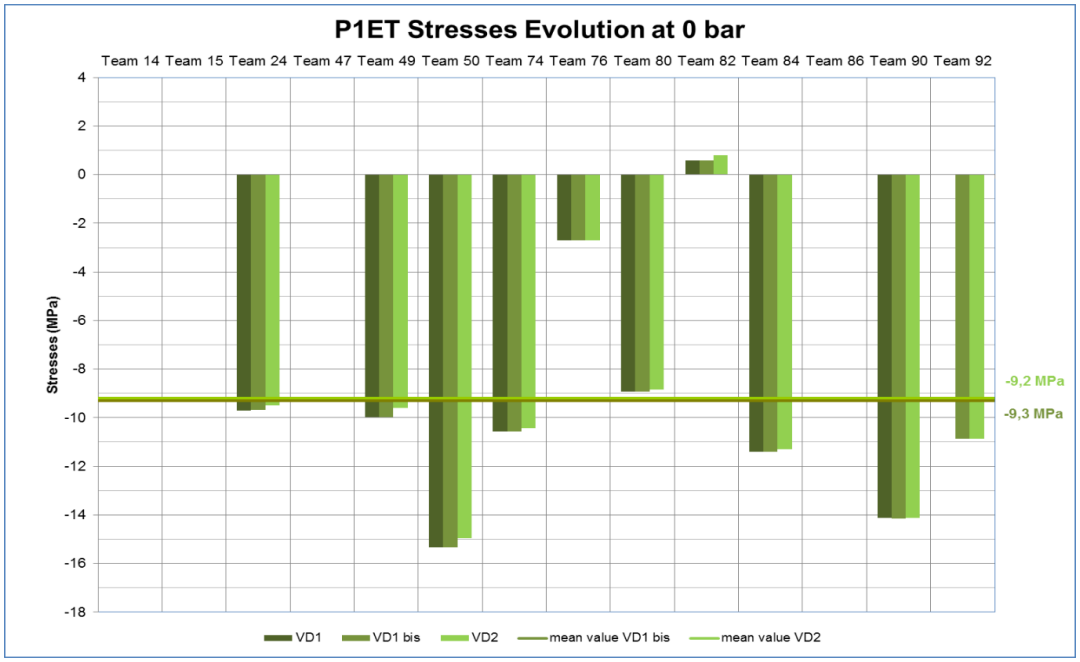

Figure 137. Stresses evolution at 0 bar: Cylindrical part – Tangential direction – Intrados

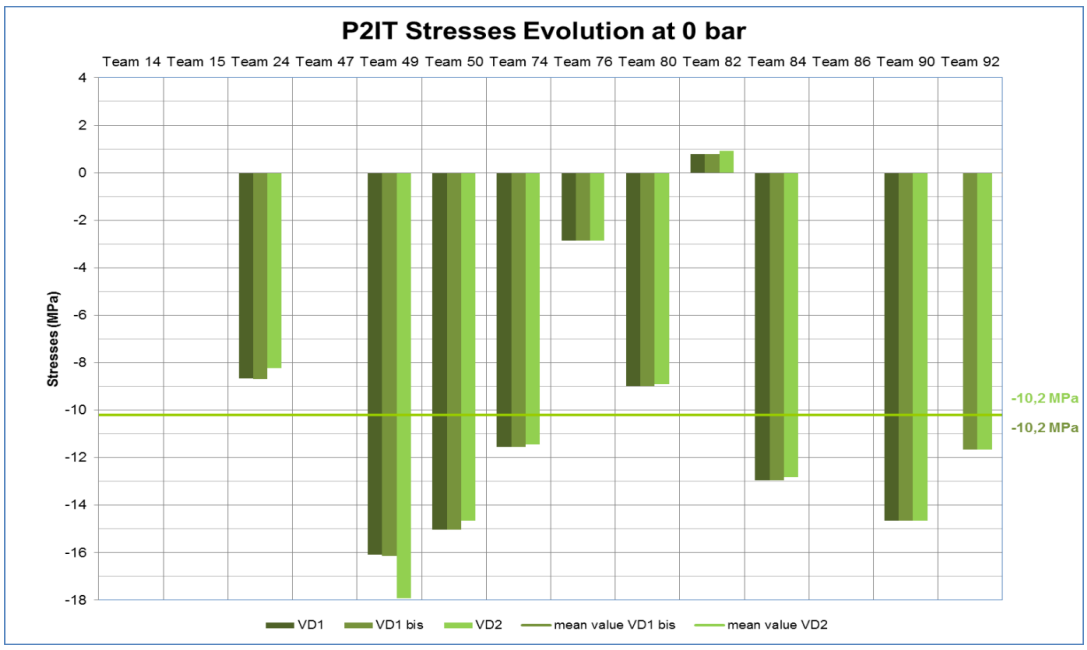

Figure 138. Stresses evolution at 0 bar: Cylindrical part – Tangential direction – Extrados

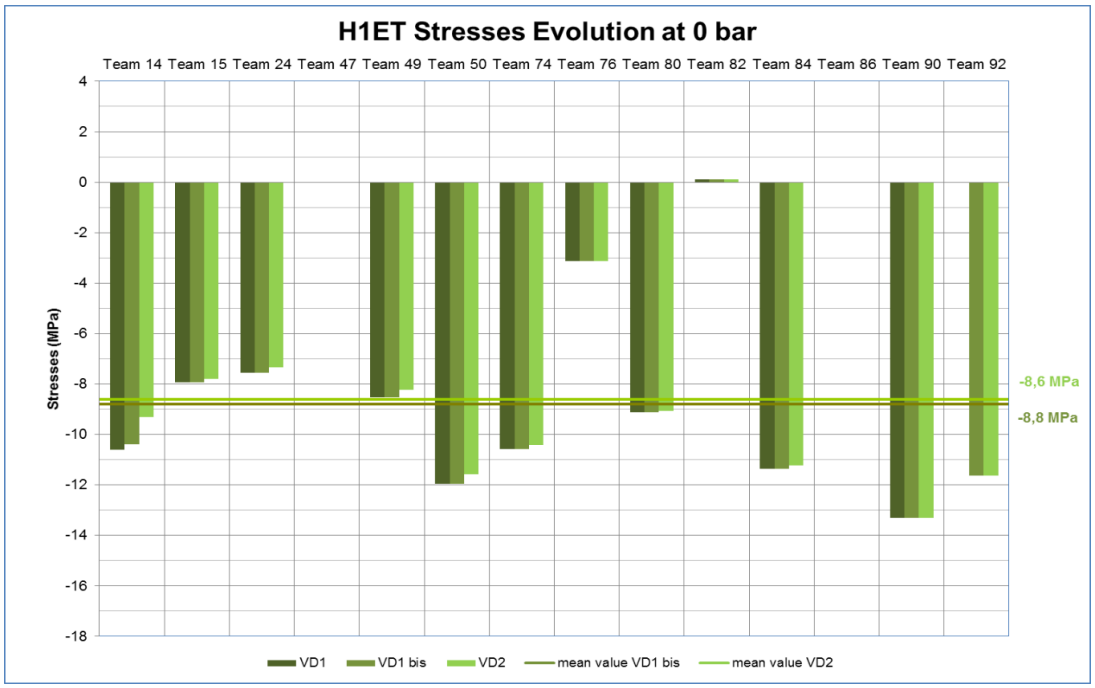

Figure 139. Stresses evolution at 0 bar: Cylindrical part – Tangential direction – Intrados

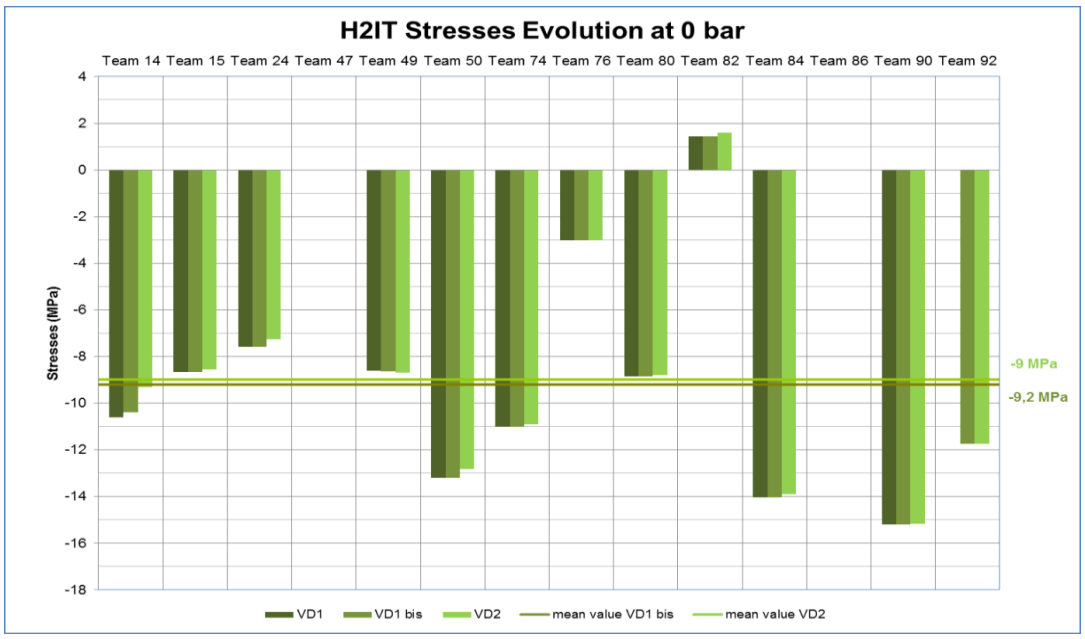

Figure 140. Stresses evolution at 0 bar: Cylindrical part – Tangential direction – Extrados

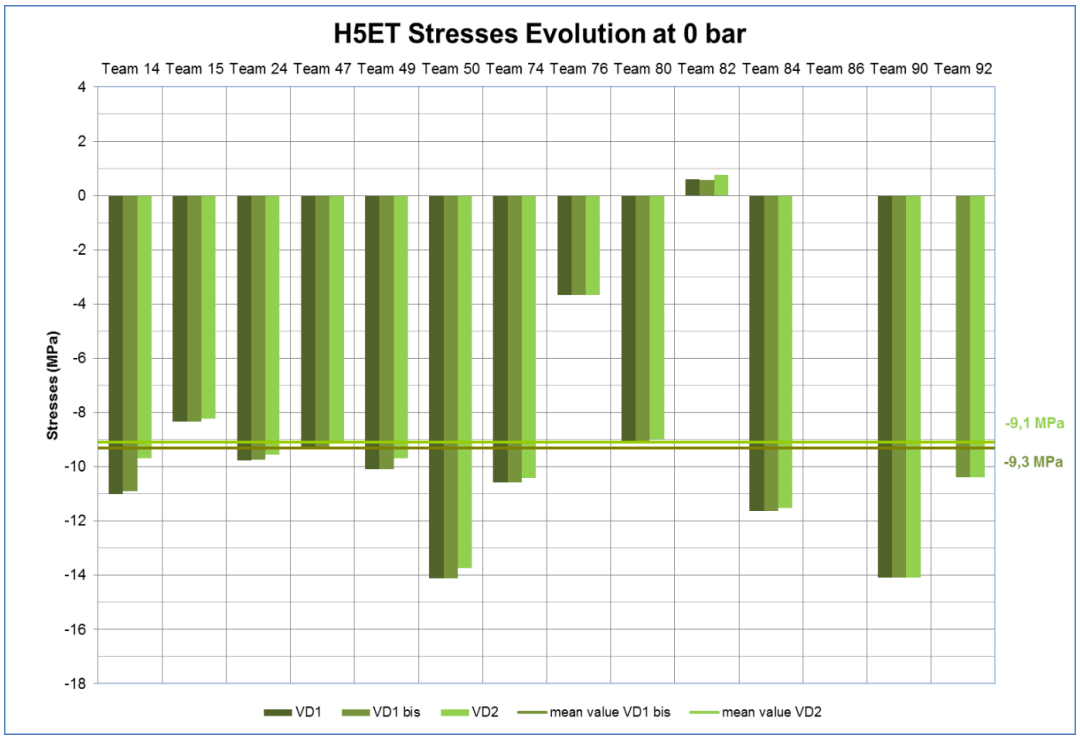

Figure 141. Stresses evolution at 0 bar: Cylindrical part – Tangential direction – Intrados

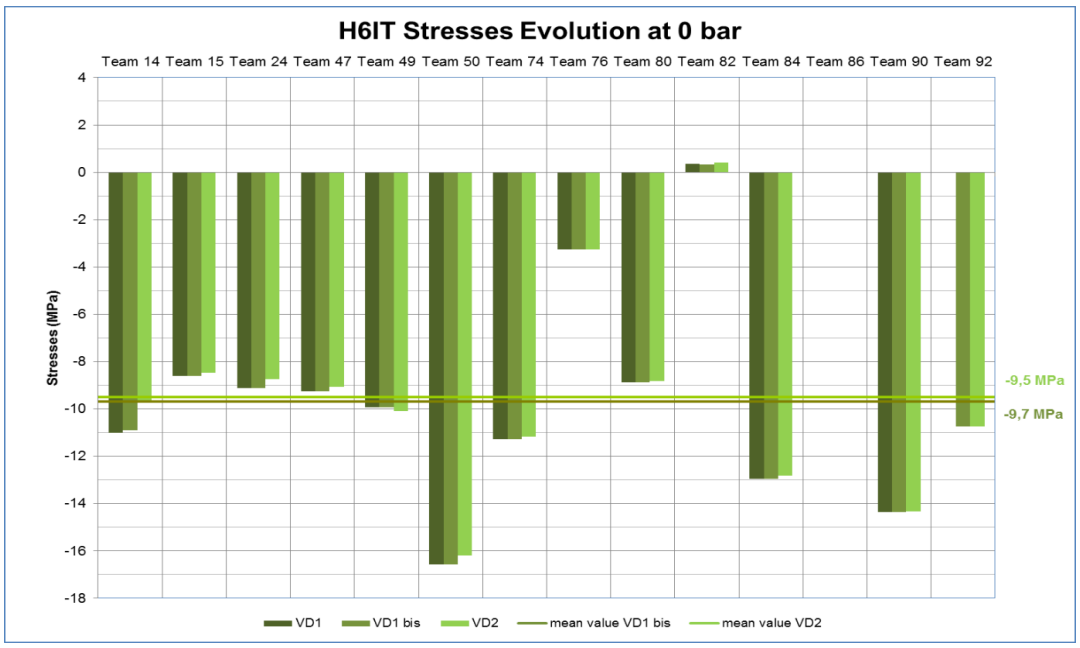

5.4.3.3.3 Comments on cylindrical wall stresses evolution

For this area, there are 12 or 13 stress values to compare. Results are less scattered than in the gusset.

Like in the gusset, Team 82 gave very low values of compressive stress, even tensile stress in some cases. Team 92's results were close to the mean value, except for two sensors – H5EV and H6IV – probably due to a mistake.

In the vertical direction, participants gave, on average, a value of 5.5 MPa of compressive stress. Results ranged from 1.5 MPa to 10.4 MPa, without mistake values. Except for Team 82, the smallest compressive stress value was given by Team 76 on each point. Team 49 gave strange values for sensors P1EV and P2IV, with higher values of stress for this point in comparison to H1, H2, H5 and H6 located in the same area.

In the tangential direction, on average, participants gave a compressive stress of 9.4 MPa. Stresses range from -16.6 MPa to -2.7 MPa. With the exception of Team 82, the smallest compressive stress value was given by Team 76, which gave about -3 MPa on each point. The highest values were given by Teams 49, 50 and 90.

Table 22 presents the distribution of participants' results concerning the stress evolution between VD1 bis and VD2.

Table 22. Distribution of participants' results for the cylindrical wall stresses evolution between VD1 bis and VD2

	Stress decreases in all points at mid-height	Stress decreases in some points at mid-height	Stress does not decrease at mid-height
Vertical direction	Teams 14, 15, 24, 47, 50, 74, 80, 84	Teams 49	Teams 76, 82, 90, 92
Tangential direction	Teams 14, 15, 24, 47, 50, 74, 80, 84, 90	Teams 49	Teams 76, 82, 92

The majority of the teams found that compressive stress decreases over time.

5.4.3.4 Equipment hatch stresses evolution

5.4.3.4.1 Side of the hatch

Figure 142. Stresses evolution at 0 bar: Side of the hatch – Vertical – Extrados

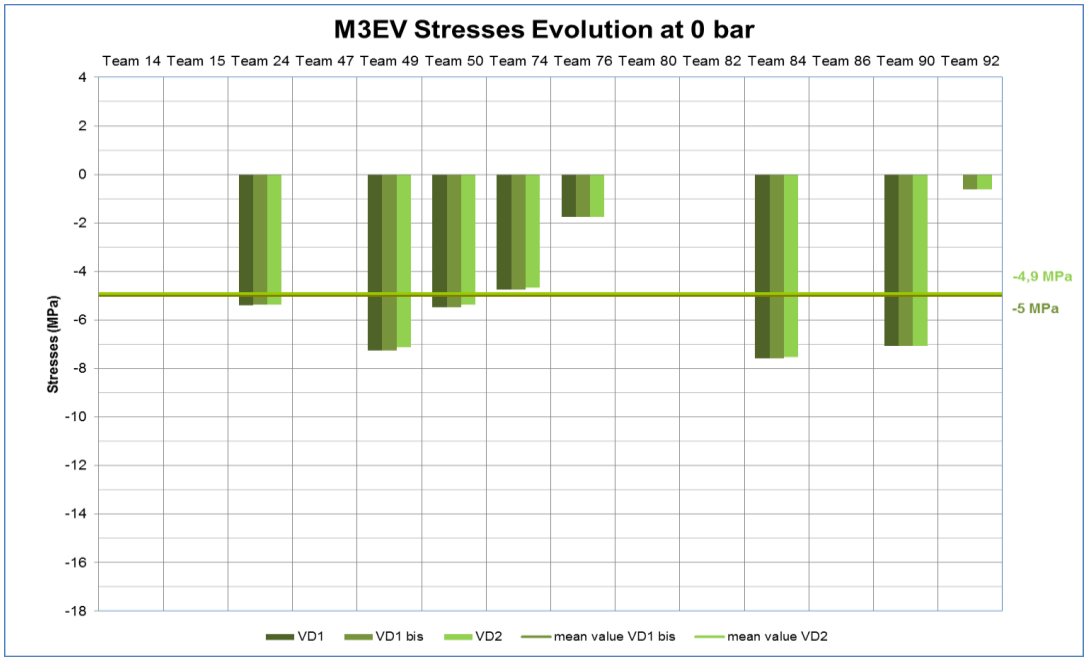

Figure 143. Stresses evolution at 0 bar: Side of the hatch – Tangential – Extrados

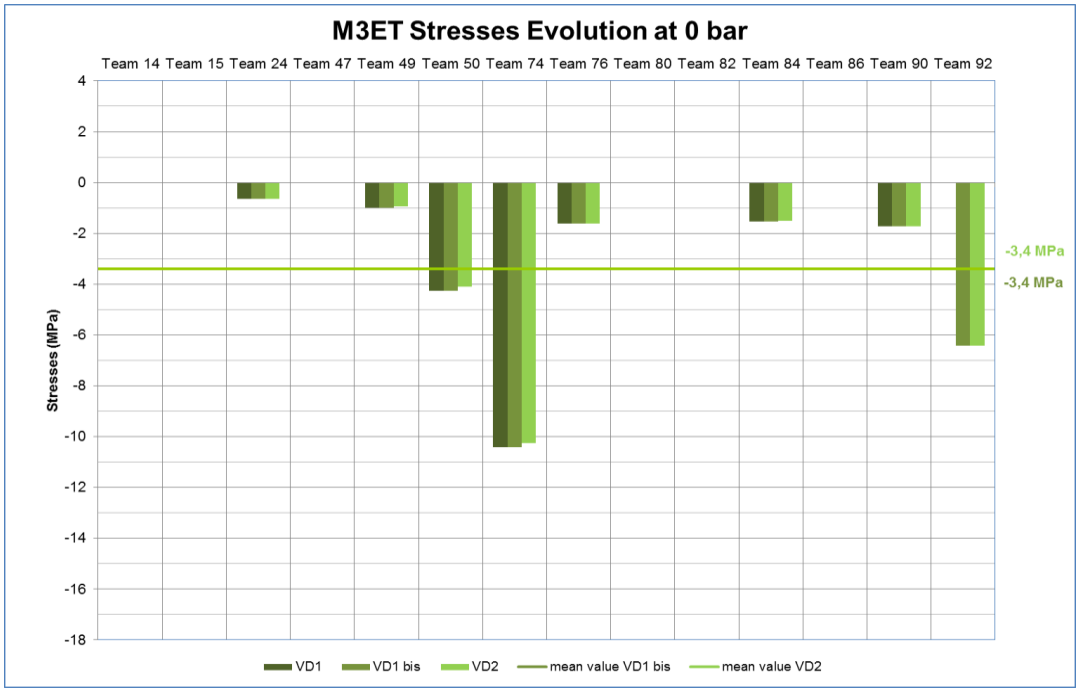

Figure 144. Stresses evolution at 0 bar: Side of the hatch – Vertical – Intrados

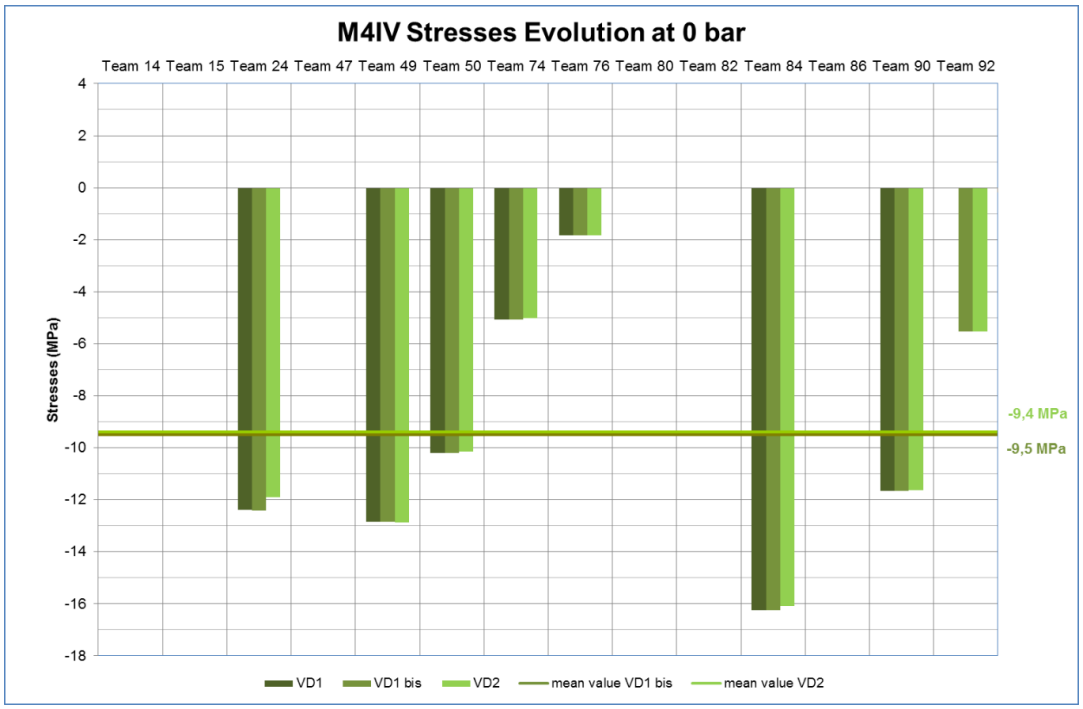

Figure 145. Stresses evolution at 0 bar: Side of the hatch – Tangential – Intrados

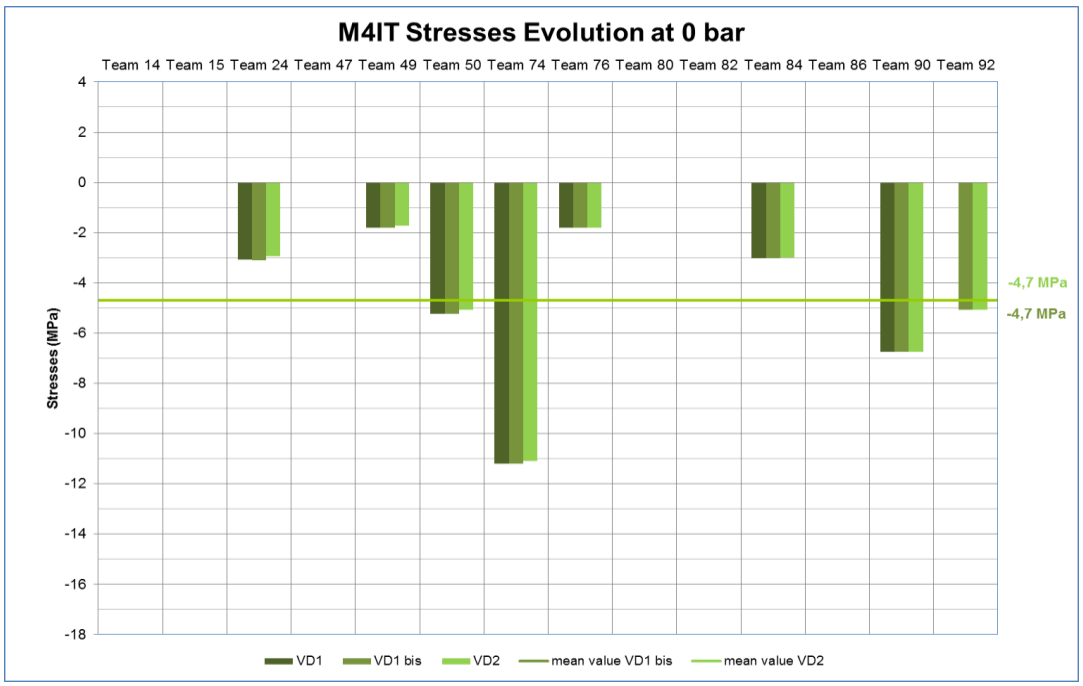

5.4.3.4.2 Above the hatch

Figure 146. Stresses evolution at 0 bar: Above the hatch – Vertical – Extrados

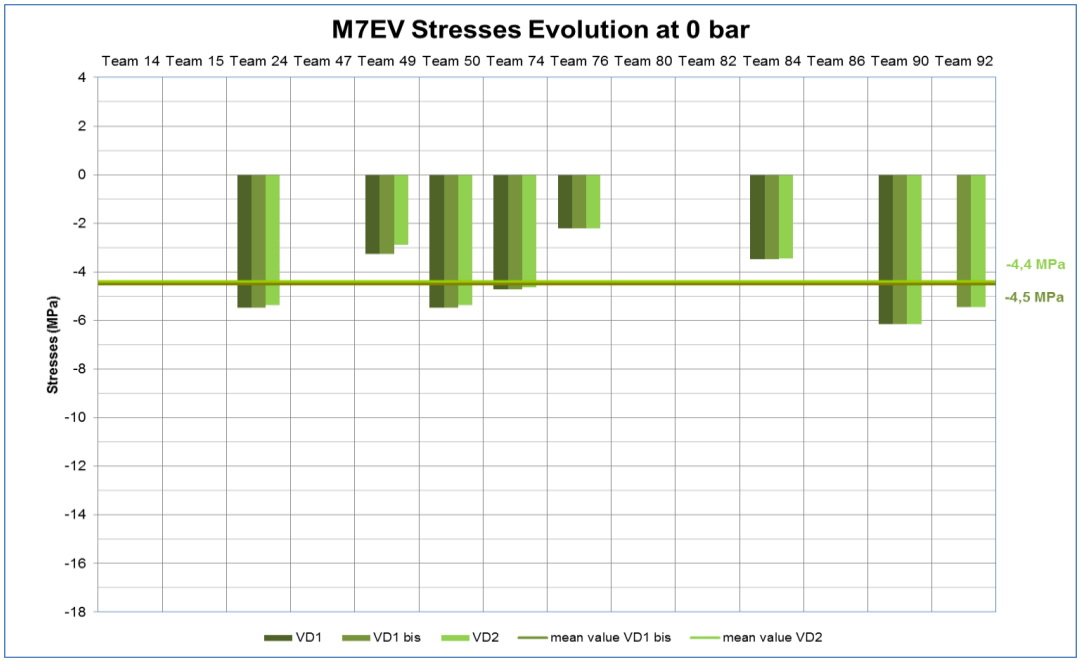

Figure 147. Stresses evolution at 0 bar: Above the hatch – Tangential – Extrados

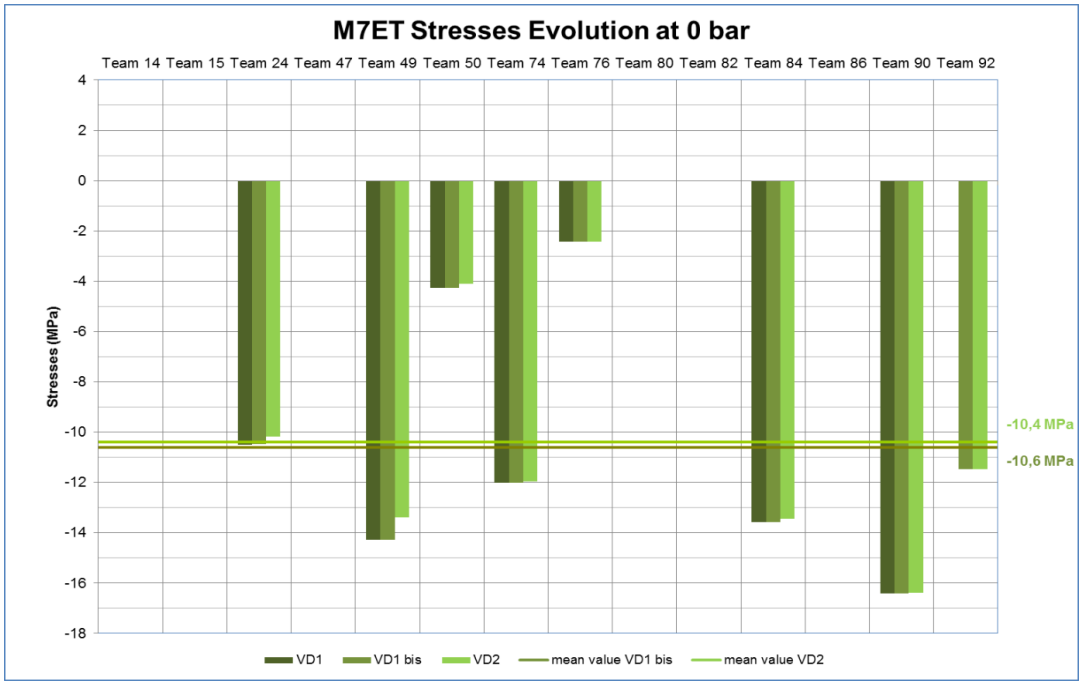

Figure 148. Stresses evolution at 0 bar: Above the hatch – Vertical – Intrados

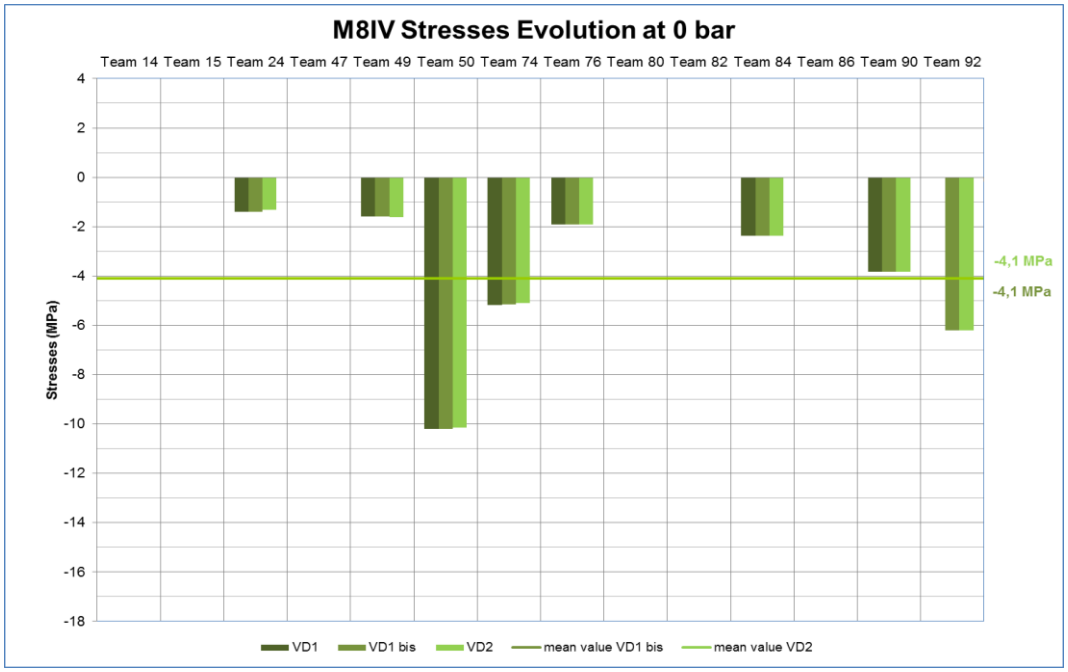

Figure 149. Stresses evolution at 0 bar: Above the hatch – Tangential – Intrados

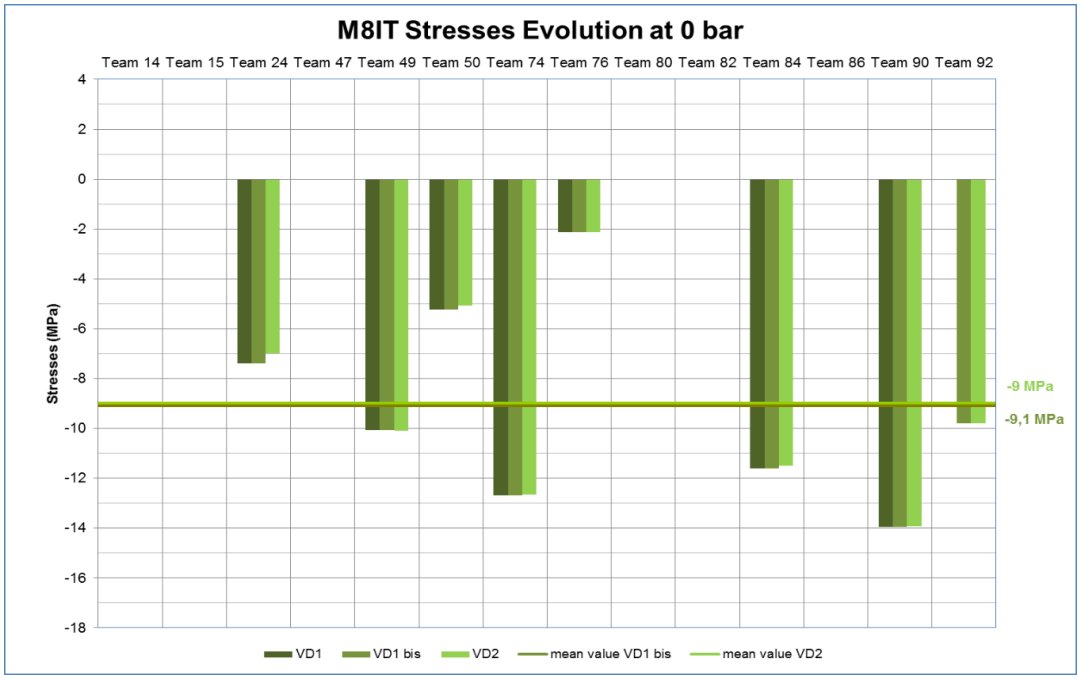

5.4.3.4.3 Comments

Only eight participants gave some stress results in this area.

Due to the tendons' deviation around the hatch, the stresses are different in this area compared to the current part of the cylinder.

On the side of the hatch, except for Team 74, all participants found this result and gave a higher compressive stress in the vertical direction than in the tangential direction. In this part, participants gave, on average, a compressive stress of about 4 MPa in the tangential direction (in comparison to the current part, where the mean value was about 5.5 MPa).

Conversely, above the hatch, the compressive stress was much higher in the tangential direction, except for Team 50. The vertical compressive stress was, on average, about 4 MPa above the hatch. It was less than for the current part of the cylinder, where the mean value was around 5.5 MPa.

5.4.3.5 Dome stresses evolution

5.4.3.5.1 Results

Figure 150. Stresses evolution at 0 bar: Top of the dome – Extrados (194 Gr)

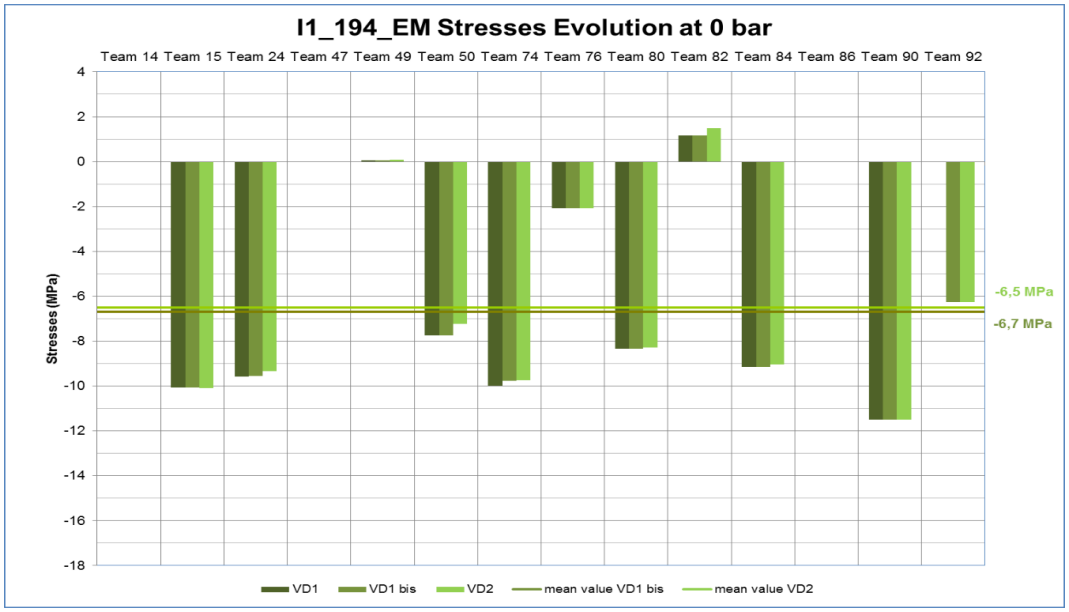

Figure 151. Stresses evolution at 0 bar: Top of the dome – Extrados (94 Gr)

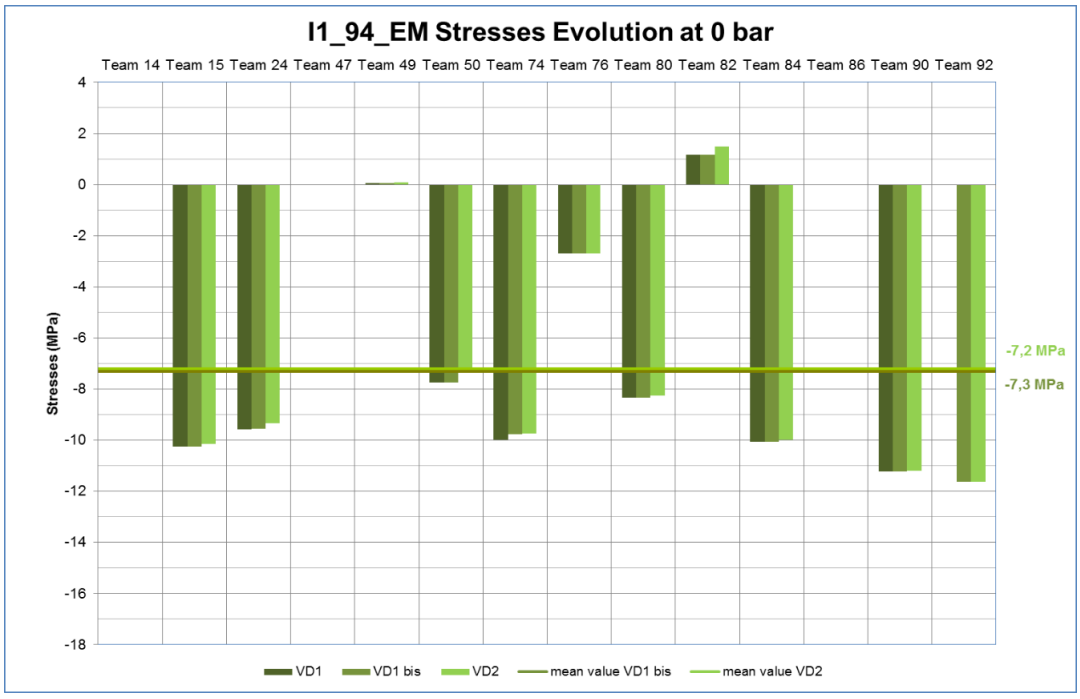

Figure 152. Stresses evolution at 0 bar: Top of the dome – Intrados (194 Gr)

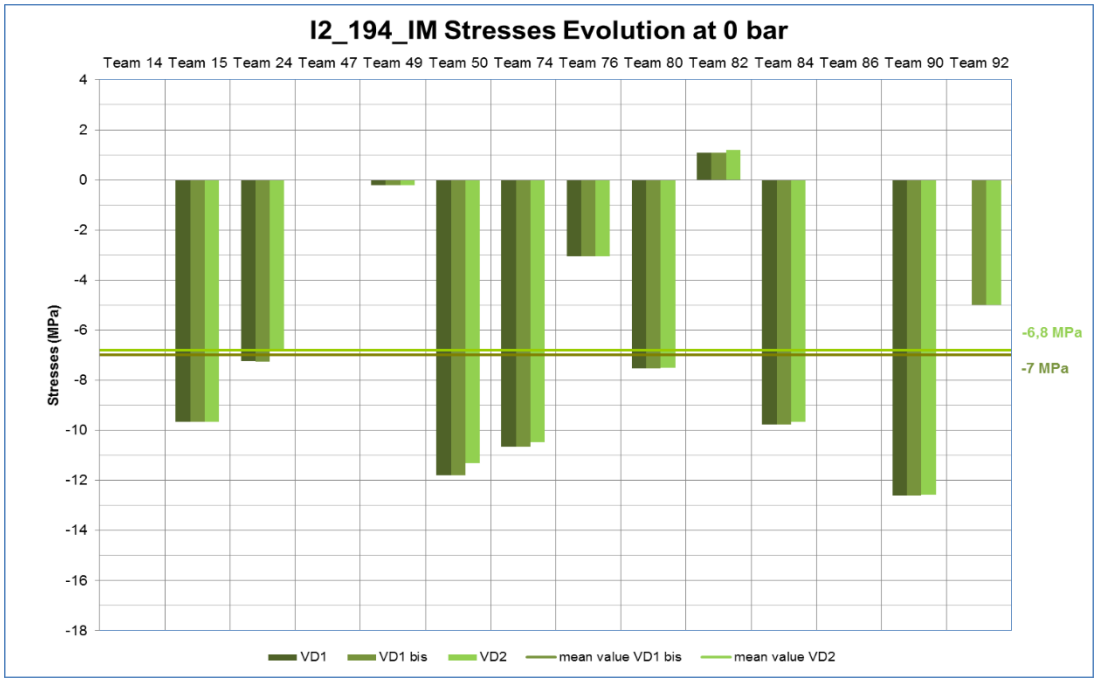

Figure 153. Stresses evolution at 0 bar: Top of the dome – Intrados (94 Gr)

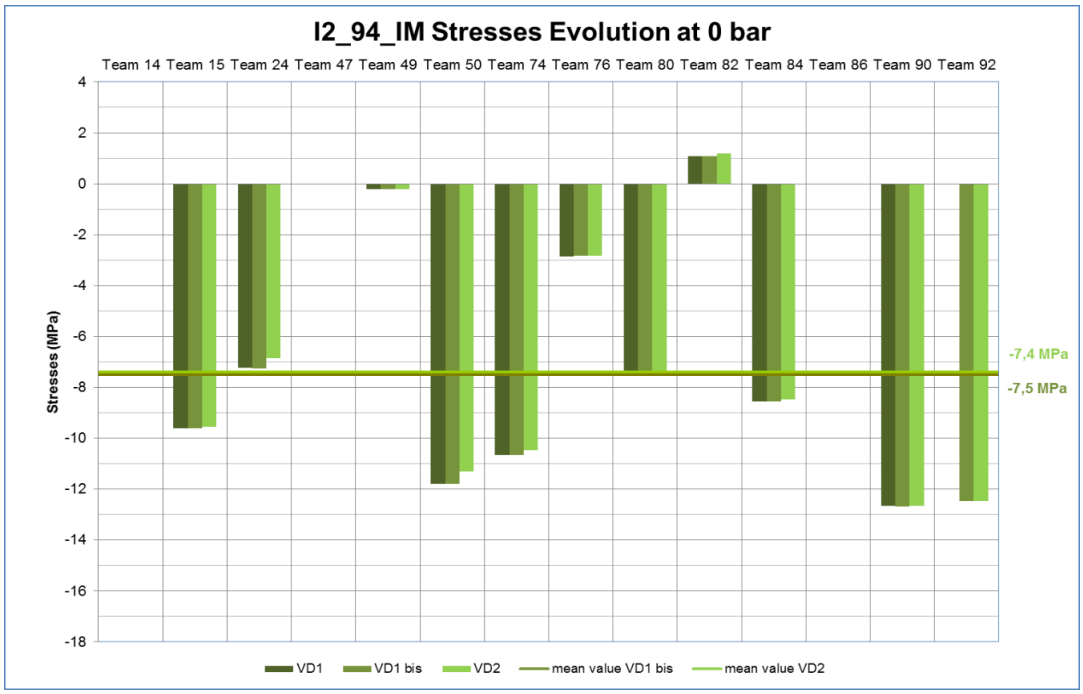

Figure 154. Stresses evolution at 0 bar: Meridian part of the dome – Meridian direction – Extrados

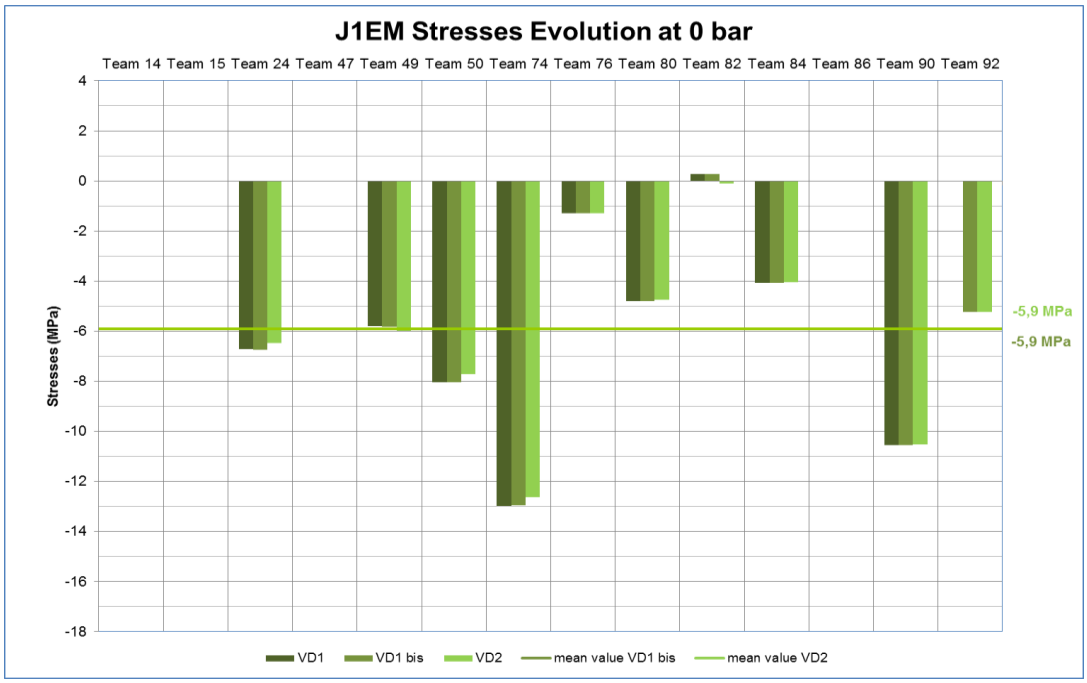

Figure 155. Stresses evolution at 0 bar: Meridian part of the dome – Tangential direction – Extrados

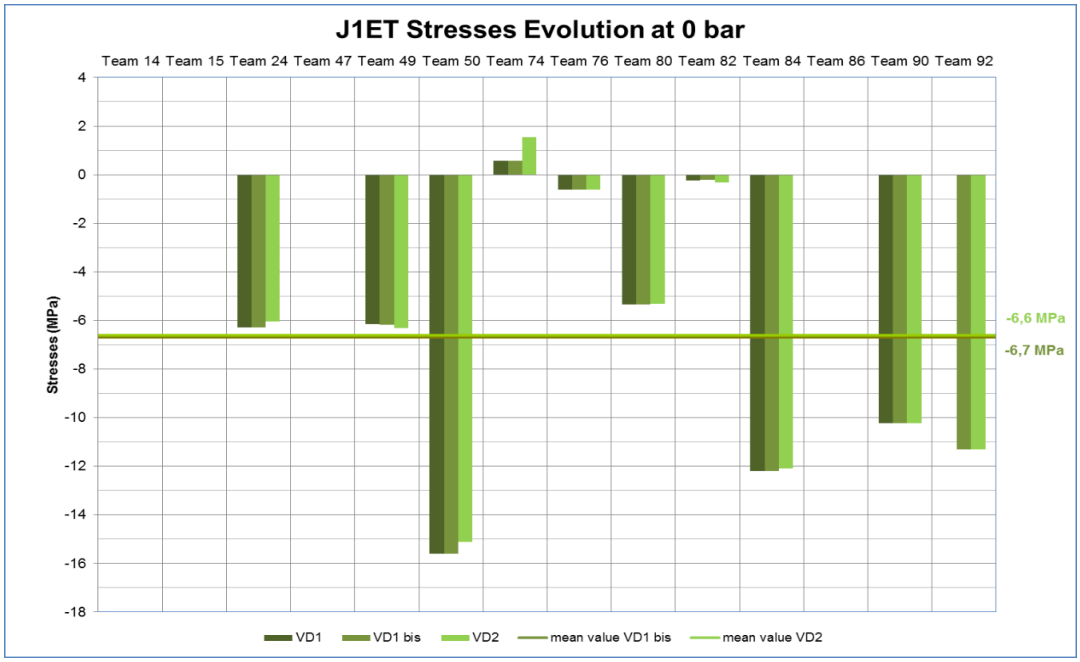

Figure 156. Stresses evolution at 0 bar: Meridian part of the dome – Meridian direction – Intrados

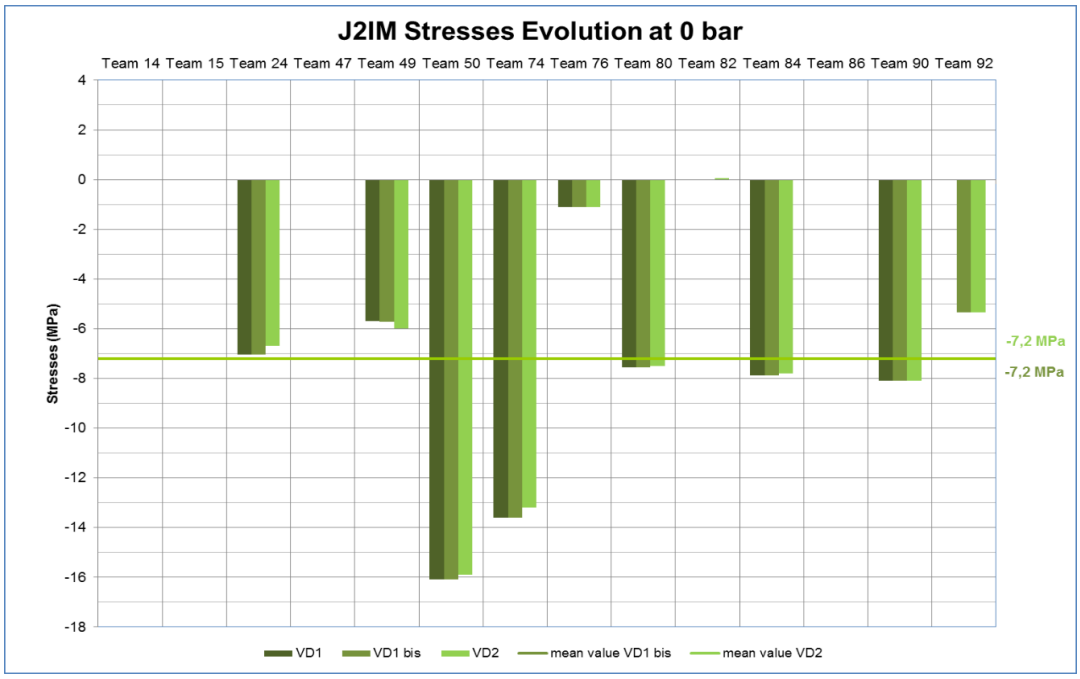

Figure 157. Stresses evolution at 0 bar: Meridian part of the dome – Tangential direction – Intrados

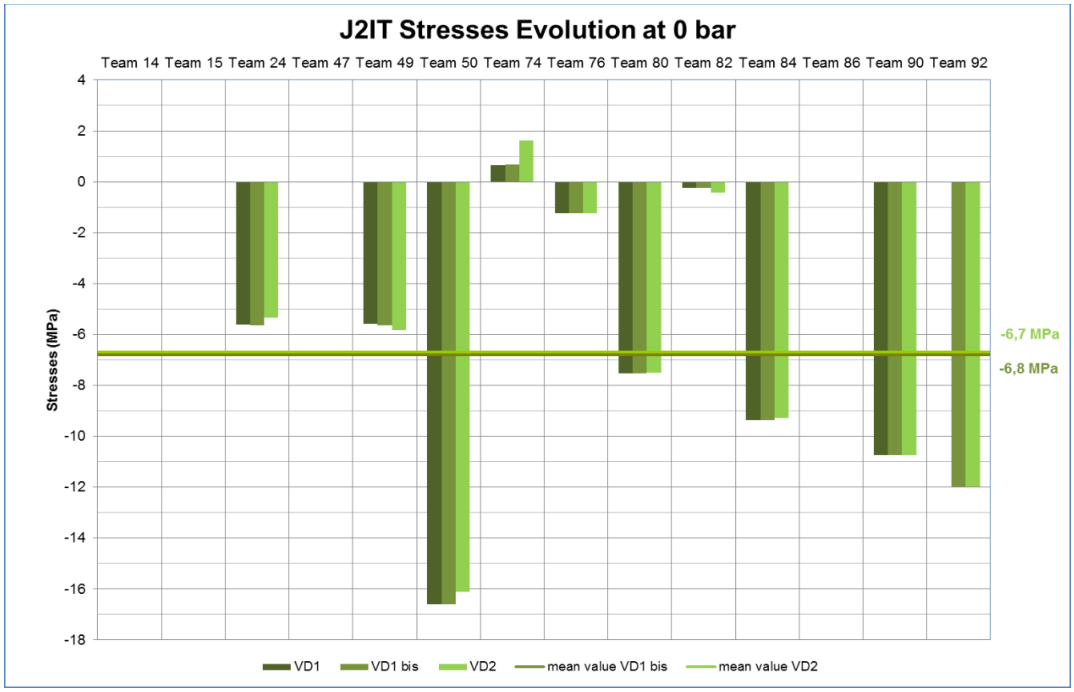

5.4.3.5.2 Comments on the dome stresses evolution

The teams' results are more scattered in this area.

There are still strange values for Team 82, which gave very low stress values, even some tensile stress values. At the top of the dome, Team 49 also gave some quite null stresses. Team 76 gave low values in both the top and the meridian part of the dome.

On average, the compressive stress at the top of the dome is about 7 MPa.

Table 23 gives the distribution of participants' results concerning the stress evolution between VD1 bis and VD2.

Table 23. Distribution of participants' results for the dome stresses evolution between VD1 bis and VD2

	Stress decreases	Stress decreases in some points	Stress does not decrease
Top of the dome	Teams 24, 50, 74, 80, 84, 90	Team 15	Teams 49, 76, 82, 92
Meridian zone	Teams 24, 50, 74, 80, 84, 90		Teams 49, 76, 82, 92

The majority of the teams found that compressive stress decreases over time.

5.4.4. Stresses evolution at 4.2 bar relative

This part analyses stresses at 4.2 bar during pressure test plateau and for several pressure tests over time. This analysis shows the compressive state of the concrete in the whole containment and gives an indication of the risk of cracks appearing due to local tensile stress.

5.4.4.1 Raft stresses evolution

5.4.4.1.1 Lower level

Figure 158. Stresses evolution at 4.2 bar: Raft – Lower level (95 Gr)

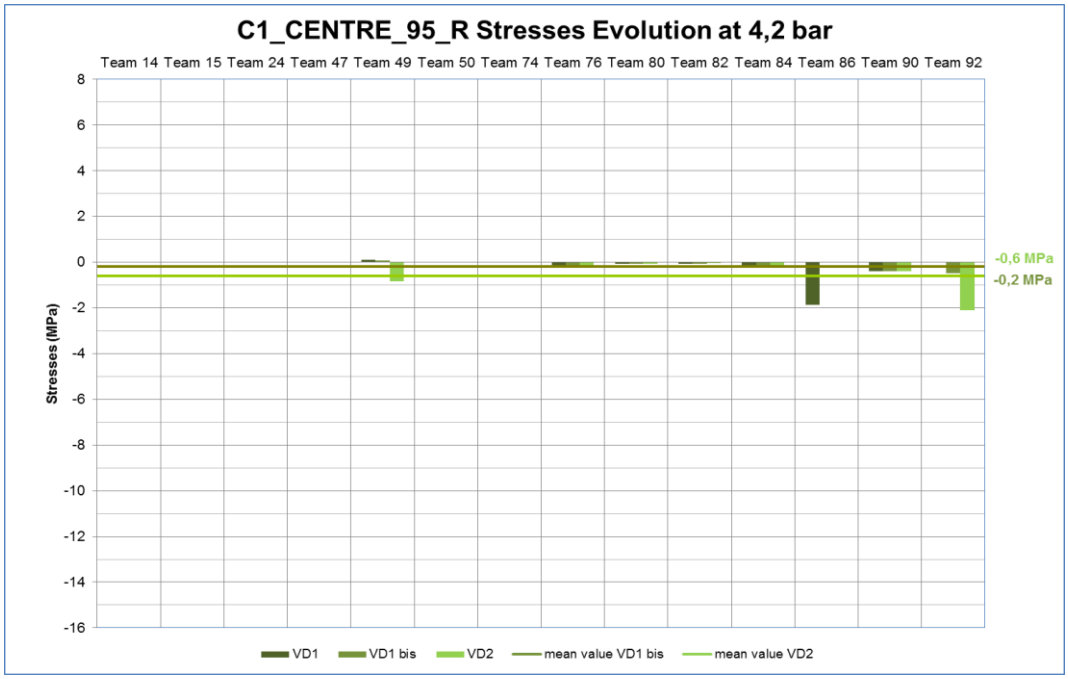

Figure 159. Stresses evolution at 4.2 bar: Raft – Lower level (195 Gr)

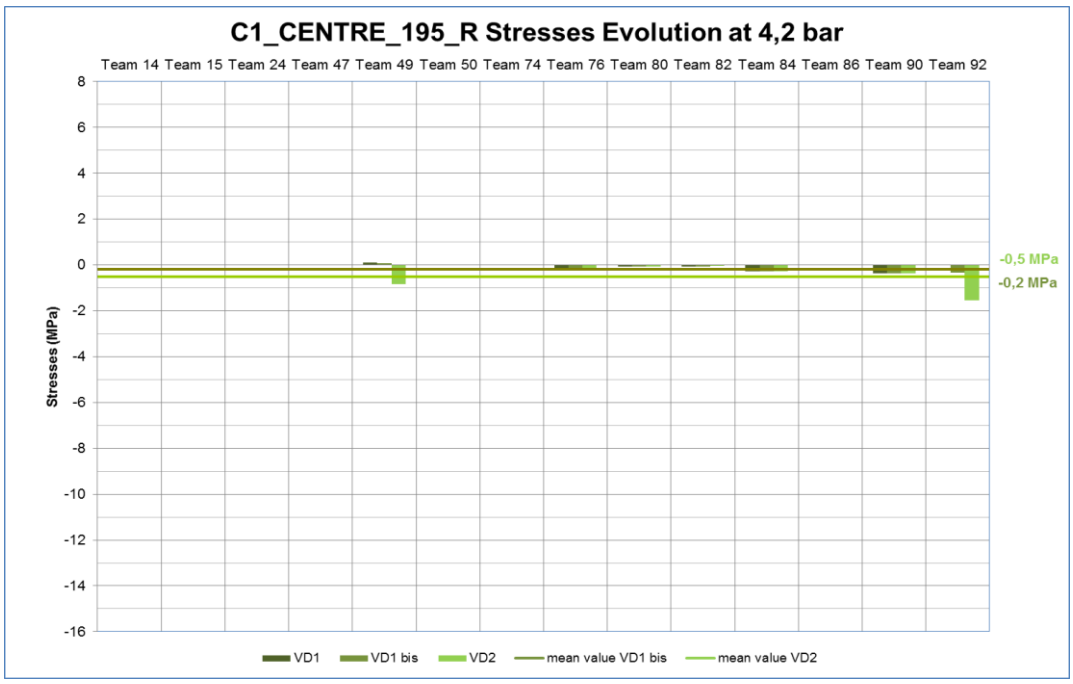

5.4.4.1.2 Upper level

Figure 160. Stresses evolution at 4.2 bar: Raft – Upper level (95 Gr)

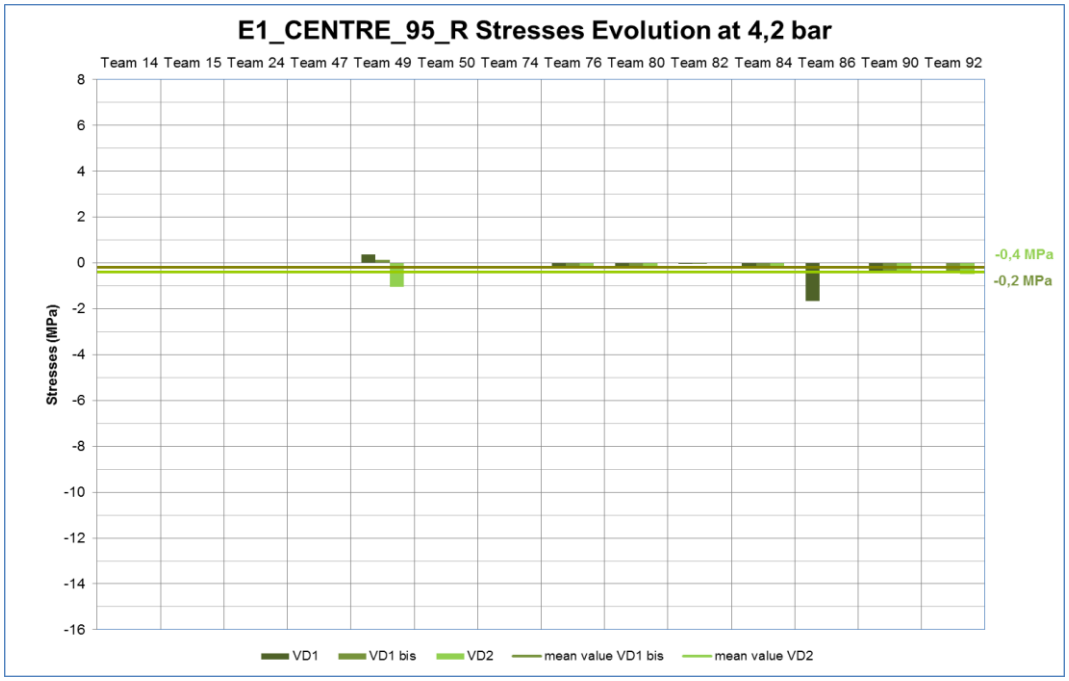

Figure 161. Stresses evolution at 4.2 bar: Raft – Upper level (195 Gr)

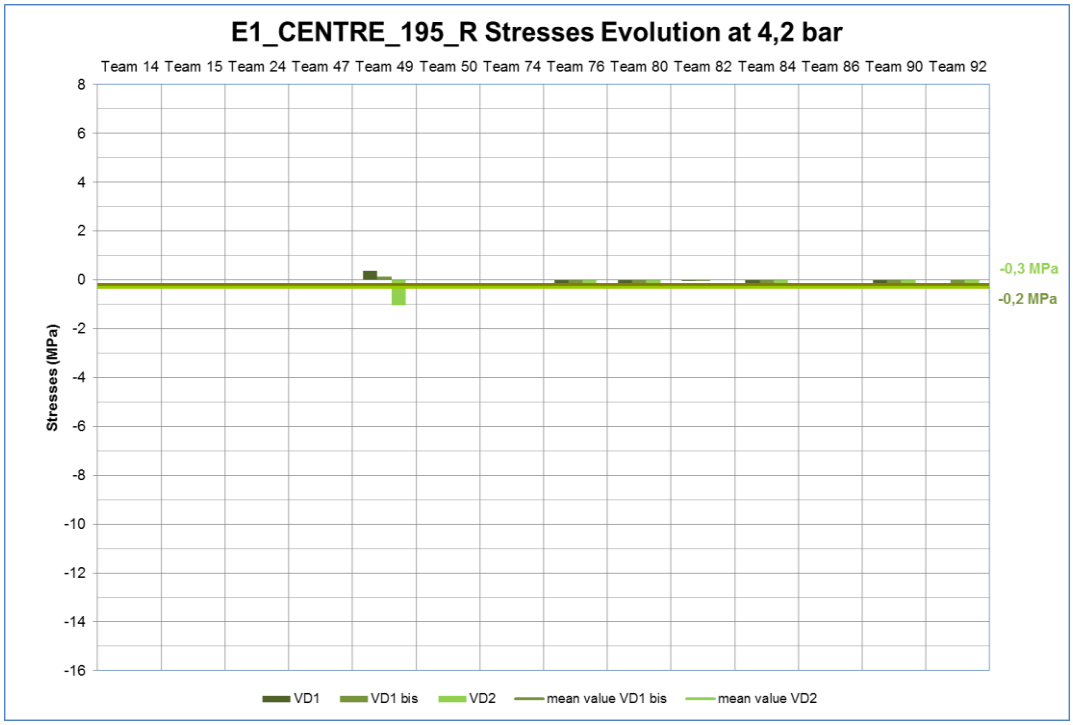

5.4.4.1.3 Comments

At 4.2 bar relative, participants gave on average no stresses in the centre of the raft, except for Teams 49, 86 and 90. Team 46 predicted an evolution from slight tensile stress to slight compressive stress over time. Teams 86 and 90 gave a compressive stress of almost 2 MPa for some sensor locations.

5.4.4.2 Gusset stresses evolution

5.4.4.2.1 Vertical direction

Figure 162. Stresses evolution at 4.2 bar: Gusset – Vertical direction – Bottom – Intrados

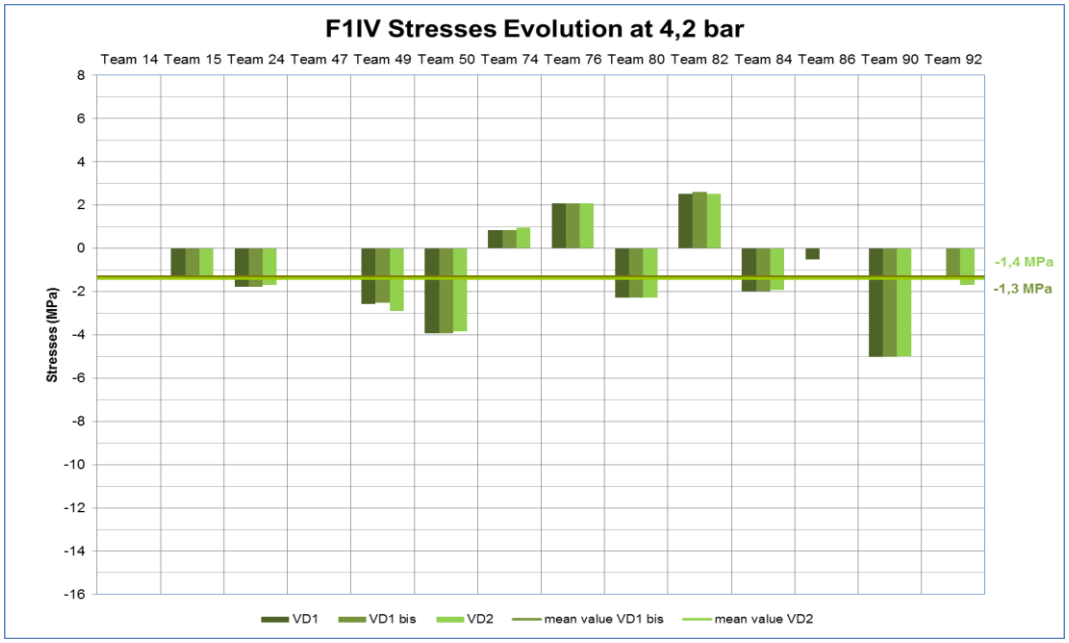

Figure 163. Stresses evolution at 4.2 bar: Gusset – Vertical direction – Bottom – Extrados

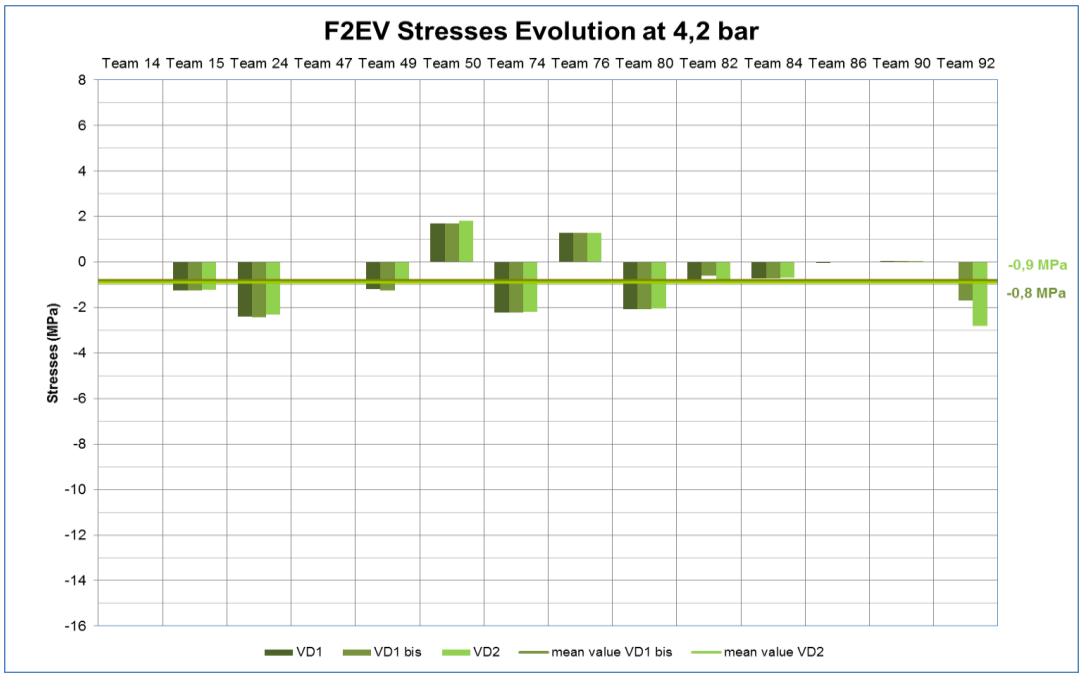

Figure 164. Stresses evolution at 4.2 bar: Gusset – Vertical direction – Top – Intrados

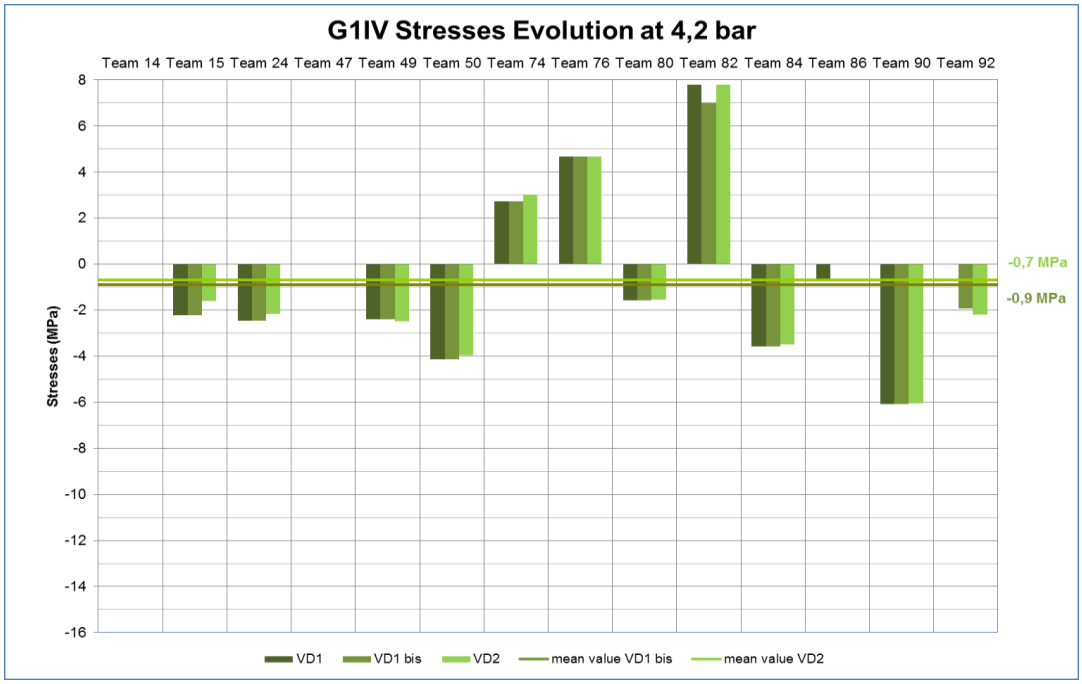

Figure 165. Stresses evolution at 4.2 bar: Gusset – Vertical direction – Top – Extrados

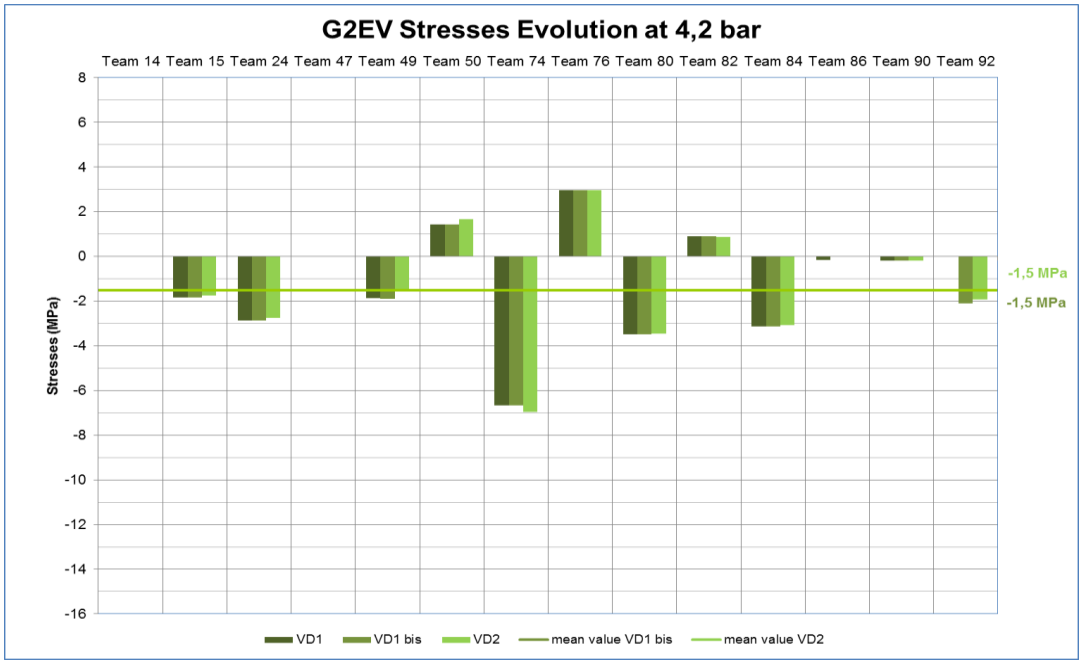

5.4.4.2.2 Tangential direction

Figure 166. Stresses evolution at 4.2 bar: Gusset – Tangential direction – Bottom – Intrados

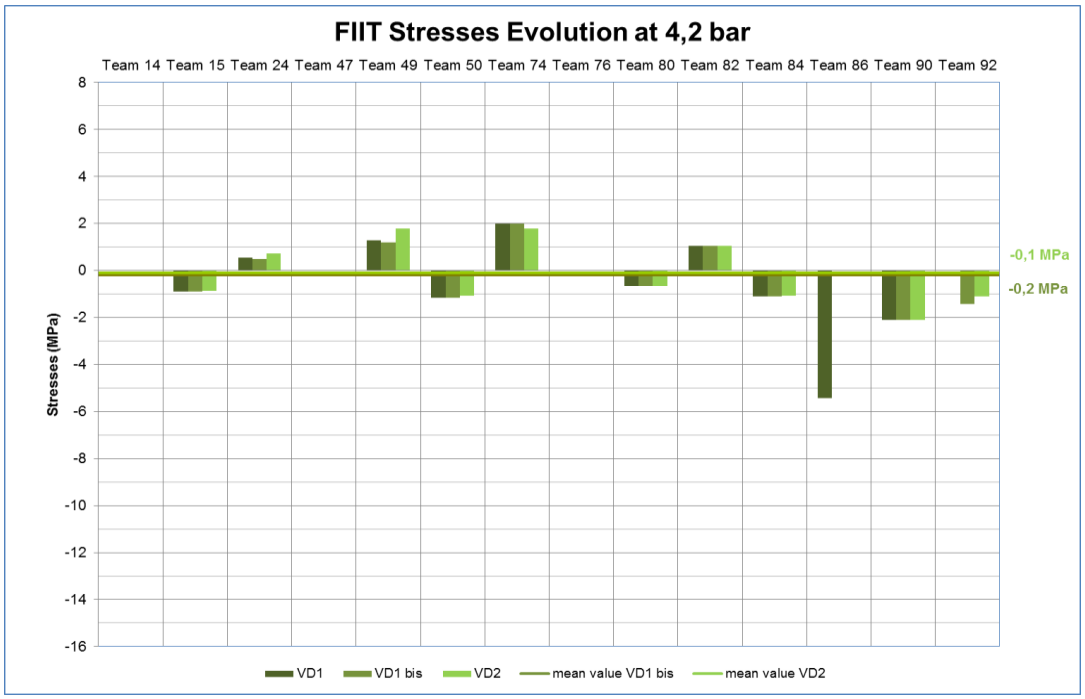

Figure 167. Stresses evolution at 4.2 bar: Gusset – Tangential direction – Bottom – Extrados

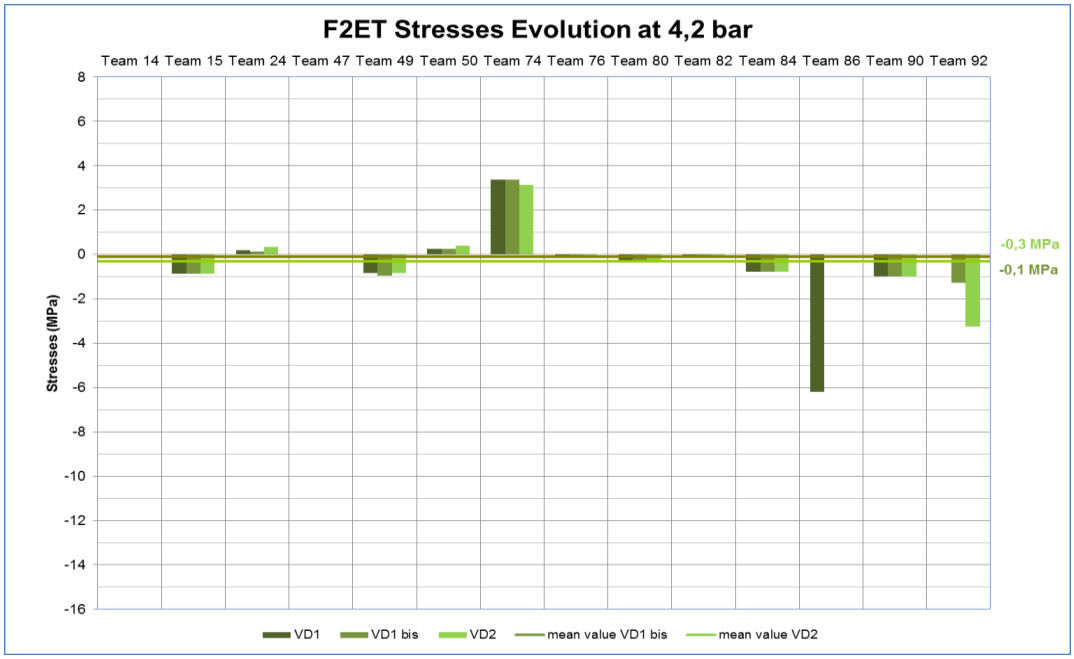

Figure 168. Stresses evolution at 4.2 bar: Gusset – Tangential direction – Top – Intrados

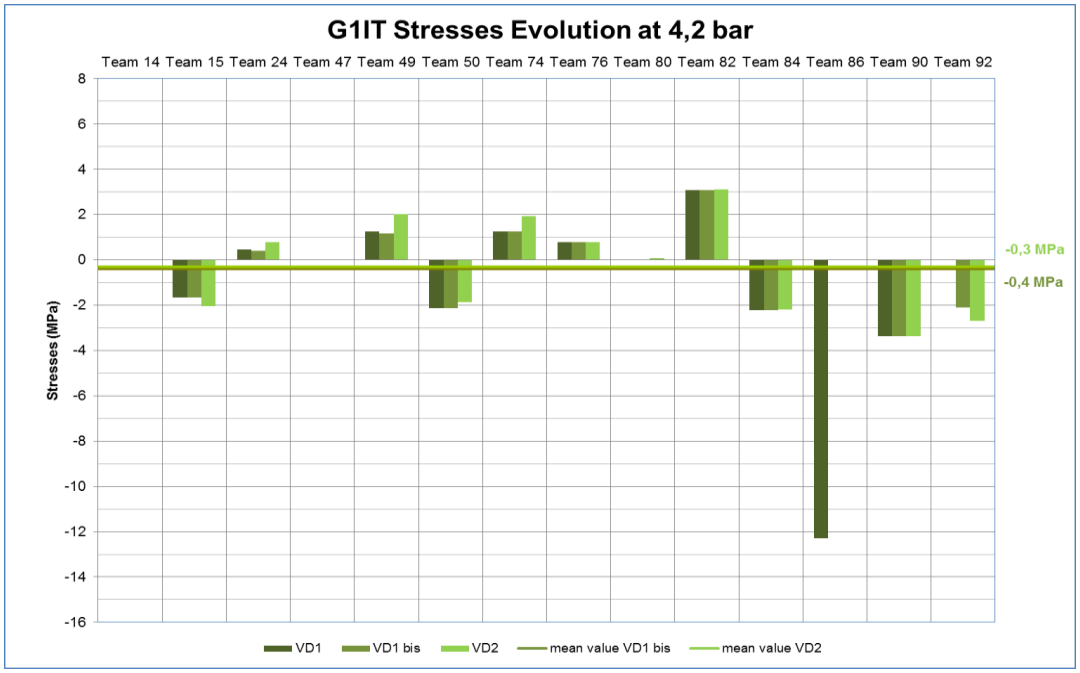

Figure 169. Stresses evolution at 4.2 bar: Gusset – Tangential direction – Top – Extrados

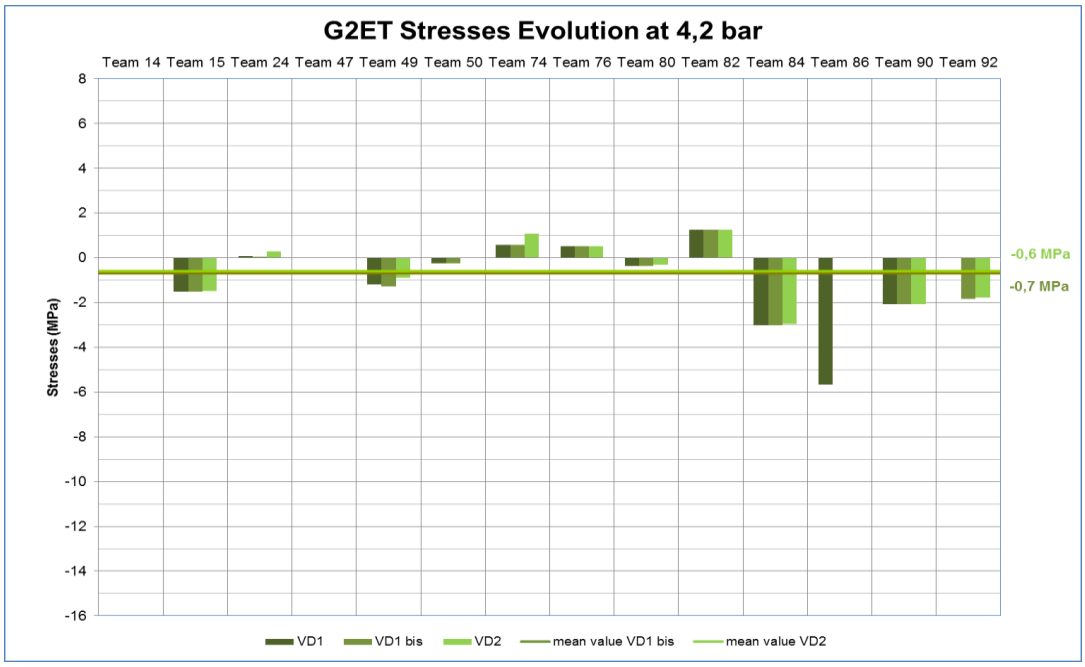

5.4.4.2.3 Comments

The results are still very scattered in this area.

In the vertical direction, eight teams gave a compressive stress under pressure ranging from 0 MPa to 6 MPa, and three gave a tensile stress of about 2 MPa in the lower part and up to 8 MPa in the upper part. With these predicted values, some horizontal cracks could appear in this part of the gusset. Team 82, which gave a very low compressive stress at 0 bar, gave the highest tensile stress (about 8 MPa in G1IV).

In the horizontal direction, seven teams gave a compressive stress under pressure ranging from 0 MPa to 12 MPa. Team 86's results seem strange, like the results submitted at 0 bar. Five teams predicted a tensile stress in the gusset, more on intrados than on extrados. Teams 74 and 82 gave the highest values of tensile stress.

5.4.4.3 Cylindrical wall stresses evolution

5.4.4.3.1 Vertical direction

Figure 170. Stresses evolution at 4.2 bar: Cylindrical part – Vertical direction – Extrados

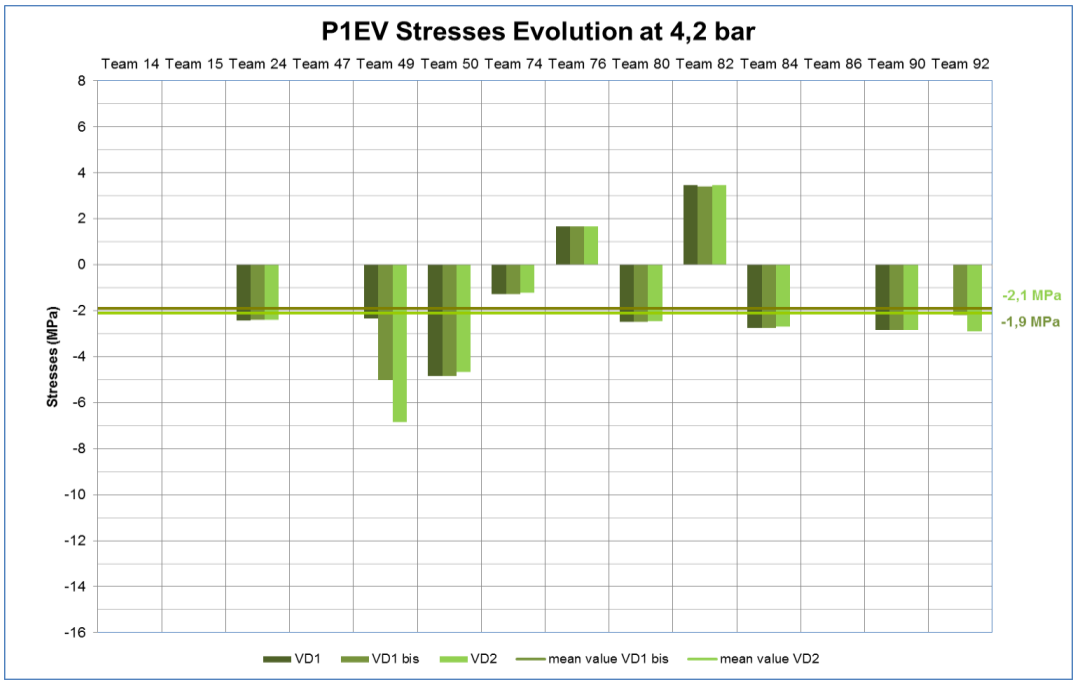

Figure 171. Stresses evolution at 4.2 bar: Cylindrical part – Vertical direction – Intrados

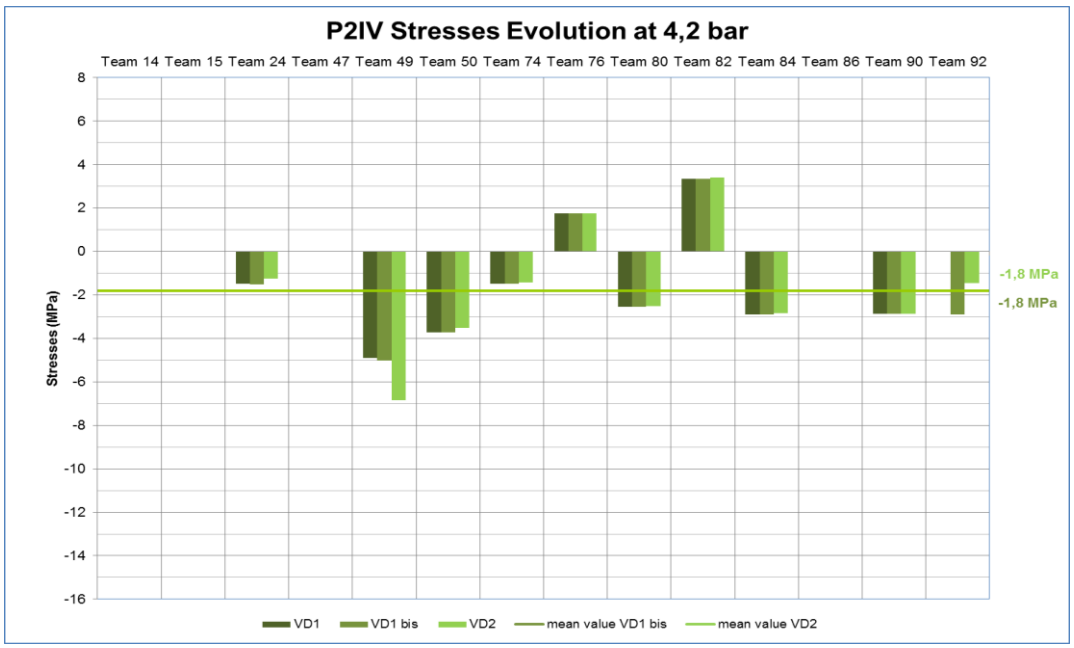

Figure 172. Stresses evolution at 4.2 bar: Cylindrical part – Vertical direction – Extrados

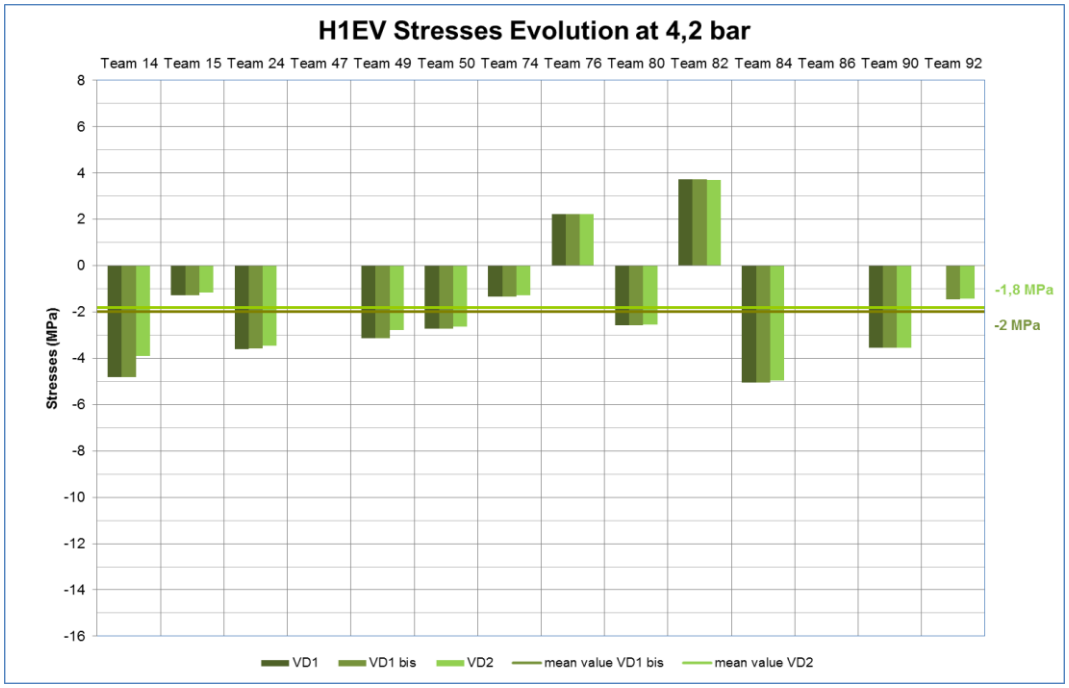

Figure 173. Stresses evolution at 4.2 bar: Cylindrical part – Vertical direction – Intrados

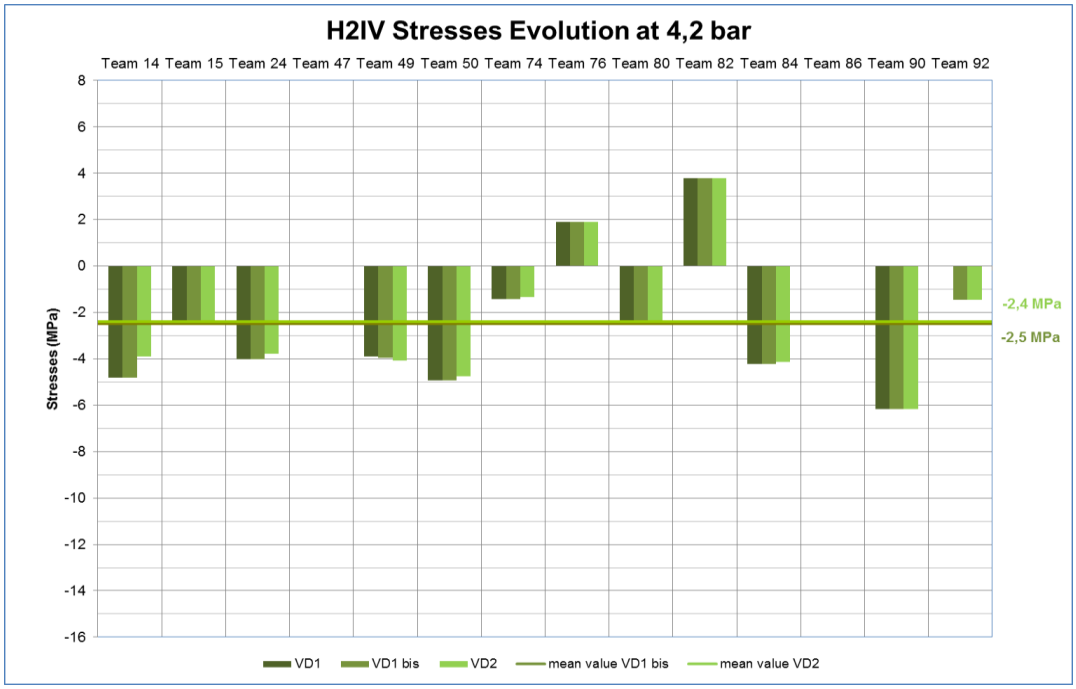

Figure 174. Stresses evolution at 4.2 bar: Cylindrical part – Vertical direction – Extrados

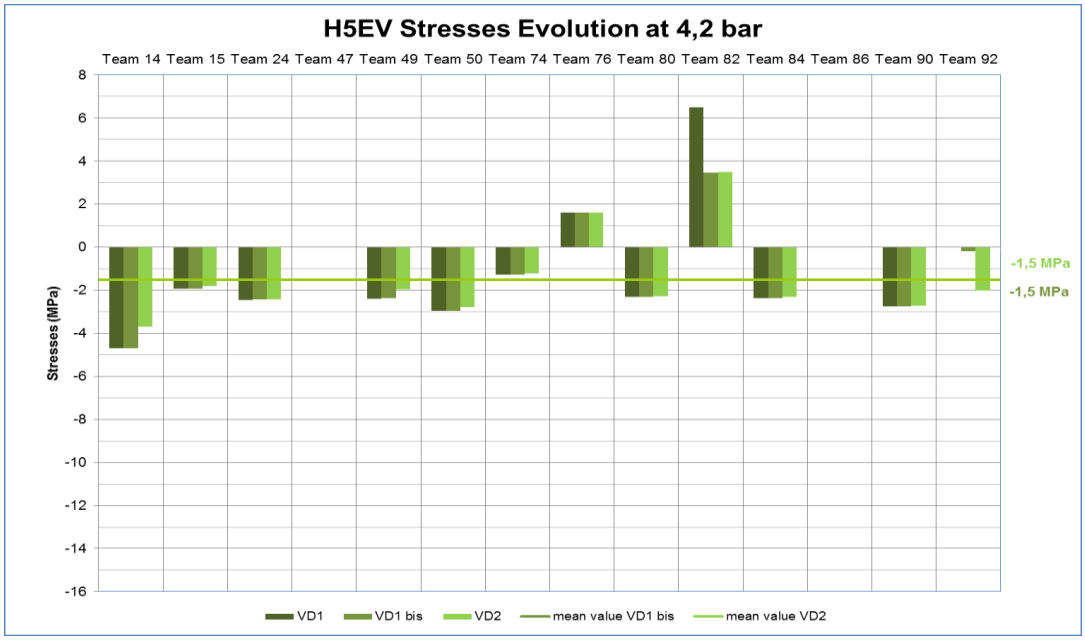

Figure 175. Stresses evolution at 4.2 bar – Cylindrical part – Vertical direction – Intrados

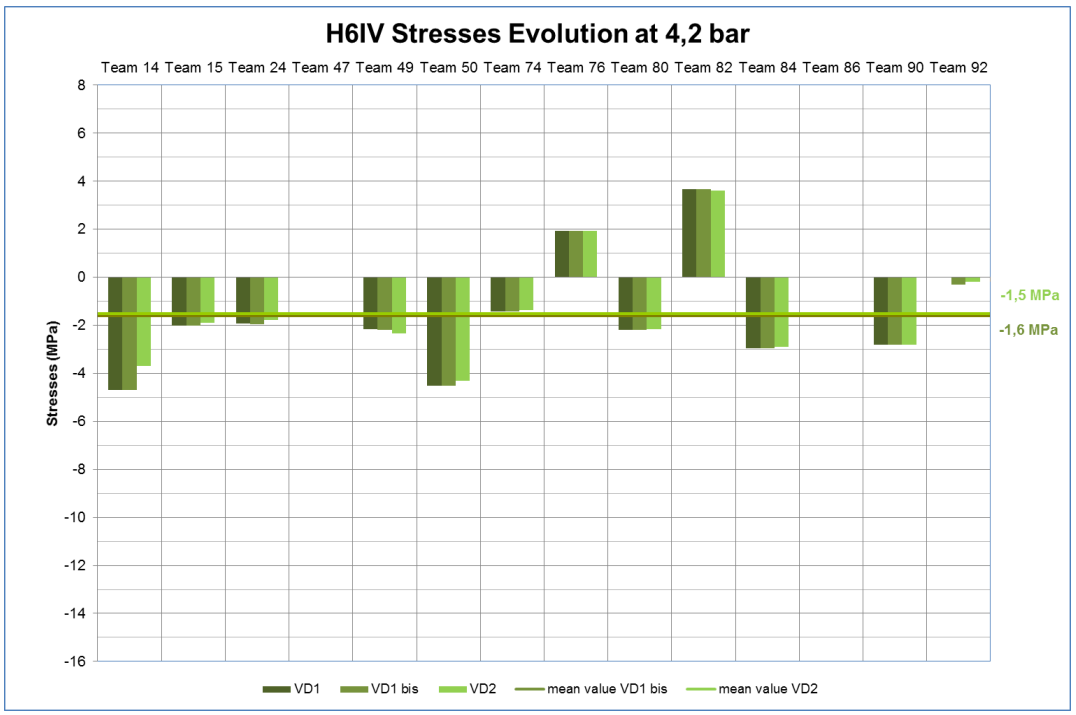

5.4.4.3.2 Tangential direction

Figure 176. Stresses evolution at 4.2 bar: Cylindrical part – Tangential direction – Extrados

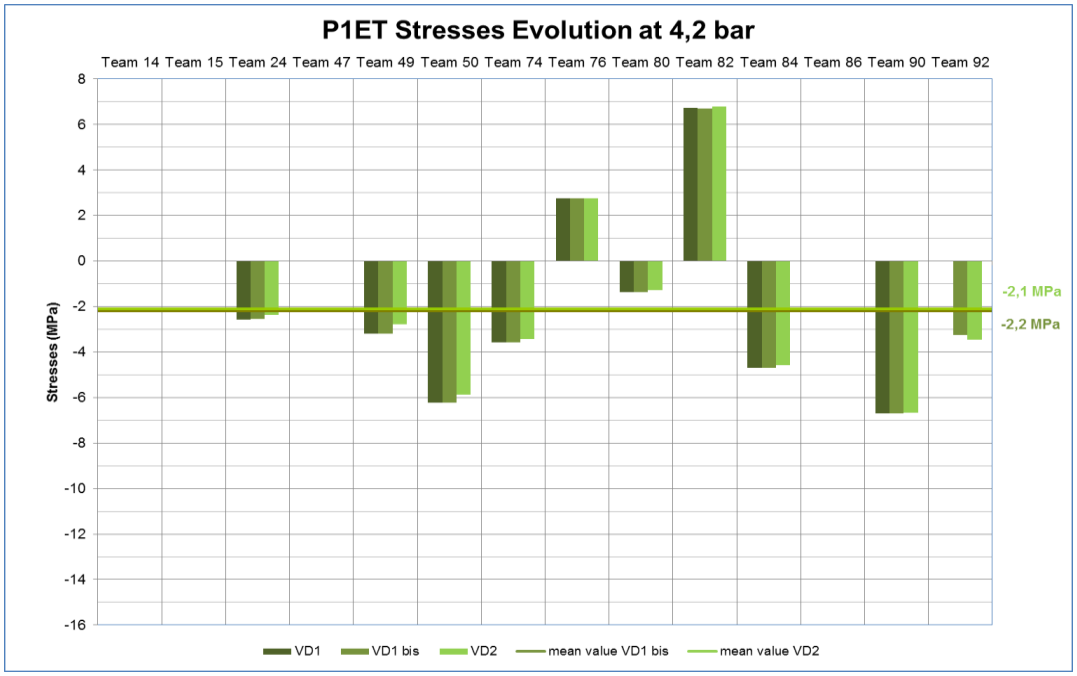

Figure 177. Stresses evolution at 4.2 bar: Cylindrical part – Tangential direction – Intrados

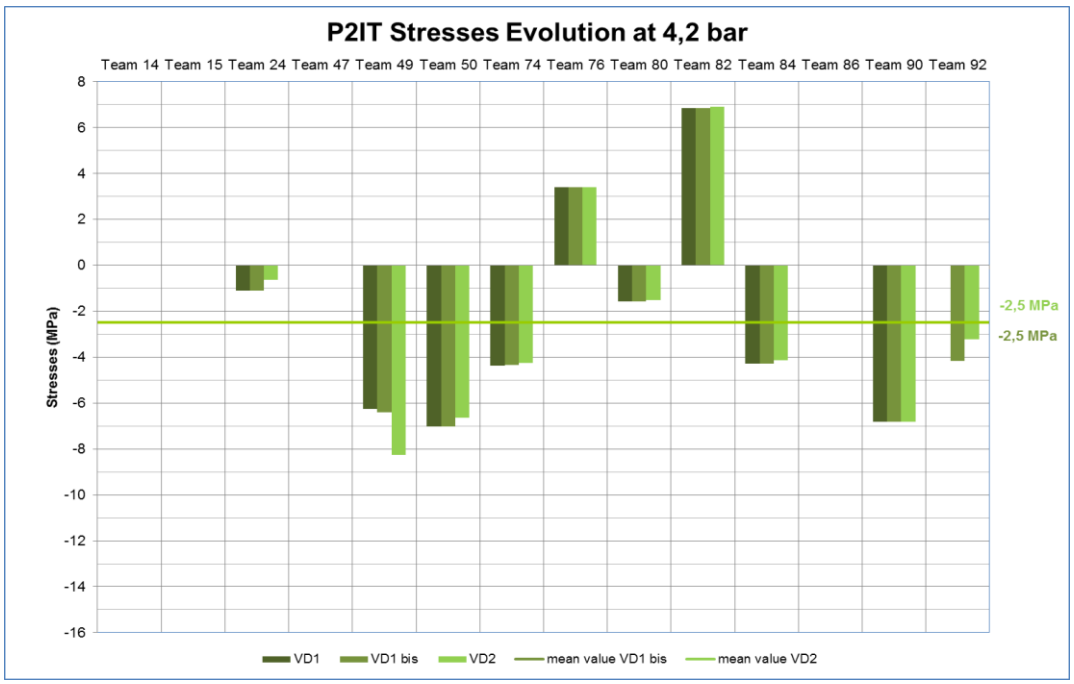

Figure 178. Stresses evolution at 4.2 bar: Cylindrical part – Tangential direction – Extrados

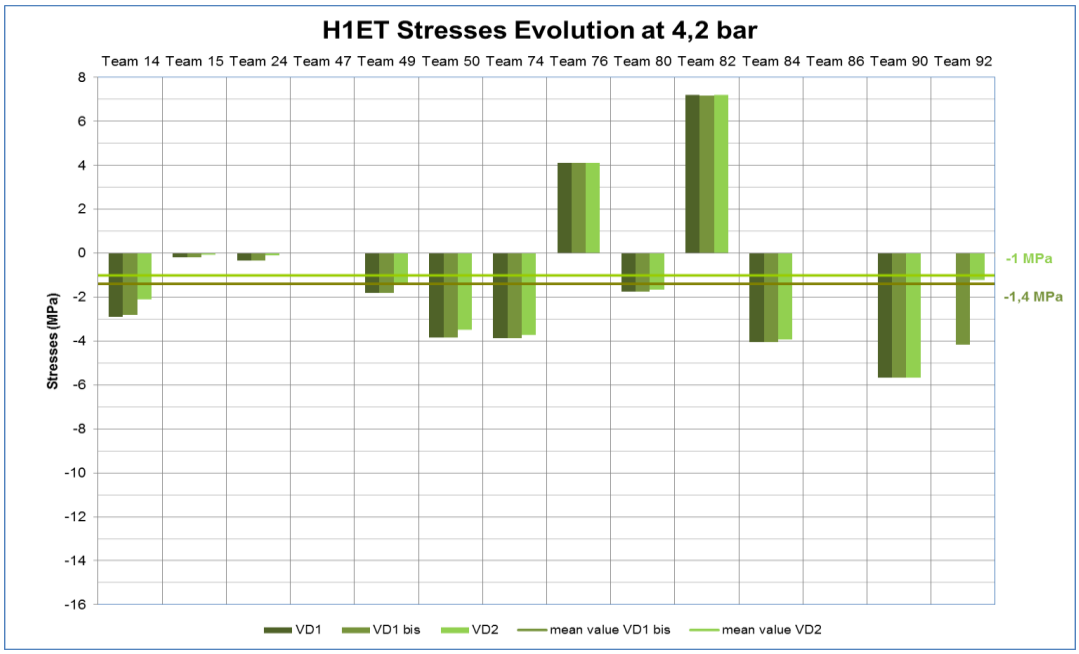

Figure 179. Stresses evolution at 4.2 bar: Cylindrical part – Tangential direction – Intrados

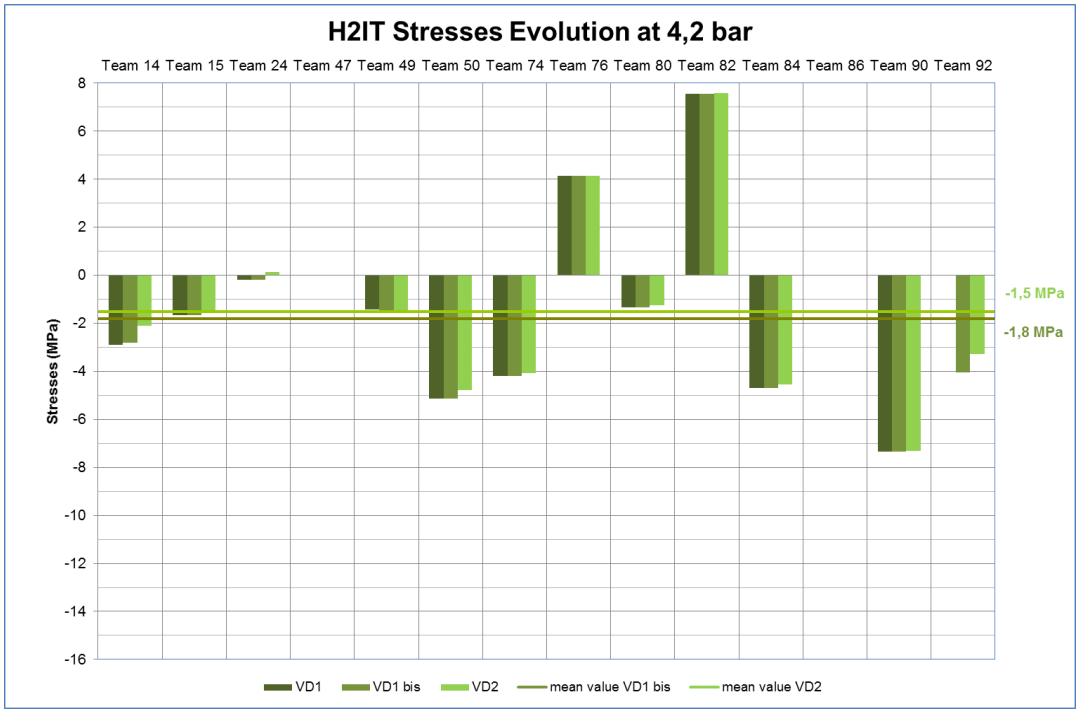

Figure 180. Stresses evolution at 4.2 bar: Cylindrical part – Tangential direction – Extrados

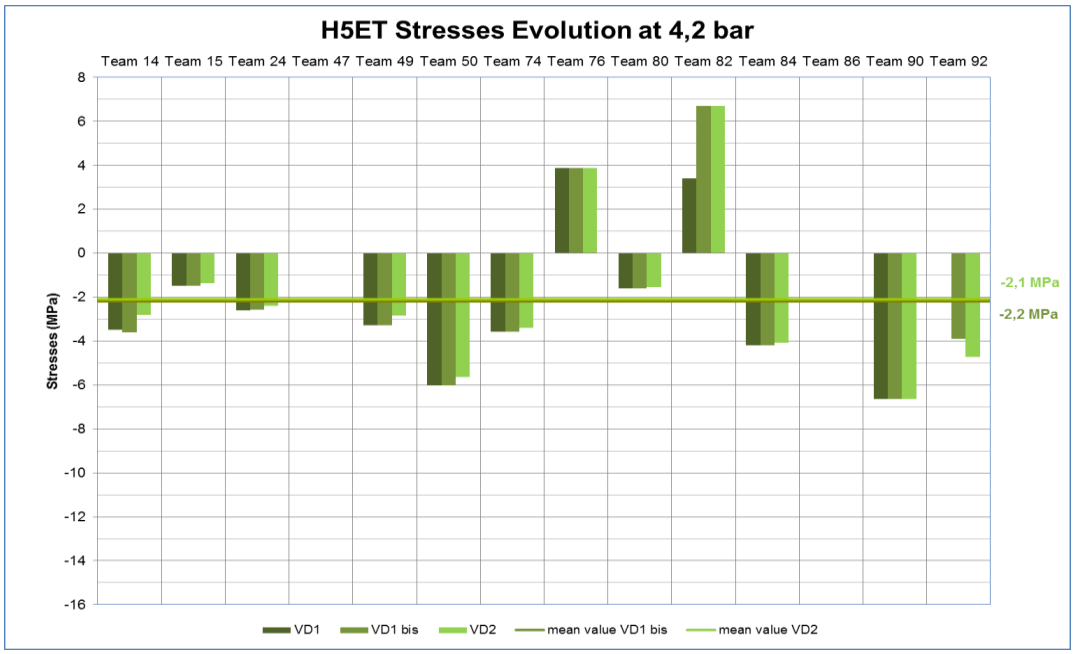

Figure 181. Stresses evolution at 4.2 bar: Cylindrical part – Tangential direction – Intrados

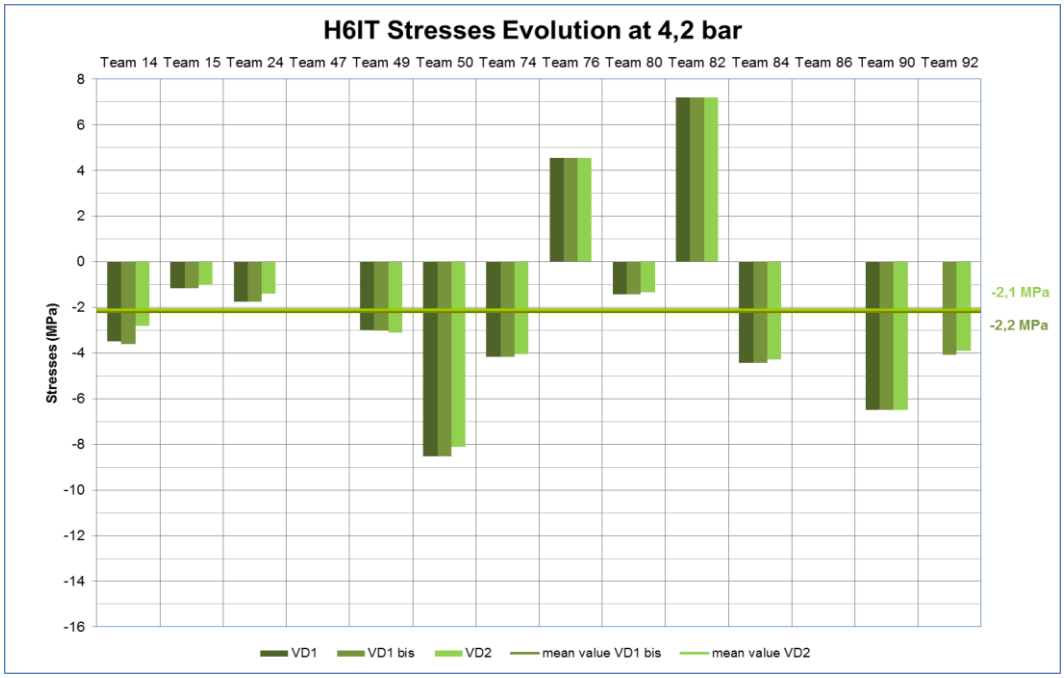

5.4.4.3.3 Comments on the cylindrical wall stresses

For this area, there are 12 stress values to compare. Results are less scattered than in the gusset.

As Team 82 had given very low values of compressive stress (even tensile stress in some cases) at 0 bar, this team predicted an important tensile stress of this area at 4.2 bar relative in both directions (about 4 MPa in the vertical direction and 7 MPa in the tangential direction).

In the vertical direction, all but two teams (Teams 76 and 82) gave a compressive stress at 4.2 bar ranging from 1 MPa to 7 MPa. As for results at 0 bar, Team 49 gave strange values for sensors P1EV and P2IV, with higher values of stress for this point in comparison to H1, H2, H5 and H6 located in the same area.

In the tangential direction, all but two teams (Teams 76 and 82) gave a compressive stress at 4.2 bar ranging from 0 MPa to 8 MPa. The highest values were given by Teams 49, 50 and 90.

Table 24 shows the distribution of participants' results for the stress evolution between VD1 bis and VD2.

Table 24. Distribution of participants' results for the cylindrical wall stresses evolution between VD1 bis and VD2

	Compressive stress decreases in all points at mid-height	Compressive stress decreases in some points at mid-height	Compressive stress does not decrease at mid-height
Vertical direction	Teams 14, 15, 24, 50, 74, 80, 84	Team 49	Teams 76, 82, 90, 92
Tangential direction	Teams 14, 15, 24, 50, 74, 80, 84, 90	Team 49	Teams 76, 82, 92

The majority of the teams found that compressive stress decreases over time.

5.4.4.4 Equipment hatch stresses evolution

5.4.4.4.1 Side of the hatch

Figure 182. Stresses evolution at 4.2 bar: Side of the hatch – Vertical – Extrados

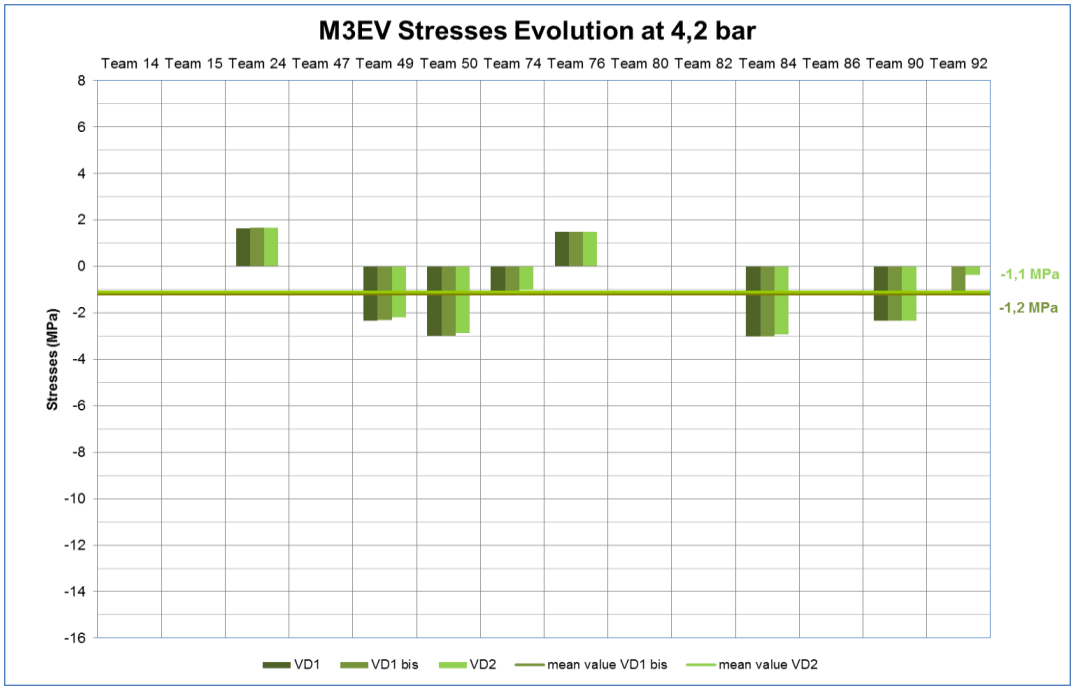

Figure 183. Stresses evolution at 4.2 bar: Side of the hatch – Tangential – Extrados

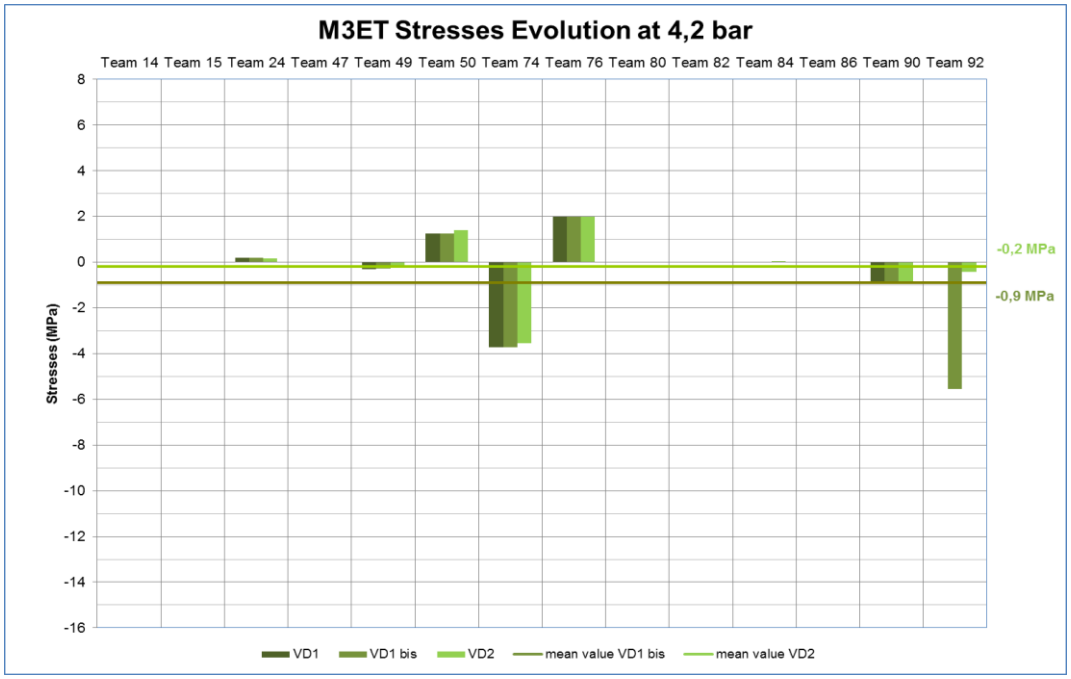

Figure 184. Stresses evolution at 4.2 bar: Side of the hatch – Vertical – Intrados

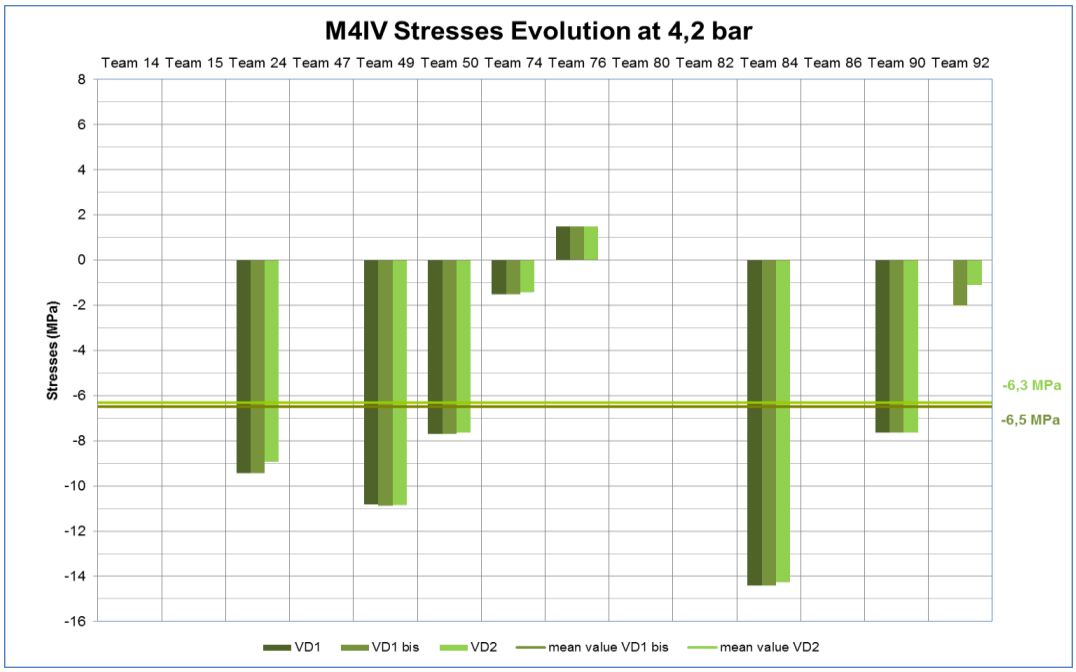

Figure 185. Stresses evolution at 4.2 bar: Side of the hatch – Tangential – Intrados

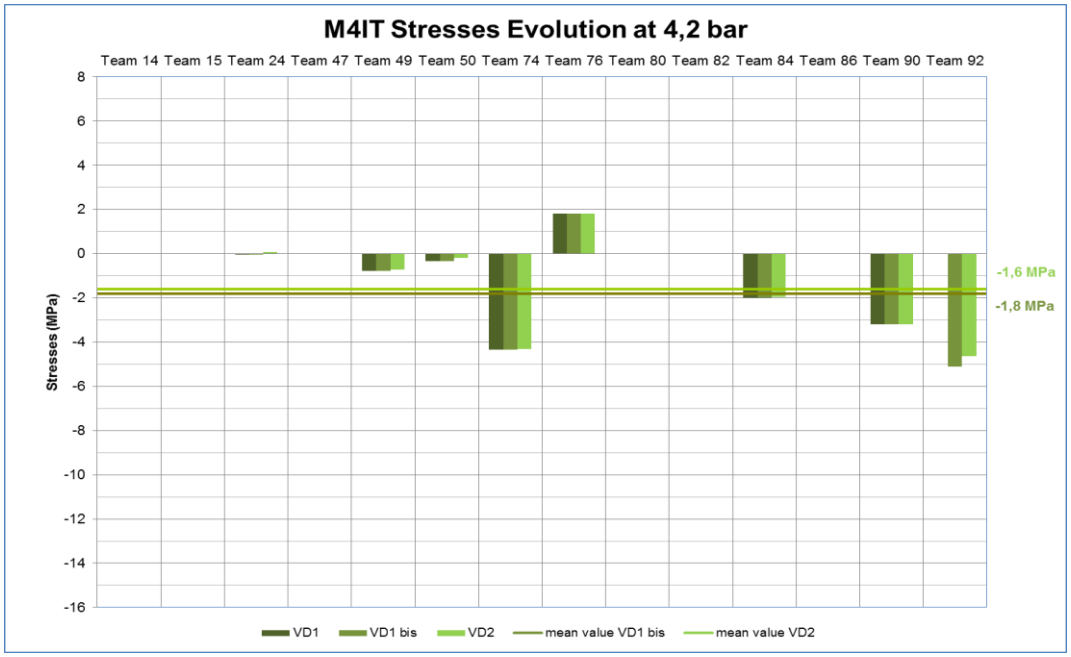

5.4.4.4.2 Above the hatch

Figure 186. Stresses evolution at 4.2 bar: Above the hatch – Vertical – Extrados

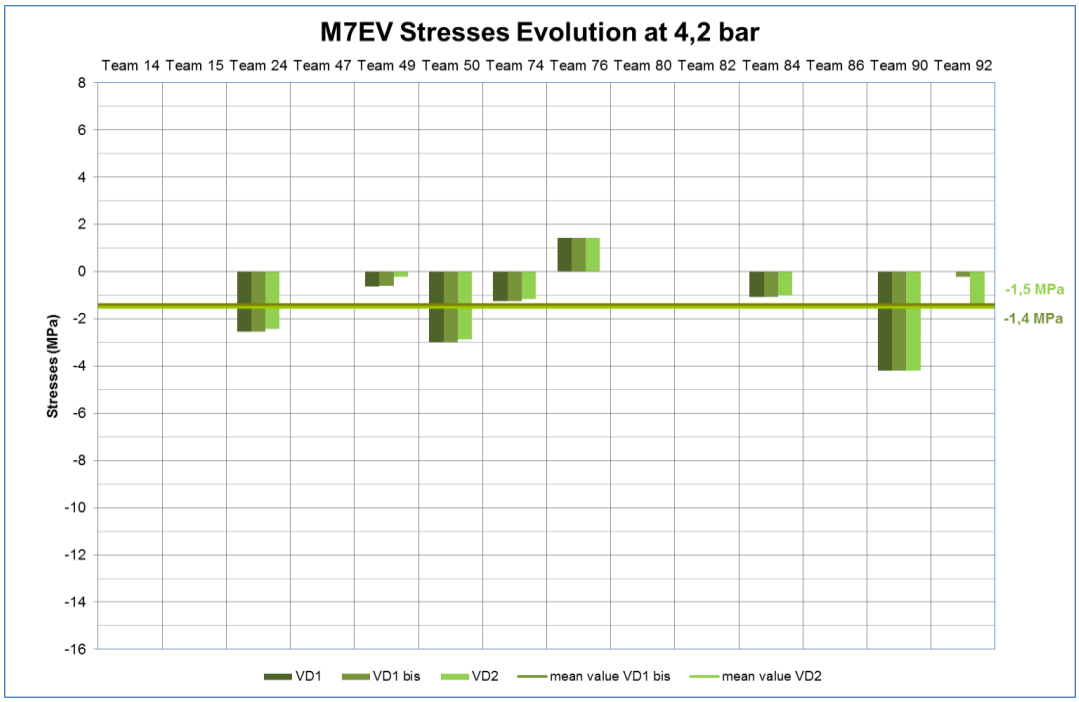

Figure 187. Stresses evolution at 4.2 bar: Above the hatch – Tangential – Extrados

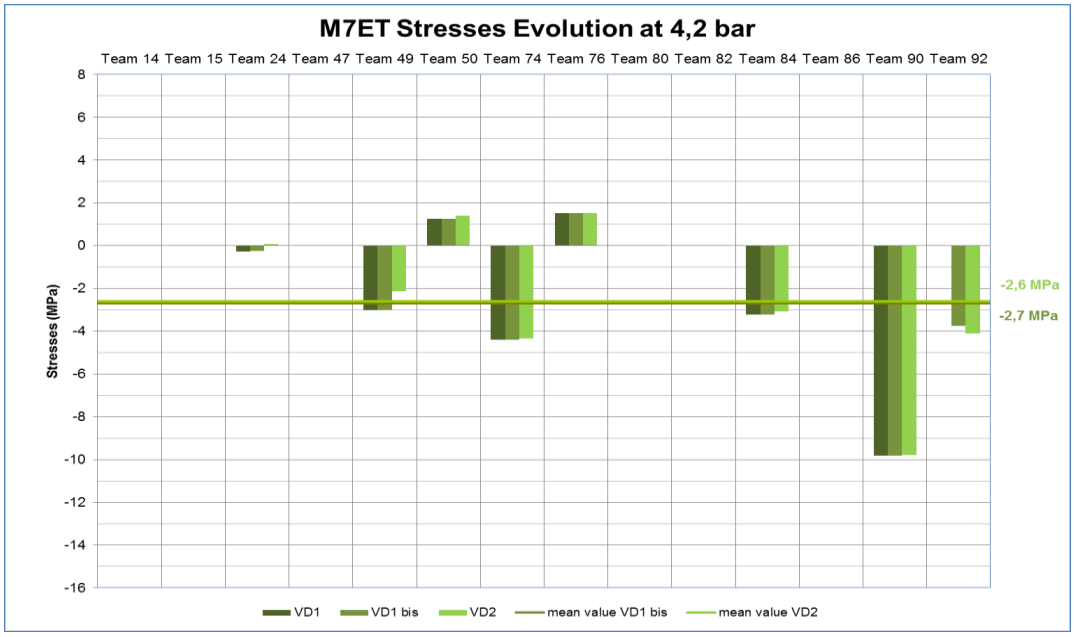

Figure 188. Stresses evolution at 4.2 bar: Above the hatch – Vertical – Intrados

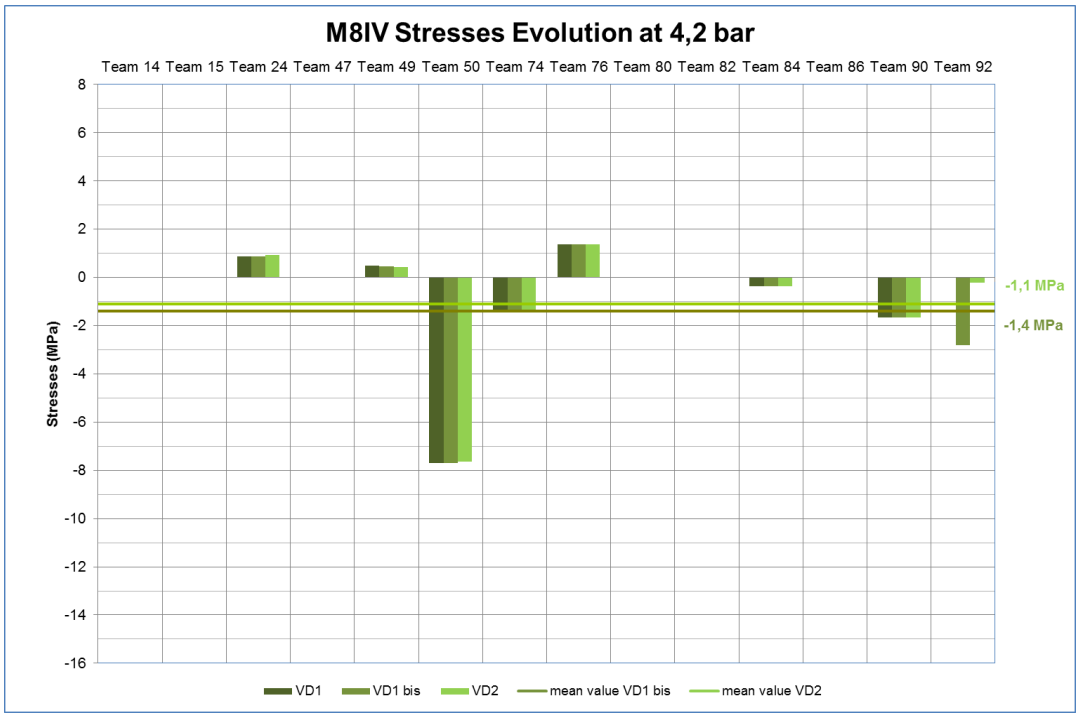

Figure 189. Stresses evolution at 4.2 bar: Above the hatch – Tangential – Intrados

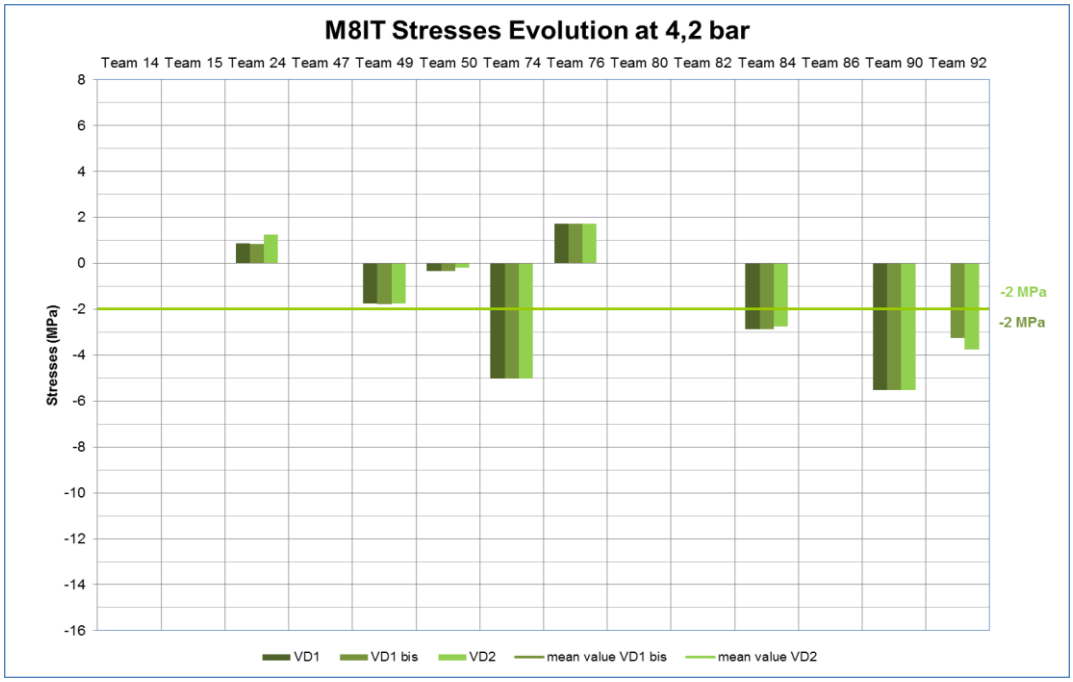

5.4.4.4.3 Comments

Only eight participants gave some stress results in this area.

On the side of the hatch, all participants gave a compressive stress in all points with the exception of three teams. Team 76 gave a tensile stress of about 1.5 MPa in both directions, Team 24 gave a tensile stress in M3 and Team 50 gave a tensile stress in the tangential direction (M3ET) of about 1 MPa. In contrast to Team 76, which gave a very low value of compressive stress at 0 bar, Teams 24 and 50 gave a compressive stress of about 4 MPa at 0 bar. The effects of inner pressure in this area (M3) are higher for these two teams.

Above the hatch, all but three teams gave a compressive stress in all points. As for the side of the hatch, Team 76 gave a tensile stress of about 1.5 MPa in both directions. Team 24 gave a low tensile stress in M8 (1 MPa), Team 49 a very low tensile stress (< 1 MPa) in M8IV and Team 50 a tensile stress in the tangential direction (M7ET) of about 1 MPa. These results are due to low values of compressive stresses at 0 bar.

Even if Teams 24 and 50 predicted an increase of tensile stress between VD1 bis and VD2, these tensile stresses remain lower than concrete tensile strength.

5.4.4.5 Dome stresses evolution

5.4.4.5.1 Results

Figure 190. Stresses evolution at 4.2 bar: Top of the dome – Extrados (194 Gr)

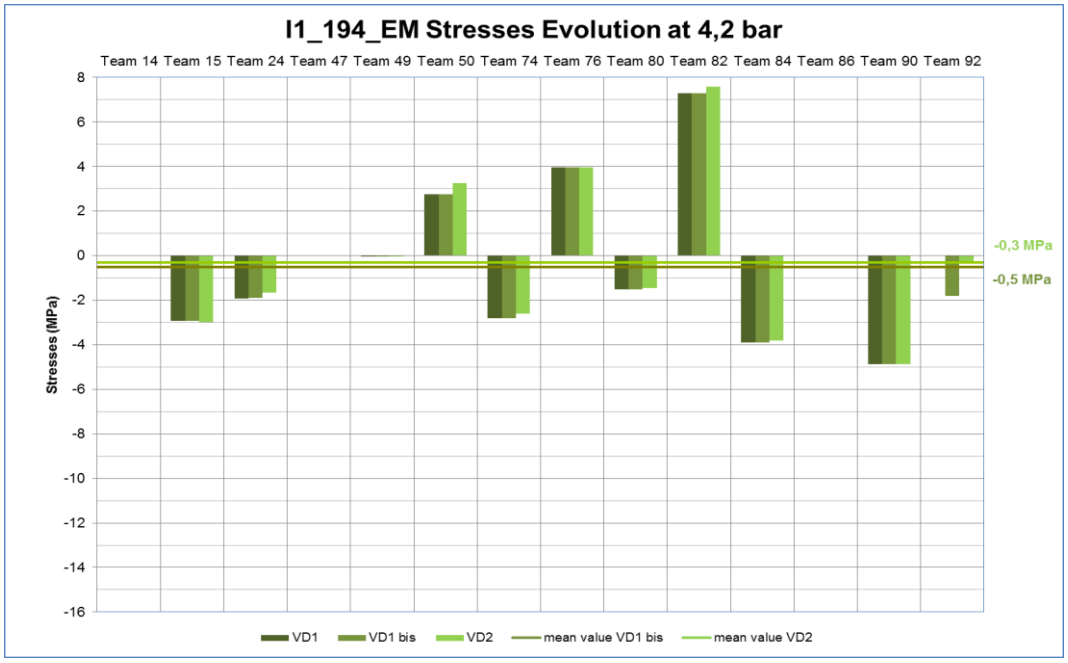

Figure 191. Stresses evolution at 4.2 bar: Top of the dome – Extrados (94 Gr)

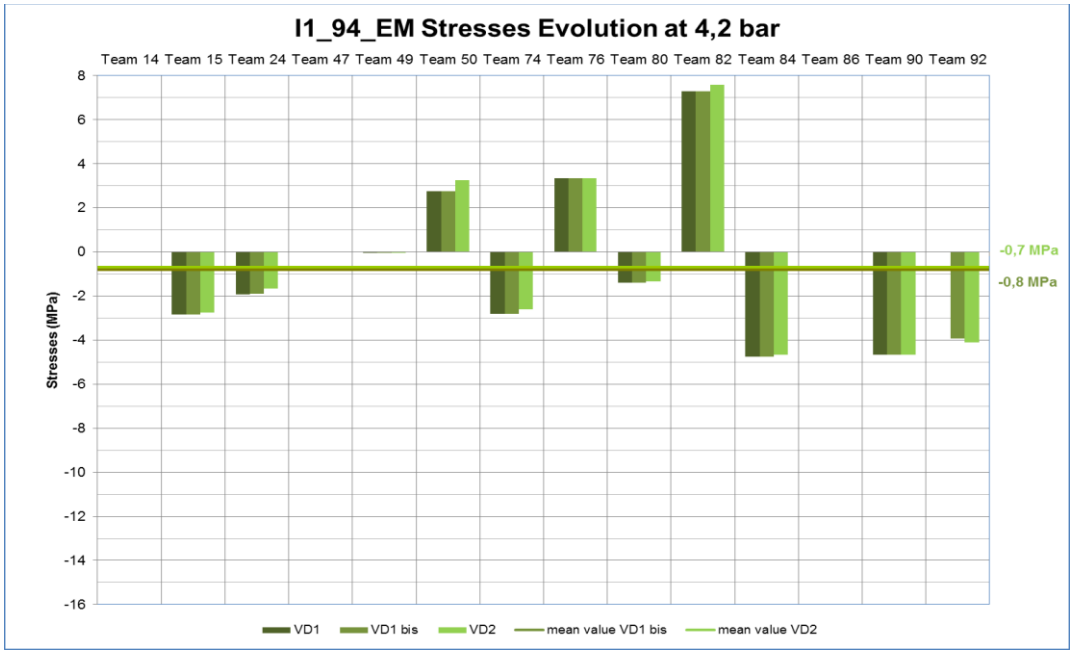

Figure 192. Stresses evolution at 4.2 bar: Top of the dome – Intrados (194 Gr)

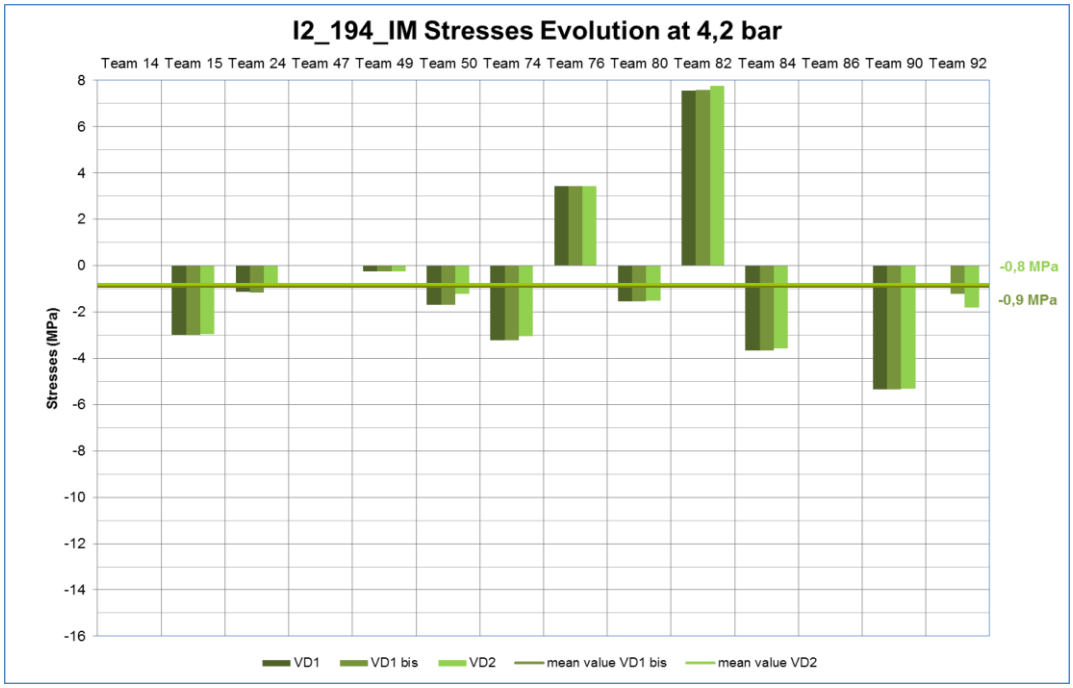

Figure 193. Stresses evolution at 4.2 bar: Top of the dome – Intrados (94 Gr)

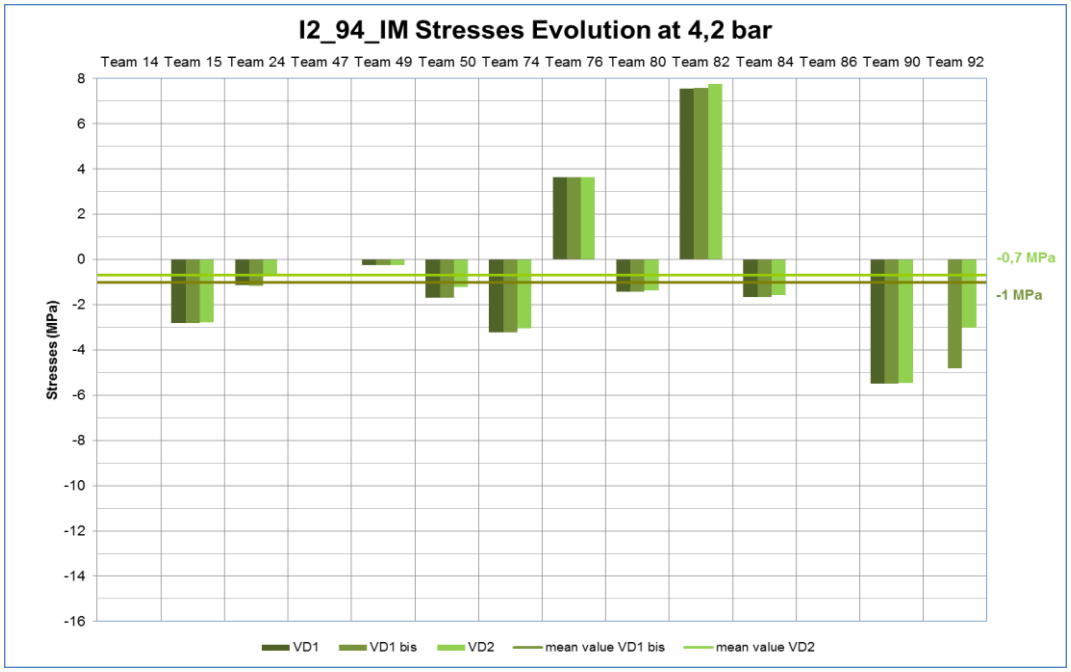

Figure 194. Stresses evolution at 4.2 bar: Meridian part of the dome – Meridian direction – Extrados

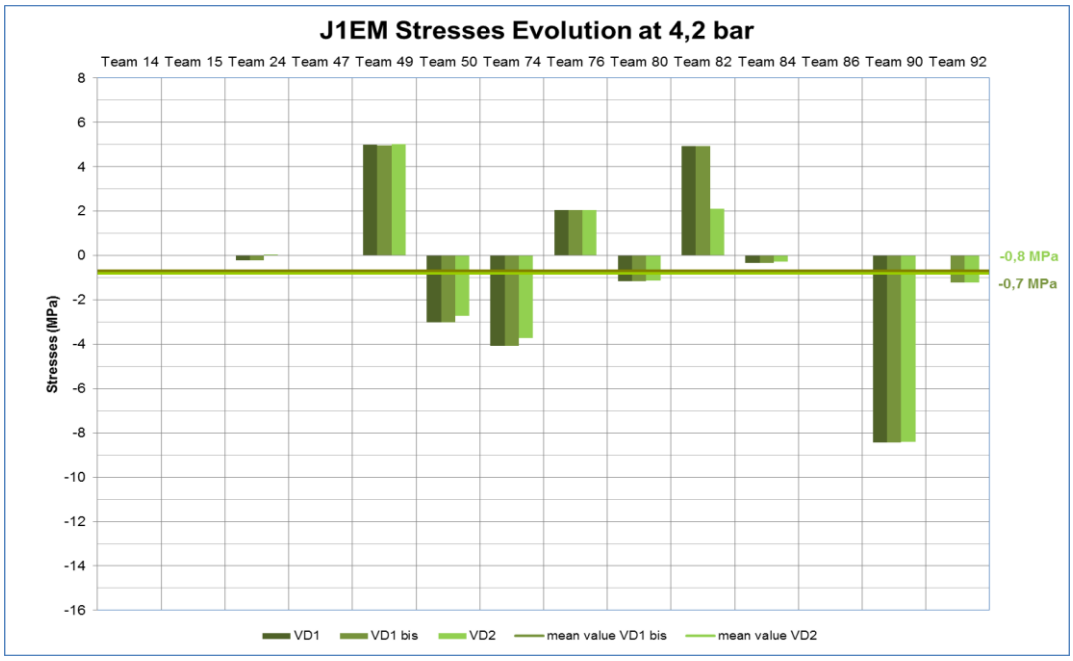

Figure 195. Stresses evolution at 4.2 bar: Meridian part of the dome – Tangential direction – Extrados

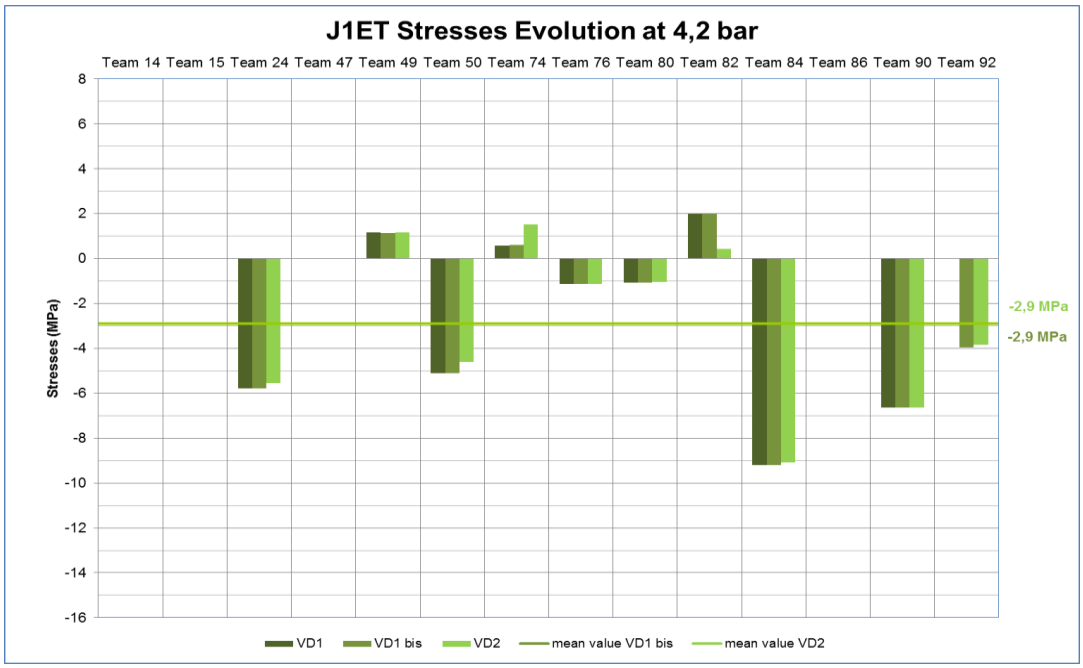

Figure 196. Stresses evolution at 4.2 bar: Meridian part of the dome – Meridian direction – Intrados

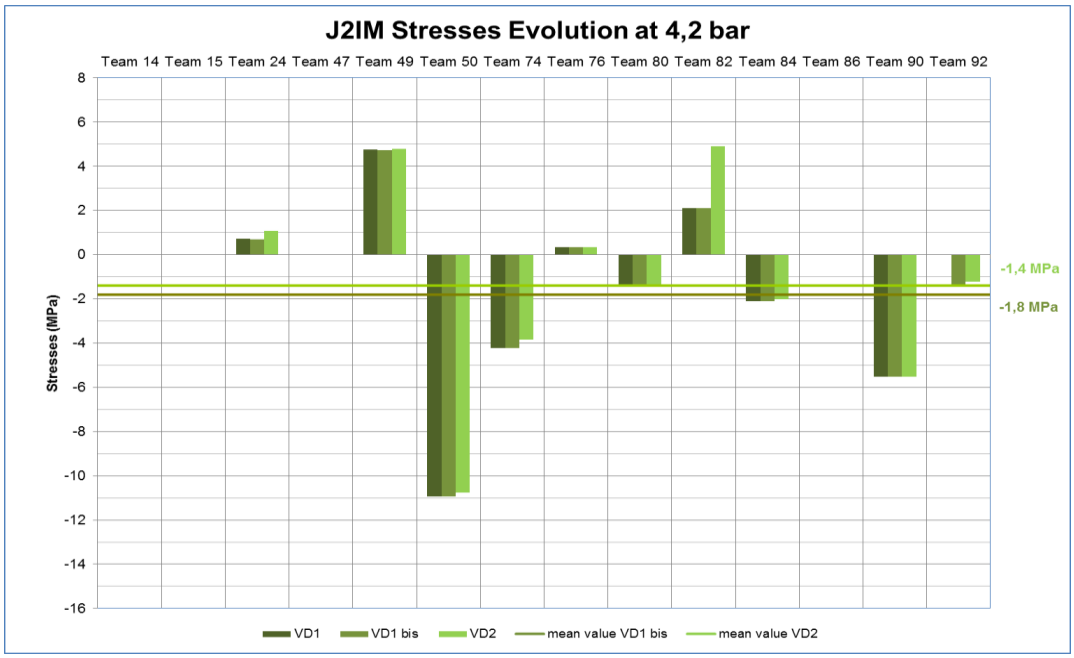

Figure 197. Stresses evolution at 4.2 bar: Meridian part of the dome – Tangential direction – Intrados

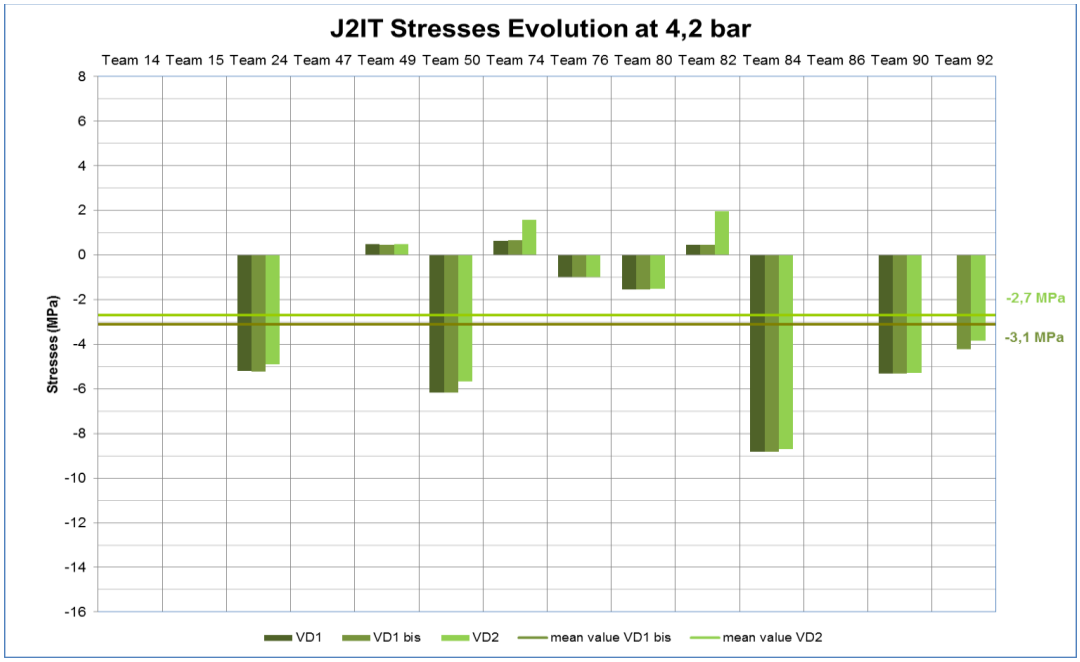

5.4.4.5.2 Comments

The teams' results are more scattered in this area.

There are still strange values for Team 82, which gave very high tensile stress values. Team 76 also gave high values of tensile stress at the top of the dome.

At the top of the dome, Team 50 also gave some tensile stress of about 3 MPa on extrados. This tensile stress could lead to cracks appearing. Teams 76 and 82, however, gave low values of compressive stress at 0 bar.

In the meridian part, except for Teams 76 and 82, more teams predicted tensile stress: Team 24 (1 MPa in J2IM), Team 49 (5 MPa in the meridian direction and about 1 MPa in the tangential direction) and Team 74 (about 1 MPa in the tangential direction). The values predicted by Team 49 should lead to the apparition of cracks.

5.5. Cracks

5.5.1. Expected results

Teams were asked to predict cracking in the whole containment during the pressure tests, per zone, on each face of the wall. The results could be presented through various crack indicators, as described in Table 25.

Table 25. Crack indicators used to present the predictions of cracking in the whole containment during the pressure tests

	VD1 bis				VD2			
	Inner face cracks (include through cracks)							
Area	Total length	Maximum opening	Spacing	Other	Total length	Maximum opening	Spacing	Other
Gusset								
Hatch area								
Cylindrical part (wall)								
Dome								
	Outer face cracks (include through cracks)							
Gusset								
Hatch area								
Cylindrical part (wall)								
Dome								
	Through cracks only							
Gusset								
Hatch area								
Cylindrical part (wall)								
Dome								

5.5.2. Experimental results

The experimental results shown in this part correspond to the visual inspection made during pressurisation tests or just after pressurisation tests. The results for the outer face come from visual inspections made during pressurisation tests. For reasons of inaccessibility during the pressurisation tests, the results for the inner face were obtained just after the pressurisation tests.

5.5.2.1 Total length and maximum opening measured

The cracks identified in the dome inner face are located on precast slab forms and don't reflect the dome mechanical behaviour. These results are not presented here.

During the last pressurisation tests, cracks were only observed on the gusset. In addition to the visual inspections, optical fibres interrogated with a specific and refined interrogator gave some precise locations of the vertical cracks inside the wall.

Tables 26 and 27 give the main characteristics of the observed cracks in the gusset over time on the inner and outer faces. Crack opening is an indicative value. No precise measure was made.

Table 26. Vertical cracks on the inner face of the gusset

	After VD1	After VD1 bis	After VD2
Number	Not available	101	Not available
Total length (m)	Not available	37.4	Not available
Maximum length (m)	Not available	1.00	Not available
Average length (m)	Not available	0.37	Not available
Maximum opening (mm)	Not available	~0.17	Not available

Table 27. Vertical cracks on the outer face of the gusset

	During VD1	During VD1 bis	During VD2
Number	47	48	49
Total length (m)	35.4	35.9	37.0
Maximum length (m)	1.10	1.10	1.10
Average length (m)	0.88	0.88	0.88
Maximum opening (mm)	~0.2	~0.2	~0.2

On the inner face, the last visual inspection revealed about 100 vertical cracks, for a total length of 37 m. The average length was 0.37 m.

On the outer face, the number of vertical cracks is divided by two compared to the inner face. Over time, the number of cracks increased from 47 in VD1 to 49 in VD2. The total length is equal to the total length on the inner face, which leads to a higher average length equal to 0.88 m.

For a better visualisation of the cracks repartition, some maps are given below.

5.5.2.2 Mapping of the observed vertical cracks after the VD1 bis test

The location of vertical cracks on the inner face is given in Figure 198.

Figure 198. Location of vertical cracks on the inner face of the gusset after VD1 bis

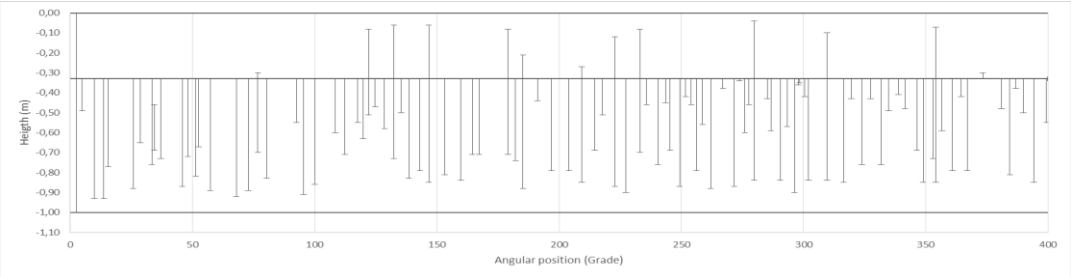

The location of vertical cracks on the outer face is given in Figure 199.

Figure 199. Location of vertical cracks on the outer face of the gusset after VD1 bis

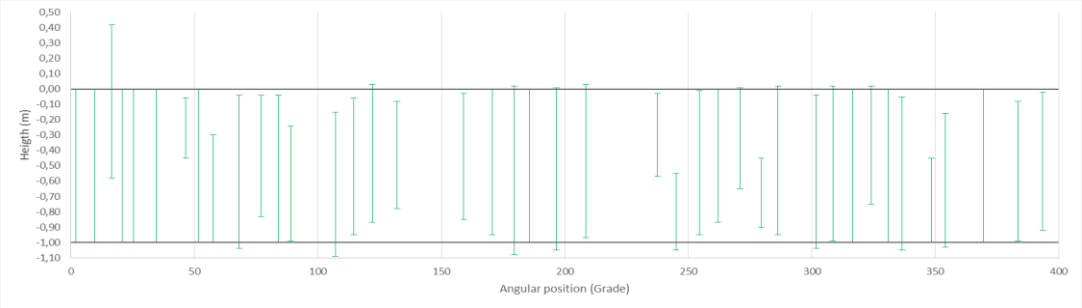

5.5.2.3 Vertical through cracks in the gusset

With the data collected with three embedded optical fibres during the VD2 pressurisation test, it was possible to identify vertical through cracks in the gusset.

With these data, 31 through cracks were identified in the gusset in VD2 (Figure 200). On average these cracks are spaced about 1.1 m.

Figure 200. Location of vertical through cracks in the gusset: Top sectional view of the gusset

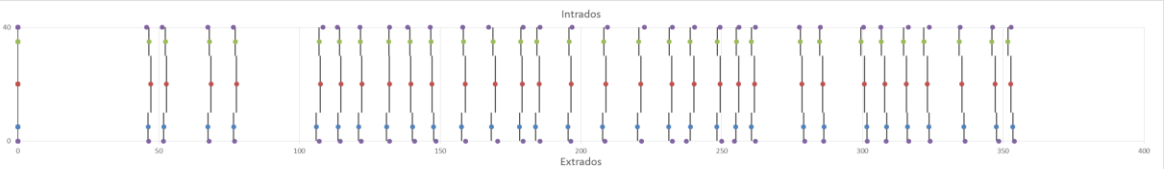

5.5.3. Submitted results

Nine teams provided answers to this topic: Teams 14, 23, 49, 50, 56, 74, 76, 84 and 92.

Three teams predicted that no crack would be observed: Teams 56, 74 and 92.

Team 50 considered early age cracks. The given results for this team are the early age cracks only.

Team 76 only gave some views about the cracking area.

5.5.4. Cracking state results

Out of the nine teams which gave results, only six predicted some cracks appearing: Teams 14, 23, 49, 50, 76 and 84. Team 50 talked about early age cracks evolution.

Except for Team 76, which provided only some views of cracking areas, all the results are given in the tables below, even if some are partial.

5.5.4.1 Inner face cracks (including through cracks)

Table 28. Inner face cracks total length (in metres)

	VD1 bis						VD2				
Team	Exp.	14	23	49	50	84	14	23	49	50	84
Gusset	37.4		2		0.98			2		0.98	
Hatch area	–		2		0			2		0	
Cylindrical part	–		5		0			5		0	
Dome	–		1		0			1		0	

Table 29. Inner face cracks maximum opening (in µm)

	VD1 bis					VD2				
Team	14	23	49	50	84	14	23	49	50	84
Gusset	172	100	160	38	2	198	100	220	55	3
Hatch area	41	100	80	0	17	59	100	66	0	17
Cylindrical part	20	10	34	0	109	20	10	38	0	109
Dome		10	91	0	18		10	110	0	9

5.5.4.2 Outer face cracks (including through cracks)

Table 30. Outer face cracks total length (in metres)

	VD1 bis						VD2					
Team	Exp.	14	23	49	50	84	Exp.	14	23	49	50	84
Gusset	35.9		2		0.98		37.0		2		0.98	
Hatch area	–		2		0		–		2		0	
Cylindrical part	–		5		0		–		5		0	
Dome	–		1		0		–		1		0	

Table 31. Outer face cracks maximum opening (in µm)

	VD1 bis					VD2				
Team	14	23	49	50	84	14	23	49	50	84
Gusset	28	100	44	40	100	31	100	51	58	149
Hatch area	10	100	42	0	189	20	100	46	0	188
Cylindrical part	30	10	44	0	555	40	10	52	0	439
Dome		10	50	0	317		10	93	0	415

5.5.4.3 Through cracks

Table 32. Through cracks total length (in metres)

	VD1 bis						VD2					
Team	Exp.	14	23	49	50	84	Exp.	14	23	49	50	84
Gusset	27.1		2		0.98		27.6		2		0.98	
Hatch area	–		2		0		–		2		0	
Cylindrical part	–		2		0		–		2		0	
Dome	–		1		0		–		1		0	

Table 33. Through cracks max opening (in µm)

	VD1 bis					VD2				
Team	14	23	49	50	84	14	23	49	50	84
Gusset	172	10		40		198	10		58	
Hatch area		10		0			10		0	
Cylindrical part		5		0			5		0	
Dome		5		0			5		0	

5.5.4.4 Comments

Concerning the cracks repartition, experimental results only show cracks in the gusset. Team results also show cracks in other parts of the containment (hatch area, cylindrical part and dome), except for Team 50, which predicted cracks only in the gusset. But Team 50's results are early age cracks only. By predicting only the early age cracks, Team 50 predicted the cracks repartition well.

Only two teams gave total lengths for some cracks (Teams 23 and 50). The results clearly underestimate the measures and show no evolution between VD1 bis and VD2.

Participants' predictions concerning crack openings give very scattered results.

On the gusset inner face, the highest values were given by Teams 14 and 49. These two teams predicted an increase of the maximum opening between VD1 bis and VD2. When comparing the inner face and outer face, Teams 14 and 49 gave higher crack openings on

the inner face, Teams 23 and 50 predicted the same openings on both sides, and Team 84 predicted a higher opening on the outer face of the gusset.

In the cylindrical part, crack openings range from 10 µm to 109 µm on the inner face and participants predicted no evolution between VD1 bis and VD2. On the outer face, crack openings range from 10 µm to 555 µm and 2 teams (Teams 14 and 49) predicted a small increase of the maximum opening between VD1 bis and VD2 while Team 84 predicted a decrease.

On the hatch area, crack openings are given to be higher on the inner face than on the outer face, except for Team 84. Values range from 10 µm to 189 µm.

In the dome, values range from 10 µm to 415 µm. Team 84 gave the highest values.

Three teams predicted the existence of through cracks in the gusset (Teams 14, 23 and 50), but with a very low value of total length. Crack opening values in the gusset given by teams range from 10 µm to 198 µm. Regarding the spacing of through cracks, only one team (Team 23) gave a spacing value of 0.1 m. The experimental value was, on average, a spacing of 1.1 m.

6. Results on Theme 3: Air leakage during the pressurisation test

6.1. Problem to solve

The VeRCoRs mock-up underwent five pressurisation tests between November 2015 and March 2018. The global air leakage was measured at the end of the 5.2 bar abs. plateau of each of these pressurisation tests.

During the pressurisation test, at the 5.2 bar abs. plateau, the containment wall was sprayed in order to locate leakage faults and quantify the flow through these defects.

Theme 3 of this benchmark consists of predicting air leakage during the pressurisation test, at the end of the 5.2 bar abs. plateau.

6.2. Results

The air leakage flow is expressed in Nm^3/h (normal m^3 per hour).

The normal volume of a gas (expressed in Nm^3) is the volume it occupies in normal conditions of temperature and pressure: TN = 273.15 K (0°C) and PN = 1 013.25 hPa (102 Pa).

6.2.1. Global air leakage

Seven teams replied to Theme 3. Their global air leakage results are given in Table 34 along with the experimental results.

Table 34. Global air leakage results (in Nm^3/h)

	Experimental	Team 14	Team 23	Team 49	Team 50	Team 74	Team 76	Team 88
Global air leakage VD1	29.6	14.2	3.0	22.0	31.9	7.0	12.3	7.8
Global air leakage VD1 bis	31.3	14.2	3.0	23.0	33.26	7.91	16.9	7.9
Global air leakage VD2		17.9	3.0	27.0	41.5	8.94	22.5	12.6

There is a factor of about 14 between the highest and lowest predictions of global air leakage. In the previous benchmark in 2015, the factor was about 200. The mean distance from the experimental value is 55%. Considering the difficulty of the models combining hydro-mechanical phenomena and specific leak calculation laws, this is a good result.

Global air leakage has been underestimated by all teams except by Team 50, which gives the best prediction. All of the teams except Teams 14 and 23 predicted the air leakage increase between VD1 and VD1 bis.

Figure 201. Global air leakage at 4.2 bar (rel.): Evolution over experimental programme

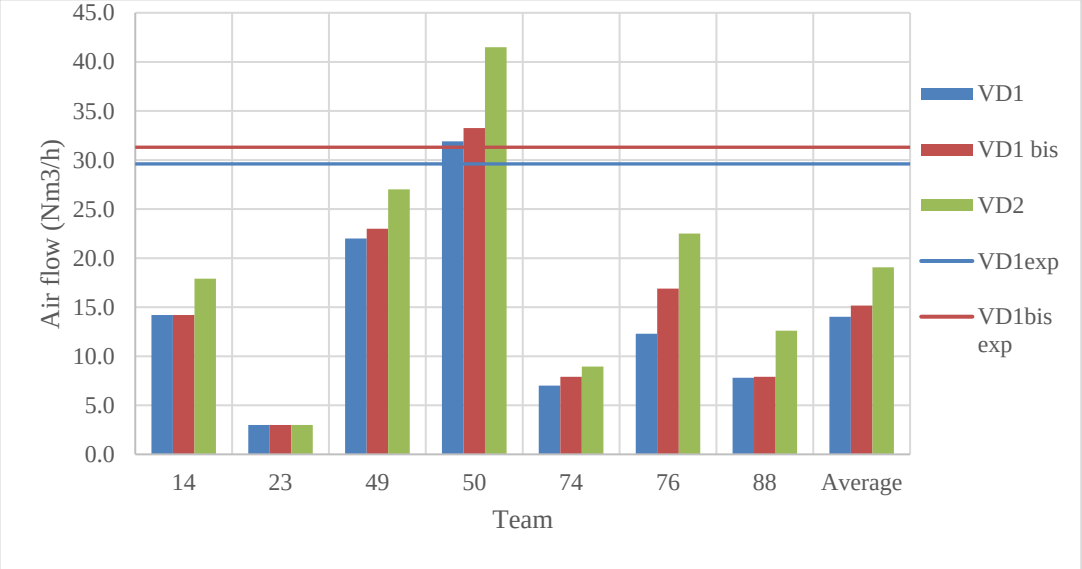

6.2.2. Air leakage repartition

6.2.2.1 Experimental results

During each pressure test, a spraying phase with soaped water was undergone to detect local air leakage. Then local measurements of air flow were made on the whole outer face of the containment.

Respectively, 28.544 Nm^3/h and 24.772 Nm^3/h were measured during the spraying phase of the VD1 and VD1 bis pressurisation tests. These flows represent 96% and 79% of the global air leakage. This corresponds to the air leakage of the containment wall defects (cracks, porosity lines). It is important to keep in mind that this kind of measurement has significant uncertainty in comparison to the global air leakage measurement.

The repartition of local measurements is given in Tables 35 and 36.

Table 35 Measured air leakage repartition in VD1

Area	Air leakage (Nm^3/h)	Measured air leakage percentage
Gusset	23.949	84%
Hatch area	0.812	3%
Cylindrical part	2.955	10%
Dome	0.828	3%

Table 36. Measured air leakage repartition in VD1 bis

Area	Air leakage (Nm^3/h)	Measured air leakage percentage
Gusset	20.758	84%
Hatch area	0.796	3%
Cylindrical part	2.996	12%
Dome	0.222	1%

The experimental results show that approximately 85% of the local air leakage is in the gusset. This result confirms, like in the previous benchmark, that the entire containment wall history, especially at an early age, matters in the air leakage study.

6.2.2.2 Comparison between experimental and predicted air leakage

Seven teams estimated the air leakage repartition. The predicted air leakage repartition is given in Table 37.

Table 37. Air leakage repartition given by participants (in Nm^3/h)

VD1	Global air leakage	Gusset	Hatch area	Cylindrical part	Dome
Team 50	31.9	0.77	0.78	17.08	13.28
Team 49	22	3.54	1.51	13.9	4.01
Team 74	7	3.9	1.1	1.8	0.2
Team 23	3	1	1	0.5	0.5
Team 76	12.3	7.85	1.012	3.283	0.16
Team 14	14.2	4.3	0.1	9.1	0.7
Team 88	7.8	1.2	0.4	4.3	0.2
VD1 bis					
Team 50	33.26	0.79	0.79	18.35	13.32
Team 49	23	3.58	1.53	14	4.06
Team 74	7.91	4.4	1.2	2	0.23
Team 23	3	1	1	0.5	0.5
Team 76	16.9	8.1	1.055	7.496	0.25
Team 14	14.2				
Team 88	7.9	1.2	0.4	4.3	0.2
VD2					
Team 50	41.5	1.01	0.86	23.86	15.78
Team 49	27	4.11	1.79	16.3	4.7
Team 74	8.94	5	1.4	2.3	0.26
Team 23	3	1	1	0.5	0.5
Team 76	22.5	8.16	1.121	15.868	0.35
Team 14	17.9	4.5	0.2	12.3	0.9
Team 88	12.6	3.6	0.5	6	0.2

To allow comparison with participants' results, it is supposed in Figure 202 that the global air leakage follows the same repartition as the local air leakage. The repartition given in the following graphs is in percentage of the global air leakage.

Figure 202. Air leakage repartition in VD1

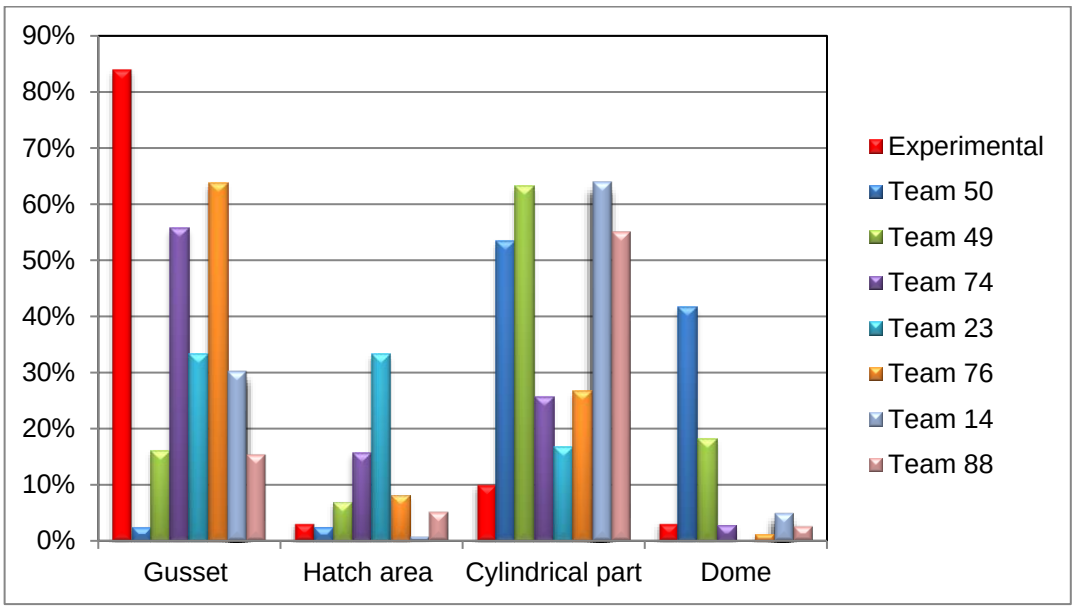

Figure 203. Air leakage repartition in VD1 bis

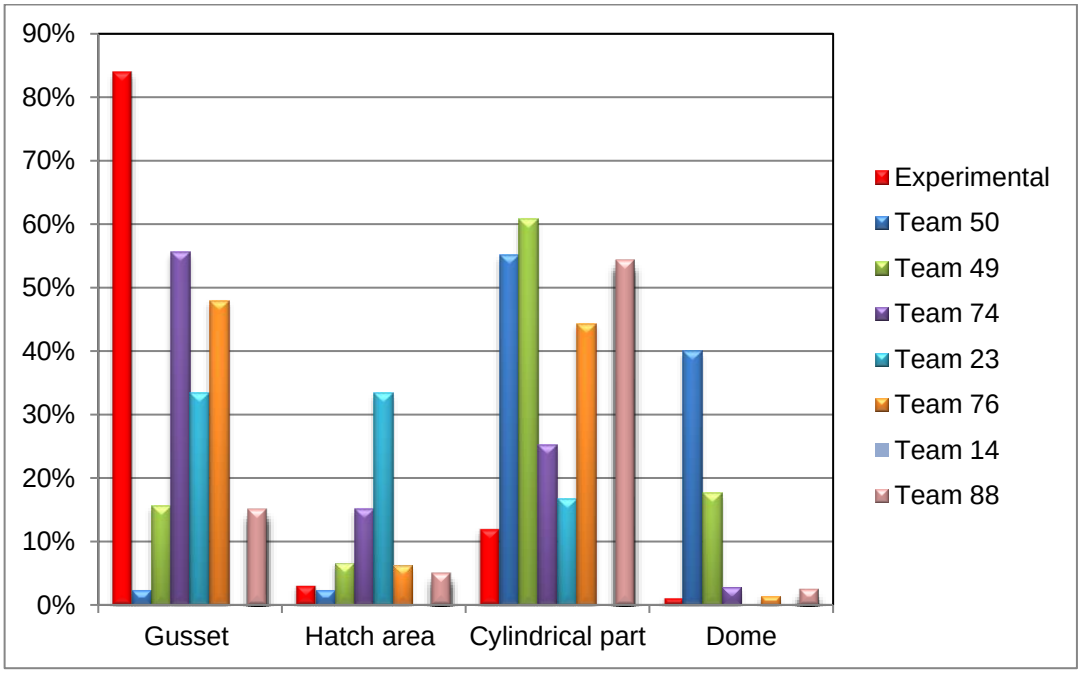

Figure 204. Air leakage repartition in VD2

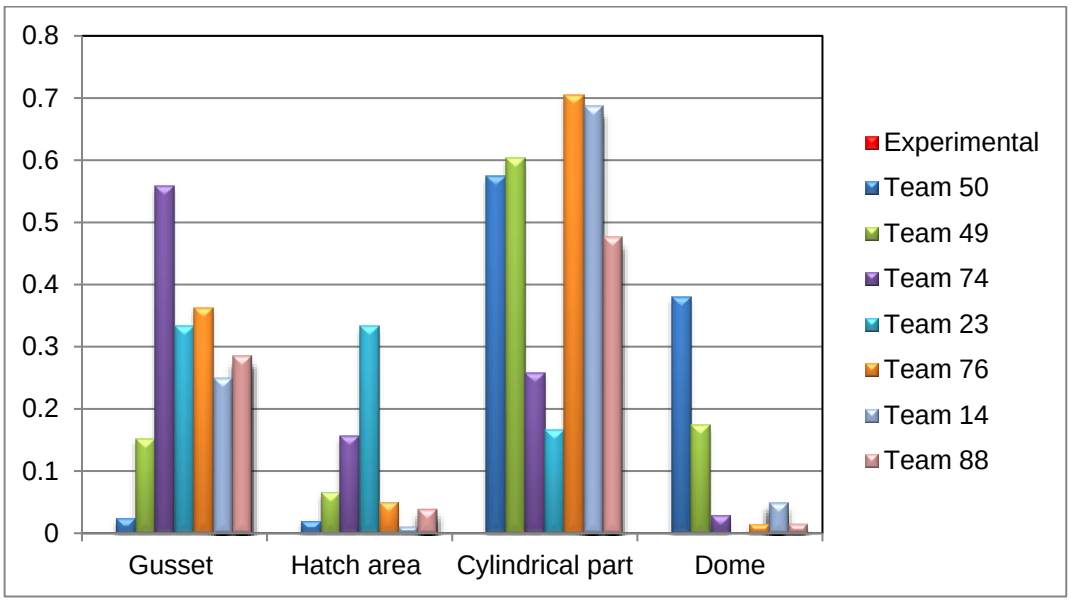

The experimental leakage repartition is roughly the same between VD1 and VD1 bis.

If the experimental repartition is compared with the repartitions given by the teams, it can be noted that only two teams ranked the area contributions in the right order: Team 74 and Team 76. But these two teams did not give the same evolution between VD1 and VD1 bis. Team 74 predicted a slow evolution of air leakage in the cylindrical part while Team 76 predicted an increase from 26% to 44% for the contribution of this area between the two tests.

Among the other teams, four predicted that the cylindrical part is the major contributor to the global air leakage. One team predicted an equal contribution of the gusset and the hatch area as major contributors to the global air leakage.

All teams overestimated the cylindrical part's contribution and underestimated the gusset's contribution.

The hatch area contribution to air leakage was significantly overestimated by Teams 74 and 23.

Dome contribution to air leakage was globally well estimated, except for Teams 49 and 50, which overestimated its contribution significantly.

6.2.3. Local leakage in the gusset

As the gusset is the major part contributing to global air leakage, specific measures were taken during the VD2 test in this area. The three optical fibres embedded at a level of -0.20 m in the gusset were continuously interrogated during the VD2 pressure test in order to detect and localise vertical cracks inside the wall.

Figure 205. Radial position of optic fibres in the gusset

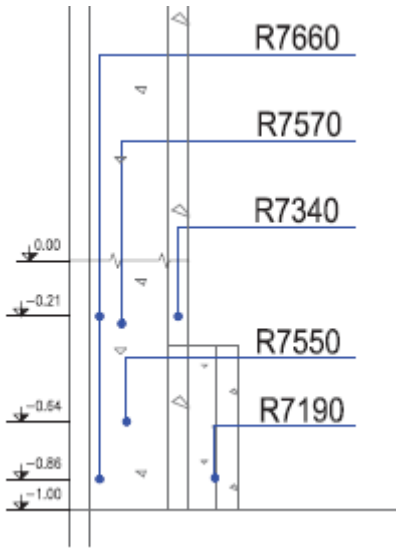

This measure also made it possible to evaluate the crack opening evolution during the pressure test. Some results are presented in the following graphs. On these graphs, blue and red vertical lines represent crack opening increases in microns during the pressure test. Each black dotted line represents a local air flow measured on the outer face of the gusset. The superposition of these two measures is only made here to evaluate the positions of cracks inside the wall and on the outer face.

Figure 206. Location of vertical cracks in the gusset during VD2 pressure test – Intrados

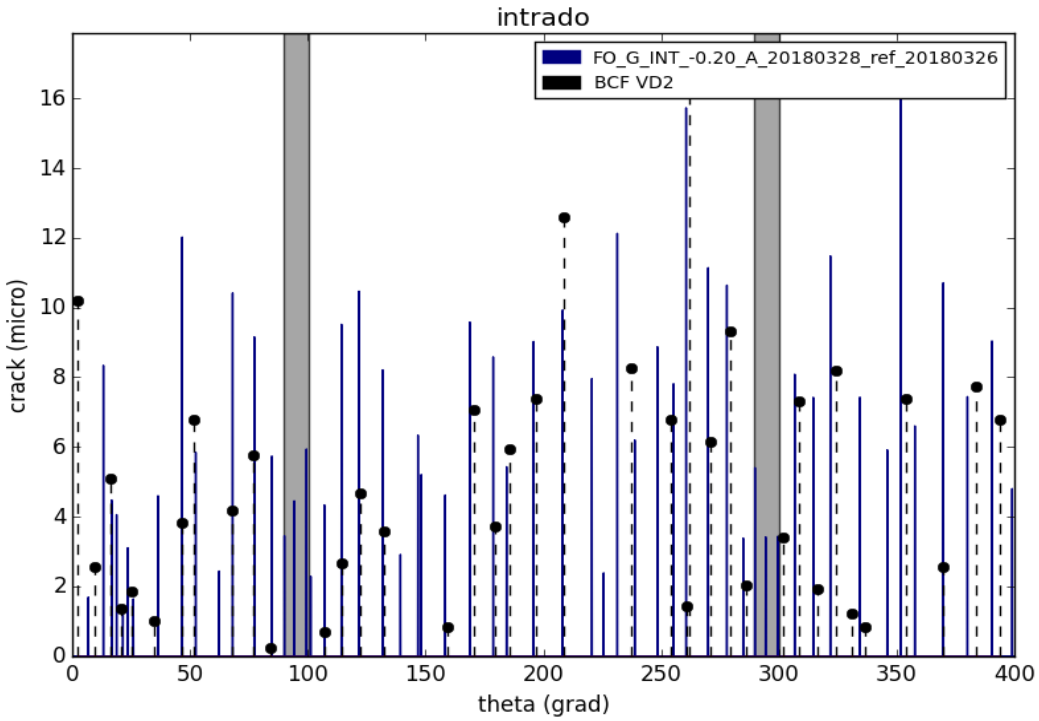

Figure 207. Localisation of cracks in the gusset during VD2 pressure test: Middle of the wall

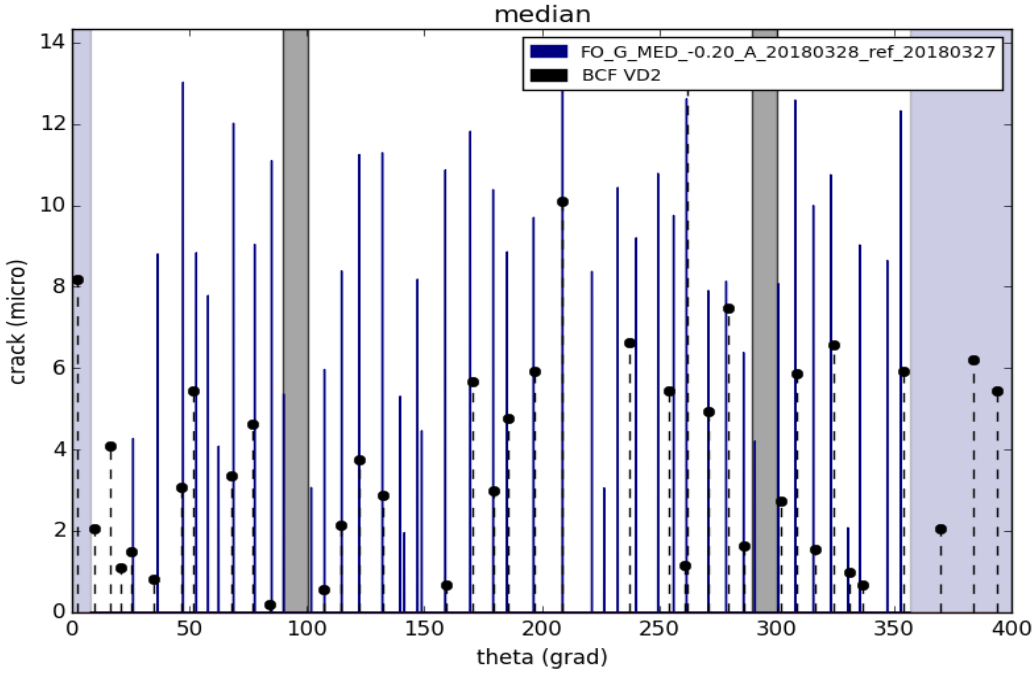

Figure 208. Localisation of cracks in the gusset during VD2 pressure test: Extrados

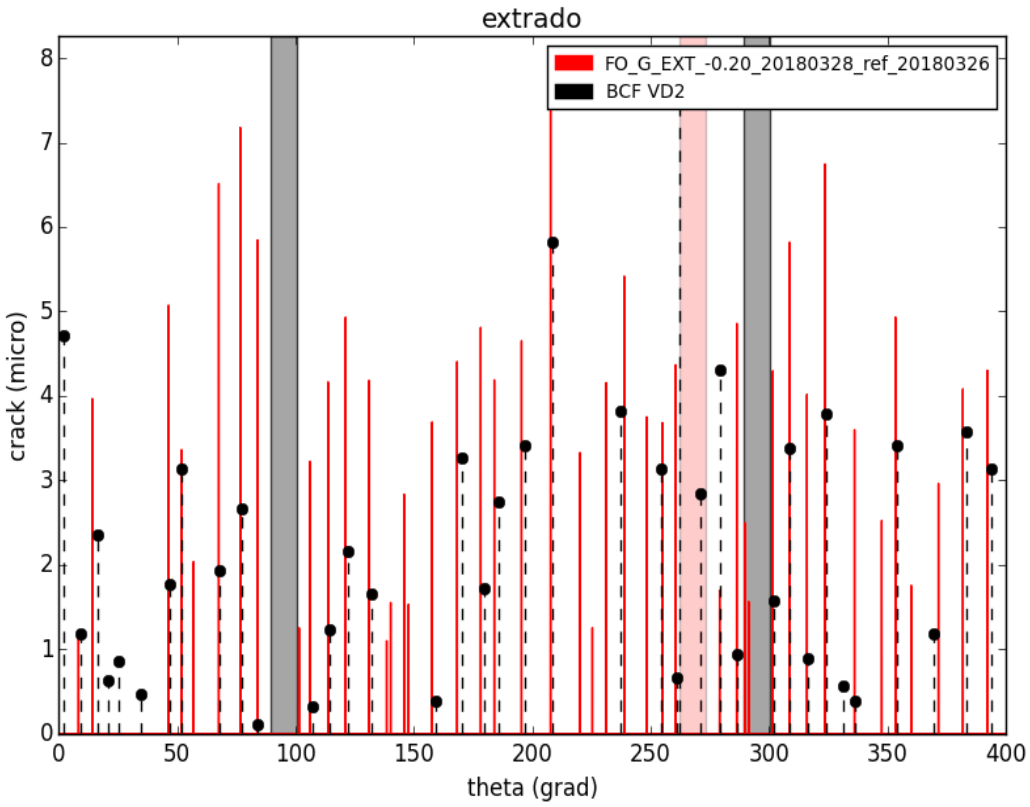

The previous figures show that there is a good correspondence between the position of the detected cracks inside the wall and the visible cracks on the outer face during the VD2 test.

Other measures were made during the VD2 pressure test. On five vertical cracks of the gusset, the air flow was continuously registered during the whole pressure test. This measure is show in Figure 209.

Figure 209. Local air flows evolution during the VD2 pressure test

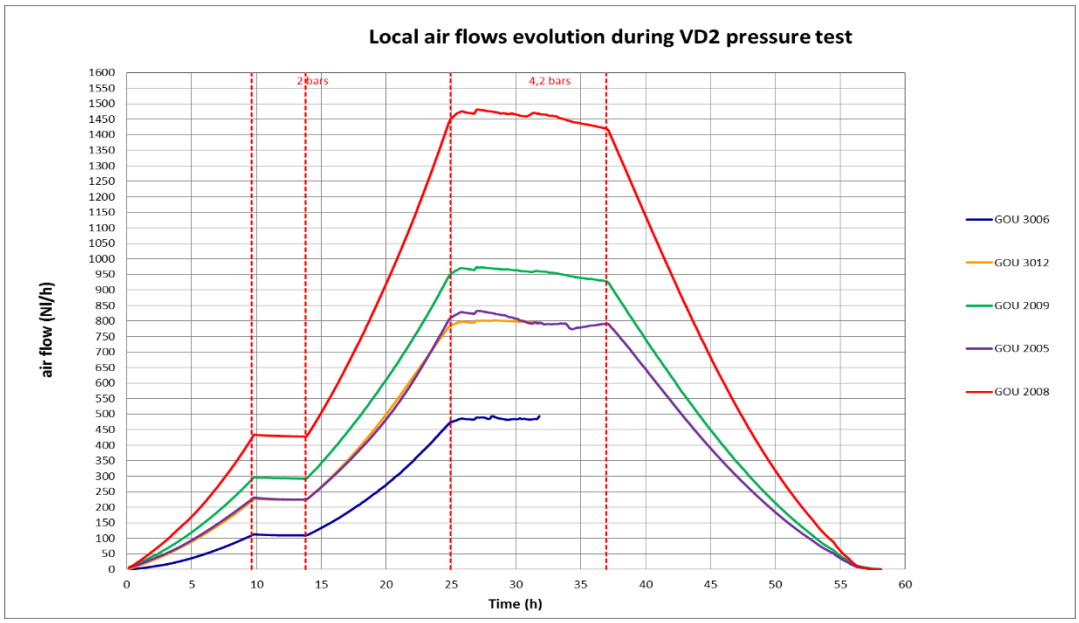

For these five vertical cracks, it will be possible to try to find a correlation between air flow and crack openings. These kinds of data will surely be very helpful to better understand the air flow through cracks and to improve models.

6.3. Global comments on air leakage

Global air leakage prediction has improved since the previous benchmark both as regards the difference between the predictive values and the experimental measurement as well as regarding the dispersion of the values provided by the participants.

Nevertheless, in the representation of the leakage phenomena, the prediction remains imprecise. For example, Team 50 gave the best global air flow prediction (only 8% from the experimental value), but not the right repartition of this leakage. Indeed, this team predicted an air flow in the gusset more than 20 times lower than the experimental value.

This confirms that the leakage through cracks is preponderant and requires additional modelling. The last measures on the vertical cracks during the VD2 pressure tests combined with other measures coming in the future will provide important data to try to improve air flow modelling through cracks.

7. Conclusions

For this second benchmark, three main themes were proposed:

- Theme 1: Creep modelling – micromechanics and/or multiphysics approaches;
- Theme 2: Mechanical behaviour of the containment during pressurisation tests;
- Theme 3: Air leakage.

Global participation was significant: the involvement of 18 teams from 9 countries shows the interest of the scientific community in advanced modelling in civil engineering. There were 14 teams in the previous benchmark in 2015. Seven new teams from Canada, the People's Republic of China, Finland, France, Korea and Spain, which had not participated in the first benchmark, participated in the second benchmark exercise and some of them submitted exhaustive and good quality results.

For this second benchmark, Themes 2 and 3 proposed quite the same exercises as in 2015 but on an advanced age of the mock-up. Eighteen teams submitted results on Theme 2 in 2018. This is twice as many as in 2015. This provides a global overview of all the advanced modelling practices in civil engineering. On Theme 3, dealing with air leakage, six teams had submitted results in 2015. In 2018, that number rose to seven, of which two are new teams and one had not participated in Theme 3 in 2015. This confirms that the participants already involved in the first benchmark on this highly specialised subject continued in their efforts to improve their models and that others want to propose their approach to deal with this topic. It is a real asset to have so many motivated participants and this allows for significant progress in the long term.

As in the previous benchmark, the quality of the work done by the participants was good.

Theme 1 proposed to compare approaches for creep modelling at different material scales or in various environmental conditions. Regarding different scale approaches, only one participant tried modelling the creep behaviour of cement paste in the framework of this benchmark. It is too little to draw any conclusions. For creep modelling at concrete scale, the results provided are more numerous. Although some results obtained are good and close to the experimental values, there are significant differences between the results provided by the participants, even when the model chosen to represent creep is the same for several teams. Beyond the choice of the model, it is the use of the input data and sometimes the presentation of the results that are at the origin of such deviations.

The results for modelling the containment behaviour and the effects of ageing (Theme 2) are numerous. These calculations are indeed more common in the profession.

Some teams obtained results that were very similar to the experimental measurements, showing a good understanding of the behaviour of the structure. Nevertheless, there are sometimes significant differences both between participants and compared with the experimental measurements.

The gusset area in particular remains complex to model and its behaviour is poorly mastered. But looking at the dispersion of the results given in the 2015 and 2018 benchmarks per zone of the containment (Figure 210), even if the gusset is an area where results should be improved in the future, the dispersion has strongly decreased in this area, like in all other areas of the containment.

Figure 210. Values dispersion per zone of the containment: Evolution between 2015 and 2018

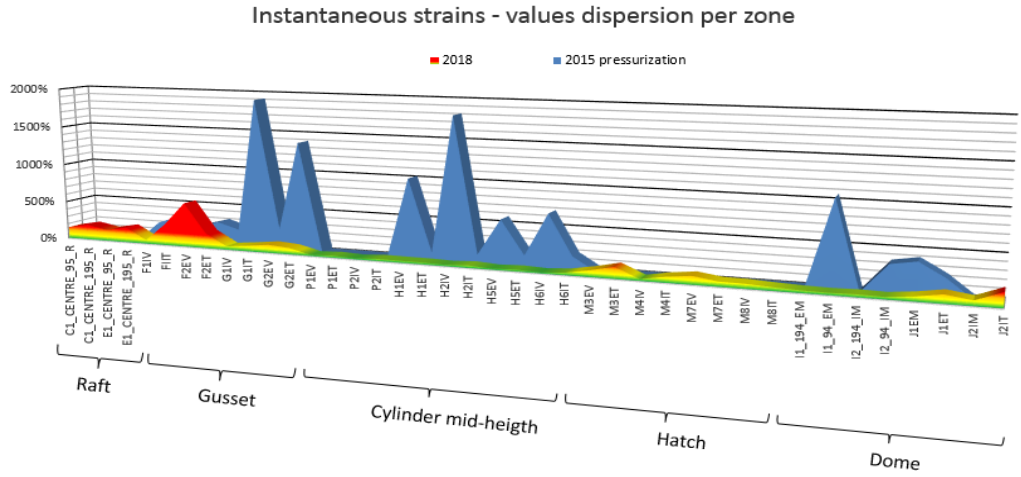

One can also note that the results for cracks are far from the experimental results. In particular, one can note and then confirm that as in the first benchmark, ignoring the effects associated with early age creates a gap in forecasting the state of active cracking during pressurisation (particularly in the gusset).

It seems that no evident progress has been made since 2015 in modelling strategies integrating non-linearities along the whole history of the building and some efforts are necessary on this point.

Finally, regarding the prediction of the leakage flow, even if it is a difficult exercise, some improvements have been made. In 2015, the results showed a factor of 1:200 between the lowest flow and the highest. For this second benchmark, the factor has decreased to 1:14. On average, the global leakage predicted values were 30 times higher than the experimental ones in 2015. In 2018, the average value underestimated the experimental value by 55%, and one team was only 8% from the experimental value.

Calculating a leak through a concrete wall seems to have been better approached by participants, even if new teams tried the exercise for the first time in this second benchmark. Of course, the knowledge of the previous behaviour of the mock-up regarding air leakage also helps to obtain better predictions. These good results only concern the global air flow prediction.

However, it is clear that the determination of the cracking state is a major element to forecast leakage since the leakage through cracks is preponderant. It is therefore necessary to make additional efforts on modelling both the appearance of cracks and air flow through cracks to obtain better air leakage predictions for industrial use.

8. Synthesis of the restitution workshop

The three-day workshop was organised on the following principles:

- 1st half-day, presentation of the VeRCoRs programme and its progress.
- 2nd half-day, review of Theme 1 of the benchmark and presentation of the work done by the participants on this theme.
- 2nd day, review of Themes 2 and 3 and presentation of the work done by the participants on these themes.
- 3rd day, presentation of the technical innovations in the field of monitoring and the results. Presentations of the digital twin digital platform.
- Conclusions and visit of the VeRCoRs model installation.

Discussion areas were included in the programme, with the main elements given below.

1st half-day: Presentation of the VeRCoRs programme and its progress

An introductory message was first issued by the R&D Director of EDF. He stressed the importance of analysing the ageing of concrete in French nuclear power plants and that it is with this objective that the VeRCoRs mock-up was built. EDF welcomes the significant progress made since the first benchmark, which is a sign of the interest of the international scientific community in this type of concern.

The main conclusions following the presentations of the research programme are:

- Concerning the experimentation and more particularly the localisation of the leaks:
  - Significant damage appears around the hatch and no particular leakage is measured; the reason is that the damage does not go through the wall.
  - The number of active cracks appears to be lower in the first tests than in recent tests. At the beginning of the test programme, a crack was identified as a through crack when it appeared in intrados and extrados of the gusset; however, the recent local measurements (using optical fibres) show that there are also active cracks that do not fall into this category; active cracks are therefore more numerous than initially listed.
- Concerning modelling:
  - It is necessary to identify the type of improvement to models.
  - It is necessary to take into account thermoactivation on drying.
  - It is necessary to improve the link between ageing and increased leakage rate.
  - The dependence between loss of prestressing and increasing local leakage must be quantified.
  - It is necessary to find how and where to repair leakage zones.
  - It is necessary to better understand the path of leaks.

2nd half-day: Restitution of the benchmark on Theme 1.

In the presentation of the creep modelling report, it was pointed out that:

- Concerning the effectiveness of the waterproof coating in clean creep experiments, the technique has reached a good level of reliability.
- The results concerning the incidence of a biaxial creep state have shown that a well-designed 1D-based model works well in 2D.

Other issues were raised while presenting this topic to participants:

- In relation to the modelling resulting from the EC2:
  - EC2 replicates basic creep, but what about "drying creep"? In response to this question, it is indicated that the EC2 does not make this distinction but that the results are a mixture of the two effects. It is also specified that the formulas proposed by MC 2010 and the future EC2 parameters must be calibrated for each use on a dedicated experiment (the tests must be done especially at the time of prestressing) and this gives very good results.
  - Some consider that EC2 does not always reproduce creep in the long term.

In relation to the importance of drying creep:

- An American presentation based on modelling uses the average between basic and drying creep and questions the importance of drying shrinkage. The discussion led to the reminder that the US containment enclosures are all equipped with a liner and that the problem of drying is largely diminished.

During the general discussion, the following topics were discussed:

- How to scale up in modelling early age creep, tensile creep/compressive creep, 3D creep, the effects of temperature, relative humidity, etc.
- The conclusion is that the experimental database has yet to be enriched and as a result modelling will evolve.

2nd day: Restitution of the benchmark on Themes 2 and 3

The presentations were organised into two sessions:

- Analysis of the behaviour of the containment: eight teams treated this part independently of the "prediction of leakage from the enclosure".
- Analysis of the behaviour and tightness of the containment: seven teams presented results.

The following points emerged from the presentations:

- The models used are based on discretisation ranging from a few hundred elements to more than 700 000, which can lead to very long and expensive calculations.
- Some participants already present in the 2015 benchmark showed progress in their approach. This is the case of Team 74, which used shell elements enriched in a simplified mesh and introduced a creep law mix (MC2010 and ACI209) and associated a hollow cylinder experiment under internal air pressure leading to a real "flow rate/crack opening" analysis. The results are promising.
- There are two options to take into account early age cracks in the gusset, either to integrate the treatment of early age in the analysis or to introduce cracks observed in the mesh used. Team 50 proposed a complete treatment of the problem integrating early age into a probabilistic approach (probabilistic thermo-hydro-

mechanical [THM] model) conducted after having selected the most influential parameters (parameters of drying, permeability and certain mechanical parameters) and treating the problem at the level of structurally representative volumes whose boundary conditions are derived from an axisymmetric computation. The results regarding global leakage are convincing. In the category of cracks introduced, a post-benchmark calculation presented by Team 14 notes that very good predictive results are obtained for the VD2 when the characteristics of the flow in the cracked zones are deduced from the measurements resulting from the first tests (VD0, VD1, VD1 bis).

The discussions that took place at the end of the presentation led to the following points:

- Some participants reported the need for additional data:
  - On the forces in the prestressing cables – two cables were instrumented after calibration, and adjustment of a certain number of uncertainties for these data will be available soon.
  - On the material uncertainties, on the permeability around ducts and reinforcement, on the opening and closing of cracks, on the evolution of the Poisson's ratio during a 3D creep, on the effects of scale, etc. as many topics that are not always easy to answer.
- In general, the calibration of the models is difficult and anything that will improve this will be a step in the right direction. The sensitivity of certain phenomena can be important:
  - This is the case of the impact of temperature variations on creep and, to a certain extent, relative humidity. Note that the temperature also acts on the prestressing.
  - It is also the case of the characteristics to be attributed to the cracks (average opening, tortuosity) in hope of a good estimate of the leak.
- A question was asked about the need to reproduce the construction phases. In response it was indicated that if the concreting phases are essential in the analysis of the dams, it is especially the prestressing phases that are important.

3rd day: Presentations on measurement techniques, digital clone work and perspective work

The general conclusions on the benchmark are:

The interest of the international community *vis-à-vis* VeRCoRs is confirmed: there were 14 participants in the 2015 benchmark and 18 in the 2018 benchmark and twice as many teams (14/7) contributed to the work related to predicting the mechanical behaviour of the structure.

The mix of research teams and teams in the field of engineering leads to the use of different models (from EC2 or different numerical codes), especially for creep and cracking, which leads to very successful comparative reviews. This also leads to the emergence of new models, such as those based on probabilistic approaches.

Some data are important (temperature) or to be perfected (measurement of the forces of prestressing in the cables, variability of the mechanical characteristics of the materials).

The scientific mastery of the problem is reinforced, particularly because of the contribution of 11 teams to the 2 benchmarks. Indeed:

- For the prediction of strains due to pressurisation, in most of the structure, the dispersion of the results went from thousands of per cent to 30%.
- With regard to the global leakage forecast, the gap between the strongest and weakest forecasts has been divided by 15 between the 2 benchmarks and the best result is close to that of the experiment (of the order of 10%).

Progress is still expected, especially in the predictions of cracking at early age and the behaviour of this cracking over time and during pressurisation tests.

For the future, it is suggested to make the best use of the VeRCoRs mock-up to further improve local measurement capacities (water content, permeability, cracking, etc.) and continue the tests, especially the "severe accident" test by analysing finely its consequences.

With respect to a future benchmark, it is recommended that it not be postponed for too long (two years) so that the teams invested remain mobilised and benefit fully from the acquired know-how.

9. Lessons learnt

Some lessons learnt may be drawn from this second benchmark:

- Early age concrete behaviour is the major contributor to cracking, which may lead to leakage. It is a complex phenomenon and difficult to model. It would be a good practice to study and try to detect these early cracks at the beginning of the structure's life in the frame of extended periodic inspections.
- It is very difficult to consider those early cracks in the modelling of concrete structures under thermo-mechanical loading. More advanced methods have to be developed.
- Progress has been achieved in recent years in the use of advanced instrumentations such as acoustic sensors. They give indirect information that may lead to promising results to detect where the cracks are and how much gas leaks through those cracks.
- The use of optical fibres in nuclear reactor buildings is also an advanced instrumentation technology that gives very dense and rich information. However, it is still hard to master without some preliminary precautions.
- It is known that water content is the "engine" of ageing of the VeRCoRs mock-up. The mock-up is at a scale of 1/3, which allows it to age about nine times faster. The physical laws of creep and shrinkage are directly linked to water content, which leads to the evolution of the cracking state of the mock-up. It is currently possible to measure the water content of concrete. Therefore, technical equipment for practical use should be developed to capture this parameter.
- No data were available during this benchmark regarding the water content evolution of the concrete as it was still not readily available at the time. In the future, water content data will be made available because it is a key parameter.
- Further research and development should be carried out to better predict the location of cracks and leaks.
- One of the main lessons learnt related to nuclear safety is that the determination of the cracking state is a major element to forecast leakage since leakage mainly occurs through cracks. It is therefore necessary to make additional efforts on modelling the appearance of cracks and the air flow through cracks to obtain better air leakage predictions for industrial use.

References

Irfan-ul-Hassan, B. Pichler, R. Reihsner and Ch. Hellmich (2016), "Elastic and creep properties of young cement paste, as determined from hourly repeated minute-long quasi-static tests", *Cement and Concrete Research*, Volume 82, 2016, pp. 36-49, DOI: 10.1016/j.cemconres.2015.11.007.